

Imidazolium Carboxylate Based [C–H]^{δ+} Functionalized Discrete and Polymeric Coordination Assemblies: Synthesis and Characterization

Paladugu Suresh

A Dissertation Submitted to
Indian Institute of Technology Hyderabad
In Partial Fulfillment of the Requirements for
The Degree of Master of Technology/ Doctor of Philosophy



भारतीय प्रौद्योगिकी संस्थान हैदराबाद
Indian Institute of Technology Hyderabad

Department of Chemistry

October, 2014

Declaration

I declare that this written submission represents my ideas in my own words, and where others' ideas or words have been included, I have adequately cited and referenced the original sources. I also declare that I have adhered to all principles of academic honesty and integrity and have not misrepresented or fabricated or falsified any idea/data/fact/source in my submission. I understand that any violation of the above will be a cause for disciplinary action by the Institute and can also evoke penal action from the sources that have thus not been properly cited, or from whom proper permission has not been taken when needed.



(Signature)

Paladugu Suresh

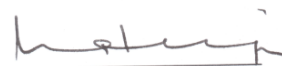
(—Student Name—)

CY10P013

(Roll No)

Approval Sheet

This thesis entitled “Imidazolium Carboxylate Based [C–H]^{δ+} Functionalized Discrete and Polymeric Coordination Assemblies: Synthesis and Characterization” by Paladugu Suresh is approved for the Doctor of Philosophy from IIT Hyderabad.



Prof. Srinivasan Natarajan

Professor

Solid State Structural Chemistry Unit

Indian Institute of Science Bangalore

Examiner



Prof. M. S. Balakrishna

Professor

Department of Chemistry

Indian Institute of Technology Bombay

Examiner



Dr. G. Prabusankar

Assistant Professor

Department of Chemistry

Indian Institute of Technology Hyderabad

Adviser



Dr. Saket Asthana

Assistant Professor

Department of Physics

Indian Institute of Technology Hyderabad

Chairman

Acknowledgements

I sincerely acknowledge my thesis advisor Dr. Ganesan Prabusankar for giving me the opportunity to work in the area of metal-organic assemblies. The targeted work was accomplished due to his continuous support, motivation and suggestions.

I would like to specially thank my doctoral committee members Dr. Ch. Subrahmanyam and Dr. Tarun Kanti Panda for their valuable suggestions and fruitful discussions. I gratefully acknowledge Dr. Natarajan Sampath for solving some of my crystal data's. I would like to thank Dr. Ranjith Ramadurai for studying magnetic properties of some of my molecules.

I thank Department of Chemistry, Indian Institute of Technology Hyderabad for providing sophisticated facilities like NMR, Single-Crystal XRD, Powder XRD, FT-IR, TGA, UV-vis and Fluorescence spectroscopy.

I am very much thankful to my lab members for their support and suggestions. I would like to express my special thanks to my colleagues and friends at Department of Chemistry, Indian Institute of Technology Hyderabad for their technical and moral support during my stay in IIT Hyderabad.

I would like to also thank CSIR and IIT Hyderabad for providing fellowship. I thank DST (Project No: SR/FT/CS-94/2010) for providing research grants for research.

I would like to especially thank my mother, father and sister for their support throughout my carrier. I thank my friends, teachers and relatives for their moral support.

Dedicated to

My parents and sister

Abstract

The construction of functionalized coordination polymers (FCPs) have been the subject of interest over the last few decades due to their fascinating architectures and versatile applications in catalysis, gas storage, separation, luminescence, electrical conductivity, magnetism and nonlinear optics. Suitable organic spacers, metal precursors and synthetic methodologies are essential criteria to design FCPs with different physical properties. In addition, non-covalent interactions such as hydrogen bonds, $\pi \cdots \pi$, $M \cdots \pi$, $C-H \cdots \pi$ and $anion \cdots \pi$ interactions play a key role in FCPs to increase their dimensionality, supramolecular topology and porosity. Therefore, the choice of organic spacer is extremely important to fine-tune the structural and desired functional properties of FCPs through the coordination mode or non-covalent interaction mode. Amongst these organic spacers, the imidazolium carboxylic acids are of special interest as they have a $[C-H]^{\delta+}$ functional group (potential functional group for anion reorganization and post modification to generate N-heterocyclic carbene tethered catalytically active metal centers) along with excellent functional group tolerance at the N-positions. Thus, the thesis dealt (i) the design, synthesis and characterization of new imidazolium carboxylic acid organic spacers, (ii) synthesis and characterization of novel imidazolium carboxylate based coordination polymers, (iii) structural diversity and close interracial relationships between main group, transition metal and rare earth imidazolium carboxylate based coordination assemblies. A thorough literature survey on imidazolium carboxylate coordination polymers (till August 2014) and seven new imidazolium carboxylate organic spacers along with their thirty synthetically intriguing metal aggregates have been reported in the thesis. These new molecules have been fully characterized. Chapter 1 (Introduction) reviews the recent literature on imidazolium carboxylate based coordination assemblies. Chapters two to five deal with the synthesis and structural features of newly prepared imidazolium carboxylate supported coordination assemblies. The final section of each chapter lists the references from the literature, which are indicated in the text (Chapters 1-6) by appropriate numbers appearing as square brackets. Lists of abbreviations, table, scheme, and figure captions appearing in this report are collected together in the beginning of the thesis chapters.

Preface

This thesis embodies the results of synthetic, spectroscopic, structural, bonding aspects of imidazolium carboxylates and coordination assemblies. The new compounds have been characterized by FT-IR, NMR, UV-vis spectroscopy, fluorescence spectroscopy, TGA, Single-Crystal XRD and Powder XRD techniques.

Chapter 1 (Introduction) reviews the literature on imidazolium carboxylate based coordination assemblies, scope of work and the objectives.

Chapter 2 describes design, synthesis, spectral characterization of semirigid mono-imidazolium carboxylate and its series of d-block (Mn, Co, Ni, Cu, Zn and Cd) zwitterionic coordination networks.

Chapter 3 deals with the synthesis and spectral characterization of luminescent bis-imidazolium carboxylate and its infinite coordination networks of copper and zinc

Chapter 4 explains synthesis and spectral characterization of varies bis- and tris-imidazolium carboxylates based ionic calcium coordination assemblies.

Chapter 5 presents synthesis and spectral characterization of zwitterionic bis- and tris-imidazolium carboxylates based rare-earth coordination assemblies.

Chapter 6 (summary and conclusion) summarizes the results described in the Chapters 2-5, making important correlations between the compounds.

Contents

Abbreviations.....	xi
List of Figures.....	xii
List of Schemes	xix
List of Tables	xx
1 Introduction.....	1
1.1 Coordination polymers	1
1.2 Imidazolium carboxylate based transition metal coordination polymers	8
1.3 Main group imidazolium-carboxylate coordination polymers	15
1.4 Imidazolium carboxylate based lanthanide coordination polymers.....	18
1.5 Scope of the work	21
1.6 Objectives	21
1.7 References.....	22
2 Semi rigid imidazolium carboxylate controlled structural topologies in zwitterionic coordination networks.....	28
2.1 Introduction.....	28
2.2 Experimental.....	30
2.2.1 Materials and methods.....	30
2.2.2 Synthesis of L(C ₂ H ₅) ₂ Br, LH ₂ Br and 1-6	30
2.2.3 Crystallography	33
2.3 Results and discussion	33
2.3.1 Synthesis and characterization of L(C ₂ H ₅) ₂ Br, LH ₂ Br and 1-6	33
2.3.2 Crystal structural description of 1-6.....	37
2.3.3 Comparison of solid state structures of 1-6.....	45
2.3.4 TGA analysis.....	47
2.4 Conclusion	48
2.5 References.....	48
3 Luminescent Imidazolium Carboxylate Supported Aggregate and Infinite Coordination Networks of Copper and Zinc.....	51
3.1 Introduction.....	51
3.2 Experimental Section.....	52
3.2.1 Materials and methods.....	52
3.2.2 Synthesis of 2-6.....	54

3.3	Results and discussion	56
3.3.1	Synthesis and characterization	56
3.3.2	Crystal structural description of 2 and 4–6	62
3.3.3	TGA analysis.....	71
3.4	Conclusions.....	72
3.5	References.....	72
4	Imidazolium Carboxylate Based Ionic Calcium Coordination Polymers and Discrete Molecules with Diversified Calcium Coordination Geometry	75
4.1	Introduction.....	75
4.2	Experimental.....	77
4.2.1	Materials and methods.....	77
4.2.2	Synthesis of bis- and tris-imidazolium carboxylates and 1-6.....	78
4.2.3	Crystallography	83
4.3	Results and discussion	84
4.3.1	Synthesis and characterization of bis- and tris-imidazolium carboxylates and 1-6	84
4.3.2	Description of crystal structures.....	88
4.3.3	Comparison of solid state structures of 1-6.....	99
4.3.4	Thermal analyses.....	101
4.4	Conclusions.....	102
4.5	References.....	103
5	Rare-earth discrete molecules and coordination polymers from zwitterionic imidazolium carboxylate	105
5.1	Introduction.....	105
5.2	Experimental section	106
5.2.1	Materials and methods.....	106
5.2.2	Synthesis of L ¹ , L ² and 1-14.....	107
5.3	Results and discussion	110
5.3.1	Synthesis and characterization of L ¹ and 1-6	110
5.3.2	Description of crystal structures 1-6.....	114
5.3.3	Synthesis and characterization of L ² and 7-10	118
5.3.4	Description of crystal structures 7-10.....	121
5.3.5	Synthesis and characterization of 11-14.....	122
5.3.6	Description of crystal structures 11-14.....	125
5.4	Conclusions.....	133

5.5	References.....	134
6	Summary and Conclusion.....	136
	List of Publications	149
	List of Conferences and Workshops	151

Abbreviations

Å	Angstrom
DMF	Dimethyl formamide
DMSO	Dimethyl sulfoxide
FT-IR	Fourier transform-infrared
GOF	Goodness of fit
h	Hour
FCP	Functionalised coordination polymer
IRMOF	Isorecticular metal-organic framework
m	Multipet (NMR), medium (IR)
MHz	Mega hertz
ml	Millileter
mmol	Millimole
MOF	Metal-organic framework
NHC	N-heterocyclic carbene
NMR	Nuclear magnetic resonance
PCP	Porous coordination polymer
ppm	Parts per million
PXRD	Powder X-ray diffraction technique
q	Quartet
RT	Room temperature
s	Singlet (NMR), strong (FT-IR)
SBU	Secondary building unit
SXRD	Single-crystal X-ray diffraction technique
t	Triplet
w	Weak
δ	Chemical shift
TGA	Thermogravimetric analysis

List of Figures

Chapter 1

Figure 1.1: Classification of porous materials.

Figure 1.2: The number of publications containing keywords “coordination polymers” or “metal organic frameworks” in graph with respect to five years period from 1990, survey by SciFinder.

Figure 1.3: Applications of porous coordination polymers.

Figure 1.4: Probable metal-binding modes of carboxylate spacers.

Figure 1.5: Functional centers in imidazolium salt.

Figure 1.6: Number of publications related to imidazolium carboxylate based coordination polymers.

Figure 1.7: The known imidazolium carboxylic acid spacers.

Figure 1.8: View into the helical tube of $[(\text{ZnBr}(\text{H}_2\text{O})_4(\text{L}^1))(\text{H}_2\text{O})]_\infty$ with the one-dimensional water chain in the center.

Figure 1.9: Molecular structure of $[\text{Cu}_4(\text{Cl})(\text{L}^5)_4]_\infty$.

Figure 1.10: Molecular structure of IRMOF-77.

Figure 1.11: A view of the lamellar network $\{[\text{Cu}_2(\text{L}^{12})_2(\text{MeOH})_2].4\text{NO}_3.\text{H}_2\text{O}\}_\infty$.

Figure 1.12: Six metallomacrocycles connected to the core $\{\text{Zn}_8\text{O}\}$ cluster.

Figure 1.13: Packing diagram of $\{[\text{Zn}(\text{L}^{13})(\text{Cl})_2].8\text{H}_2\text{O}\}_\infty$, showing the 1D opening channels as view along the c axis.

Figure 1.14: Molecular packing in $\{[\text{Ca}_2(\text{L}^1)_3(\text{Br})].5\text{H}_2\text{O}\}_\infty$ along the a axis.

Figure 1.15: 3D framework of $[\text{Pb}(\text{Cl})(\text{L}^1)]_\infty$.

Figure 1.16: 1D chains of $[\text{PrL}^1(\text{H}_2\text{O})_4\text{Cl}].\text{Br}.\text{H}_2\text{O}$ along the a axis.

Figure 1.17: 3D network of $[\text{Ce}(\text{L}^5\text{-Cl})(\text{L}^5\text{-Cl-H})\text{CuCl}]_\infty$.

Chapter 2

Figure 2.1: Schematic illustrations of $\text{L}^1\text{H}_2\text{X}$ ($\text{X} = \text{Br}$ or Cl), L^1H , $\text{L}^2\text{H}_2\text{X}$, $\text{L}^3\text{H}_2\text{Cl}$ and LH_2Br organic spacers.

Figure 2.2: FT-IR (neat) spectrum of LH_2Br .

Figure 2.3: ^1H NMR spectrum of LH_2Br in DMSO-d_6 at RT.

Figure 2.4: ^{13}C NMR spectrum of LH_2Br in DMSO-d_6 at RT.

Figure 2.5: FT-IR (neat) spectrum of LH_2Br vs **1-6**.

Figure 2.6: PXRD profiles for compounds **1-6**.

Figure 2.7: The solid-state UV-vis absorption spectra of LH_2Br and **1-6**.

Figure 2.8: (a) Coordination environment of the Mn(II) center in **1**. The hydrogen atoms have been omitted for clarity. (b) Polyhedron view of the Mn(II) center. (c) View of the 1D chain in **1**.

Figure 2.9: (a) The mononuclear zwitterion nickel imidazolium carboxylate. The hydrogen atoms have been omitted for clarity. (b) Polyhedron view of the Ni(II) center in **3**. (c) View of the 3D supramolecular network through inter and intra molecular $\text{O-H}\cdots\text{O}_{\text{COO}}$ hydrogen bonds. (d) View of hydrogen bonding network through c -axis.

Figure 2.10: (a) Coordination environment of Cu(II) ion in **4**. The hydrogen atoms have been omitted for clarity. (b) Polyhedron view of the Cu(II) center in **4**. (c) View of the 1D chain in **4**. (d) The close packing of independent chains in **4** (view along b axis).

Figure 2.11: (a) Coordination environment of the Cd(II) centers in **6**. (b) Polyhedron view of the Cd(II) centers. (c) Representation of two-dimensional framework in **6**. (d) The bridging mode of the Cd(II) centers in the two dimensional framework.

Figure 2.12: Schematic illustrations of the metal-binding motifs of the carboxylate linker (**LH₂Br**) (a) Orientation of $-\text{CH}_2-\text{COO}^-$ and $-\text{C}_6\text{H}_4-\text{COO}^-$ functional groups in **1–6**; (b) $\mu^1-\eta^0:\eta^1$ in **1**, **2** and **5**; (c) $\mu^1-\eta^0:\eta^1$ and $\mu^0-\eta^0:\eta^0$ in **3**; (d) $\mu^1-\eta^1:\eta^1$ and $\mu^1-\eta^0:\eta^1$ in **4**; (e) $\mu^1-\eta^1:\eta^1$ and $\mu^2-\eta^1:\eta^1$ in **6**.

Figure 2.13: TGA curves for compounds **1–5**.

Chapter 3

Figure 3.1: Known bis-azolium carboxylate spacers that are employed for the MOF synthesis.

Figure 3.2: ^1H NMR spectrum of **3** in D_2O at RT.

Figure 3.3: ^{13}C NMR spectrum of **3** in D_2O at RT.

Figure 3.4: FT-IR (neat) spectrum of **2–6**.

Figure 3.5: (a) The UV-vis absorption spectra of **2–6** in water at RT (1.6×10^{-6} M). (b) The solid-state UV-vis absorption spectra of **2–6**.

Figure 3.6: (a) The fluorescent spectra of **2–6** in water at RT with excitation wavelength of 370 nm (1.6×10^{-6} M). (d) The solid-state fluorescent spectra of **2–6**.

Figure 3.7: Structure of the asymmetric unit of **2**. Hydrogen atoms have been omitted for clarity.

Figure 3.8: Packing diagram of molecule **2**.

Figure 3.9: Structure of the Cu dimer **4**. Hydrogen atoms, NO_3^- and DMF have been omitted for clarity.

Figure 3.10: Structure of the asymmetric unit of **5**. Hydrogen atoms have been omitted for clarity.

Figure 3.11: Top: A view of the 2D layer of **5** where polyhedra represent CuO_6 ; Bottom: A close view of the hydrogen bonding between the neighboring 2D layer in **5** viewed along the *a*-axis showing the 3D framework by hydrogen bonding between Br and C–H groups.

Figure 3.12: Structure of the asymmetric unit of **6**. Hydrogen atoms have been omitted for clarity.

Figure 3.13: Top: A view of the 2D layer of **6** where polyhedral represent ZnO_6 ; Bottom: A close view of the hydrogen bonding between the neighboring 2D layer in **6** viewed along the *a*-axis showing the 3D framework by hydrogen bonding between Br and C–H groups.

Figure 3.14: TGA curves for compounds **2-6**.

Chapter 4

Figure 4.1: The structure of 1,3-bis(carboxymethyl)imidazolium (**BCI**) and 1,3-bis(carboxymethyl)benzimidazolium (**BCBI**) salts.

Figure 4.2: Molecular structure of bis-imidazolium carboxylic acids ($\text{L}^1\text{H}_2\text{Br}_2$, $\text{L}^2\text{H}_2\text{Br}_2$, $\text{L}^3\text{H}_2\text{Br}_2$ and $\text{L}^4\text{H}_2\text{Br}_2$) and tris-imidazolium carboxylic acids ($\text{L}^5\text{H}_2\text{Br}_2$ and $\text{L}^6\text{H}_2\text{Br}_2$).

Figure 4.3: Molecule **4** shows color variation in different lights (Visible, short UV and long UV); a = sample in water, b = powder form, c = pellet form.

Figure 4.4: The solid-state UV-vis absorption spectra of **1-6** and corresponding organic spacers.

Figure 4.5: The solid-state fluorescent spectra of **1-6** and corresponding organic spacers.

Figure 4.6: (a) Coordination environment of the Ca(II) centers in **1**. The hydrogen atoms have been omitted for clarity. (b) View of the edge shared polyhedrons in **1**. (c) View of the 1D coordination polymer. (d) 3D supramolecular network through hydrogen bond $\text{O}-\text{H}\cdots\text{Br}$ and $\text{C}-\text{H}\cdots\text{Br}$.

Figure 4.7: (a) Molecular structure of the Ca(II) centers in **2**. The hydrogen atoms have been omitted for clarity. (b) Core unit of molecule **2**. (c) Polyhedron view of Ca(II) centers.

Figure 4.8: (a) Coordination environment of the Ca(II) centers in **3**. The hydrogen atoms have been omitted for clarity. (b) Core unit of molecule **3**. (c) View of zig-zag arrangement of Ca(II) centers. (d) View of molecule **3** in the direction of the *c* axis. (e) Space filling model of **3** (views along *c* axis).

Figure 4.9: (a) Coordination environment of the Ca(II) center in **4**. The hydrogen atoms have been omitted for clarity. (b) The polyhedron arrangement in two-dimensional layer of **4**. (c) Three-dimensional network through Br[⋯]H hydrogen bonding. (d) Space filling model of 3D network of **4**.

Figure 4.10: (a) One-dimensional coordination polymer of **5**. The hydrogen atoms have been omitted for clarity. (b) Repeating unit of molecule **5**. (c) Polyhedron view of the Ca(II) centers in molecule **5**.

Figure 4.11: (a) Coordination environment of the Ca(II) centers in **6**. The hydrogen atoms and bromine ions have been omitted for clarity. (b) Core unit of molecule **6**. (c) Polyhedron view of the Ca(II) centers.

Figure 4.12: Polyhedra of Ca coordination compounds **1-6** and reported Ca molecules based on imidazolium carboxylates; a = $\{[\text{Ca}_2(\text{BCI})_3(\text{Br})](\text{H}_2\text{O})_5\}_\infty$ and b = $[\text{Ca}(\text{BCBI})_2(\text{H}_2\text{O})_4] \cdot 2\text{H}_2\text{O}$.

Figure 4.13: The TGA curves of compounds **1-6**.

Chapter 5

Figure 5.1: Zwitterionic bis- and tris- imidazolium carboxylates.

Figure 5.2: ¹H NMR spectrum of **L**¹ in D₂O at RT.

Figure 5.3: ¹³C NMR spectrum of **L**¹ in D₂O at RT.

Figure 5.4: FT-IR (neat) spectrum of **L**¹ and **1-6**.

Figure 5.5: The solid-state UV-vis absorption spectra of **L**¹ and **1-6**.

Figure 5.6: (a) The solid state structure of **1**. The hydrogen atoms have been omitted for clarity. (b) Core unit of **1**. (c) Polyhedron view of La(III) centers in **1**.

Figure 5.7: (a) The solid state structure of **3**. The hydrogen atoms have been omitted for clarity. (b) Core unit of **3**. (c) Polyhedron view of Sm(III) centers in **3**.

Figure 5.8: (a) The solid state structure of **5**. The hydrogen atoms have been omitted for clarity. (b) Core unit of **5**. (c) Polyhedron view of Dy(III) center in **5**.

Figure 5.9: ^1H NMR spectrum of L^2 in D_2O at RT.

Figure 5.10: ^{13}C NMR spectrum of L^2 in D_2O at RT.

Figure 5.11: FT-IR (neat) spectrum of L^2 and **7–10**.

Figure 5.12: The solid-state UV-vis absorption spectra of L^2 and **7–10**.

Figure 5.13: (a) The 1D nano tubular coordination polymer of **9**. The hydrogen atoms have been omitted for clarity. (b) Core unit of molecule **9**. (c) Polyhedron view of Dy(III) center in **9**. (d) Space filling model of **9**.

Figure 5.14: FT-IR (neat) spectrum of L^2 and **11–14**.

Figure 5.15: The solid-state UV-vis absorption spectra of L^2 and **11–14**.

Figure 5.16: FT-IR spectra of L^1 , L^2 and Dy molecules (**5**, **9** and **13**).

Figure 5.17: (a) Coordination environment of the Dy(III) center in **13**. The hydrogen atoms have been omitted for clarity. (b) Polyhedron view of Dy(III) center in **13**. (c) View through phenyl ring of molecule **13**.

Figure 5.18: Molecular packing of **13**.

Chapter 6

Figure 6.1: Functional centers in imidazolium salt.

Figure 6.2: (a) Molecular structure of $[(\text{L}^1)_2\text{Mn}(\text{H}_2\text{O})_2]_\infty$. (b) Molecular structure of $[(\text{L}^1)_2\text{Cu}]_\infty$.

Figure 6.3: Representation of two-dimensional framework in $[(\text{L}^1)_3\text{Cd}_2(\text{Br})_2]_\infty$.

Figure 6.4: Top: A view of the 2D layer of $[(\text{L}^2)_2\text{Cu}(\text{H}_2\text{O})_2]_2(\text{Br})_2]_\infty$ where polyhedra represent CuO_6 ; Bottom: A close view of the hydrogen bonding between

the neighboring 2D layer in $[(L^2)_2Cu(H_2O)_2]_2(Br)_2\}_\infty$ viewed along the a axis showing the 3D framework by hydrogen bonding between Br and C–H groups.

Figure 6.5: The structure of 1,3-bis(carboxymethyl)imidazolium (BCI) and 1,3-bis(carboxymethyl)benzimidazolium (BCBI) salts.

Figure 6.6: Molecular structure of bis-imidazolium carboxylic acids ($L^3H_2Br_2$, $L^4H_2Br_2$, $L^5H_2Br_2$ and $L^2H_2Br_2$) and tris-imidazolium carboxylic acids ($L^6H_2Br_2$ and $L^7H_2Br_2$).

Figure 6.7: (a) 3D supramolecular network through hydrogen bond of $\{[(L^3)_2Ca_2(H_2O)_4](Br)_4.6H_2O\}_\infty$. (b) Molecular structure of $\{[(L^4)_2Ca_2(H_2O)_9](Br)_4.4H_2O\}$. (c) Three-dimensional network through Br \cdots H hydrogen bonding of $\{[(L_2)_2Ca(H_2O)_2]_2(Br)_2\}_\infty$. (d) Molecular structure of $\{[(L^7)_2Ca_2(H_2O)_9](Br)_6\}$. (e) One-dimensional coordination polymer of $\{[(L^6)_2Ca_3(Na)(H_2O)_9(Cl)](Br)_6.2H_2O\}_\infty$.

Figure 6.8: Space filling model of 3D MOF $\{[(L^5)_2Ca_2(H_2O)_2]_2(Br)_2\}_\infty$.

Figure 6.9: 1D nano tubular coordination polymer of $\{[(L^6)(Dy)(NO_3)(H_2O)](H_2O)_3(NO_3)_2\}_\infty$.

Figure 6.10: Molecular packing of $\{[(L^6)_2(Dy)](NO_3)_3\}$.

List of Schemes

Chapter 2

Scheme 2.1: Synthesis of $\mathbf{LH_2Br}$.

Chapter 3

Scheme 3.1: Synthesis of $\mathbf{L(C_2H_5)_2Br_2}$ (**2**) and $\mathbf{LH_2Br_2}$ (**3**).

Scheme 3.2: Synthesis of $\{[(\mathbf{L})\text{Cu}(\text{DMF})]_2(\text{NO}_3)_4(\text{H}_2\text{O})(\text{DMF})_2\}$ (**4**), $\{[(\mathbf{L})_2\text{Cu}(\text{H}_2\text{O})_2]_2(\text{Br})_2\}_\infty$ (**5**) and $\{[(\mathbf{L})_2\text{Zn}(\text{H}_2\text{O})_2]_2(\text{Br})_2\}_\infty$ (**6**)

Chapter 4

Scheme 4.1: Synthesis of $\mathbf{L^1H_2Br_2}$.

Scheme 4.2: Synthesis of $\mathbf{L^5H_3Br_3}$.

Chapter 5

Scheme 5.1: Synthesis of $\mathbf{L^1}$.

Scheme 5.2: Synthesis of $\mathbf{L^2}$.

Chapter 6

Scheme 6.1: Synthesis of $\mathbf{L^1H_2Br}$.

Scheme 6.2: Synthesis of $\mathbf{L^2H_2Br_2}$.

Scheme 6.3: Synthesis of $\{[(\mathbf{L}^2)\text{Cu}(\text{DMF})]_2(\text{NO}_3)_4(\text{H}_2\text{O})(\text{DMF})_2\}$, $[(\mathbf{L}^2)_2\text{Cu}(\text{H}_2\text{O})_2]_2(\text{Br})_2\}_\infty$ and $\{[(\mathbf{L}^2)_2\text{Zn}(\text{H}_2\text{O})_2]_2(\text{Br})_2\}_\infty$.

Scheme 6.4: Synthesis of $\mathbf{L^6H_3Br_3}$.

Scheme 6.5: Synthesis of $\mathbf{L^3}$ and $\mathbf{L^6}$.

List of Tables

Chapter 2

Table 2.1: Summary of crystallographic data and structure refinement results for **1-3**

Table 2.2: Summary of crystallographic data and structure refinement results for **4-6**

Chapter 3

Table 3.1: Summary of crystallographic data and structure refinement results for **2** and **4**

Table 3.2: Summary of crystallographic data and structure refinement results for **5** and **6**

Table 3.3: Selected bond lengths and angles of **5** and **6**

Chapter 4

Table 4.1: Selected FT-IR spectra and NMR peak values for bis- and tris-imidazolium carboxylate spacers and corresponding calcium molecules (**1-6**)

Table 4.2: Summary of crystallographic data and structure refinement results for **1-3**

Table 4.3: Summary of crystallographic data and structure refinement results for **4-6**

Chapter 5

Table 5.1: Selected bond lengths and bond angles of **1-3**

Table 5.2: Selected bond lengths and bond angles of **4-6**

Table 5.3: Selected bond lengths and bond angles of **7-10**

Table 5.4: Selected bond lengths and bond angles of **11-14**

Table 5.5: Summary of crystallographic data and structure refinement results for **1-3**

Table 5.6: Summary of crystallographic data and structure refinement results for **4-6**

Table 5.7: Summary of crystallographic data and structure refinement results for **7-9**

Table 5.8: Summary of crystallographic data and structure refinement results for **10-12**

Table 5.9: Summary of crystallographic data and structure refinement results for **13 and 14**

Chapter 1

Introduction

1.1 Coordination polymers

Porous solids are of scientific and technological interest because of their ability to interact with atoms, ions and molecules not only at their surfaces, but throughout the bulk of the material. Not surprisingly, traditional applications of porous materials thus involve ion exchange, adsorption (for separation) and catalysis, and many of these benefit from the high order [1]. The pores of solids are classified according to size: pore sizes in the range of 2 nm and below are called micropores, those in the range of 2 nm to 50 nm are denoted mesopores, and those above 50 nm are macropores. The distribution of sizes, shapes and volumes of the void spaces in porous materials directly relates to their ability to perform the desired function in a particular application. The need to create uniformity within the pore size, shape and volume has steadily increased over recent years because it can lead to superior applications properties. Classically porous materials are inorganic materials, carbon-based materials and inorganic-organic polymers (Figure 1.1). A large number of inorganic porous materials have been developed e.g. Zeolites.

Zeolites are traditional inorganic microporous crystalline materials, which are built from an infinitely extending three dimensional network of $[\text{SiO}_4]^{4-}$ and $[\text{AlO}_4]^{5-}$ tetrahedral units linked to each other by the sharing oxygen atoms [2,3]. The general formula for a zeolite is $M_{x/n}[(\text{AlO}_2)_x(\text{SiO}_2)_y].m\text{H}_2\text{O}$, where M is an alkali or alkaline earth cation, n is the valence of the cation, m is the number of water molecules per unit cell, x and y are the total number of tetrahedral per unit cell [4]. The first zeolite, stilbite, was discovered by Cronstedt in 1756, who found that the mineral lost water rapidly on heating and seemed to boil. The name “zeolite” comes from the Greek words “Zeo” (boil) and “Lithos” (stone), literally meaning “the rock that boils”. The crystallization water of zeolite is in the form of water molecules existing in the framework structure of zeolite. So, this is particularly called "zeolitic water." Even when dehydrated by heating or the like, the structure of zeolite is not destroyed. The space areas, where crystallization

water used to be, remain as they are in the form of a cavity. This looks like the structure of a piece of sponge. Zeolite, according to its characteristics, strongly absorbs gas and moisture into those cavities. Zeolites naturally form when fresh groundwater or sea water reacts with volcanic ash and take anywhere from 50 to 50,000 years to complete their formation. Natural zeolites were first used by the Romans to filter their drinking water. Synthetic zeolites were first observed in 1862 [5]. Synthetic zeolites can produce much faster and in phase-pure state and in more uniform fashion. More than 150 zeolite types have been synthesized and 40 naturally occurring zeolites are known [6]. Zeolites are traditionally used in water filtration, refrigeration, construction, and aquariums. Zeolites came to prominence industrially, when Mobil patented the synthetic ZSM-5 catalyst in 1977 for the conversion of methanol to petroleum [7].

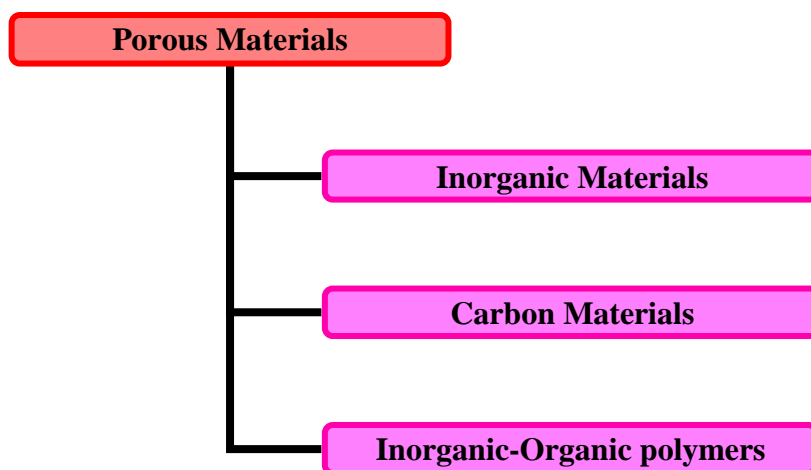


Figure 1.1: Classification of porous materials.

Aluminophosphates ($\text{AlPO}_4\text{-n}$, n represents a particular structure type) are constructed by alternation of corner sharing AlO_4 and PO_4 tetrahedrons units, and which build up a 3D neutral framework with channels and/or pores of molecular dimensions. The new family of microporous crystalline aluminophosphates was reported in 1982 [8]. The general formula is represented as $[\text{Al}^{\text{III}}\text{P}^{\text{V}}\text{O}_4]_y\text{R}\cdot\text{nH}_2\text{O}$, where R denotes organic template and many AIPOs have crystal structures, which are not perceived in zeolites. Further AIPOs developed through substitution *via* incipient wetness impregnation, ion exchange or isomorphous substitution. Thus examples are silicoaluminophosphates, metalloaluminophosphate, metalaluminophosphates and metallophosphates [9-11]. Pyrolysis of carbon-rich materials leads to the formation of perhaps the most well-known carbon porous compound known as activated carbon [12]. Due to their high

surface areas and porous nature, activated carbons have been used as adsorbents throughout time by a wide array of industries ranging from medical to military [13]. While activated carbon has the benefit of possessing high surface areas and adsorption capacities, their graphene structures suffer from a lack of order. This inconsistency prevents activated carbons from being used as materials for application in catalysis. In fact, the distribution of the pores in activated carbons may range as widely as 20 Å to several thousand Å [14]. However, despite their lack of order, activated carbons have been a useful material for applications in gas adsorption and separation, solvent removal and recovery, and water purification for many years.

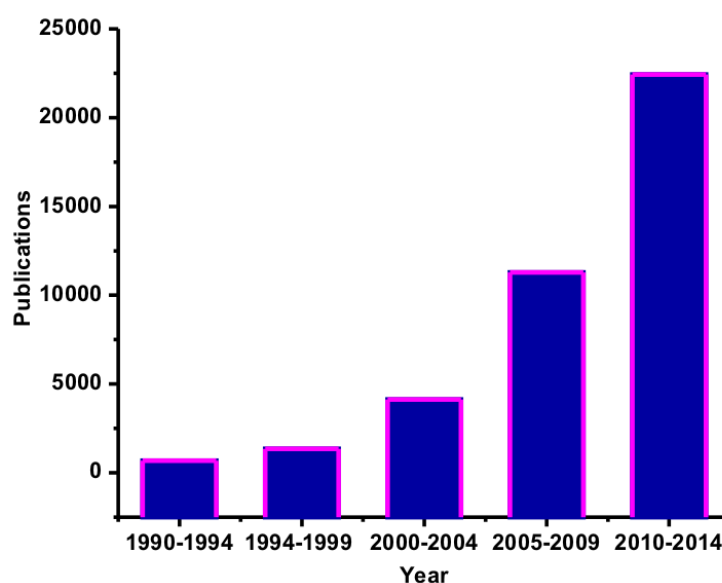


Figure 1.2: The number of publications containing keywords “coordination polymers” or “metal organic frameworks” in graph with respect to five years period from 1990, survey by SciFinder.

Porous coordination polymers (PCPs) are an emerging class of hybrid porous materials fashioned by a self-assembled network in between the inorganic units and multidentate organic spacers. Now a day, porous coordination polymers have been an alternative to the former two classes of porous materials, based on its structure regularity, high porosity, high surface area and highly designable frameworks. The progress on “coordination polymer” from 1990 to 2014 is shown in Fig. 1.2. The phrase, “coordination polymers” appeared in the beginning of 1960s, and the area was first reviewed in 1964 [15]. Prior to the late 1980s, a variety of polymeric metal-organic coordination compounds were exposed, such as the Holfmann type complexes and

Prussian blue compounds. Those examples are motivated by scientists towards aiming to discovery a new class of materials. Since the early 1990s, research on the structures of porous coordination polymers has increased greatly, and examples with functional micropores soon started to appear. Robson *et al.* reported a porous coordination polymer capable of an anion exchange in 1990 [16]. The first catalytic properties of the 2D $[\text{Cd}^{\text{II}}(4,4'\text{-bpy})_2(\text{NO}_3)_2]$ coordination polymer were studied with the reaction of benzaldehyde and cynotrimethylsilane by Fujita *et al.* in 1994 [17]. The adsorption of guest molecules was studied separately by Yaghi [18] and Moore [19] in 1995. The metal-organic framework (MOF) word was promoted by Yaghi *et al.* in 1995 [20]. In 1997, Kitagawa *et al.* reported the gas adsorption phenomena at ambient temperature [21]. The motivated report is delivered by Yaghi *et al.* in 1999, which is the isolation of MOF-5 [22] and also the concept of isorecticular MOFs, which is reported in 2002 [23].

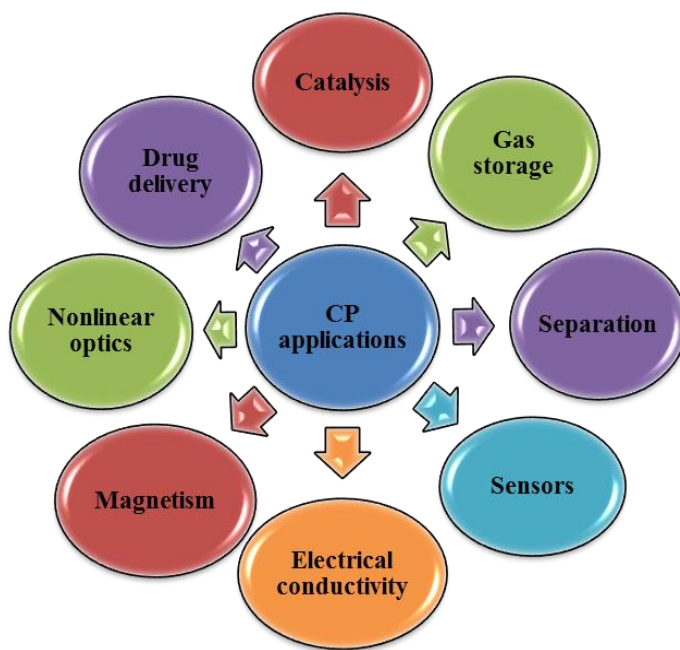


Figure 1.3: Applications of porous coordination polymers [34-40].

PCPs can be made *via* different methods such as solvothermal, hydrothermal, direct mixing, sonochemical, vapour diffusion, microwave heating and etc. The solvothermal method is normally used and involves heating a mixture of organic spacers and metal precursor in the solvent medium. The solvents include, for example, dimethylformamide (DMF), diethylformamide (DEF), dimethyl sulfoxide (DMSO), water, ethanol, methanol, dioxane and mixtures thereof. Among these solvents, DMF

dissolve the reactants but also deprotonate the carboxylic acids. In addition, variables in the reaction conditions including reagent concentration, time, temperature, p^H and fractional volume filling of the vessel are important parameters as well [24].

PCPs/MOFs are commercially produced by BASF and Sigma-Aldrich. Preferably, PCPs/MOFs are constructed by using two components, namely metal/metal nodes/SBU and organic spacers [25]. The porous coordination polymer of pore size/shape and overall porous activity can be tuned by the logically designing of suitable organic spacers [26]. In general, the organic spacers may be N-functionalised (pyridyl, imidazole and triazoles) [27,28], O-functionalised (carboxylates) [29], S-functionalised (sulfonate) [30], P-functionalised (phosphates) [31] and mixed thereof [32]. Among those, the bidentate or multidentate organic spacers are extensively utilized [33]. PCPs/MOFs are used extensively in different application such as gas adsorption, storage and separation, catalysis, drug delivery, sensors and etc. (Fig. 1.3) [34-40].

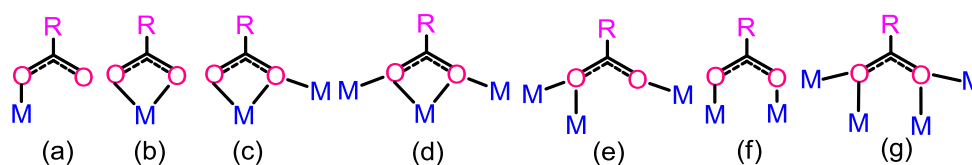


Figure 1.4: Probable metal-binding modes of carboxylate spacers [41]: (a) $\mu_1-\eta^0:\eta^1$; (b) $\mu_1-\eta^1:\eta^1$; (c) $\mu_2-\eta^1:\eta^2$; (d) $\mu_3-\eta^2:\eta^2$; (e) $\mu_3-\eta^1:\eta^2$; (f) $\mu_2-\eta^1:\eta^1$; (g) $\mu_4-\eta^2:\eta^2$.

The multidentate carboxylate organic spacers are excellent ligands for the synthesis of coordination polymers affording structures with a diverse range of topologies and conformation with the carboxylate group able to a metal center as a mono-, bi-, or multidentate ligand. The possible metal-binding motifs of carboxylate linkers are shown in Fig 1.4 [41]. The suitable organic spacers, metal precursors and synthetic methodologies are essential criteria to design the FCPs with different physical properties. In addition, the non-covalent interactions such as hydrogen bonding, $\pi \cdots \pi$, $M \cdots \pi$, $C-H \cdots \pi$ and $anion \cdots \pi$ interactions play a key role in FCPs to increase the dimensionality, supramolecular topology and porosity. Therefore, the choice of organic spacer is extremely important to fine-tune the structural and desired functional properties of FCPs through coordination or non-covalent interaction modes. Within these organic spacers, the imidazolium carboxylic acids are of special interest as they have $[C-H]^\delta+$ functional group (potential functional group for anion reorganization and

post modification to generate N-heterocyclic carbene tethered catalytically active metal centers) along with excellent functional group tolerance at N-positions.

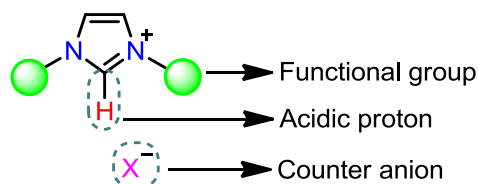


Figure 1.5: Functional centers in imidazolium salt.

Imidazolium salts are having different structural versatilities like water solubility, chirality, functionalization, chelation, chirality, immobilization, ionic liquids, water solubility and catalysis [42]. Moreover other interesting structural features are having that acidic proton and counter anions (Fig. 1.5). The acidic proton is NCHN. Preferably, this proton forms the efficient hydrogen bonding network with counter anions, solvent molecules and other guest molecules. Notably, the counter ions play a key role in the anion exchange with F^- , PF_6^- , BF_4^- , $H_2PO_4^-$, HPO_4^{2-} and HSO_4^- not only those common anions, and also some biologically important anions like DNA, RNA, ADP, ATP, GTP and etc [43].

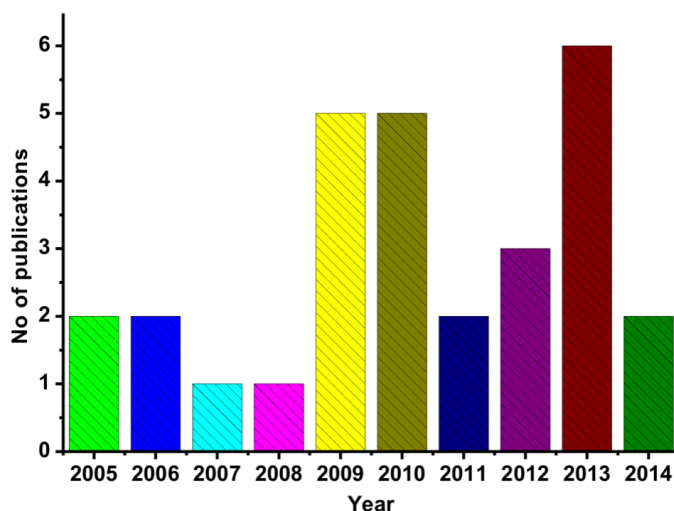


Figure 1.6: Number of publications related to imidazolium carboxylate based coordination polymers.

Imidazolium salts can be synthesized easily and the starting materials are readily available [44]. Besides the NNC-H group in imidazolium salts can be a potential

functional group for pre/post modified M-NHC synthesis. Since the discovery of stable N-heterocyclic carbenes (NHCs), these complexes have found widespread use in catalysis, in which they serve both as nucleophilic catalysts and as ligands in metal-mediated reactions [45]. Thus the imidazolium carboxylate coordination polymer chemistry is considerably different from the conventional neutral carboxylate coordination polymers. The publications of imidazolium carboxylate based coordination polymers with respect to the year are shown in Fig. 1.6.

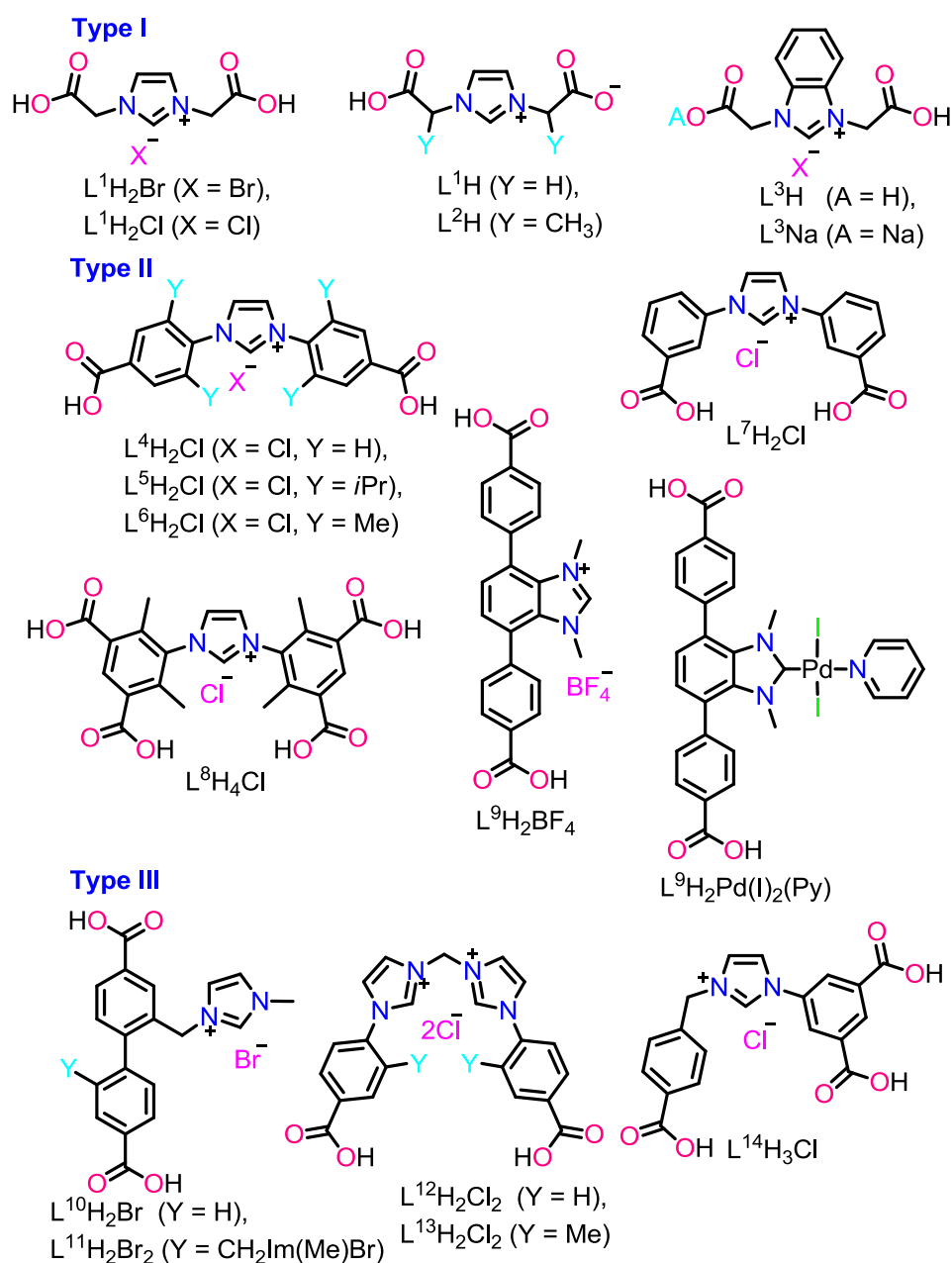


Figure 1.7: The known imidazolium carboxylic acid spacers.

The known imidazolium carboxylates can be classified as three types (Fig 1.7).

Type I, Imidazolium with flexible carboxylate arms;

Type II, Imidazolium with rigid carboxylate arms;

Type III, Imidazolium with flexible CH₂ and rigid carboxylate arms.

1.2 Imidazolium carboxylate based transition metal coordination polymers

The first imidazolium carboxylate coordination polymer was reported by Dyson *et al.* in 2005 using ionic imidazolium carboxylate linker [46]. The bio-inspired supramolecular network of water was trapped by zinc zwitterionic tubular coordination polymer $[(\text{ZnBr}(\text{H}_2\text{O})_4(\text{L}^1))(\text{H}_2\text{O})]_\infty$ derived from *N,N'*-diacetic acid imidazolium bromide with zinc. The supramolecular network of water chain found in $[(\text{ZnBr}(\text{H}_2\text{O})_4(\text{L}^1))(\text{H}_2\text{O})]_\infty$ is comparable to the water chain present in aquaporin channels (Fig. 1.8).

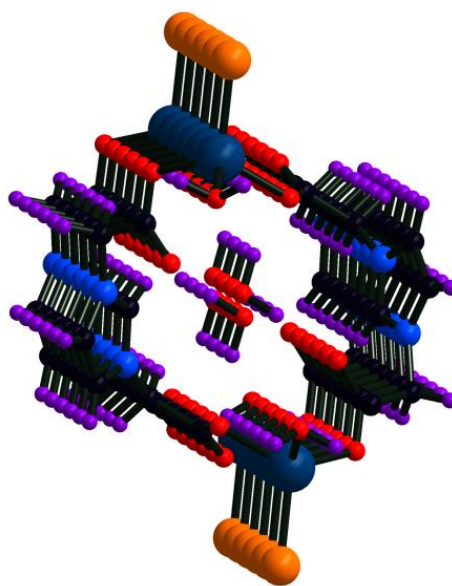


Figure 1.8: View into the helical tube of $[(\text{ZnBr}(\text{H}_2\text{O})_4(\text{L}^1))(\text{H}_2\text{O})]_\infty$ with the one-dimensional water chain in the center.

Later, the zinc $\{\text{ZnCl}(\text{H}_2\text{O})_4(\text{L}^1)\}(\text{H}_2\text{O})_\infty$ and cobalt $\{[\text{Co}(\text{H}_2\text{O})_4(\text{L}^1)]\text{Br}(\text{H}_2\text{O})\}_\infty$ coordination polymers were isolated from *N,N'*-diacetic acid imidazolium chloride with corresponding elemental zinc and cobalt in water [47]. The structure of $\{\text{ZnCl}(\text{H}_2\text{O})_4(\text{L}^1)\}(\text{H}_2\text{O})_\infty$ was similar to the reported molecule $\{\text{ZnBr}(\text{H}_2\text{O})_4(\text{L}^1)\}(\text{H}_2\text{O})_\infty$. In $\{[\text{Co}(\text{H}_2\text{O})_4(\text{L}^1)]\text{Br}(\text{H}_2\text{O})\}$, Co(II) coordination geometry

is octahedral with cis-carboxylate bonds and four coordinated water molecules. The $\{[\text{Co}(\text{H}_2\text{O})_4(\text{L}^1)]\text{Br}(\text{H}_2\text{O})\}$ was built as self-possessed of interlocking cobalt imidazolium carboxylate polymeric chains, separated by discrete layer of bromide anions.

In 2009, Son *et al.* isolated the first example of the organometallic NHC-metal complex. The most interesting 2D undulating Cu grid $[\text{Cu}_4(\text{Cl})(\text{L}^5)]_\infty$ consisting of NHC-Cu was isolated using $\text{L}^5\text{H}_2\text{Cl}$ and $\text{Cu}(\text{NO}_3)_2$ in DMF at 110 °C [48]. In $[\text{Cu}_4(\text{Cl})(\text{L}^5)]_\infty$, two different types of copper centers are observed, which are copper(II) paddlewheel with distorted octahedron geometry and copper(I) with linear geometry (Fig. 1.9). Besides, 1D cadmium coordination polymer $\{[\text{Cd}(\text{L}^5)_4(\text{Cl})_2](\text{DMF})_2\}_\infty$ was isolated from the reaction between $\text{L}^5\text{H}_2\text{Cl}$ and $\text{Cd}(\text{NO}_3)_2$ in DMF at 110 °C. In $\{[\text{Cd}(\text{L}^5)_4(\text{Cl})_2](\text{DMF})_2\}_\infty$, two carboxylates were coordinated to a single cadmium ion and two chlorine atoms were bridged between two cadmium metals.

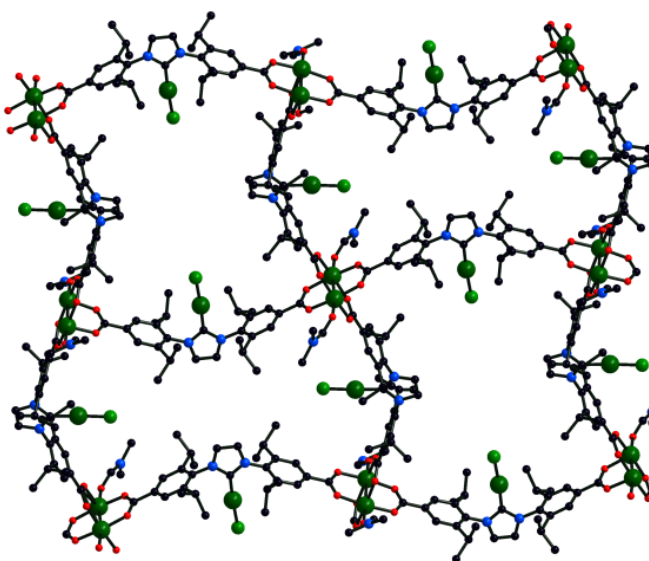


Figure 1.9: Molecular structure of $[\text{Cu}_4(\text{Cl})(\text{L}^5)]_\infty$.

The microporous coordination polymer $\{[\text{Cu}_2(\text{L}^8)(\text{DMSO})_2]\cdot 2\text{H}_2\text{O}\}_\infty$ was successfully isolated from the reaction of $\text{Cu}(\text{NO}_3)_2\cdot 2.5\text{H}_2\text{O}$ and novel imidazolium tetracarboxylic acid ($\text{L}^8\text{H}_4\text{Cl}$) in DMSO under solvothermal method [49]. $\{[\text{Cu}_2(\text{L}^8)(\text{DMSO})_2]\cdot 2\text{H}_2\text{O}\}_\infty$ was formed as 2D coordination polymer with Cu paddle-wheel secondary building unit. The sample was thermally activated as three ways *i.e.* (100 °C, 24 h), (200 °C, 24 h) and (200 °C, 4 h). Among the activated samples, heating under vacuum at 200 °C for 4 h produced the optimally activated sample, which was demonstrating an upright

adsorption selectively for CO₂ over methane, probably because of interactions with open metal sites and the unusual ionic environment within the MOF generated from the positively charged aromatic imidazolium components.

The 2D coordination polymer {[Cd₂(L²)₂(SO₄)(4,4'-bpy)₂(H₂O)₂].5H₂O}_∞ was isolated using mixed organic spacers strategy from L³Na, 4,4'-bpy and CdSO₄.H₂O in the mixture of solvents H₂O, MeOH and DMF in 2009 [50]. In {[Cd₂(L²)₂(SO₄)(4,4'-bpy)₂(H₂O)₂].5H₂O}_∞, the mixed carboxylate (L²) and SO₄⁻² linked [Cd₂(μ₂-η²-L²-η²)₂(SO₄)]_∞ chains were bridged by 4,4'-bpy ligands.

1D necklace-type coordination polymer {[Zn₂(μ₂-HCOO)(L⁷)₂](NO₃).1.5DMF}_∞ was isolated by Sumby *et al.* from the reaction between 3-bis(4-carboxyphenyl)imidazolium bromide (L⁷H₂Br) and Zn(NO₃)₂.6H₂O in dimethylformamide in 2010 [51]. The porous structure was designed from the close packing of 1D polymer, which was filled with disordered DMF solvate molecules. The zinc secondary building units in the 1D polymer were also connected through the formate anion, which is an undulating structure from the U-shaped conformation of the imidazolium carboxylate spacer (L⁷H₂Br).

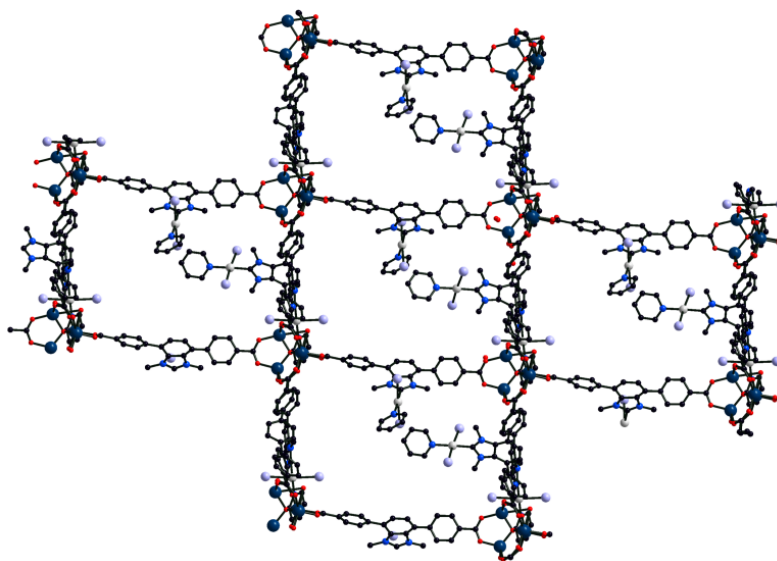


Figure 1.10: Molecular structure of IRMOF-77.

Yaghi *et al.* have reported the imidazolium-carboxylate organic spacer 4,7-bis(4-carboxyphenyl)-1,3-dimethylbenzimidazolium tetrafluoroborate (L⁹H₂BF₄) and the first of pre-modified Pd-NHC imidazolium-carboxylate linker [4,7-bis(4-carboxyphenyl)-1,3-dimethylbenzimidazol-2-ylidene](pyridyl)palladium(II) iodide (L⁹H₂PdI₂(Py)) in

2010 [52]. The IRMOF-76 $[\text{Zn}_4\text{O}(\text{L}^9)_3(\text{BF}_4)_{0.5}(\text{PF}_6)_{1.6}(\text{OH})_{0.9}]_\infty$ was isolated from the reaction of $\text{Zn}(\text{BF}_4)_2 \cdot x\text{H}_2\text{O}$, KPF_6 and $\text{L}^9\text{H}_2\text{BF}_4$ in DMF at 100 °C. In IRMOF-76, Zn_4O units were connected to six L^9 links to form a cubic framework of *pcu* topology. Subsequently, the covalently bound Pd-NHC complex IRMOF-77 $[\text{Zn}_4\text{O}(\text{L}^9(\text{Py})\text{PdI}_2)_3(\text{H}_2\text{O})_4]_\infty$ was isolated from the reaction between $\text{L}^9\text{H}_2\text{PdI}_2(\text{Py})$ with $\text{Zn}(\text{NO}_3)_2 \cdot 6\text{H}_2\text{O}$, Py in DEF at 100 °C. IRMOF-77 is another example of hetero metallic porous coordination polymer and also it is isorecticular with MOF-5 (Fig. 1.10). In IRMOF-77, ligand exchange experiments were carried out by quinolone. The Langmuir and BET surface areas of activated IRMOF-77 were by calculated to be 1610 and 1590 $\text{m}^2 \text{g}^{-1}$, respectively. The amount of N_2 uptake in the pores ($P/P_0 = 0.9$) corresponds to 46 N_2 molecules per formula unit, or 552 per unit cell.

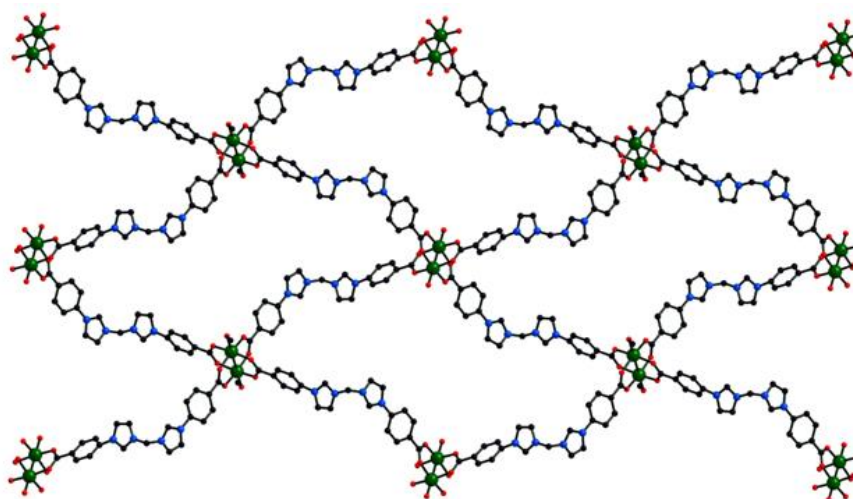


Figure 1.11: A view of the lamellar network $\{[\text{Cu}_2(\text{L}^{12})_2(\text{MeOH})_2] \cdot 4\text{NO}_3 \cdot \text{H}_2\text{O}\}_\infty$.

The first post modified NHC-MOF was reported by Wu *et al.* in 2011 [53]. The copper coordination polymers $\{[\text{Cu}_2(\text{L}^{12})_2(\text{MeOH})_2] \cdot 4\text{NO}_3 \cdot \text{H}_2\text{O}\}_\infty$ and $\{[\text{Cu}(\text{L}^{12})(\text{Cl})_2] \cdot \text{H}_2\text{O}\}_\infty$ were isolated using 4-carboxy phenyl imidazolium derivative ($\text{L}^{12}\text{H}_2\text{Cl}_2$) as an organic spacer. $\{[\text{Cu}_2(\text{L}^{12})_2(\text{MeOH})_2] \cdot 4\text{NO}_3 \cdot \text{H}_2\text{O}\}_\infty$ was built as interesting wave-like lamellar network in the *ac* plane with cross dimensions $18 \times 34 \text{ \AA}^2$ (Fig. 1.11), while $\{[\text{Cu}(\text{L}^{12})(\text{Cl})_2] \cdot \text{H}_2\text{O}\}_\infty$ was formed as 3D supramolecular network through hydrogen bonding between independent 1D zigzag chains. The coordination polymers $\{[\text{Cu}_2(\text{L}^{12})_2(\text{MeOH})_2] \cdot 4\text{NO}_3 \cdot \text{H}_2\text{O}\}_\infty$ and $\{[\text{Cu}(\text{L}^{12})(\text{Cl})_2] \cdot \text{H}_2\text{O}\}_\infty$ were post modified by using $\text{Pd}(\text{OAc})_2$ in THF. The post modified $\{[\text{Cu}_2(\text{L}^{12})_2(\text{MeOH})_2] \cdot 4\text{NO}_3 \cdot \text{H}_2\text{O}\}_\infty$ was

demonstrated the high catalytic activity towards Suzuki–Miyaura coupling reaction of various phenylhalides with phenylboronic acids under heterogeneous phases.

The four metal organic frameworks $\text{Cu}_2(\text{L}^{10})_2 \cdot 2(\text{DMF}_x/\text{EtOH}_{1-x})$ (NU-501), $\text{Cu}_2(\text{L}^{11})_2 \cdot 2(\text{DMF}_x/\text{EtOH}_{1-x})$ (NU-502), $\text{Zn}_4\text{O}(\text{L}^{10})_3$ (NU-503) and $\text{Zn}_4\text{O}(\text{L}^{11})_3$ (NU-504) were isolated from corresponding metal nitrate and corresponding imidazolium salts ($\text{L}^{10}\text{H}_2\text{Br}$ or $\text{L}^{11}\text{H}_2\text{Br}_2$) in DMF or DMF/EtOH [54]. NU-501 involved catenation between two independent 2D sheets with binuclear paddle-wheel units. NU-502 was constructed by two independent 2D sheets with similar binuclear paddle-wheel units as NU-501, and the morphology is different from NU-501. NU-503 was reported as analogous to IRMOF-9, while NU-504 was reported as analogous to IRMOF-10. It was observed that the incorporation of different numbers of azolium cores (one or two) into porous materials can impact the level of catenation or morphology.

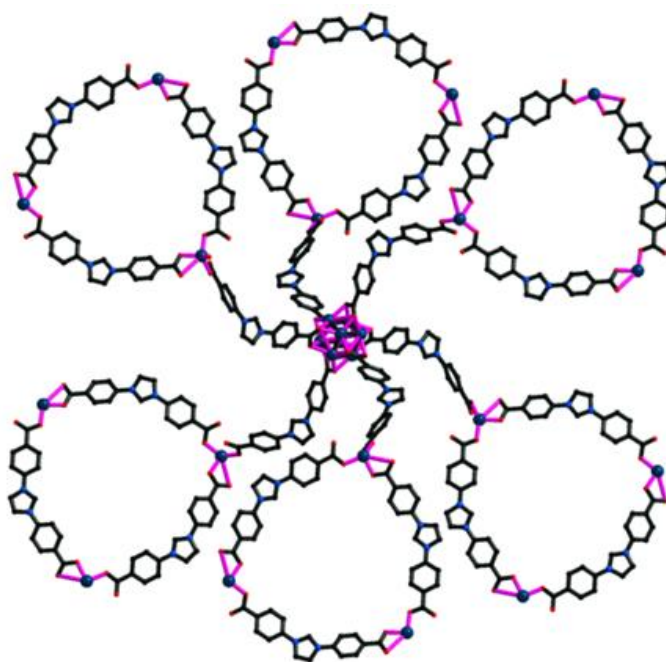


Figure 1.12: Six metallomacrocycles connected to the core $\{\text{Zn}_8\text{O}\}$ cluster.

The zinc and cadmium coordination polymers $\{[\text{Zn}(\text{L}^3)_2(\text{H}_2\text{O})_4] \cdot 5\text{H}_2\text{O}\}_\infty$, $\{[\text{Cd}(\text{L}^3)(\text{H}_2\text{O})_2](\text{NO}_3) \cdot 5\text{H}_2\text{O}\}_\infty$ and $[\text{Cd}(\text{L}^3)\text{Cl}]_\infty$ were derived from organic spacer L^3H by Wu *et al.* in 2011 [55]. $\{[\text{Cd}(\text{L}^3)(\text{H}_2\text{O})_2](\text{NO}_3) \cdot 5\text{H}_2\text{O}\}_\infty$ and $[\text{Cd}(\text{L}^3)\text{Cl}]_\infty$ were shown second-order non-linear optically (NLO) active. $\{[\text{Cd}(\text{L}^3)(\text{H}_2\text{O})_2](\text{NO}_3) \cdot 5\text{H}_2\text{O}\}_\infty$ formed as a 3D supramolecular network through the hydrogen bonding between lamellar networks with lattice water molecules. Supramolecular network of

$\{[\text{Zn}(\text{L}^3)_2(\text{H}_2\text{O})_4]\cdot 5\text{H}_2\text{O}\}_\infty$ was isolated with large channels, which are accommodating with water guests. $[\text{Cd}(\text{L}^3)\text{Cl}]_\infty$ was formed as square grid lamellar network with cross dimensions of $11 \times 11 \text{ \AA}^2$.

A rare 3D porous coordination polymer $\{[(\text{Zn}_{0.25})_8(\text{O})]\text{Zn}_6(\text{L})_{12}(\text{H}_2\text{O})_{29}(\text{DMF})_{69}(\text{NO}_3)_2\}_n$ constructed by Zn_8O cluster as a secondary building unit (SBU) was reported by Bharadwaj *et al.* in 2012 (Fig 1.12) [56]. The 3D porous coordination polymer $\{[(\text{Zn}_{0.25})_8(\text{O})]\text{Zn}_6(\text{L}^4)_{12}(\text{H}_2\text{O})_{29}(\text{DMF})_{69}(\text{NO}_3)_2\}_n$ was isolated using 1,3-bis(4-carboxyphenyl)imidazolium chloride ($\text{H}_2\text{L}^4\text{Cl}$) and $\text{Zn}(\text{NO}_3)_2\cdot 6\text{H}_2\text{O}$ in DMF under solvothermal route. The voids in $\{[(\text{Zn}_{0.25})_8(\text{O})]\text{Zn}_6(\text{L}^4)_{12}(\text{H}_2\text{O})_{29}(\text{DMF})_{69}(\text{NO}_3)_2\}_n$ were occupied by several water and DMF molecules through H-bonding. Proton conductivity studies on this compound revealed that the conductivity increases with humidity and reaches a maximum value of $2.3 \times 10^{-3} \text{ S cm}^{-1}$ at $25 \text{ }^\circ\text{C}$ and 95% RH. It $\{[(\text{Zn}_{0.25})_8(\text{O})]\text{Zn}_6(\text{L}^4)_{12}(\text{H}_2\text{O})_{29}(\text{DMF})_{69}(\text{NO}_3)_2\}_n$ was showed high thermal stability ($\sim 400 \text{ }^\circ\text{C}$) and proton conductivity (comparable with Nafion) with low activation energy.

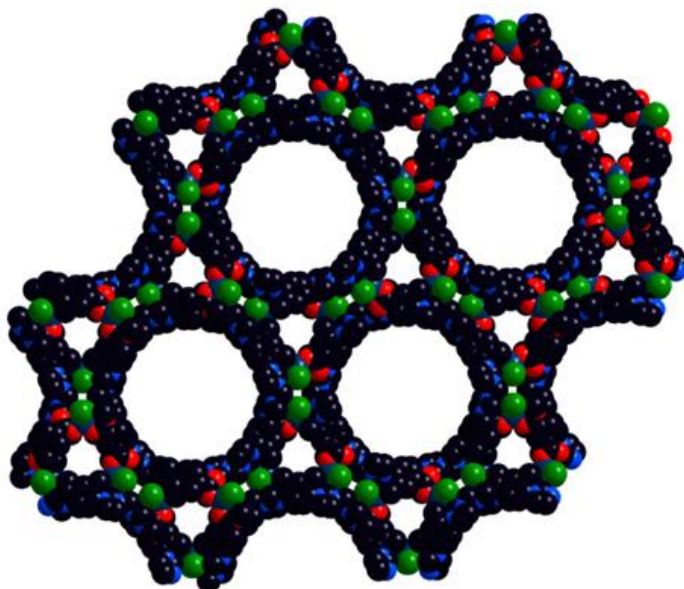


Figure 1.13: Packing diagram of $\{[\text{Zn}(\text{L}^{13})_2(\text{Cl})_2]\cdot 8\text{H}_2\text{O}\}_\infty$, showing the 1D opening channels as view along the *c* axis.

A novel chiral metal-organic nanotube (MONT), $\{[\text{Zn}(\text{L}^{13})_2(\text{Cl})_2]\cdot 8\text{H}_2\text{O}\}_\infty$ was synthesized using 1,1'-methylenebis(3-(4-carboxy-2-methylphenyl)-1*H*-imidazol-3-ium) $\text{L}^{13}\text{H}_2\text{Cl}_2$ and $\text{Zn}(\text{NO}_3)_2\cdot 6\text{H}_2\text{O}$ in the mixture of solvents (H_2O and EtOH) at room temperature by Wu *et al.* in 2012 (Fig 1.13) [57]. The MONT of

$\{[\text{Zn}(\text{L}^{13})(\text{Cl})_2] \cdot 8\text{H}_2\text{O}\}_\infty$ was post modified by $\text{Pd}(\text{OAc})_2$ in THF. The post modified solid synergizes the multiple functionalities of MOFs, SNTs, and NHCs with high catalytic activity for a number of reactions, including Suzuki–Miyaura and Heck cross-coupling reactions, hydrogenation of olefins, and reduction of nitrobenzene. With these the catalytic reactions were preceded smoothly under the mild conditions and also with low catalyst loadings.

The coordination polymers $[\text{Cu}(\text{L}^6)(\text{H}_2\text{O})](\text{Cl})_x(\text{NO}_3)_{1-x}$ and $[\text{Zn}_4(\text{L}^6)_5](\text{Cl})_x(\text{NO}_3)_{3-x}$ were reported from 3-bis(4-carboxy-2,6-dimethylphenyl)-1*H*-imidazolium chloride ($\text{L}^6\text{H}_2\text{Cl}$) by Kaskel *et al.* in 2013 [58]. $[\text{Cu}(\text{L}^6)(\text{H}_2\text{O})](\text{Cl})_x(\text{NO}_3)_{1-x}$ was isolated from the reaction between $\text{L}^6\text{H}_2\text{Cl}$ and $\text{Cu}(\text{NO}_3)_2 \cdot 3\text{H}_2\text{O}$ in ethanol at 80 °C, while $[\text{Zn}_4(\text{L}^6)_5](\text{Cl})_x(\text{NO}_3)_{3-x}$ was isolated from the reaction of $\text{L}^6\text{H}_2\text{Cl}$ and $\text{Zn}(\text{NO}_3)_2 \cdot 4\text{H}_2\text{O}$ in ethanol at 90 °C. The $[\text{Cu}(\text{L}^6)(\text{H}_2\text{O})](\text{Cl})_x(\text{NO}_3)_{1-x}$ was formed as two-dimensional cationic layers with uninodal *sql* topology. Furthermore, the centers of the mesh are occupied by the knots of the next net in such way, that a catenated 3D structure was formed. $[\text{Zn}_4(\text{L}^6)_5](\text{Cl})_x(\text{NO}_3)_{3-x}$ was formed as a three-dimensional structure through intercalation of double layers consisting of binuclear paddle-wheel units. $[\text{Cu}(\text{L}^6)(\text{H}_2\text{O})](\text{Cl})_x(\text{NO}_3)_{1-x}$ shows dye adsorption in ethanol, while $[\text{Zn}_4(\text{L}^6)_5](\text{Cl})_x(\text{NO}_3)_{3-x}$ does not show dyes adsorption due to small pore size (9.2 Å). Among dyes, Nile blue was shown adsorption and desorption, whereas fluorescein and methyl red were adsorbed irreversibly. Nile red was not adsorbed. In contrast, $[\text{Cu}(\text{L}^6)(\text{H}_2\text{O})](\text{Cl})_x(\text{NO}_3)_{1-x}$ adsorbs and desorbs dyes selectively depending on the nature of the dye molecule.

The charge-separated porous coordination polymer $\{[\text{Zn}_2(\text{L}^{14})_2](\text{DMF})\}_\infty$ was isolated from the reaction between imidazolium tricarboxylate ligand, N-(3,5-dicarboxyphenyl)-N'-(4-carboxylbenzyl)imidazolium chloride ($\text{L}^{14}\text{H}_3\text{Cl}$) and $\text{Zn}(\text{NO}_3)_2 \cdot 6\text{H}_2\text{O}$ in DMF/ H_2O at 80 °C by Su and co-workers in 2013 [59]. The coordination polymer $\{[\text{Zn}_2(\text{L}^{14})_2](\text{DMF})\}_\infty$ was built with a zinc(II) dimeric secondary building units, which displays an unprecedented 3,6-connected two-dimensional net topology with the point (Schläfli) symbol $(4^2 \cdot 6)_2(4^4 \cdot 6^9 \cdot 8^2)$. The framework comprises of one-dimensional highly polar intralayer channels. DFT calculations spectacle that positive charges are located on the imidazolium/phenyl rings and negative charges on the carboxylate moieties. The charge-separated nature of the pore surface has a profound effect in their adsorption behavior, resulting in remarkable hysteretic sorption of various gases and vapors. For CO_2 , the hysteretic sorption was observed to occur even up to 298 K. Moreover, the

trace chloride anions present in the pore channels were able to modulate the gas-sorption behavior.

The Mn(II) coordination polymers $[\text{Mn}(\text{L}^1)(\text{N}_3)]$, $[\text{Mn}(\text{R,R-L}^2)(\text{N}_3)] \cdot 0.5\text{CH}_3\text{OH}$, $[\text{Mn}(\text{S,S-L}^2)(\text{N}_3)] \cdot 0.5\text{CH}_3\text{OH}$ and $[\text{Mn}(\text{R,S-L}^2)(\text{N}_3)]$ were derived from achiral and chiral imidazolium-carboxylate zwitterionic ligands: 1,3-bis(carboxylatomethyl)imidazolium (L^1), (S,S)-, (R,R)-, and (R,S)-1,3-bis(1-carboxylatoethyl)imidazolium (S,S-L^2 , R,R-L^2 and R,S-L^2) by Gao *et al.* in 2013 [60]. Both L^1 and S,S-L^2 (or R,R-L^2) lead to 2D coordination polymers based on Mn(II) chains with (azide)bis(carboxylate) bridges, but the inter-chain connecting topologies were different. With R,S-L^2 , a 3D framework $[\text{Mn}(\text{R,S-L}^2)(\text{N}_3)]$ was formed, in which the linear trinuclear units were formed through (azide)bis(carboxylate) bridges linked by μ -1,3 azides and 1,3-dimethyleneimidazolium tethers. Magnetic analyses of those compounds suggested that $[\text{Mn}(\text{L}^1)(\text{N}_3)]$, $[\text{Mn}(\text{R,R-L}^2)(\text{N}_3)] \cdot 0.5\text{CH}_3\text{OH}$ and $[\text{Mn}(\text{S,S-L}^2)(\text{N}_3)] \cdot 0.5\text{CH}_3\text{OH}$ behave as 1D antiferromagnetic systems, while $[\text{Mn}(\text{R,S-L}^2)(\text{N}_3)]$ showed canted antiferromagnetism with a weak ferromagnet with $T_C = 12.2$ K.

Recently, a novel entangled architecture of cadmium coordination polymer $\{[\text{Cd}_2(\text{L}^4)_3(\text{DMF})(\text{NO}_3)] \cdot 3\text{DMF} \cdot 8\text{H}_2\text{O}\}_\infty$ was isolated from the reaction of 1,3-bis(4-carboxyphenyl)imidazolium chloride ($\text{L}^4\text{H}_2\text{Cl}$) with $\text{Cd}(\text{NO}_3)_2 \cdot 6\text{H}_2\text{O}$ in DMF under solvothermal method [61]. The $\{[\text{Cd}_2(\text{L}^4)_3(\text{DMF})(\text{NO}_3)] \cdot 3\text{DMF} \cdot 8\text{H}_2\text{O}\}_\infty$, displayed an interesting 6,3-connected polycatenated structure with channels occupied by large numbers of DMF and water molecules. On removal of these solvent molecules, the compound maintains its overall structure. Furthermore, the proton conductivity investigation afforded a proton conductivity of $1.3 \times 10^{-5} \text{ S cm}^{-1}$ at 25 °C and 98% RH, when water molecules were introduced into the empty channels. This $\{[\text{Cd}_2(\text{L}^4)_3(\text{DMF})(\text{NO}_3)] \cdot 3\text{DMF} \cdot 8\text{H}_2\text{O}\}_\infty$ showed low conductivity compared to the previous Zn(II) compound $\{[\text{Zn}_{0.25}(\text{O})]_8\text{Zn}_6(\text{L})_{12}(\text{H}_2\text{O})_{29}(\text{DMF})_{69}(\text{NO}_3)_2\}_n$ due to loose packing of imidazolium groups.

1.3 Main group imidazolium-carboxylate coordination polymers

Imidazolium carboxylate based main group porous coordination polymer was first reported by Dyson *et al.* in 2005 [62]. Where they isolated the strontium-imidazolium coordination network $\{[\text{Sr}(\text{L}^1)_2] \cdot 4\text{H}_2\text{O}\}_\infty$, which was obtained from the reaction of zwitterionic 1,3-bis(carboxymethyl)-imidazolium with SrCO_3 in water. The geometry of strontium(II) is a distorted hexagonal bipyramid. Each strontium(II) cation was

surrounded by eight oxygen atoms halting from six different imidazolium molecules. The macromolecular Sr coordination polymer structure was assembled from 8-coordinate strontium, which binds to six different imidazolium carboxylate molecules. The two-dimensional polymer was separated by water sheets, in which the water molecules were formed near-planar hexagons in *bc* plane. The overall structure further bears a close resemblance to montmorillonite clays, where water molecules are easily absorbed between the layers, leading swelling of the mineral. Yet, it was the combination of several features in compound $\{[\text{Sr}(\text{L}^1)_2]\cdot 4\text{H}_2\text{O}\}_\infty$, that make this structure special: (i) both the water layer and the coordination compound form a two-dimensional polymer, (ii) the water layer shows a relatively planar structure, and (iii) there was no direct bonding interaction between the water molecules and the imidazolium salt and only one strong hydrogen bond per asymmetric unit between the different layers.

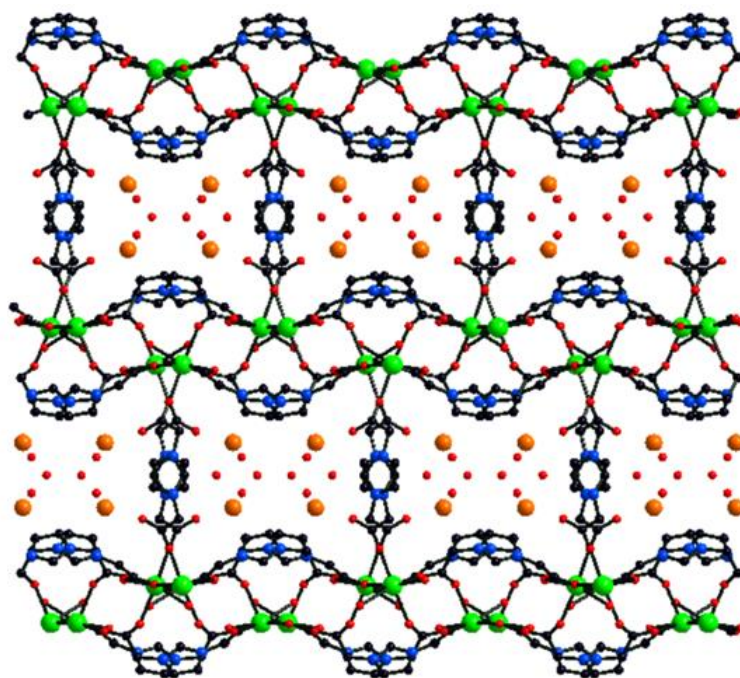


Figure 1.14: Molecular packing in $\{[\text{Ca}_2(\text{L}^1)_3(\text{Br})]\cdot 5\text{H}_2\text{O}\}_\infty$ along the *a* axis.

Later, a series of porous coordination polymers containing Group I or II metal ions were reported [63]. Ca and Sr coordination polymer, $\{[\text{Ca}_2(\text{L}^1)_3(\text{Br})]\cdot 5\text{H}_2\text{O}\}_\infty$ and $\{[\text{Sr}(\text{L}^1)(\text{Br})]\cdot 5.5\text{H}_2\text{O}\}_\infty$ were synthesized from the reaction between $\text{L}^1\text{H}_2\text{Br}$ and corresponding metal carbonates in water. Ba coordination polymer $\text{Ba}[\text{L}^1\text{Br}]\cdot 9\text{H}_2\text{O}$ was derived from the reaction between $\text{L}^1\text{H}_2\text{Br}$ and BaO in water. Cs coordination

compound $\text{CsL}^1.4\text{H}_2\text{O}$ was isolated from the reaction between L^1H and CsCO_3 in water. Although the starting materials are closely related and the molar ratio of the acids and metal salt were the same in the reactions described above, the resulting structures of the isolated solid products were diverse. It appeared that the resulting macrostructure depends markedly on the orientation of the two carboxylate moieties. In $\{[\text{Sr}(\text{L}^1)(\text{Br})].5.5\text{H}_2\text{O}\}_\infty$, carboxylate moieties were *pseudo-trans* to each other, whereas in $\{[\text{Ca}_2(\text{L}^1)_3(\text{Br})].5\text{H}_2\text{O}\}_\infty$, both arms point in the same direction. The three-dimensional coordination polymer $\{[\text{Ca}_2(\text{L}^1)_3(\text{Br})].5\text{H}_2\text{O}\}_\infty$ was consisting of sinusoidal-shaped double layers of calcium ions, composed of rows of calcium cations ($\text{Ca}(\text{II})$ separation distance 4.98(5)) that were linked *via* bridging imidazolium carboxylate (Fig. 1.14). Notably, coordination of the bromide to the metal is not observed with the “harder”, more oxophilic, alkaline earth metal centers. The $\{[\text{Sr}(\text{L}^1)(\text{Br})].5.5\text{H}_2\text{O}\}_\infty$ was formed as two-dimensional network, in which the polymeric sheets are held together *via* hydrogen bonding between bromide anions and water molecules. The coordination polymer $\{[\text{Ba}(\text{L}^1)(\text{Br})].9\text{H}_2\text{O}\}_\infty$ was mentioned as complicated framework built with three independent barium, imidazolium and bromine ions along with approximately nine water molecules.

The barium coordination polymer $\{[\text{Ba}(\text{L}^3)_2(\text{H}_2\text{O})_2].2\text{H}_2\text{O}\}_\infty$ was isolated from the reaction of 1,3-bis(carboxymethyl)benzimidazolium (HL^3) and $\text{Ba}(\text{OH})_2$ in water by using hydrothermal method [64]. The $\{[\text{Ba}(\text{L}^3)_2(\text{H}_2\text{O})_2].2\text{H}_2\text{O}\}_\infty$ was constructed as one-dimensional polymeric zigzag chain along the *c*-axis. Similar method was applied for Mg and Ca hydroxides, but which were isolated as discrete monomers.

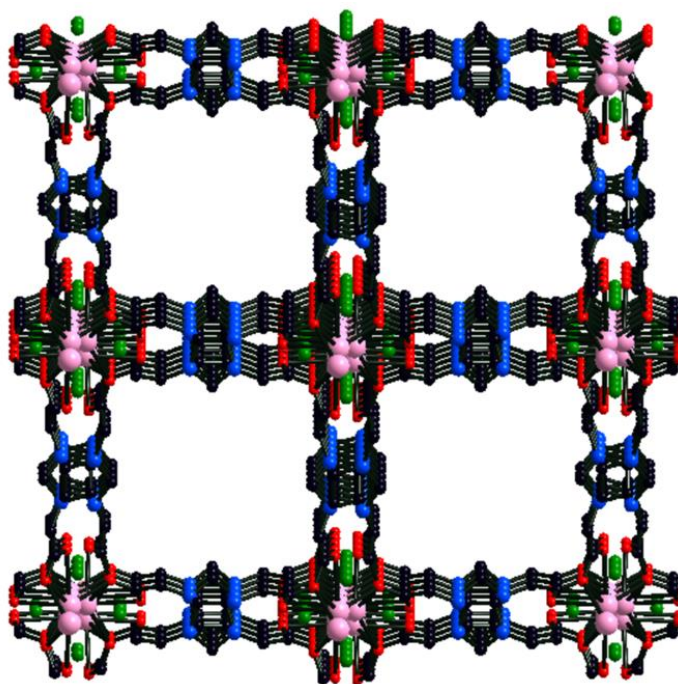


Figure 1.15: 3D framework of $[\text{Pb}(\text{Cl})(\text{L}^1)]_\infty$.

The first p-block imidazolium carboxylate based coordination polymer was reported by Zheng *et al.* in 2007 [65]. A novel chiral 2-fold interpenetrating three-dimensional (3D) metal-organic framework (MOF), $[\text{Pb}(\text{Cl})(\text{L}^1)]_\infty$, was constructed from the flexible ligand N,N'-diacetic acid imidazolium chloride ($\text{L}^1\text{H}_2\text{Cl}$) and $\text{Pb}(\text{NO}_3)_2$ in water, where Pb(II) coordination geometry is distorted monocapped pentagonal bipyramidal. In $[\text{Pb}(\text{Cl})(\text{L}^1)]_\infty$, one-dimensional right-handed helical was built through the monocapped pentagonal bipyramidally coordinated Pb atoms and bridging L^1 anions. The right-handed helical chains were held together to form a 3D homochiral MOF with interpenetrated 3D nets. After the 2-fold interpenetration, the void spaces 30.6% (calculated through PLATON) still exist *via* along *b*-axis. Interestingly, the 3D MOF exhibits tetragonal right-handed helical nanochannels with an opening of 1.2×1.2 nm. Coordination polymer $[\text{Pb}(\text{Cl})(\text{L}^1)]_\infty$, adopted a doubly folded interpenetrating structure to avoid the formation of very large open cavities. Coordination polymer $[\text{Pb}(\text{Cl})(\text{L}^1)]_\infty$, represents as the first even number-fold interpenetrating 3D chiral MOF fabricated from the symmetrical flexible ligand without any chiral auxiliary (Fig. 1.15).

1.4 Imidazolium carboxylate based lanthanide coordination polymers

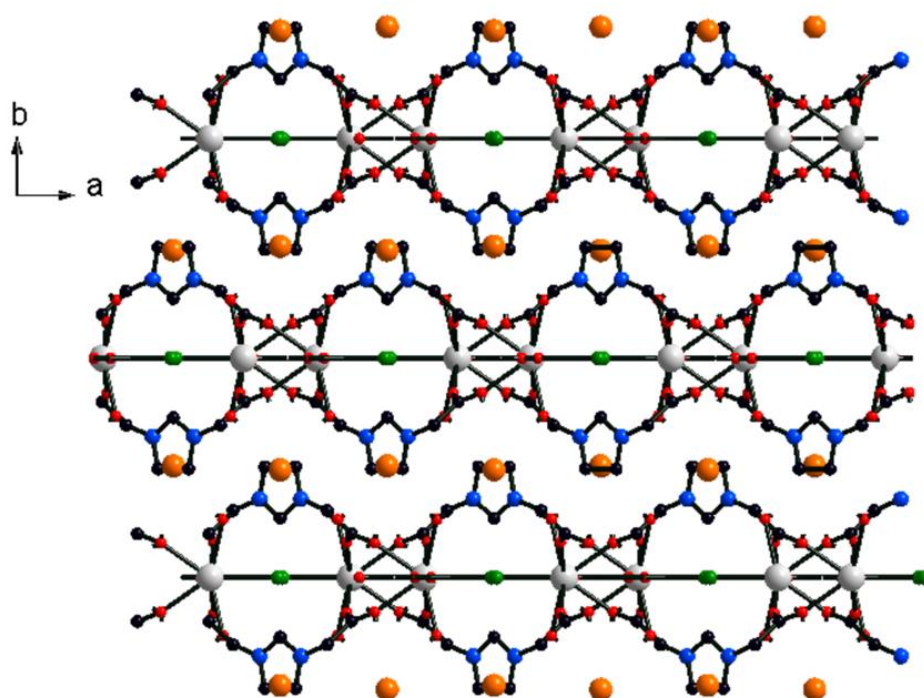


Figure 1.16: 1D chains of $[\text{PrL}^1(\text{H}_2\text{O})_4\text{Cl}]\cdot\text{Br}\cdot\text{H}_2\text{O}$ along the a axis.

Imidazolium carboxylate based lanthanide coordination polymers were first reported by Lu *et al.* in 2009 [66]. $[\text{Er}_4(\mu_3\text{-OH})_4(\mu_2\text{-O})_{0.5}\text{OL}^1_4(\text{H}_2\text{O})_3]\cdot\text{Br}_{2.90}\cdot\text{Cl}_{1.10}\cdot 2\text{H}_2\text{O}$ (MOF-1) and $[\text{PrL}^1(\text{H}_2\text{O})_4\text{Cl}]\cdot\text{Br}\cdot\text{H}_2\text{O}$ (MOF-2) were isolated from the reaction of $\text{L}^2\text{H}_2\text{Br}$ and $\text{LnCl}_3\cdot 6\text{H}_2\text{O}$ ($\text{Ln} = \text{Er}$ or Pr). $[\text{Er}_4(\mu_3\text{-OH})_4(\mu_2\text{-O})_{0.5}\text{OL}^1_4(\text{H}_2\text{O})_3]\cdot\text{Br}_{2.90}\cdot\text{Cl}_{1.10}\cdot 2\text{H}_2\text{O}$ was constructed as 3D framework through bridging ligands with $\text{Er}\cdots\text{Er}$ distance of 4.863 Å. $[\text{PrL}^1(\text{H}_2\text{O})_4\text{Cl}]\cdot\text{Br}\cdot\text{H}_2\text{O}$ was built as 1D chain through the bridging imidazolium carboxylate ligand (Fig 1.16), which was further assembled as 2D network through hydrogen bonding.

Later, Zhang *et al.* reported the different modes of a series of La(III) and Nd(III) with zwitterionic flexible organic spacer (L^1H) [67]. LnX_3 ($\text{Ln} = \text{La}, \text{Nd}$; $\text{X} = \text{ClO}_4^-, \text{NO}_3^-,$ or Cl^-) were treated with L^1H in different solvents (H_2O or $\text{H}_2\text{O}/\text{DMF}$) under the same pH to yield a series of lanthanide compounds at room temperature. With varied coordination modes of L^1 leads to La(III) 3D frameworks with non-interpenetrating topologies. The $\{[\text{La}(\text{trans-}\text{L}^1)(\text{cis-}\text{L}^1)(\text{H}_2\text{O})_2](\text{ClO}_4)_3\cdot 3\text{H}_2\text{O}\}_\infty$ and $\{[\text{La}_2(\text{trans-}\text{L}^1)_3(\text{H}_2\text{O})_6](\text{OH})_3\cdot 7\text{H}_2\text{O}\}_\infty$ were constructed as 2D corrugated layers bridged by L^1 with different bridging modes to form different 3D structures, which were shown *tcs* and (4,6)- connected topologies, respectively. The $\{[\text{La}(\text{trans-}\text{L}^1)_2(\text{H}_2\text{O})_2](\text{Cl})_3\cdot 4\text{H}_2\text{O}\}_\infty$ was isolated as 3D *ant* net. The $\{[\text{Nd}(\text{trans-}\text{L}^1)_2(\text{H}_2\text{O})_2](\text{ClO}_4)_3\cdot 3\text{H}_2\text{O}\}_\infty$ and $\{[\text{Nd}(\text{trans-}$

$L^1)_2(H_2O)_2](NO_3)_3 \cdot 3H_2O\}_\infty$ exist in 4-connected *sql* net, which are analogous to cationic structures of $\{[La(trans-L^1)(cis-L^1)(H_2O)_2](ClO_4)_3 \cdot 3H_2O\}_\infty$ and $\{[La_2(trans-L^1)_3(H_2O)_6](OH)_3 \cdot 7H_2O\}_\infty$. The compound $\{[Nd(trans-L^1)(cis-L^1)(H_2O)_2](Cl)_3 \cdot 5H_2O\}_\infty$ exist in a (4,5)-connected network, resulting from the different modes of flag-like (L^1)⁻ above and below the layers. $\{[Nd(trans-L^1)_2(H_2O)_2](Cl)_3 \cdot 5H_2O\}_\infty$ built in 2D double-layer, consisting of a couple of (4,4) rectangular grid layers.

The 3D Ce^{+3} self-assembly network $[Ce(L^5-Cl)_2(NO_3)]_\infty$ and heterometallic NHC-Cu decorated 3D Ce^{+3} supramolecular network $[Ce(L^5-Cl)(L^5-Cl-H)CuCl]_\infty$ (Fig. 1.17) were reported by Son *et al.* in 2010 [68]. The self-assembly between cerium nitrate and imidazolium carboxylate (L^5H_2Cl) was resulted in the formation of a 3D-porous supramolecular structure $[Ce(L^5-Cl)_2(NO_3)]_\infty$. Whereas the reaction between L^5H_2Cl , cerium nitrate and Cu_2O resulted the formation of porous $[Ce(L^5-Cl)(L^5-Cl-H)CuCl]_\infty$ with *in-situ* decorated NHC-copper. In $[Ce(L^5-Cl)(L^5-Cl-H)CuCl]_\infty$, the helical chains were built in both $[Ce(L^5-Cl)_2(NO_3)]_\infty$ and $[Ce(L^5-Cl)(L^5-Cl-H)CuCl]_\infty$. Large void space was generated in between the helical chains. In which, the narrowest pore size was calculated as $6.5 \times 8.4 \text{ \AA}^2$.

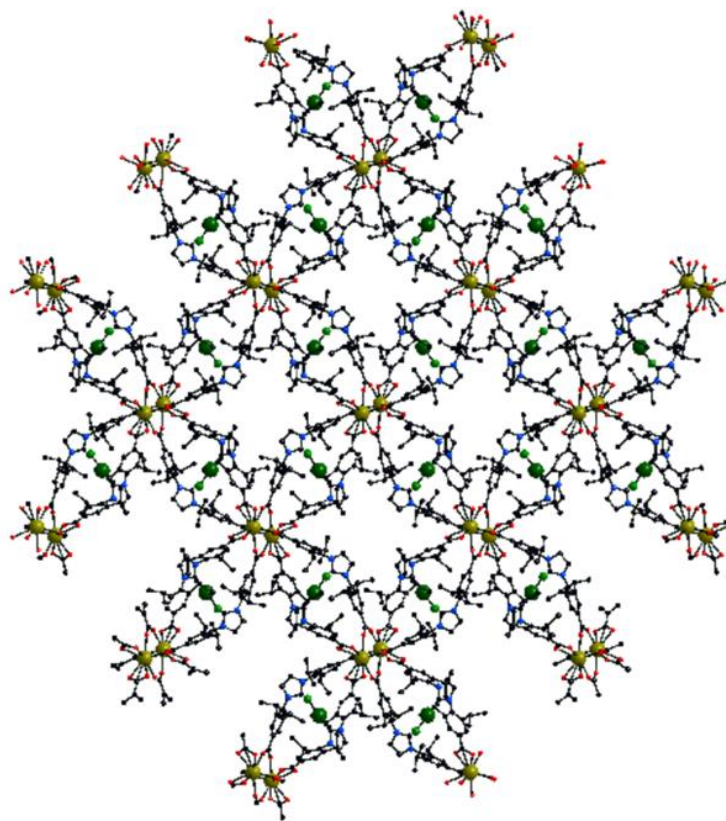


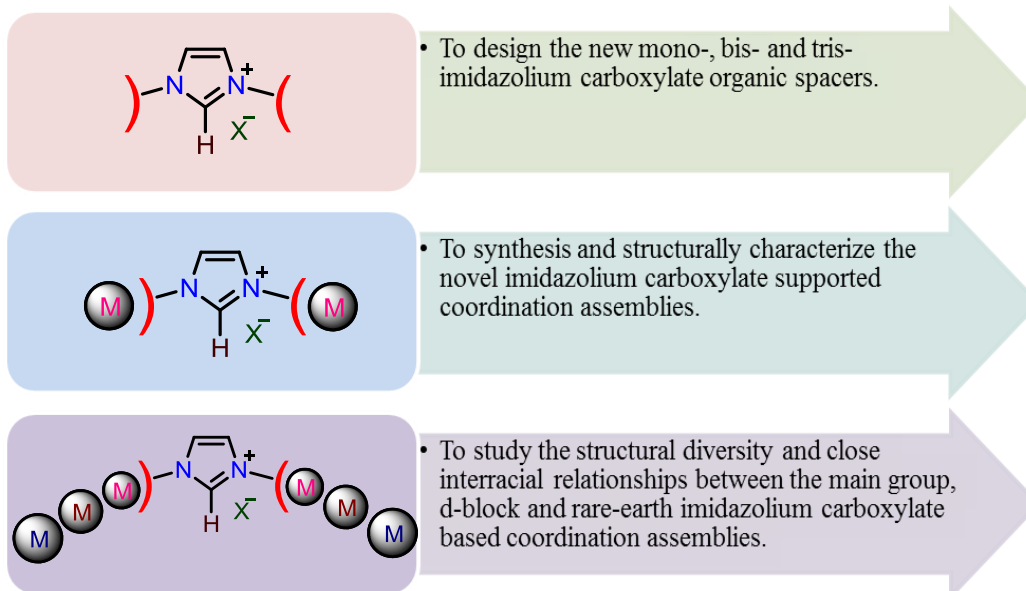
Figure 1.17: 3D network of $[Ce(L^5-Cl)(L^5-Cl-H)CuCl]_\infty$.

1.5 Scope of the work

- ❖ As discussed in the introduction (Chapter 1, *vide supra*), the imidazolium carboxylates supported metal coordination polymers are rare.
- ❖ The known metal-imidazolium carboxylate coordination assemblies are derived using mono or bis-imidazolium carboxylic acids. The coordination assemblies supported by tris-imidazolium carboxylic acids are not known.
- ❖ Flexible carboxylic acid groups ($-\text{CH}_2\text{COOH}$) linked bis- and tris-imidazolium carboxylates are not reported.
- ❖ The functionalized imidazolium carboxylates like luminescent imidazolium carboxylates supported coordination assemblies are not reported.
- ❖ Unlike the d-block imidazolium carboxylate coordination aggregates, the main group and lanthanides based imidazolium carboxylate coordination assemblies are least explored.

1.6 Objectives

Our objectives are:



1.7 References

- [1] S. Kitagawa, R. Kitaura, and S.-I. Noro. *Angew. Chem., Int. Ed.* 43, (2004) 2334.
- [2] D. W. Breck. *Zeolite Molecular Sieves: Structure, Chemistry and Use*. John Wiley & Sons, p.4.
- [3] G. D. Stucky, and J. E. MacDougall. *Science* 247, (1990) 669.
- [4] V. H. Bakkum, E. M. Flanigen, P. A. Jacobs, and J. C. Jansen. *Introduction to zeolite science and practice*. 2nd. Revised Edn., Elsevier, Amsterdam, 1991.
- [5] H. de Sainte Claire Deville. *C. R. Hebd. Séance Acad. Sci.* 52, (1862) 324.
- [6] “Zeolites: Industry Trends and Worldwide Markets in 2010” (Review of report, www.newsletters.com/map/prod/722220.html), Technical insights, Inc.
- [7] F. G. Dwyer, F. V. Hanson, and A. B. Schwartz. US patent 4,035,430, “Conversion of methanol to gasoline product”, mobil oil corporation, New York, NY (dated 12 july, 1977).
- [8] S. T. Wilson, B. M. Lok, C. A. Messina, T. R. Cannan, and E. M. Flanigen. *J. Am. Chem. Soc.* 102, (1982) 1146.
- [9] B. M. Lok, C. A. Messina, R. L. Patton, R. T. Gajek, T. R. Cannan, and E. M. Flanigen. *J. Am. Chem. Soc.* 106, (1984) 6092.
- [10] E. M. Flanigen, B. M. Lok, R. L. Patton, and S. T. Wilson. *Pure and Applied Chemistry* 58, (1986) 1351.
- [11] M. Hartmann, and L. Kevan. *Chem. Rev.* 99, (1999) 635.
- [12] S. M. Manocha. *Sadhana* 28, (2003) 335.
- [13] H. Marsh. *Activated Carbon*. Elseviser, Amsterdam, 2006.
- [14] D. W. Breck. *Zeolite Molecular Sieves: Chemistry, and Use*. John Wiley & Sons, New York, 1974.
- [15] “Coordination Polymers”: J. C. Bailar, Jr., *Prep. Inorg. React.* (1964) 1.
- [16] B. F. Hoskins, and R. Robson. *J. Am. Chem. Soc.* 112, (1990) 1546.

- [17] M. Fujita, Y. J. Kwon, S. Washizu, and K. Ogura. *J. Am. Chem. Soc.* 116, (1994) 1151.
- [18] O. M. Yaghi, G. Li, and H. Li. *Nature* 378, (1995) 703.
- [19] D. Venkataraman, G. B. Gardner, S. Lee, and J. S. Moore. *J. Am. Chem. Soc.* 117, (1995) 11600.
- [20] (a) O. M. Yaghi, and H. Li. *J. Am. Chem. Soc.* 117, (1995) 10401; (b) O. M. Yaghi, and G. Li. *Angew. Chem.*, 34, (1995) 207.
- [21] M. Kondo, T. Yoshitomi, K. Seki, H. Matsuzaka, and S. Kitagawa. *Angew. Chem.*, 117, (1997) 1844.
- [22] H. Li, M. Eddaoudi, M. O'Keeffe, and O. M. Yaghi. *Nature* 402, (1999) 276.
- [23] (a) M. Eddaoudi, J. Kim, N. Rosi, D. Vodak, J. Wachter, M. O'Keeffe, and O. M. Yaghi. *Science* 295, (2002) 469; (b) O. M. Yaghi, M. Eddaoudi, H. Li, J. Kim, and N. Rosi. Patent, WO 2002/088148, 2002; (c) H. K. Chae, D. Y. Siberio-Pérez, J. Kim, Y. B. Go, M. Eddaoudi, A. J. Matzger, M. O'Keeffe, and O. M. Yaghi. *Nature* 427, (2004) 523.
- [24] N. Stock, and S. Biswas. *Chem. Rev.* 112, (2012) 933.
- [25] (a) D. J. Tranchemontagne, J. L. Mendoza-Cortes, M. O'Keeffe M, and O. M. Yaghi. *Chem. Soc. Rev.* 38, (2009) 1257; (b) J. J. Perry IV, J. A. Perman, and M. J. Zaworotko. *Chem. Soc. Rev.* 38, (2009) 1400.
- [26] F. A. A. Paz, J. Klinowski, S. M. F. Vilela, J. P. C. Tomé, J. A. S. Cavaleiro, and J. Rocha. *Chem. Soc. Rev.* 41, (2012) 1088.
- [27] S. Hasegawa, S. Horike, R. Matsuda, S. Furukawa, K. Mochizuki, Y. Kinnoshita, and S. Kitagawa. *J. Am. Chem. Soc.* 129, (2007) 2607.
- [28] (a) J. Yang, T. Hu, and T. C. W. Mak. *Cryst. Growth Des.* 14, (2014) 2990; (b) J. Guo, D. Sun, L. Zhang, Q. Yang, X. Zhao, and D. Sun. *Cryst. Growth Des.* 12, (2012) 5649; c) H.-J. Lee, P.-Y. Cheng, C.-Y. Chen, J.-S. Shen, D. Nandi, and H. M. Lee. *CrystEngComm* 13, (2011) 4814.
- [29] W. Xuan, C. Zhu, Y. Liu, and Y. Cui. *Chem. Soc. Rev.* 41, (2012) 1677.

- [30] S. Horike, S. Bureekaew, and S. Kitagawa. *Chem. Commun.* (2008) 471.
- [31] A. K. Gupta, A. K. Srivastava, L. K. Mahawar, and R. Boomishankar. *Cryst. Growth Des.* 14, (2014) 1701.
- [32] (a) R. Singh, and P. K. Bharadwaj. *Cryst. Growth Des.* 13, (2013) 3722; (b) M. Li, Q. Ling, Z. Yang, B.-L. Li, and H.-Y. Li. *CrystEngComm* 15, (2013) 3630; (c) Z. Su, J. Xu, J. Fan, D.-J. Liu, Q. Chu, M.-S. Chen, S.-S. Chen, G.-X. Liu, X.-F. Wang, and W.-Y. Sun. *Cryst. Growth Des.* 9, (2009) 2801; (d) D. Sun, Z.-H. Yan, V. A. Blatov, L. Wang, and D.-F. Sun. *Cryst. Growth Des.* 13, (2013) 1277.
- [33] S. Kitagawa, R. Kitaura, and S.-I. Noro. *Angew. Chem., Int. Ed.* 52, (2013) 270.
- [34] Selected examples for catalysis: (a) J.-Y. Lee, O. K. Farha, J. Roberts, K. A. Scheidt, S. T. Nguyen, and J. T. Hupp. *Chem. Soc. Rev.* 38, (2009) 1450; (b) L. Q. Ma, C. Abney, and W. B. Lin. *Chem. Soc. Rev.* 38, (2009) 1248; (c) K. S. Jeong, Y. B. Go, S. M. Shin, S. J. Lee, J. Kim, O. M. Yaghi, and N. Jeong. *Chem. Sci.* 2, (2011) 877; (d) A. Corma, H. Garcia, F. X. Llabres, and I. Xamena. *Chem. Rev.* 110, (2010) 4606; (e) M. Yoon, R. Srirambalji, and K. Kim. *Chem. Rev.* 112, (2012) 1196.
- [35] Selected examples for gas storage: (a) L. J. Murray, M. Dincă, and J. R. Long. *Chem. Soc. Rev.* 38, (2009) 1294; (b) J. R. Li, R. J. Kuppler, and H. C. Zhou. *Chem. Soc. Rev.* 38, (2009) 1477; (c) O. K. Farha, A. O. Yazaydin, I. Eryazici, C. D. Malliakas, B. G. Hauser, M. G. Kanatzidis, S. T. Nguyen, R. Q. Snurr, and J. T. Hupp. *Nat. Chem.* 2, (2010) 944; (d) R. B. Getman, Y. S. Bae, C. E. Wilmer, and R. Q. Snurr. *Chem. Rev.* 112, (2012) 703; (e) M. P. Suh, H. J. Park, T. K. Prasad, and D.-W. Lim. *Chem. Rev.* 112, (2012) 782.
- [36] Selected examples for separation: (a) J. A. Mason, M. Veenstra, and J. R. Long. *Chem. Sci.* 5, (2014) 32; (b) J.-R. Li, J. Sculley, and H.-C. Zhou. *Chem. Rev.* 112, (2012) 869; (c) A. Shigematsu, T. Yamada, and H. Kitagawa. *J. Am. Chem. Soc.* 134, (2012) 13145.
- [37] Selected examples for luminescence: (a) Y. Cui, Y. Yue, G. Qian, and B. Chen. *Chem. Rev.* 112, (2012) 1126; (b) J. Heine, and K. M-Buschbaum. *Chem. Soc. Rev.* 42, (2013) 9232.

- [38] Selected examples for electrical conductivity: (a) A. Shigematsu, T. Yamada, and H. Kitagawa. *J. Am. Chem. Soc.* 133, (2011) 2034; (b) T. Yamada, M. Sadakiyo, and H. Kitagawa. *J. Am. Chem. Soc.* 131, (2009) 3144; (c) S. C. Sahoo, T. Kundu, and R. Banerjee. *J. Am. Chem. Soc.* 133, (2011) 17950; (d) T. Kundu, S. C. Sahoo, and R. Banerjee. *Chem. Commun.* 48, (2012) 4998.
- [39] Selected example for magnetism: M. Kurmoo. *Chem. Soc. Rev.* 38, (2009) 1353.
- [40] Selected examples for nonlinear optics: (a) Z. Yin, Q.-X. Wang, and M.-H. Zeng. *J. Am. Chem. Soc.* 134, (2012) 4857; (b) Y.-L. Wang, J.-H. Fu, J.-J. Wei, X. Xu, X.-F. Li, and Q.-Y. Liu. *Cryst. Growth Des.* 12, (2012) 4663.
- [41] Y.-Z. Zheng, Z. Zheng, and X.-M. Chen. *Coord. Chem. Rev.* 250, (2006) 2194.
- [42] (a) O. Kühl. *Functionalised N-heterocyclic carbene complexes*. Wiley, New York, 2010; (b) O. Kühl. *Chem. Soc. Rev.* 36, (2007) 592; (c) J. A. Mata, M. Poyatos, and E. Peris. *Coord. Chem. Rev.* 251, (2007) 841; (d) R. E. Douthwaite. *Coord. Chem. Rev.* 251, (2007) 702; (e) W. J. Sommer, and M. Weck. *Coord. Chem. Rev.* 251, (2007) 860; (f) P. Wasserscheid, and W. Keim. *Angew. Chem., Int. Ed.* 39, (2000) 3772; (g) Z. Fei, and P. J. Dyson. *Chem. Commun.* 49, (2013) 2594; (h) L.-A. Schaper, S. J. Hock, W. A. Herrmann, and F. F. Kühn. *Angew. Chem., Int. Ed.* 52, (2013) 270.
- [43] (a) Z. Xu, N. J. Singh, S. K. Kim, D. R. Spring, K. S. Kim, and J. Yoon. *Chem. Eur. J.* 17, (2011) 1163; (b) H. Ihm, S. Yun, H. G. Kim, J. K. Kim, and K. S. Kim. *Org. Lett.* 4, (2002) 2897; (c) V. Amendola, M. Boiocchi, B. Colasson, L. Fabbrizzi, E. Monzani, M. J. D.-Rodriguez, and C. Spadini. *Inorg. Chem.* 47, (2008) 4808; (d) D.-B. Qin, F.-B. Xu, X.-J. Wan, Y.-J. Zhao, and Z.-Z. Zhang. *Tetrahedron Lett.* 47, (2006) 5641; (e) S. Kumar, V. Luxami, and A. Kumar. *Org. Lett.* 10, (2008) 5549; (f) H. N. Kim, J. Lim, H. N. Lee, J.-W. Ryu, M. J. Kim, J. Lee, D.-U. Lee, Y. Kim, S.-J. Kim, K. D. Lee, H.-S. Lee, and J. Yoon. *Org. Lett.* 13, (2011) 1314; (g) H. N. Kim, J. H. Moon, S. K. Kim, J. Y. Kwon, Y. J. Jang, J. Y. Lee, and J. Yoon. *J. Org. Chem.* 76, (2011) 3805; (h) N. Ahmed, B. Shirinifar, I. S. Yoon, A. Bist, V. Suresh, and K. S. Kim. *Chem. Commun.* 48, (2012) 2662; (i) Z. Xu, S. K. Kim, and J. Yoon. *Chem. Soc. Rev.* 39, (2010) 1457; (j) J. Yoon, S. K. Kim, N. J. Singh, and K. S. Kim. *Chem. Soc. Rev.* 35, (2006) 355.

- [44] K. Hirano, S. Urban, C. Wang, and F. Glorius. *Org. Lett.* 11, (2009) 1019.
- [45] S. Díez-González, N. Marion, and S. P. Nolan. *Chem. Rev.* 109, (2009) 3612.
- [46] Z. Fei, D. Zhao, T. J. Geldbach, R. Scopelliti, P. J. Dyson, S. Antonijevic, and G. Bodenhausen. *Angew. Chem., Int. Ed.* 44, (2005) 5720.
- [47] Z. Fei, W. H. Ang, T. J. Geldbach, R. Scopelliti, and P. J. Dyson. *Chem. Eur. J.* 12, (2006) 4014.
- [48] J. Chun, G. Jung, H. J. Kim, M. Park, M. S. Lah, and S. U. Son. *Inorg. Chem.* 48, (2009) 6353.
- [49] J. Y. Lee, J. M. Roberts, O. K. Farha, A. A. Sarjeant, K. A. Scheidt, and J. T. Hupp. *Inorg. Chem.* 48, (2009) 9971.
- [50] L. Liu, Z. Li, B. Wang, G. Li, L. Wang, X. Meng, and Z. He. *Cryst. Growth Des.* 9, (2009) 5244.
- [51] R. S. Crees, M. L. Cole, L. R. Hanton, and C. J. Sumby. *Inorg. Chem.* 49, (2010) 1712.
- [52] K. Oisaki, Q. Li, H. Furukawa, A. U. Czaja, and O. M. Yaghi. *J. Am. Chem. Soc.* 132, (2010) 9262.
- [53] G.-Q. Kong, X. Xu, C. Zou, and C.-D. Wu. *Chem. Commun.* 47, (2011) 11005.
- [54] J. M. Roberts, O. K. Farha, A. A. Sarjeant, J. T. Hupp, and K. A. Scheidt. *Cryst. Growth Des.* 11, (2011) 4747.
- [55] G.-Q. Kong, and C.-D. Wu. *CrystEngComm* 14, (2012) 847.
- [56] S. Sen, N. N. Nair, T. Yamada, H. Kitagawa, and P. K. Bharadwaj. *J. Am. Chem. Soc.* 134, (2012) 19432.
- [57] G.-Q. Kong, S. Ou, C. Zou, and C.-D. Wu. *J. Am. Chem. Soc.* 134, (2012) 19851.
- [58] G. Nickerl, A. Notzon, M. Heitbaum, I. Senkowska, F. Glorius, and S. Kaskel. *Cryst. Growth Des.* 13, (2013) 198.
- [59] S. Wang, Q. Yang, J. Zhang, X. Zhang, C. Zhao, L. Jiang, and C.-Y. Su. *Inorg. Chem.* 52, (2013) 4198.

- [60] X. Wang, X.-B. Li, R.-H. Yan, Y.-Q. Wang, and E.-Q. Gao. *Dalton Trans.* 42, (2013) 10000.
- [61] S. Sen, T. Yamada, H. Kitagawa, and P. K. Bharadwaj. *Cryst. Growth Des.* 14, (2014) 1240.
- [62] Z. Fei, T. J. Geldbach, D. Zhao, R. Scopelliti, and P. J. Dyson. *Inorg. Chem.* 44, (2005) 5200.
- [63] Z. Fei, T. J. Geldbach, R. Scopelliti, and P. J. Dyson. *Inorg. Chem.* 45, (2006) 6331.
- [64] L. Huang, A.-G. Zhong, D.-B. Chen, D. Qiu, and H.-D. Liang. *J. Mol. Struct.* 984, (2010) 39.
- [65] X.-W. Wang, L. Han, T.-J. Cai, Y.-Q. Zheng, J.-Z. Chen, and Q. Deng. *Cryst. Growth Des.* 7, (2007) 1027.
- [66] L. Han, S. Zhang, Y. Wang, X. Yan, and X. Lu. *Inorg. Chem.* 48, (2009) 786.
- [67] X.-C. Chai, Y.-Q. Sun, R. Lei, Y.-P. Chen, S. Zhang, Y.-N. Cao, and H.-H. Zhang. *Cryst. Growth Des.* 10, (2010) 658.
- [68] J. Chun, H. S. Lee, G. Jung, S. W. Lee, H. J. Kim, and S. U. Son. *Organometallics* 29, (2010) 1518.

Chapter 2

Semi Rigid Imidazolium Carboxylate Controlled Structural Topologies in Zwitterionic Coordination Networks

2.1 Introduction

The construction of functionalized coordination polymers (FCPs) have been the subject of interest over the last few decades due to their fascinating architectures and versatile applications in different fields [1-7]. Suitable organic spacers, metal precursors and synthetic methodologies are essential criteria to design the FCPs with different physical properties [8]. In addition, non-covalent interactions such as hydrogen bonding, $\pi \cdots \pi$, $M \cdots \pi$, $C-H \cdots \pi$ and $anion \cdots \pi$ interactions play a key role in FCPs to increase their dimensionality, supramolecular topology and porosity [9]. Therefore, the choice of organic spacer is extremely important to fine-tune the structural and desired functional properties of FCPs through the coordination mode or non-covalent interaction mode. Amongst these organic spacers, imidazolium carboxylic acids are of special interest as they have $[C-H]^{\delta+}$ functional group (potential functional group for anion reorganization and post modification to generate N-heterocyclic carbene tethered catalytically active metal centers) along with excellent functional group tolerance at N-positions [10-16]. However, the structurally characterized coordination polymers using imidazolium carboxylic acids are hampered due to the ionic nature of the organic spacer (often yielding an insoluble powder with metal salts).

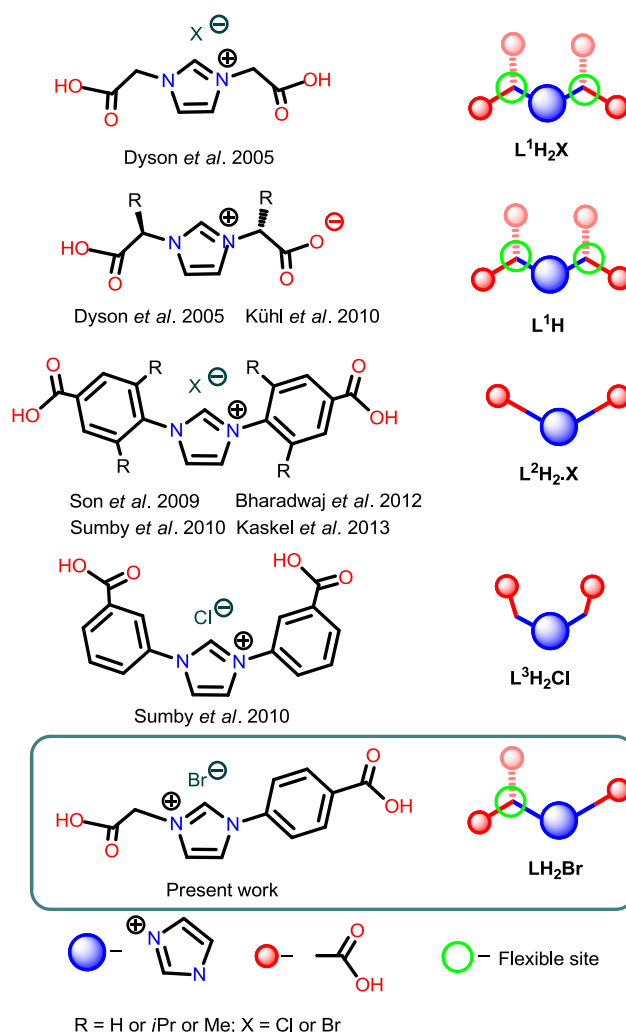


Figure 2.1: Schematic illustrations of L^1H_2X ($X = Br$ or Cl), L^1H , L^2H_2X , L^3H_2Cl and LH_2Br organic spacers.

Among the known imidazolium carboxylic acid ligands, N,N'-diacetic acid imidazolium halides [L^1H_2X] and the zwitter ionic (L^1H) ligands (Fig. 2.1) are the extensively studied systems for the FCPs construction with transition metals (Zn, Cd and Co), main group metals (Ca, Sr, Ba, Cs, Pb and Bi) and rare earth metals (Er, Pr, La and Nd) [16b,17]. Notably, L^1 contains two flexible carboxylate wings, which allows the maximum degree of freedom. Later, the Zn_8O cluster incorporated zinc coordination polymer $[\{(Zn_{0.25})_8(O)\}Zn_6(L^2)_{12}(H_2O)_{29}(DMF)_{69}(NO_3)_2]_{\infty}$ was derived from the rigid carboxylate imidazolium ligand (L^2H_2X), where the carboxylate wings are in a fixed position [16c,18]. In addition, several coordination polymers derived from the substituted ligands of L^1H_2X , L^2H_2X and L^3H_2Cl were reported (Fig. 2.1) [19]. To the best of our knowledge, the rigid and flexible biscarboxylates linked mono imidazolium

salts have not been employed yet for the synthesis of coordination polymers [16d,16e,19h-k]. Thus, we report the flexible and rigid carboxylate linked imidazolium salt (**LH₂Br**) (Fig. 2.1) supported series of zwitterionic late transition metal (II) coordination polymers, [**L₂Mn(H₂O)₂**]_∞ (**1**), [**L₂Co(H₂O)₂**]_∞ (**2**), [**L₂Ni(H₂O)₄**]_∞ (**3**), [**L₂Cu**]_∞ (**4**), [**L₂Zn(H₂O)₂**]_∞ (**5**) and [**L₃Cd₂(Br)₂**]_∞ (**6**). The compounds **1-6** have been characterized by FT-IR, TGA, SXRD, PXRD and UV-vis spectroscopy.

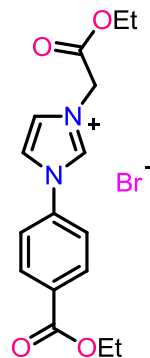
2.2 Experimental

2.2.1 Materials and methods

The solvents were purchased from commercial sources and purified according to standard procedures [20]. Unless otherwise stated, the chemicals were purchased from commercial sources. **LH₂Br** was prepared as reported [21]. FT-IR measurement (neat) was carried out on a Bruker Alpha-P Fourier transform spectrometer. The UV-vis spectra were measured on a T90+ UV-visible spectrophotometer. The thermogravimetric analysis (TGA) was performed using a TA-SDT Q600, Tzeropress. Powder X-ray diffraction (PXRD) studies were carried out on a PANalytical X'pert Pro powder X-ray diffractometer operated at an acceleration voltage of 40 kV and an applied current of 30 mA. Elemental analyses were performed by the Euro Vector EA-300 elemental analyzer.

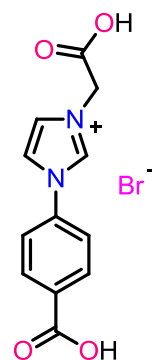
2.2.2 Synthesis of **L(C₂H₅)₂Br**, **LH₂Br** and **1-6**

L(C₂H₅)₂Br: A mixture of ethyl 4-(1*H*-imidazol-1-yl)benzoate (2 g, 9.249 mmol) and ethyl 2-bromoacetate (1.6 g, 9.58 mmol) in acetone (15 mL) was refluxed for 12 h. The solvent was filtered using cannula and solid was washed with acetone (5 mL) and diethyl ether (10 mL). The solid was subsequently dissolved in water (10 mL) and filtered. The solvent was removed under reduced pressure and dried under high vacuum. Yield: 82% (based on ethyl 4-(1*H*-imidazol-1-yl)benzoate). Anal. Calcd. (%) for C₁₆H₁₉N₂O₄Br (383.24): C, 50.14; H, 5.00; N, 7.31; found: C, 50.2; H, 5.2; N, 7.1. ¹H NMR (400 MHz, D₂O): δ = 9.51 (s, 1H, ImH), 8.17 (d, 2H, ArH), 8.04 (s, 1H, ImH),



7.79 (s, 1H, ImH), 7.75 (d, 2H, ArH), 5.33 (s, 2H, CH₂), 4.36 (m, 4H, 2 x CH₂), 1.39 (t, 3H, CH₃), 1.33 (t, 3H, CH₃) ppm. ¹³C NMR (100 MHz, D₂O): δ = 167.74 (C=O), 167.20 (C=O), 137.94 (ArC), 136.20 (ImC), 131.45 (ArC), 124.68 (ImC), 122.19 (ImC), 121.49 (ArC), 121.44 (ImC), 63.78 (OCH₂), 62.70 (OCH₂), 50.50 (CH₂), 13.40 (CH₃), 13.26 (CH₃) ppm. FT-IR (neat): $\bar{\nu}$ = 3409 (w), 3126 (w), 3094 (w), 3052 (w), 2986 (w), 2932 (w), 1742 (s), 1712 (s), 1607 (m), 1568 (w), 1550 (s), 1512 (w), 1464 (w), 1422 (w), 1393 (w), 1370 (m), 1331 (w), 1315 (w), 1276 (s), 1221 (s), 1198 (w), 1183 (m), 1106 (s), 1064 (s), 1017 (s), 955 (m) cm⁻¹.

LH₂Br: To the ester compound [**L**(C₂H₅)₂]**Br** (3 g, 7.83 mmol) added 12% HCl aqueous solution (60 mL) and refluxed for 12 h. The solution was removed under reduced pressure and the remaining solid was washed with acetone (20 mL) and diethyl ether (10 mL). The solvent removed under reduced pressure and dried under high vacuum. Yield: 88% (based on [**L**(C₂H₅)₂]**Br**). Anal. Calcd. (%) for C₁₂H₁₁N₂O₄Br (327.13): C, 44.06; H, 3.39; N, 8.56; found: C, 44.2; H, 3.5; N, 9.1. ¹H NMR (400 MHz, DMSO-d₆): δ = 10.15 (s, 1H, ImH), 8.46 (s, 1H, ImH), 8.17 (d, 2H, ArH), 8.07 (s, 1H, ImH), 7.96 (d, 2H, ArH), 5.30 (s, 2H, CH₂) ppm. ¹³C NMR (100 MHz, DMSO-d₆): δ = 167.62 (C=O), 166.06 (C=O), 137.62 (ArC), 136.86 (ImC), 131.84 (ArC), 131.21 (ArC), 124.92 (ImC), 121.89 (ArC), 120.62 (ImC), 50.16 (CH₂) ppm. FT-IR (neat): $\bar{\nu}$ = 3121 (w), 3103 (w), 2992 (w), 2829 (w), 2591 (w), 2490 (w), 1713 (s), 1608 (m), 1571 (m), 1547 (s), 1511 (w), 1432 (m), 1404 (w), 1386 (s), 1333 (w), 1316 (w), 1226 (w), 1200 (s), 1115 (s), 1064 (s), 1016 (w), 975 (w), 956 (w) cm⁻¹.



[L₂Mn(H₂O)₂]_∞ (1): **LH₂Br** (0.1 g, 0.306 mmol) and Mn(NO₃)₂·4H₂O (0.039 g, 0.155 mmol) were taken into Schlenk tube and 1:1 DMF and water (3 mL) were added. The reaction mixture was heated at 130 °C for 12 h then slowly brought to room temperature to obtain colorless crystals. The crystals were washed with MeOH and dried under vacuum. Yield: 76% (based on Mn(NO₃)₂·4H₂O). Anal. Calcd. (%) for C₂₄H₂₂N₄O₁₀Mn (581.40): C, 49.58; H, 3.81; N, 9.45; found: C, 49.7; H, 3.7; N, 9.4. FT-IR (neat): $\bar{\nu}$ = 3111 (w), 1609 (s), 1545 (s), 1383 (s), 1324 (m), 1217 (m), 1128 (w), 1070 (m) cm⁻¹.

[L₂Co(H₂O)₂]_∞ (2): Compound **2** was synthesized using a similar method as for **1**, but with Co(NO₃)₂·6H₂O (0.045 g, 0.155 mmol) instead of Mn(NO₃)₂·4H₂O. Yield: 81%

(based on $\text{Co}(\text{NO}_3)_2 \cdot 6\text{H}_2\text{O}$). Anal. Calcd. (%) for $\text{C}_{24}\text{H}_{22}\text{N}_4\text{O}_{10}\text{Co}$ (585.40): C, 49.24; H, 3.79; N, 9.57; found: C, 49.3; H, 3.8; N, 9.5. FT-IR (neat): $\bar{\nu} = 3108$ (w), 1608 (s), 1577 (w), 1544 (s), 1381 (s), 1325 (m), 1216 (m), 1129 (w), 1069 (m), 954 (m) cm^{-1} .

$[\text{L}_2\text{Ni}(\text{H}_2\text{O})_4]_\infty$ (3): Compound **3** was synthesized using a similar method as for **1**, but with $\text{Ni}(\text{NO}_3)_2 \cdot 6\text{H}_2\text{O}$ (0.045 g, 0.155 mmol) instead of $\text{Mn}(\text{NO}_3)_2 \cdot 4\text{H}_2\text{O}$. Yield: 85% (based on $\text{Ni}(\text{NO}_3)_2 \cdot 6\text{H}_2\text{O}$). Anal. Calcd. (%) for $\text{C}_{24}\text{H}_{26}\text{N}_4\text{O}_{12}\text{Ni}$ (621.20): C, 46.40; H, 4.22; N, 9.02; found: C, 46.3; H, 4.3; N, 9.2. FT-IR (neat): $\bar{\nu} = 3036$ (w), 2910 (w), 1605 (s), 1530 (w), 1433 (w), 1385 (s), 1306 (m), 1228 (m), 1130 (w), 1075 (m) cm^{-1} .

$[\text{L}_2\text{Cu}]_\infty$ (4): The compound **4** was synthesized using a similar method as for **1**, but with $\text{Cu}(\text{NO}_3)_2 \cdot 3\text{H}_2\text{O}$ (0.037 g, 0.153 mmol) instead of $\text{Mn}(\text{NO}_3)_2 \cdot 4\text{H}_2\text{O}$. Yield: 79% (based on $\text{Cu}(\text{NO}_3)_2 \cdot 3\text{H}_2\text{O}$). Anal. Calcd. (%) for $\text{C}_{24}\text{H}_{18}\text{N}_4\text{O}_8\text{Cu}$ (553.98): C, 52.03; H, 3.28; N, 10.11; found: C, 51.9; H, 3.4; N, 10.1. FT-IR (neat): $\bar{\nu} = 3068$ (w), 2991 (w), 2946 (w), 1630 (w), 1610 (s), 1579 (w), 1548 (s), 1511 (w), 1367 (s), 1315 (m), 1231 (m), 1140 (m), 1072 (m), 1042 (w) cm^{-1} .

$[\text{L}_2\text{Zn}(\text{H}_2\text{O})_2]_\infty$ (5): The compound **5** was synthesized using a similar method as for **1**, but with $\text{Zn}(\text{NO}_3)_2 \cdot 6\text{H}_2\text{O}$ (0.046 g, 0.154 mmol) instead of $\text{Mn}(\text{NO}_3)_2 \cdot 4\text{H}_2\text{O}$. Yield: 88% (based on $\text{Zn}(\text{NO}_3)_2 \cdot 6\text{H}_2\text{O}$). Anal. Calcd. (%) for $\text{C}_{24}\text{H}_{22}\text{N}_4\text{O}_{10}\text{Zn}$ (591.86): C, 48.71; H, 3.75; N, 9.47; found: C, 48.8; H, 3.8; N, 9.4. FT-IR (neat): $\bar{\nu} = 3108$ (w), 1609 (s), 1577 (w), 1544 (s), 1381 (s), 1326 (m), 1301 (w), 1218 (m), 1130 (w), 1070 (m), 974 (m) cm^{-1} .

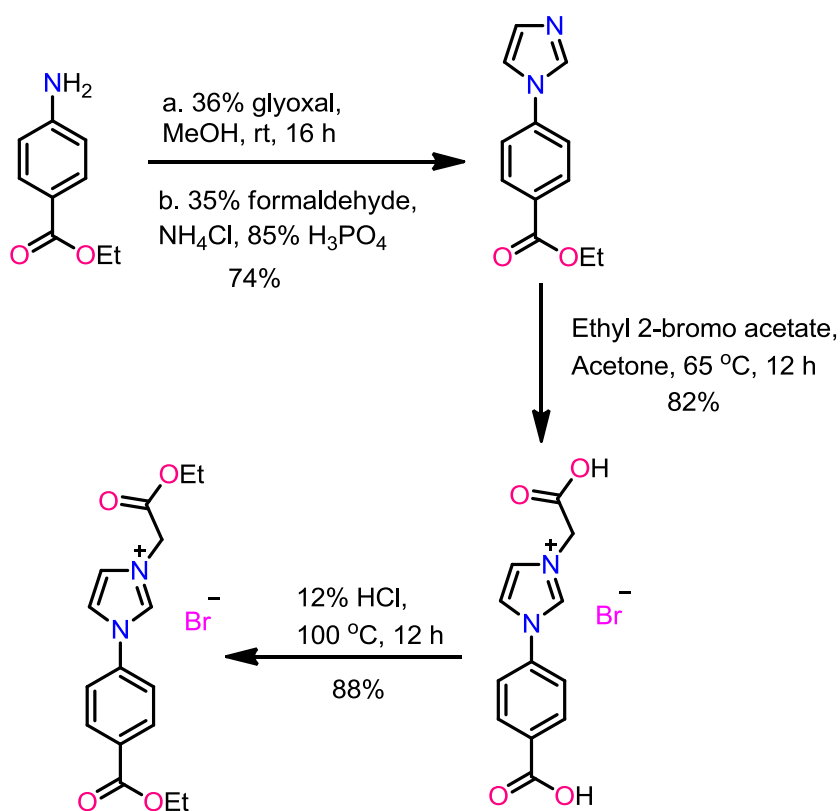
$[\text{L}_3\text{Cd}_2(\text{Br})_2]_\infty$ (6): The compound **6** was synthesized using a similar method as for **1**, but with $\text{Cd}(\text{NO}_3)_2 \cdot 4\text{H}_2\text{O}$ (0.095 g, 0.308 mmol) instead of $\text{Mn}(\text{NO}_3)_2 \cdot 4\text{H}_2\text{O}$. Yield: 82% (based on $\text{Cd}(\text{NO}_3)_2 \cdot 4\text{H}_2\text{O}$). Anal. Calcd. (%) for $\text{C}_{12}\text{H}_9\text{N}_2\text{O}_4\text{CdBr}$ (437.52): C, 32.94; H, 2.07; N, 6.40; found: C, 32.8; H, 2.2; N, 6.4. FT-IR (neat): $\bar{\nu} = 3119$ (w), 3098 (m), 2940 (w), 1621 (s), 1609 (s), 1577 (w), 1532 (s), 1392 (s), 1363 (w), 1332 (w), 1310 (w), 1295 (m), 1270 (w), 1214 (m), 1186 (w), 1129 (w), 1106 (w), 1067 (m), 1035 (w), 1013 (m), 954 (w) cm^{-1} .

2.2.3 Crystallography

The crystal structures of **1-6** were measured on an Oxford Xcalibur 2 diffractometer. A suitable crystal was selected and mounted on a SuperNova, Dual, Cu at zero, Eos diffractometer. Data were collected at 150 K or 298 K. Using Olex2 [22], the structures **1-6** were solved with the olex2.solve structure solution program using Charge Flipping and refined with the olex2.refine refinement package using Gauss-Newton minimization. CCDC 1010010-1010015 contains the supplementary crystallographic data for this paper. These data can be obtained free of charge from the Cambridge Crystallographic Data Centre via www.ccdc.cam.ac.uk/data_request/cif or from the Cambridge Crystallographic Data Centre, 12 Union Road, Cambridge CB2 1EZ, UK; fax: +44 1223 336 033; or e-mail: deposit@ccdc.cam.ac.uk

2.3 Results and discussion

2.3.1 Synthesis and characterization of $L(C_2H_5)_2Br$, LH_2Br and **1-6**



Scheme 2.1: Synthesis of LH_2Br .

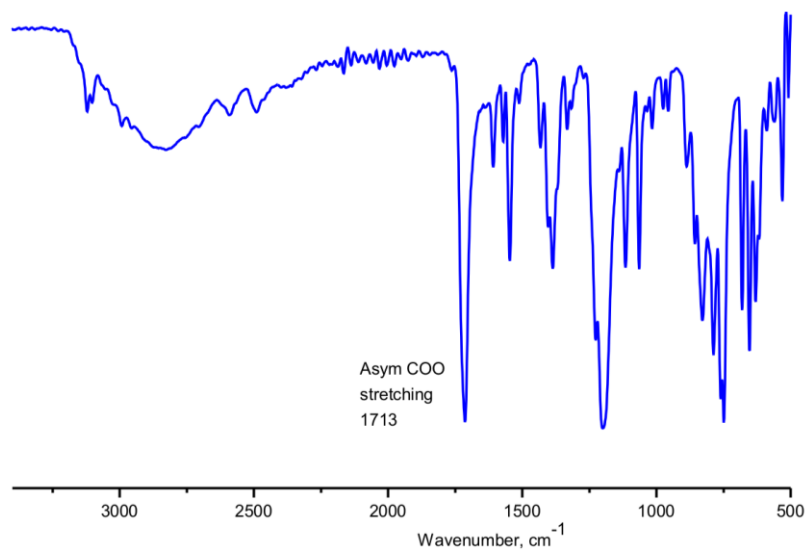


Figure 2.2: FT-IR (neat) spectrum of LH₂Br.

Compound L(C₂H₅)₂Br was synthesized from reaction of ethyl 4-(1*H*-imidazol-1-yl)benzoate and ethyl 2-bromoacetate in acetone under refluxing condition (Scheme 2.1). Subsequently compound LH₂Br was synthesized from the acid hydrolysis of L(C₂H₅)₂Br. The FT-IR spectrum of LH₂Br showed a characteristic peak for asymmetric stretching frequency at 1713 cm⁻¹ (Fig. 2.2).

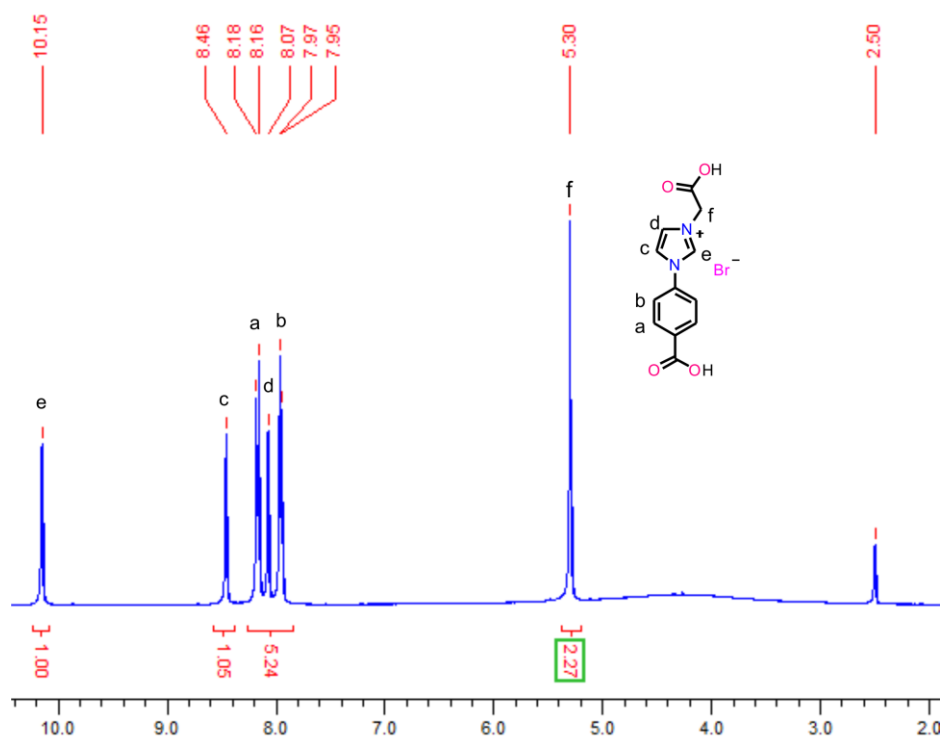


Figure 2.3: ¹H NMR spectrum of LH₂Br in DMSO-d₆ at RT.

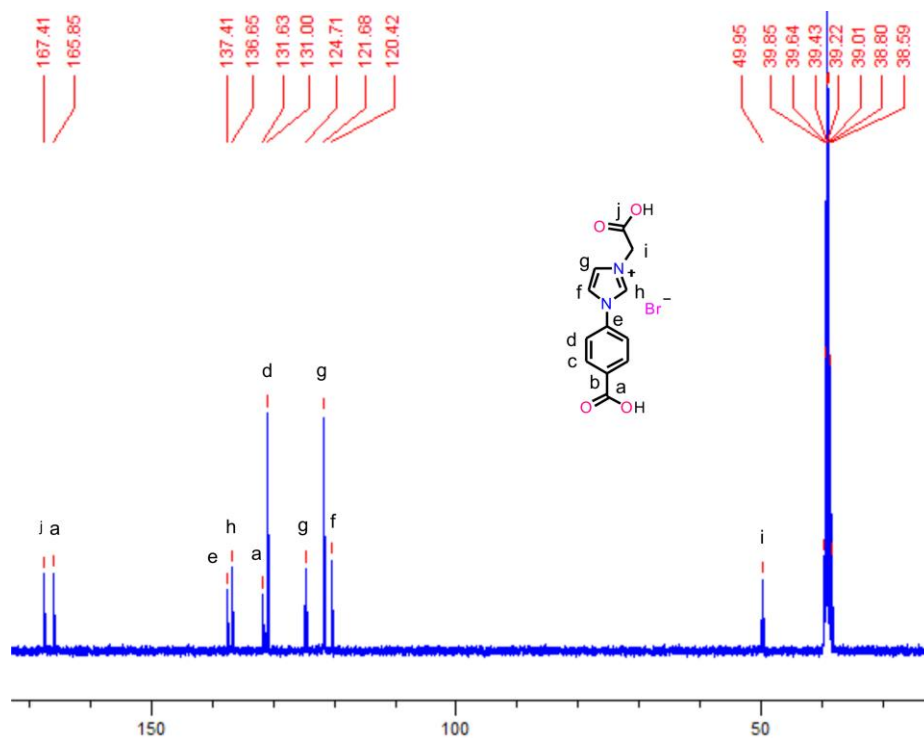


Figure 2.4: ^{13}C NMR spectrum of LH_2Br in DMSO-d_6 at RT.

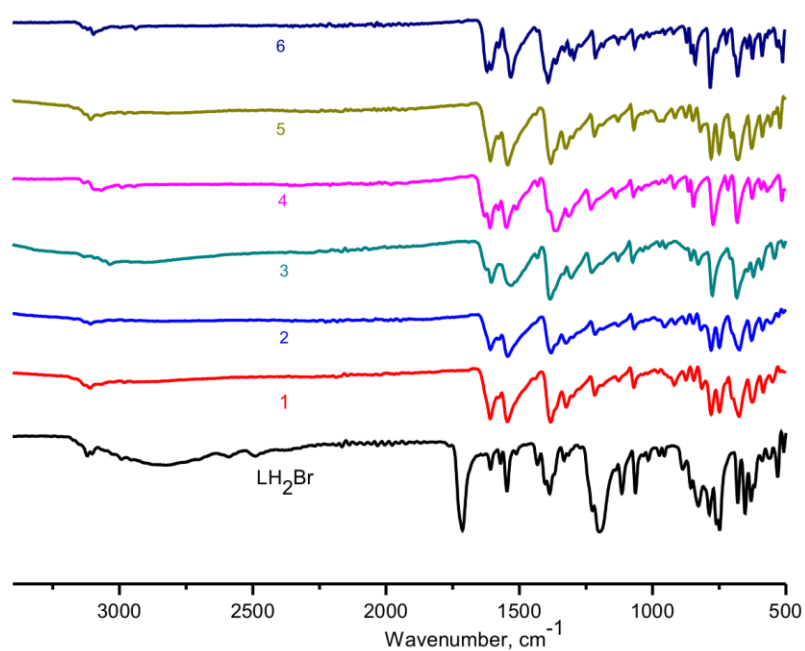


Figure 2.5: FT-IR (neat) spectrum of LH_2Br vs 1-6.

The ^1H NMR spectrum of LH_2Br showed the diagnostic peak for NCHN at 10.5 ppm (Fig. 2.3), while ^{13}C NMR spectrum of LH_2Br showed the diagnostic peak for NCHN at 136.86 ppm (Fig. 2.4). Compounds **1-6** were synthesized from the reaction of LH_2Br

with $M(\text{NO}_3)_2 \cdot x\text{H}_2\text{O}$ ($M = \text{Mn}, \text{Co}, \text{Ni}, \text{Cu}, \text{Zn}, \text{and Cd}$) in DMF and water at 130 °C. Compounds **1-6** were isolated as colorless (**1**, **5** and **6**), light pink (**2**), light green (**3**) and sky blue (**4**) crystals. The FT-IR spectra of **1-6** are depicted in the Fig 2.5. Evidently, the strong adsorption peaks in the region of $1621\text{-}1530\text{ cm}^{-1}$ are assigned to the asymmetric resonance of the carboxylate stretching bands and the peaks in the region $1392\text{-}1365\text{ cm}^{-1}$ are attributed to the symmetric stretching vibrations of the carboxylate groups. In order to check the phase purity of the bulk samples of **1-6**, PXRD patterns were recorded. The PXRD patterns were virtually identical to the corresponding simulated PXRD patterns from the single-crystal diffraction data (Fig. 2.6), which indicates a good purity and homogeneity of the samples.

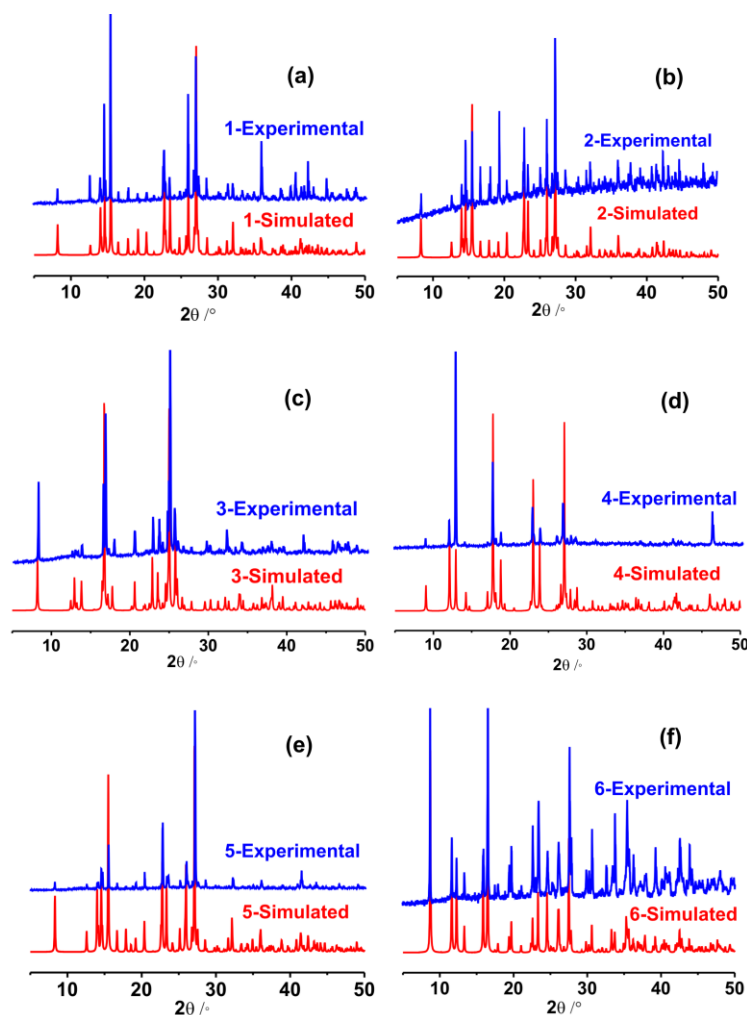


Figure 2.6: PXRD profiles for compounds 1-6.

The solid-state UV-vis absorption spectra of LH_2Br and **1-6** were measured at room temperature (Fig. 2.7). LH_2Br exhibits broad absorption bands in the range of 220-300

nm with absorption maxima at 235 and 283 nm. The absorption patterns of **1-6** in the ultraviolet region are comparable to the organic spacer (**LH₂Br**) ($\lambda_{\text{max}} = 227$ and 282 nm for **1**, $\lambda_{\text{max}} = 232$ nm for **2**, $\lambda_{\text{max}} = 231$ and 282 nm for **3**, $\lambda_{\text{max}} = 225$ and 286 nm for **4**, $\lambda_{\text{max}} = 237$ and 282 nm for **5** and $\lambda_{\text{max}} = 235$ and 280 nm for **6**) due to the π to π^* transitions of the ligand. Additionally, **3** shows an absorption maximum at 397 nm and **6** shows absorption maximum at 340 nm, which can be attributed to metal-to-ligand charge-transfer (MLCT) transitions. Compounds **2-4** exhibits a broad band in the visible region with absorption maxima at 518 nm for **2**, 728 nm for **3** and 648 nm for **4**, which are assigned to $d \rightarrow d$ transitions of the corresponding metal(II) complexes [23]. The solid-state structures of **1-6** were confirmed by the single crystal X-ray diffraction technique. Data collection parameters are listed in Table 2.1 and Table 2.2.

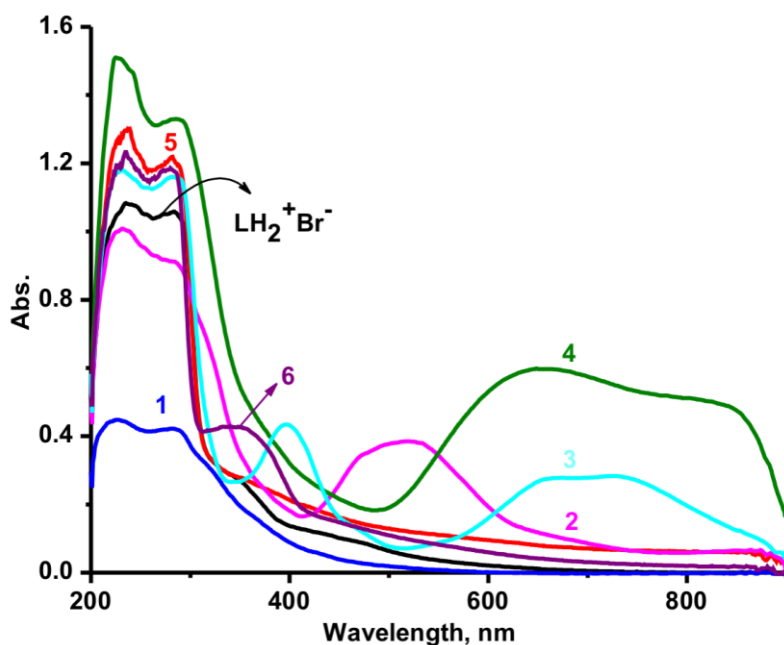


Figure 2.7: The solid-state UV-vis absorption spectra of **LH₂Br** and **1-6**.

2.3.2 Crystal structural description of **1-6**

Single crystal X-ray structure of [L₂Mn(H₂O)₂]_∞ (1**):** The molecular structure of **1** is depicted in Fig. 2.8a. The molecule **1** crystallized in the triclinic space group *P* $\bar{1}$. The geometry of the manganese (II) is distorted octahedral. The coordination environment of manganese is fulfilled by four carboxylate oxygen atoms of the ligands and two oxygen atoms of water molecules. The manganese center and four coordinated carboxylate

oxygen atoms (O2, O2a, O4 and O4a) are arranged in the basal plane, while the coordinated water molecules (O1 and O1a) are arranged in the axial plane (Fig. 2.8b). The Mn centers are bridged by an organic spacer to form the one dimensional coordination chain (Fig. 2.8c). The Mn and Mn separation within the 1D chain is 13.1623(12) Å. The carboxylic groups of each organic spacer are coordinated to the manganese centers in $\mu_1-\eta^0:\eta^1$ mode. Interestingly, the imidazolium cation charge is balanced by one of the coordinated carboxylate groups.

The manganese imidazolium carboxylate coordination polymers are rare. The only report known up until now concerns the manganese imidazolium carboxylate coordination polymers derived using imidazolium carboxylate in the presence of azide [19g]. The Mn–O_{COO} bond distances are 2.160(14) and 2.210(14) Å. The Mn–O_{water} bond length is 2.215(14) Å. The O_{COO}–Mn–O_{COO} angles fall in the range of 86.79(5)° to 180.0°, O_{water}–Mn–O_{water} 180.0. The O_{water}–Mn–O_{COO} angles are almost perpendicular (from 87.99(5)° to 92.01(5)°).

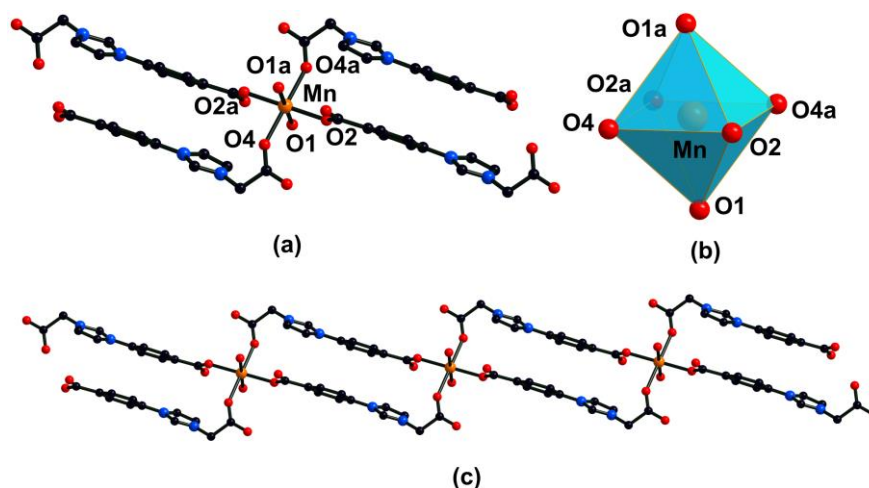


Figure 2.8: (a) Coordination environment of the Mn(II) center in **1**. The hydrogen atoms have been omitted for clarity. (b) Polyhedron view of the Mn(II) center. (c) View of the 1D chain in **1**.

Single crystal X-ray structure of [L₂Co(H₂O)₂]_∞ (2**):** The single crystal X-ray structure of **2** is isostructural with **1**. Thus, the structural features of **2** are not discussed in detail. However, the structural parameters of **1** and **2** are significantly different. The molecule **2** crystallized in the triclinic space group *P* $\bar{1}$. In **2**, the Co–O_{COO} bond distances are 2.076(3) and 2.145(3) Å. The Co–O_{water} bond length is 2.134(2) Å. The structural metrics of **2** are comparable with the known one dimensional cationic cobalt

imidazolium carboxylate coordination polymer, $[\text{Co}(\text{H}_2\text{O})_4(\text{L}^1)]\text{Br}(\text{H}_2\text{O})_\infty$, where the cationic charge is balanced by bromide ion [17a]. The $\text{O}_{\text{COO}}-\text{Co}-\text{O}_{\text{COO}}$ angles fall in the range from $86.30(7)^\circ$ to 180.0° . The $\text{O}_{\text{water}}-\text{Co}-\text{O}_{\text{water}}$ 180.0° and $\text{O}_{\text{water}}-\text{Co}-\text{O}_{\text{COO}}$ angles are nearly a perpendicular (from $88.07(6)^\circ$ to $91.93(6)^\circ$). The Co and Co separation within the 1D chain is $13.0980(12)$ Å.

Table 2.1: Summary of crystallographic data and structure refinement results for **1-3**

Parameters	1	2	3
Empirical formula	$\text{C}_{24}\text{H}_{22}\text{N}_4\text{O}_{10}\text{Mn}$	$\text{C}_{24}\text{H}_{22}\text{N}_4\text{O}_{10}\text{Co}$	$\text{C}_{24}\text{H}_{26}\text{N}_4\text{O}_{12}\text{Ni}$
Formula weight	581.40	585.40	621.20
Temperature (K)	150	298	150
Crystal system	Triclinic	Triclinic	Triclinic
Space group	$P\bar{1}$	$P\bar{1}$	$P\bar{1}$
$a/\text{Å}$	7.3845(6)	7.3753(7)	7.6500(9)
$b/\text{Å}$	7.8414(6)	7.9003(7)	7.9162(9)
$c/\text{Å}$	11.2217(10)	11.1179(10)	11.5971(11)
α°	85.382(7)	85.277(7)	98.507(9)
β°	74.061(7)	73.544(8)	105.439(9)
γ°	63.215(8)	62.907(9)	111.347(11)
Volume (Å^3)	557.06(9)	552.27(10)	606.63(12)
Z	1	1	1
$\rho_{\text{calc}}/\text{mg mm}^{-3}$	1.733	1.760	1.700
Absorption coefficient (mm^{-1})	5.475	6.755	1.859
$F(000)$	299.0	301.0	322.0

Data collected	3512	3480	3842
Unique data	2082	2054	2265
R_{int}	0.0193	0.0285	0.0177
GOF on F^2	1.045	1.054	1.048
$R_1 (I > 2\sigma(I))$	0.0359	0.0406	0.0302
$wR_2 (I > 2\sigma(I))$	0.1014	0.1095	0.0860
R_1 values (all data)	0.0359	0.0406	0.0317
wR_2 values (all data)	0.1014	0.1095	0.0876

Table 2.2: Summary of crystallographic data and structure refinement results for **4-6**

Parameters	4	5	6
Empirical formula	$\text{C}_{24}\text{H}_{18}\text{N}_4\text{O}_8\text{Cu}$	$\text{C}_{24}\text{H}_{22}\text{N}_4\text{O}_{10}\text{Zn}$	$\text{C}_{12}\text{H}_9\text{N}_2\text{O}_4\text{BrCd}$
Formula weight	553.98	591.86	437.52
Temperature (K)	150	298	298
Crystal system	Triclinic	Triclinic	Triclinic
Space group	$P\bar{1}$	$P\bar{1}$	$P\bar{1}$
$a/\text{\AA}$	6.9546(6)	7.3787(6)	7.7419(5)
$b/\text{\AA}$	8.0346(8)	7.9006(6)	7.9854(5)
$c/\text{\AA}$	10.4551(9)	11.0983(8)	10.7897(6)
α°	100.687(8)	85.353(6)	72.371(5)
β°	103.018(7)	73.412(7)	80.030(5)
γ°	108.818(8)	62.985(7)	86.863(5)
Volume (\AA^3)	517.23(9)	551.50(7)	626.11(7)

<i>Z</i>		1	1	2
$\rho_{\text{calc}}/\text{mg mm}^{-3}$		1.778	1.782	2.321
Absorption coefficient (mm^{-1})		2.081	2.211	17.871
<i>F</i> (000)		283.0	304.0	420.0
Data collected		3222	3526	4053
Unique data		1927	2056	2350
<i>R</i> _{int}		0.0173	0.0252	0.0551
GOF on <i>F</i> ²		1.053	1.052	1.105
<i>R</i> ₁ (<i>I</i> > 2σ(<i>I</i>))		0.0301	0.0312	0.0781
w <i>R</i> ₂ (<i>I</i> > 2σ(<i>I</i>))		0.0857	0.0888	0.2357
<i>R</i> ₁ values (all data)		0.0309	0.0319	0.0785
w <i>R</i> ₂ values (all data)		0.0867	0.0893	0.2361

Single crystal X-ray structure of [L₂Ni(H₂O)₄]_∞ (3): Compound **3** crystallized in the triclinic space group *P* $\bar{1}$. Interestingly, the molecule of **3** is a monomer (Fig. 2.9a). Nickel imidazolium carboxylate based coordination compounds have not been reported previously. **3** is the first example of a zwitterion nickel imidazolium carboxylate compound that has been reported in the literature. The coordination environment of the nickel center is fulfilled by two oxygen atoms of carboxylate group (the N-CH₂-COO⁻ group is coordinated to Ni, while the N-C₆H₄-COO⁻ group is not coordinated) of ligand and four oxygen atoms of water molecules. The acetic acid carboxylate groups are connected to the nickel in the $\mu_1\text{-}\eta^0\text{:}\eta^1$ fashion, while the N-C₆H₄COO⁻ group is free from coordination ($\mu_0\text{-}\eta^0\text{:}\eta^0$). As shown in the polyhedron view (Fig. 2.9b), four water molecules (O5, O6, O5a and O6a) and the Ni center are arranged in the basal plane, and two flexible carboxylic groups (O1 and O1a) are arranged in axial position. The geometry of the nickel(II) ion is distorted octahedron. The Ni-O_{COO} bond distance is

2.077(11) Å. The Ni–O_{water} bond lengths are nearly comparable (2.023(11) and 2.087(12) Å).

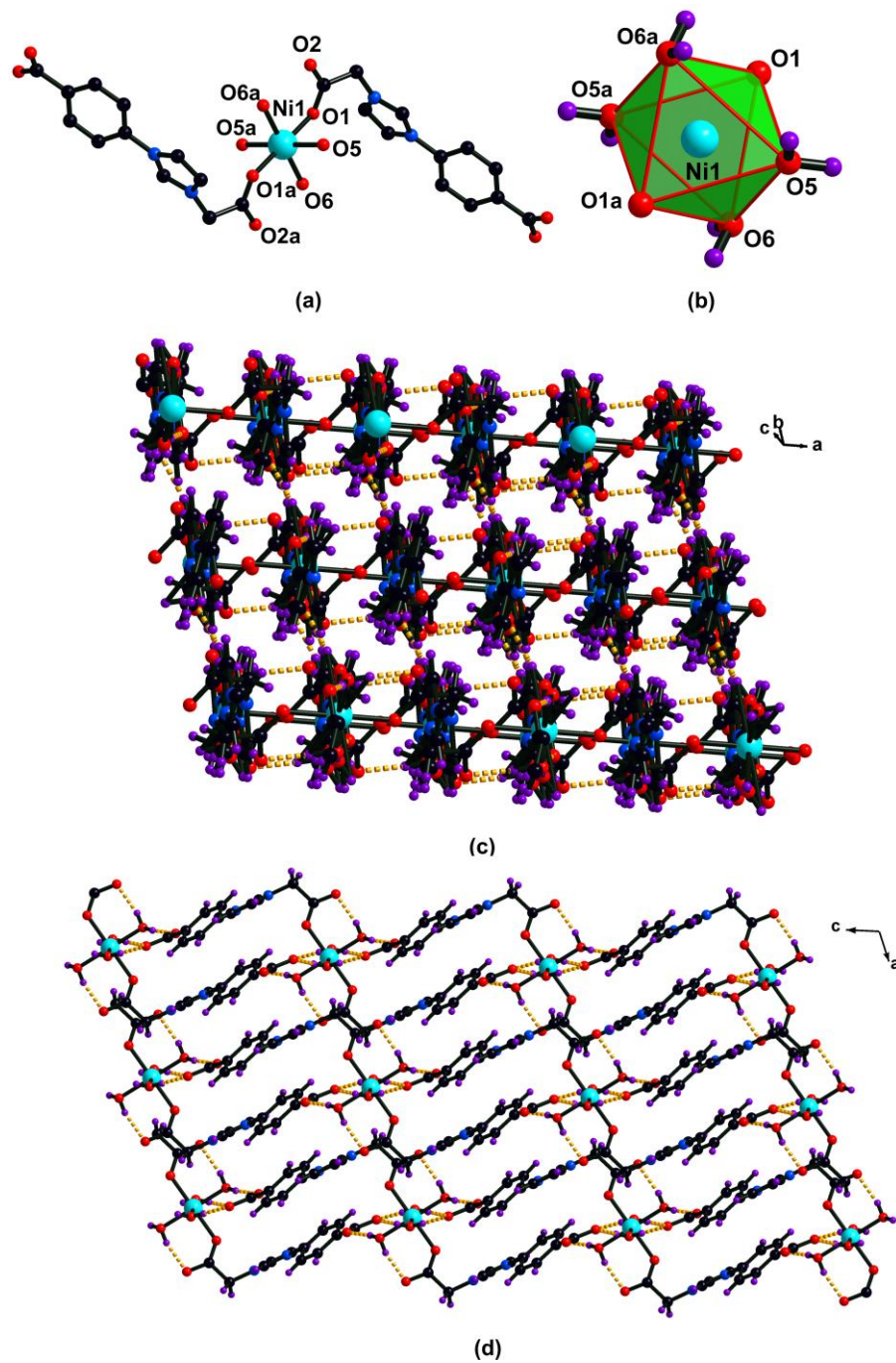


Figure 2.9: (a) The mononuclear zwitterion nickel imidazolium carboxylate. The hydrogen atoms have been omitted for clarity. (b) Polyhedron view of the Ni(II) center in 3. (c) View of the 3D supramolecular network through inter and intra molecular O–H...O_{COO} hydrogen bonds. (d) View of the hydrogen bonding network through *c*-axis.

As shown in Fig. 2.9c and Fig. 2.9d, the coordinated carboxylate oxygen (N-CH₂-COO⁻) forms an O-H \cdots O_{COO} intramolecular hydrogen bond, while the uncoordinated carboxylate oxygen (N-C₆H₄-COO⁻) forms an O-H \cdots O_{COO} intermolecular hydrogen bond with coordinated water molecules. As a result, molecule **3** is organized into a 3D supramolecular network form. The H \cdots O_{COO(aryl)} hydrogen bond distance (1.987 Å) is slightly longer than H \cdots O_{COO(acetic acid)} (1.883 Å).

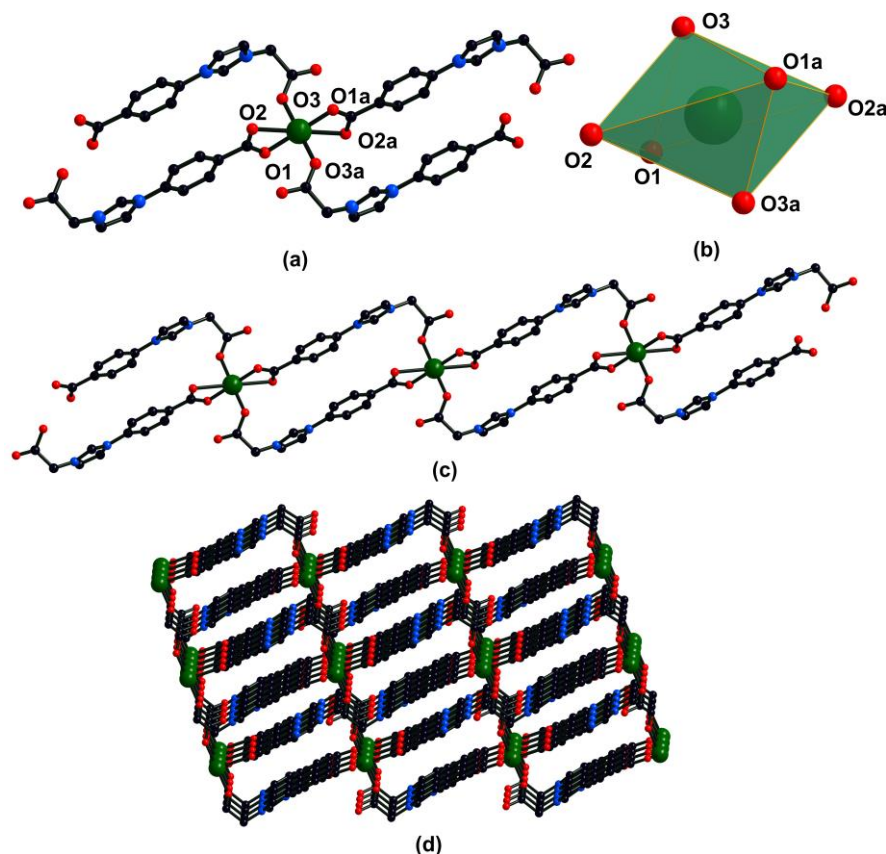


Figure 2.10: (a) Coordination environment of Cu(II) ion in **4**. The hydrogen atoms have been omitted for clarity. (b) Polyhedron view of the Cu(II) center in **4**. (c) View of the 1D chain in **4**. (d) The close packing of independent chains in **4** (view along *b* axis).

Single crystal X-ray structure of [L₂Cu]_∞ (4**):** Compound **4** crystallized in the triclinic space group *P* $\bar{1}$. Unlike **1-3**, **4** is a zwitterionic one dimensional chain (Fig. 2.10c). The coordination environment of the copper center is satisfied by six oxygen atoms of four carboxylate ligands (Fig. 2.10a). Two different types of carboxylate coordination fashions are observed, namely μ_1 - η^1 : η^1 and μ_1 - η^0 : η^1 modes (Fig. 2.10c). As expected, the geometry of the copper(II) ion is a distorted octahedron. The copper metal and four coordinated carboxylate oxygen atoms (O1, O1a, O2 and O2a) are settled in the basal

plane, while the coordinated acetic acid carboxylate oxygen atoms (O3 and O3a) are settled in the axial plane (Fig. 2.10b). The Cu and Cu separation within the 1D chain is 11.946(12) Å. The different Cu–O_{COO} bond distances are identified in the range of 1.949(12) to 2.580(13) Å. The O_{COO}–Cu–O_{COO} angle varies from 86.81(5)° to 180.0°. As shown in Fig. 2.10d, the independent one dimensional chains are closely packed in a slipped manner without any interactions.

Single crystal X-ray structure of [L₂Zn(H₂O)₂]_∞ (5): The single crystal X-ray structure of **5** is isostructural with **1** and **2**. Thus, the structural features of **5** are not deliberated in detail. Compound **5** crystallized in the triclinic space group *P* $\bar{1}$. However, the structural parameters of **5** are significantly different from **1** and **2**. In **5**, the Zn–O_{COO} bond distances are 2.071(13) and 2.184(14) Å. The Zn–O_{COO} bond distance range is slightly larger than those for reported zinc imidazolium carboxylate coordination polymers [17a,24]. The Zn–O_{water} bond length is 2.109(13) Å. The O_{COO}–Zn–O_{COO} angles fall in the range from 86.00(5)° to 180.0°. The O_{water}–Zn–O_{water} 180.0° and O_{water}–Zn–O_{COO} angles are nearly a perpendicular (from 87.80(5)° to 92.20(5)°). The Zn to Zn separation distance within the 1D chain is 13.091(12) Å.

Single crystal X-ray structure of [L₃Cd₂(Br)₂]_∞ (6): Compound **6** crystallized in the triclinic space group *P* $\bar{1}$. The molecule **6** is a zwitterionic two dimensional coordination polymer (Fig. 2.11c). As shown in figure 2.11a and 2.11b, **6** is constructed from two edge shared cadmium(II) octahedrons. The geometry of the cadmium(II) ion is a distorted octahedron (Fig. 2.11b). The coordination environment around cadmium(II) center is fulfilled by four oxygen atoms of carboxylate ligands and two μ_2 bridged bromine ions. The cadmium metal, three coordinated oxygen atoms of the carboxylate spacer and one of the bridging bromine ions are arranged in the basal plane, and an oxygen atom of the carboxylate spacer and the second bromine ion are arranged in the axial plane (Fig. 2.11b). Two Cd octahedrons are edge shared through μ_2 -bridged bromide ions. Recently, Zhang *et al.* was reported the 2D coordination polymers consisting of a [Cd₂(μ_2 -X)₂] core unit from the reaction between 1-(4-carboxybenzyl)-4,4'-bipyridinium, 4,4'-biphenyldicarboxylic acid and Cd(CH₃COO)₂ in the presence of KX (X = Cl or Br) [25]. In contrast to these known examples, in **6** the bridging bromines originate from **LH₂Br**. In the molecules reported by Zhang *et al.*, the Cd(II) is seven-coordinated with a distorted pentagonal bipyramidal geometry. The different

Cd–O_{COO} bond distances are not comparable and these are in the range from 2.228(8) Å to 2.403(8) Å. The Cd–Br bond lengths are different (2.711(19) and 2.641(18) Å). The Cd and Cd separation distance is 3.959 Å, which is very similar to that of related reported molecules. In the [Cd₂(μ₂-Br)₂] core, the Br to Br separation distance is 3.602 Å. The bond angle of Br–Cd–Br is 84.58(6)°. The different O_{COO}–Cd–O_{COO} bond angle are observed in the range from 56.6(3)° to 154.6(3)°. The carboxylate groups of each organic spacer are coordinated with three different cadmium centers in μ₁-η¹:η¹ and μ₂-η¹:η¹ modes. As a result, the bromine bridge (μ₂-Br)₂ and carboxylate bridge (μ₂-COO)₂ are linked antiparallel to the cadmium centers (Fig. 2.11c and 2.11d). The Cd···Cd separation distance between bridging mode of carboxylate (5.098 Å) is larger than the Cd···Cd separation distance between bridging mode of bromine ions (3.959 Å).

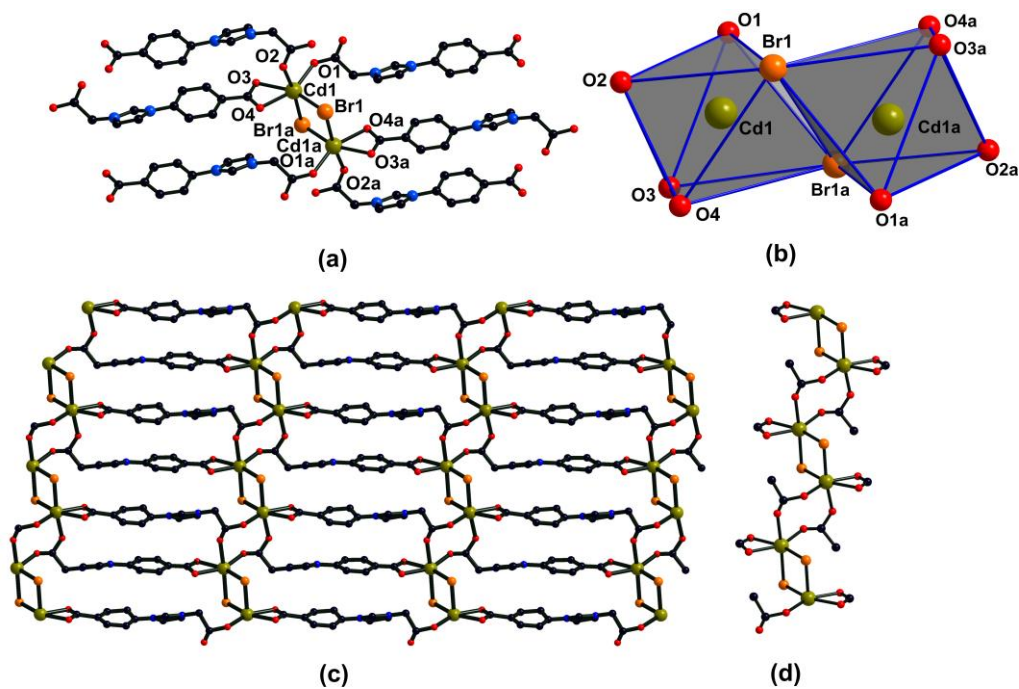


Figure 2.11: (a) Coordination environment of the Cd(II) centers in **6**. (b) Polyhedron view of the Cd(II) centers. (c) Representation of two-dimensional framework in **6**. (d) The bridging mode of the Cd(II) centers in the two dimensional framework.

2.3.3 Comparison of solid state structures of 1-6

The most common features of **LH₂Br** ligands in **1-6** are shown in Fig. 2.12, which are (i) alternative orientation of N–CH₂–COO[−] and N–C₆H₄–COO[−] functional groups in the coordination networks; (ii) monodentate and bidentate modes of coordination; (iii)

bridging nature of the ligand between metal centers in **1**, **2** and **4-6**; while **3** is an exception, where the ligand is not bridging.

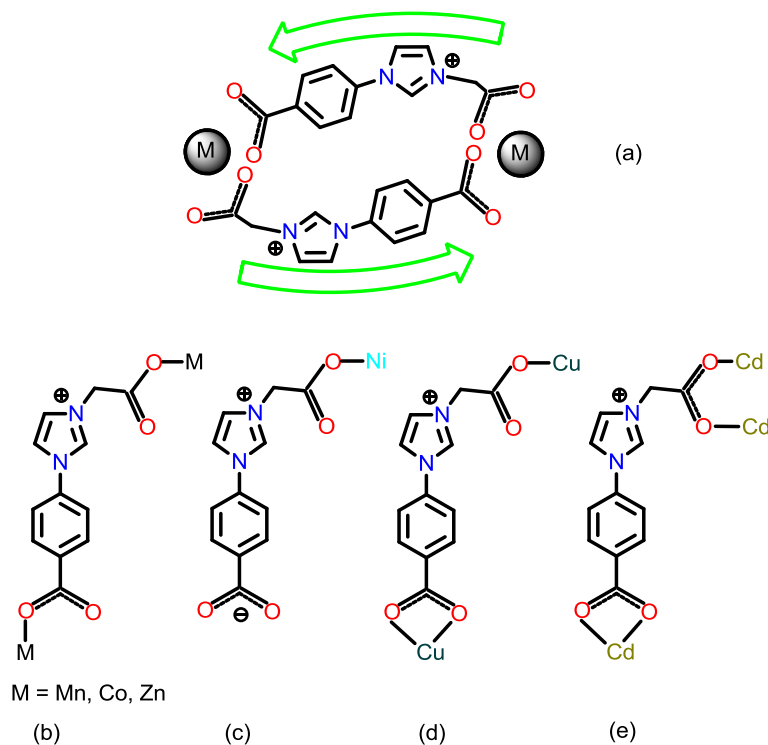


Figure 2.12: Schematic illustrations of the metal-binding motifs of the carboxylate linker (LH_2Br) (a) Orientation of $-\text{CH}_2-\text{COO}^-$ and $-\text{C}_6\text{H}_4-\text{COO}^-$ functional groups in **1-6**; (b) $\mu_1-\eta^0:\eta^1$ in **1**, **2** and **5**; (c) $\mu_1-\eta^0:\eta^1$ and $\mu_0-\eta^0:\eta^0$ in **3**; (d) $\mu_1-\eta^1:\eta^1$ and $\mu_1-\eta^0:\eta^1$ in **4**; (e) $\mu_1-\eta^1:\eta^1$ and $\mu_2-\eta^1:\eta^1$ in **6**.

The carboxylate groups in LH_2Br showed the monodentate coordination mode ($\mu_1-\eta^0:\eta^1$ and $\mu_1-\eta^0:\eta^1$) towards Mn(II), Co(II) and Zn(II) centers. The monodentate bridging coordination mode ($\mu_1-\eta^0:\eta^1$ and $\mu_0-\eta^0:\eta^0$) is observed for Ni(II) center, while the monodentate and bidentate types ($\mu_1-\eta^1:\eta^1$ and $\mu_1-\eta^0:\eta^1$) of coordination are detected in **4**. The bidentate bridging and non-bridging modes of coordination ($\mu_1-\eta^1:\eta^1$ and $\mu_2-\eta^1:\eta^1$) are identified for **6**. Among the isostructural molecules **1**, **2** and **5**, a gradual decrease in the $\text{M}-\text{O}_{\text{COO}}$ bond length is observed from Mn(II) to Co(II) and Zn(II) due to the gradual decrease in the ionic radial of the six coordinated metal ions. Similarly, a gradual decrease in the $\text{M}-\text{O}_{\text{water}}$ bond distance is measured from Mn(II) to Co(II) and Zn(II). The metal-metal separation distance ($\text{Mn}\cdots\text{Mn}$, 13.162 Å) in **1**, ($\text{Co}\cdots\text{Co}$, 13.098 Å) in **2** and ($\text{Zn}\cdots\text{Zn}$, 13.091 Å) in **5** are almost comparable, and larger than ($\text{Cu}\cdots\text{Cu}$, 11.946 Å) **4**.

2.3.4 TGA analysis

To investigate the thermal stability of compounds **1-6**, the thermogravimetric analyses were carried out under N₂ atmosphere with a heating rate of 10 °C min⁻¹ from 30 °C to 900 °C (Fig. 2.13). **1** is stable upto 188 °C then a weight loss of 7.4% is occurred at 188-245 °C due to the loss of coordinating water molecules. The framework shows stability at 245-300 °C without the coordinated water molecules. On further heating, the framework begins to decompose, with the slow release of the organic spacer, untill 750 °C. The reaming weight (12.3%, calcd 12.2%) can be attributed to manganese oxide. The TGA profiles of **2** and **5** are comparable with **1**. Compound **2** shows stability upto 133 °C and **5** shows stability upto 164 °C. The first weight loss (at 133-215 °C with a weight loss of 7.5% for **2** and at 164-213 °C with weight loss of 6.3% for **5**) can be contributed to the loss of coordinated water molecules. Although compounds **2** and **5** are stable upto 300 °C, further heating results in the break-down of the lattice structures by releasing the coordinated organic ligand.

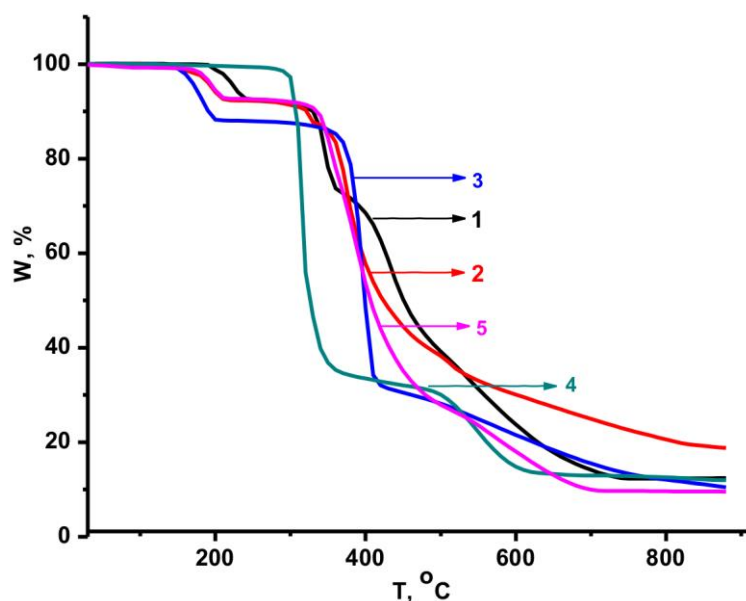


Figure 2.13: TGA curves for compounds 1-5.

The TGA profile of **3** revealed the stability of molecule up to 134 °C and about 11.7% weight loss is observed from 134 to 216 °C, which can be assigned to the loss of four coordinated water molecules. Compound **3** shows zero weight loss from 216 to 334 °C, then the major weight loss (54.6%) is observed till 442 °C, followed by a gradual weight

loss. The thermal history of **4** reveals the absence of solvent molecules (stable up to 300 °C). Subsequently, the major weight loss is observed in two stages, one starting at 300 °C and ending at 377 °C (65% weight loss) and then 380 °C to 620 °C (20.4% weight loss), which are attributed to the decomposition of the organic spacer. After 620 °C, the residue (13.7%) is due to copper oxide (calcd 14.3%). The TGA of **6** was not clear.

2.4 Conclusion

In summary, the first systematic study has been carried out on a series of late transition metals using a new semi rigid imidazolium carboxylate spacer (**LH₂Br**). The zwitterionic manganese, cobalt, nickel, copper, zinc and cadmium coordination polymers **1-6** were isolated using **LH₂Br**. Molecules **1**, **2** and **5** were isostructural 1D coordination polymers. Molecule **3** was isolated as rare nickel 3D supramolecular hydrogen bonded network through O–H···O hydrogen bonding between free rigid carboxylic groups of **LH₂Br** and coordinated water molecules. Molecule **6** was constructed as a two dimensional coordination polymer consisting of a [CdBr]₂ unit bridged by the ligand.

2.5 References

- [1] K. S. Jeong, Y. B. Go, S. M. Shin, S. J. Lee, J. Kim, O. M. Yaghi, and N. Jeong. *Chem. Sci.* 2, (2011) 877.
- [2] L. J. Murray, M. Dincă, and J. R. Long. *Chem. Soc. Rev.* 38, (2009) 1294.
- [3] J. A. Mason, M. Veenstra, and J. R. Long. *Chem. Sci.* 5, (2014) 32.
- [4] J. Heine, and K. M-Buschbaum. *Chem. Soc. Rev.* 42, (2013) 9232.
- [5] A. Shigematsu, T. Yamada, and H. Kitagawa. *J. Am. Chem. Soc.* 133, (2011) 2034.
- [6] M. Kurmoo. *Chem. Soc. Rev.* 38, (2009) 1353.
- [7] Z. Yin, Q.-X. Wang and M.-H. Zeng. *J. Am. Chem. Soc.* 134, (2012) 4857.
- [8] (a) F. A. A. Paz, J. Klinowski, S. M. F. Vilela, J. P. C. Tomé, J. A. S. Cavaleiro, and J. Rocha. *Chem. Soc. Rev.* 41, (2012) 1088; (b) N. Stock, and S. Biswas. *Chem. Rev.* 112, (2012) 933.
- [9] (a) M. Garai, and K. Biradha. *Chem. Commun.* 50, (2014) 3568; (b) B. L. Schottel, H. T. Chifotides, M. Shatruk, A. Chouai, L. M. Pérez, J. Bacsá, and K. R. Dunbar, *J. Am. Chem. Soc.* 128, (2006) 5895.

- [10] O. Köhl. *Functionalised N-heterocyclic carbene complexes*. Wiley, New York, 2010.
- [11] J. A. Mata, M. Poyatos, and E. Peris. *Coord. Chem. Rev.* 251, (2007) 841.
- [12] R. E. Douthwaite. *Coord. Chem. Rev.* 251, (2007) 702.
- [13] W. J. Sommer, and M. Weck. *Coord. Chem. Rev.* 251, (2007) 860.
- [14] (a) P. Wasserscheid, and W. Keim. *Angew. Chem., Int. Ed.* 39, (2000) 3772; (b) Z. Fei, and P. J. Dyson. *Chem. Commun.* 49, (2013) 2594.
- [15] L.-A. Schaper, S. J. Hock, W. A. Herrmann, and F. F. Kühn. *Angew. Chem., Int. Ed.* 52, (2013) 270.
- [16] (a) G.-Q. Kong, S. Ou, C. Zou, and C.-D. Wu. *J. Am. Chem. Soc.* 134, (2012) 19851; (b) Z. Fei, D. Zhao, T. J. Geldbach, R. Scopelliti, P. J. Dyson, S. Antonijevic, and G. Bodenhausen. *Angew. Chem., Int. Ed.* 44, (2005) 5720; (c) S. Sen, N. N. Nair, T. Yamada, H. Kitagawa, and P. K. Bharadwaj. *J. Am. Chem. Soc.* 134, (2012) 19432; (d) J. Y. Lee, J. M. Roberts, O. K. Farha, A. A. Sarjeant, K. A. Scheidt, and J. T. Hupp. *Inorg. Chem.* 48, (2009) 9971; (e) G.-Q. Kong, X. Xu, C. Zou, and C.-D. Wu. *Chem. Commun.* 47, (2011) 11005.
- [17] (a) Z. Fei, W. H. Ang, T. J. Geldbach, R. Scopelliti, and P. J. Dyson. *Chem. Eur. J.* 12, (2006) 4014; (b) Z. Fei, T. J. Geldbach, D. Zhao, R. Scopelliti, and P. J. Dyson. *Inorg. Chem.* 44, (2005) 5200; (c) Z. Fei, T. J. Geldbach, R. Scopelliti, and P. J. Dyson. *Inorg. Chem.* 45, (2006) 6331; (d) L. Han, S. Zhang, Y. Wang, X. Yan, and X. Lu. *Inorg. Chem.* 48, (2009) 786; (e) X.-C. Chai, Y.-Q. Sun, R. Lei, Y.-P. Chen, S. Zhang, Y.-N. Cao, and H.-H. Zhang. *Cryst. Growth Des.* 10, (2010) 658; (f) X.-W. Wang, L. Han, T.-J. Cai, Y.-Q. Zhang, J.-Z. Chen, and Q. Deng. *Cryst. Growth Des.* 7, (2007) 1027; (g) X.-C. Chai, H.-H. Zhang, S. Zhang, R. Lei, Y.-P. Chen, Y.-Q. Sun, R.-Q. Sun, and Q.-Y. Yang. (*Jiegou Huaxue*) Chinese. *J. Struct. Chem.* 28, (2009) 1343.
- [18] S. Sen, T. Yamada, H. Kitagawa, and P. K. Bharadwaj. *Cryst. Growth Des.* 14, (2014) 1240.
- [19] (a) J. Chun, G. Jung, H. J. Kim, M. Park, M. S. Lah, and S. U. Son. *Inorg. Chem.* 48, (2009) 6353; (b) J. Chun, H. S. Lee, G. Jung, S. W. Lee, H. J. Kim, and S. U. Son. *Organometallics* 29, (2010) 1518; (c) S. Wang, Q. Yang, J. Zhang, X. Zhang, C. Zhao, L. Jiang, and C.-Y. Su. *Inorg. Chem.* 52, (2013) 4198; (d) G. Nickerl, A. Notzon, M. Heitbaum, I. Senkowska, F. Glorius, and S. Kaskel. *Cryst. Growth Des.* 13, (2013) 198; (e) O. Köhl, and G. Palm. *Tetrahedron: Asym.* 21, (2010) 393; (f) C. N. Babu, A. Sathyanarayana, S. M. Mobin, and G. Prabusankar. *Inorg. Chem.*

- Commun. 37, (2013) 222; (g) X. Wang, X.-B. Li, R.-H. Yan, Y.-Q. Wang, and E.-Q. Gao. Dalton Trans. 42, (2013) 10000; (h) R. S. Crees, M. L. Cole, L. R. Hanton, and C. J. Sumbly. Inorg. Chem. 49, (2010) 1712; (i) J. M. Roberts, O. K. Farha, A. A. Sarjeant, J. T. Hupp, and K. A. Scheidt. Cryst. Growth Des. 11, (2011) 4747; (j) K. Oisaki, Q. Li, H. Furukawa, A. U. Czaja, and O. M. Yaghi. J. Am. Chem. Soc. 132, (2010) 9262; (k) B. Wang, J. Li, G. Li, L. Zhu, and G. Bao. Syn. React. Inorg., Metal-Organic, and Nano-Metal Chem. 38, (2008) 750; (l) G.-Q. Kong, and C.-D. Wu. CrystEngComm 14, (2012) 847; (m) Z. Yang, C. Wang, X. Cao, C. Wang, and G. Li. Syn. React. Inorg., Metal-Organic, and Nano-Metal Chem. 41, (2011) 1039; (n) L. Huang, A.-G. Zhong, D.-B. Chen, D. Qiu, and H.-D. Liang. J. Mol. Struct. 984, (2010) 39; (o) G. Nickerl, A. Notzon, M. Heitbaum, I. Senkowska, F. Glorius, and S. Kaskel. Cryst. Growth Des. 13, (2013) 198.
- [20] D. D. Perrin, and W. L. F. Armarego. Purification of laboratory chemicals. third ed., Pergamon Press, London, 1988.
- [21] (a) P. Suresh, S. Radhakrishnan, C. N. Babu, A. Sathyanarayana, N. Sampath, and G. Prabusankar. Dalton Trans. 42, (2013) 10838; (b) J. Liu, J. Chen, J. Zhao, Y. Zhao, L. Li, and H. Zhang. Synthesis 17, (2003) 2661.
- [22] O. V. Dolomanov, L. J. Bourhis, R. J. Gildea, J. A. K. Howard, and H. Puschmann. J. Appl. Cryst. 42, (2009) 339.
- [23] (a) L. Fan, X. Zhang, W. Zhang, Y. Ding, W. Fan, L. Sun, Y. Panga, and X. Zhao. Dalton Trans. 43, (2014) 6701; (b) J. Cui, Y. Li, Z. Guo, and H. Zheng, Cryst. Growth Des. 12, (2012) 3610; (c) W. Wang, W.-Q. Kan, J. Yang, and J.-F. Ma, CrystEngComm 15, (2013) 3824; (d) Y. Yang, P. Du, J. Yang, W.-Q. Kan, and J.-F. Ma. CrystEngComm 15, (2013) 4357.
- [24] G.-Q. Kong, and C.-D. Wu. CrystEngComm 44, (2012) 847.
- [25] X.-H. Jin, J.-K. Sun, L.-X. Cai, and J. Zhang. Chem. Commun. 47, (2011) 2667.

Chapter 3

Luminescent Imidazolium Carboxylate Supported Aggregate and Infinite Coordination Networks of Copper and Zinc

3.1 Introduction

The higher level of structural tailorability including size- and morphology-dependent properties of infinite coordination polymers (ICPs) or metal-organic frameworks (MOFs) have triggered magnificent attention in the past decades as smart materials. Functional properties of ICPs or MOFs can be carefully tuned up by the various combinations of appropriate metal salts and functional organic spaces [1]. The successful strategy in the design of ICPs and MOFs is the use of functionalized organic spacers. Among a variety of ligands employed for syntheses of ICPs or MOFs, carboxylate functionalized imidazolium organic spacers is one of the most promising chelating ligands because of the extraordinary binding affinity toward most metal ions, together with the pre-N-heterocyclic carbene centers for the wide range of applications. Furthermore, the introduction of the N-heterocyclic carbene centers into molecular network and successive complexation with particular metal ions could lead to tuneable catalytic properties. Several such examples of imidazolium carboxylate supported 1D, 2D and 3D coordination networks were synthesized and pre-/post-modifications were also performed [2,3]. For instance, the first post modified 2D MOF and its application in Suzuki–Miyaura cross-coupling reaction was demonstrated using semi-flexible carboxy-functionalized bis-imidazolium spacers such as $[\{1,1'\text{-CH}_2\text{-}3,3'\text{-(C}_6\text{H}_4\text{-}4\text{-CO}_2\text{H)}_2\}\{(\text{HCN})_2\text{CH}\}_2]\text{Cl}_2$ (**I**) by Wu *et al.* in 2011 (Fig. 3.1) [4]. Subsequently, the same spacer with a methyl substituent on the phenyl group, $[\{1,1'\text{-CH}_2\text{-}3,3'\text{-(C}_6\text{H}_3\text{-}2\text{-Me-}4\text{-CO}_2\text{H)}_2\}\{(\text{HCN})_2\text{CH}\}_2]\text{Cl}_2$ (**II**) (Fig. 3.1), resulted in the formation of a higher

dimensional MOF, which allowed post-modification for the generation of highly active catalysts for a number of reactions, including Suzuki–Miyaura and Heck cross-coupling reactions, hydrogenation of olefins, and reduction of nitrobenzene [5]. Similarly, the semi-rigid bisazoliums spacer such as, biphenyl dicarboxylate based linker with appended bis-methyl imidazolium salts (**III**) was also employed to design a 2D MOF (NU-502) (Fig. 3.1) [6].

Nevertheless, to the best of our knowledge there have been no attempts to develop materials with luminescence and optoelectronic properties using azolium spacers [2c,7]. On the basis of these findings, the complexation of the luminescence bisazoliums spacer incorporated in MOFs would easily enable the phototunable MOFs and ICPs. Bearing all these in mind, we report here our initial results on three dimensional coordination frameworks of copper, $\{[(\mathbf{L})_2\text{Cu}(\text{H}_2\text{O})_2]_2(\text{Br})_2\}_\infty$ (**5**) and zinc, $\{[(\mathbf{L})_2\text{Zn}(\text{H}_2\text{O})_2]_2(\text{Br})_2\}_\infty$ (**6**) including discrete copper dimer, $\{[(\mathbf{L})\text{Cu}(\text{DMF})]_2(\text{NO}_3)_4(\text{H}_2\text{O})(\text{DMF})_2\}$ (**4**) using a flexible bis-carboxy imidazolium anthracene spacer, $\mathbf{LH}_2\mathbf{Br}_2$ (**3**).

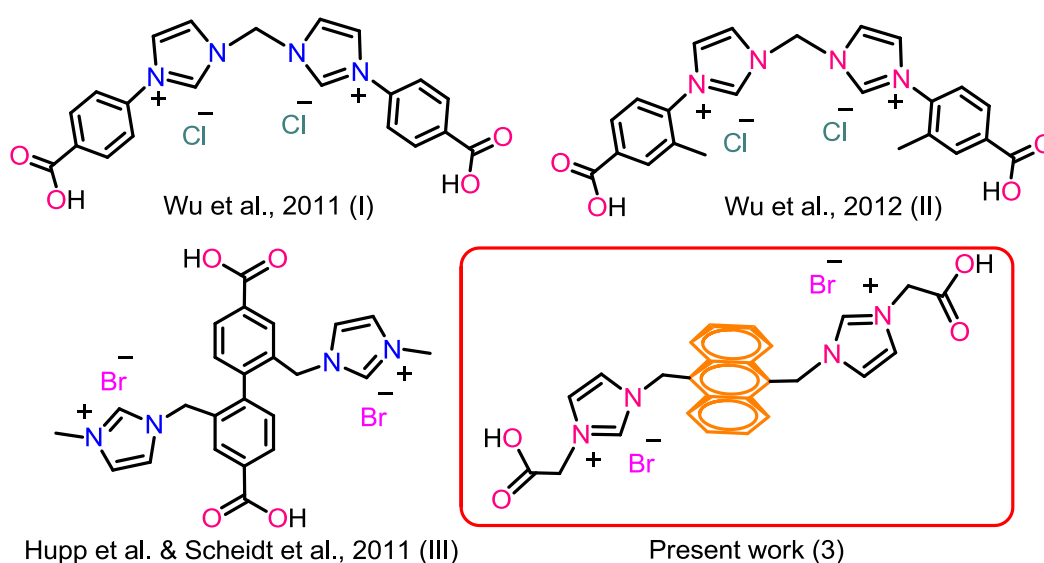


Figure 3.1: Known bis-azolium carboxylate spacers that are employed for MOF synthesis.

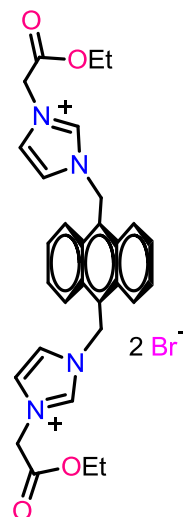
3.2 Experimental Section

3.2.1 Materials and methods

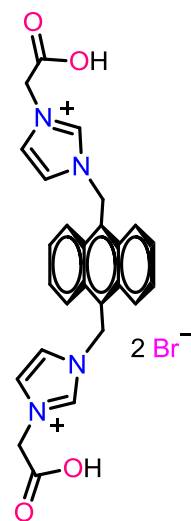
The solvents were purchased from commercial sources and purified according to standard procedures [8]. Unless otherwise stated, the chemicals were purchased from commercial sources. [9,10-Bis{(imidazol)methyl}anthracene] (**1**) was prepared as previously reported [9]. FT-IR measurement (neat) was carried out on a Bruker Alpha-P Fourier transform spectrometer. NMR spectra were recorded on Bruker Ultrashield-400 spectrometers at 25 °C unless otherwise stated. Chemical shifts are given relative to TMS and were referenced to the solvent resonances as internal standards. Thermogravimetric analysis (TGA) was performed using a TA-SDT Q600, Tzeropress. The UV-vis spectra were measured on a T90+ UV-visible spectrophotometer. The fluorescent spectra were measured on a Fluoromax-4P TCSPC, Horiba Scientific spectrophotometer. Elemental analyses were performed by the Euro EA Elemental Analysis. The crystal structure of **2** and **4-6** were measured on an Oxford Xcalibur 2 diffractometer. Data were collected at 150 K. The structure of **2** was solved by direct methods using the SIR-97 program [10] and refined with a full matrix least-squares method on F^2 using the SHELXL-97 program [11,12]. Using Olex2, [13] the structures, **4-6** were solved with the Superflip [14] structure solution program using Charge Flipping and refined with the olex2.refine [15] refinement package using Gauss-Newton minimisation. In molecule **4**, approximately 8.3% (142 \AA^3) of the unit cell volume comprises of two heavily disordered molecular fragments which could not be modelled as discrete atomic sites, were "squeezed" out with the program "Platon 1.13" [16]. The estimated total count of 75 electrons per unit cell could be attributed to the two nitrate ions per unit cell. Moreover the actual formula of **4** ($\text{C}_{64}\text{H}_{74}\text{N}_{16}\text{O}_{24}\text{Cu}_2$ /MW: 1578.46), which was calculated based on the elemental analysis data concords well with the crystallographic chemical formula weight including the squeezed nitrate ions. In molecule **6**, approximately 10% (66 \AA^3) of the unit cell volume comprises a disordered molecular fragment, which could not be modelled as discrete atomic site, was "squeezed" out with the program "Platon 1.13" [16]. The estimated 39 electrons per unit cell could be attributed to a bromide ion per unit cell. Besides, the final formula ($\text{C}_{26}\text{H}_{28}\text{N}_4\text{O}_6\text{ZnBr}_2$ / M.W: 717.71) obtained from the elemental analysis data matches well with the mass of squeezed disordered bromide ion from the unit cell. CCDC 924620-924623 contains the supplementary crystallographic data for this paper. These data can be obtained free of charge from the Cambridge Crystallographic Data Centre via www.ccdc.cam.ac.uk/data_request/cif or from the Cambridge Crystallographic Data Centre, 12 Union Road, Cambridge CB2 1EZ, UK; fax: +44 1223 336 033; or e-mail: deposit@ccdc.cam.ac.uk.

3.2.2 Synthesis of 2–6

L(C₂H₅)₂Br₂ (2): A mixture of compound **1** (0.5 g, 1.48 mmol) and ethyl 2-bromoacetate (0.493 g, 2.95 mmol) in acetone (10 mL) was refluxed for 16 h. The solvent was filtered using cannula and solid was washed with acetone (10 mL) and diethyl ether (10 mL). The resultant was subsequently dissolved in water (10 mL) and filtered. The solvent was removed under reduced pressure and dried under high vacuum. Yield: 80% (based on **1**). Elemental analysis calcd. (%) for C₃₀H₃₂N₄O₄Br₂ (672.40): C, 53.59; H, 4.80; N, 8.33; Found: C, 53.7; H, 4.7; N, 8.4. ¹H NMR (400 MHz, DMSO-d₆): δ = 9.05 (s, 2H, ImH), 8.65-8.62 (dd, 4H, AnH), 7.85 and 7.79 (s, 2 x 2H, ImH), 7.77-7.75 (dd, 4H, AnH), 6.70 (s, 4H, AnCH₂N), 5.19 (s, 4H, CH₂), 4.11 (q, 4H, CH₂), 1.14 (t, 6H, CH₃) ppm. ¹³C NMR (100 MHz, DMSO-d₆): δ = 166.5 (C=O), 136.73 (ImC), 130.49, 127.63, 126.83, 124.49 (AnC), 123.86, 122.31 (ImC), 61.63 (OCH₂), 49.48 (AnCH₂N), 45.01 (CH₂), 13.75 (CH₃) ppm. FT-IR (neat): $\bar{\nu}$ = 2970 (w), 2931 (w), 1739 (s), 1552 (m), 1220 (s), 1152 (s), 1015 (s) cm⁻¹.



LH₂Br₂ (3): 17.5% HCl aqueous solution (30 mL) was added to **2** (0.8 g, 1.19 mmol) and refluxed for 3 h. The solution was removed under reduced pressure and the remaining solid was washed with acetone (10 mL) and diethyl ether (10 mL). The resultant solid was subsequently dissolved in MeOH (20 mL) and filtered. The solvent was removed under reduced pressure and dried under high vacuum. Yield: 73% (based on **2**). Elemental analysis calcd. (%) for C₂₆H₂₄N₄O₄Br₂ (616.30): C, 50.67; H, 3.93; N, 9.09; Found: C, 50.8; H 4.0; N 9.1. ¹H NMR (400 MHz, D₂O): δ = 8.32 (s, 2H, ImH), 8.06-8.04 (dd, 4H, AnH), 7.69-7.67 (dd, 4H, AnH), 7.35 and 7.30 (s, 2 x 2H, ImH), 5.82 (s, 4H, AnCH₂N), 4.79 (s, 4H, CH₂) ppm. ¹³C NMR (100 MHz, D₂O): δ = 169.85 (C=O), 136.29 (ImC), 129.82, 128.02, 125.15, 123.65 (AnC), 123.59, 121.99 (ImC), 50.10 (AnCH₂N), 44.81 (CH₂) ppm. FT-IR (neat): $\bar{\nu}$ = 3316 (br), 3037 (w), 2881 (w), 2919 (w), 2828 (w), 1713 (s), 1552 (m), 1402 (m), 1241 (m), 1182 (m), 1152 (s) cm⁻¹.



{[(L)Cu(DMF)]₂(NO₃)₄(H₂O)(DMF)₂} (**4**): **3** (0.050 g, 0.081 mmol) and Cu(NO₃)₂·3H₂O (0.039 g, 0.162 mmol) were taken into a Schlenk tube and DMF (2 mL) added. The reaction mixture was heated at 100 °C under stirring condition for 2 h and filtered into a sample vial. After one week bluish green crystals were formed and washed with EtOH and dried under vacuum. Yield: 26% (based on **3**). Elemental analysis calcd. (%) for C₆₄H₇₄N₁₆O₂₄Cu₂ (1576.76): C, 48.76; H, 4.60; N, 14.22; Found: C, 48.3; H, 4.5; N, 14.0. ¹H NMR (400 MHz, D₂O): δ = 8.51 (s, 2 x 2H, ImH and s, 2 x 4H, AnH), 7.93 (s, 2 x 4H, AnH), 7.55 (s, 2 x 4H, ImH), 6.52-6.51 (d, 2 x 4H, AnCH₂N), 4.79 (s, 2 x 4H, CH₂), 3.04, 2.88, 2.73 (s, N(CH₃)₂) ppm. ¹³C NMR (100 MHz, D₂O): δ = 165.44 (C=O, DMF coordinated), 165.30 (C=O), 136.48 (ImC), 130.05, 128.02, 125.42, 123.73 (AnC), 121.92, 121.87 (ImC), 44.82 (AnCH₂N), 34.50 (CH₂), 36.99 (DMFCH₃), 31.44 (DMFCH₃) ppm. FT-IR (neat): $\bar{\nu}$ = 3088 (w), 1640 (s), 1564 (w), 1445 (w), 1316 (s), 1154 (m), 1101 (m) cm⁻¹.

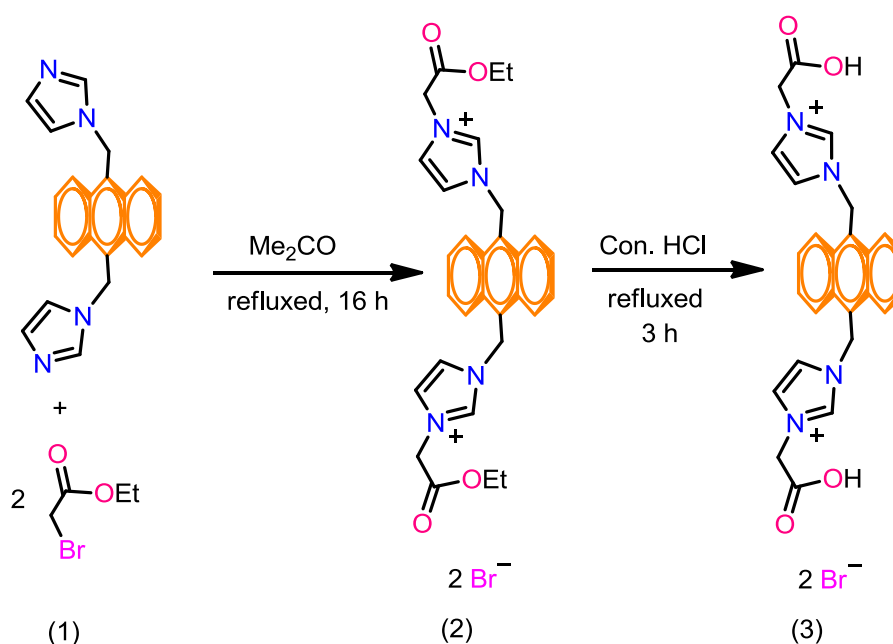
{[(L)₂Cu(H₂O)₂]₂(Br)₂}_∞ (**5**): Compound **3** (0.050 g, 0.081 mmol) was dissolved in water (3 mL) in the sample vial and the pH was maintained at 7 using 1 M NaOH aqueous solution. After that EtOH (1 mL) was added, subsequently Cu(NO₃)₂·3H₂O (0.039 g, 0.162 mmol) in EtOH (2 mL) was added slowly through a corner of the sample vial and a few drops of MeOH. Light green crystals were formed between the layers within 24 h then the reaction mixture was stored for 4 to 5 days and during this period the yellow colour disappeared. The crystals were washed with ethanol and dried under vacuum. Yield: 53% (based on **3**). Elemental analysis calcd. (%) for C₂₆H₂₈N₄O₆CuBr₂ (715.88): C, 43.62; H, 3.94; N, 7.83; Found: C, 43.6; H, 4.0; N, 7.9. ¹H NMR (400 MHz, D₂O and DMSO-d₆): δ = 8.23 (s, 2H, ImH), 8.16 (s, 4H, AnH), 7.73 (s, 4H, AnH), 7.28 (s, 4H, ImH), 5.96 (s, 4H, AnCH₂N), 4.79 (s, 4H, CH₂) ppm. ¹³C NMR (100 MHz, D₂O and DMSO-d₆): Due to very poor solubility of **5**, complete data set was not observed. δ = 136.27 (ImC), 130.08, 128.02, 125.45, 123.75 (AnC), 121.99 (ImC), 44.88 (AnCH₂N) ppm. FT-IR (neat): $\bar{\nu}$ = 3089 (w), 3032 (w), 1601 (s), 1554 (m), 1392 (s), 1313 (m), 1153 (s) cm⁻¹.

{[(L)₂Zn(H₂O)₂]₂(Br)₂}_∞ (**6**): Mixture of compound **3** (0.025g, 0.040 mmol) and elemental Zn (0.006 g, 0.091 mmol) in water (5 mL) was stirred for seven days at room temperature. The reaction mixture was filtered and light yellow crystals were formed through slow evaporation of the solution after two weeks at room temperature. The

crystals were washed with MeOH and dried under vacuum. Yield: 62% (based on **3**). Elemental analysis calcd. (%) for $C_{26}H_{28}N_4O_6ZnBr_2$ (717.71): C, 43.51; H, 3.93; N, 7.81; Found: C, 43.4; H, 4.0; N, 7.8. 1H NMR (400 MHz, D_2O): δ = 8.29 (s, 2H, ImH), 8.16-8.14 (m, 4H, AnH), 7.73-7.71 (m, 4H, AnH), 7.32 and 7.27 (s, 2 x 2H, ImH), 5.95 (s, 4H, AnCH₂N), 4.56 (s, 4H, CH₂) ppm. ^{13}C NMR (100 MHz, D_2O): δ = 171.96 (C=O), 135.94 (ImC), 129.96, 128.03, 125.33, 123.72 (AnC), 123.60, 121.78 (ImC), 51.88 (AnCH₂N), 44.77 (CH₂) ppm. FT-IR (neat): $\bar{\nu}$ = 3093 (w), 3037 (w), 1603 (s), 1565 (m), 1444 (m), 1398 (s), 1312 (m), 1159 (s) cm^{-1} .

3.3 Results and discussion

3.3.1 Synthesis and characterization



Scheme 3.1: Synthesis of $L(C_2H_5)_2Br_2$ (2**) and LH_2Br_2 (**3**).**

Compound **2** was synthesized from reaction of 9,10-bis(imidazol-1-ylmethyl)anthracene (**1**) and ethyl 2-bromoacetate in acetone under refluxing condition (Scheme 3.1). Subsequently compound **3** was synthesized from the acid hydrolysis of compound **2**. Compound **2** is more soluble than **3** in polar solvents like H_2O , MeOH and DMSO and insoluble in nonpolar solvents, chloro solvents and acetone. The bluish green crystals of compound **4** were obtained from the reaction between $Cu(NO_3)_2 \cdot 3H_2O$ and **3** in DMF at

100 °C for 2 h (Scheme 3.2). The light green crystals of compound **5** were derived from $\text{Cu}(\text{NO}_3)_2 \cdot 3\text{H}_2\text{O}$ and **3** in H_2O , EtOH and MeOH mixture at room temperature in the presence of NaOH for 1–5 days. The light yellow crystals of compound **6** were formed *via* a direct reaction of elemental Zn and **3** in water at room temperature. Compounds **4**, **5** and **6** are insoluble in common organic solvents and poorly soluble in H_2O . Compounds **2–6** were characterized by a FT-IR, multinuclear (^1H and ^{13}C) NMR, UV-vis and fluorescent spectroscopy. The FT-IR spectrum of **2** shows a characteristic peak for the C=O stretching frequency at 1739 cm^{-1} , while the unionized and uncoordinated carboxylic acid stretching frequency for compound **3** appeared at 1713 and 3316 cm^{-1} .

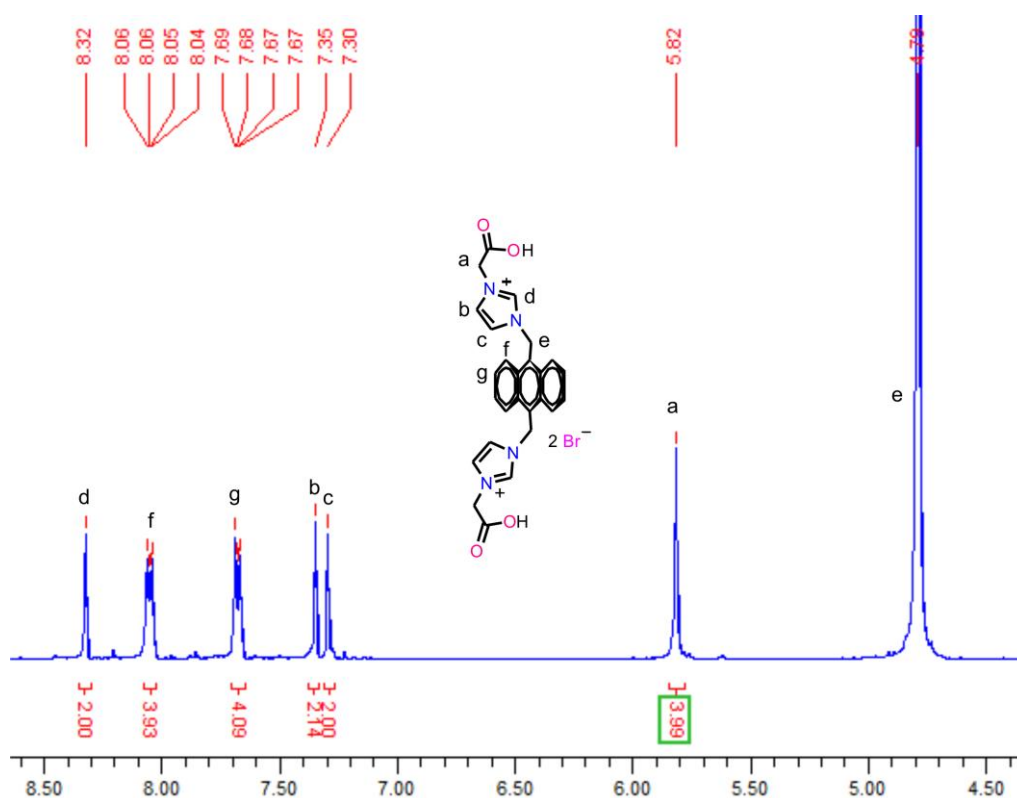


Figure 3.2: ^1H NMR spectrum of **3** in D_2O at RT.

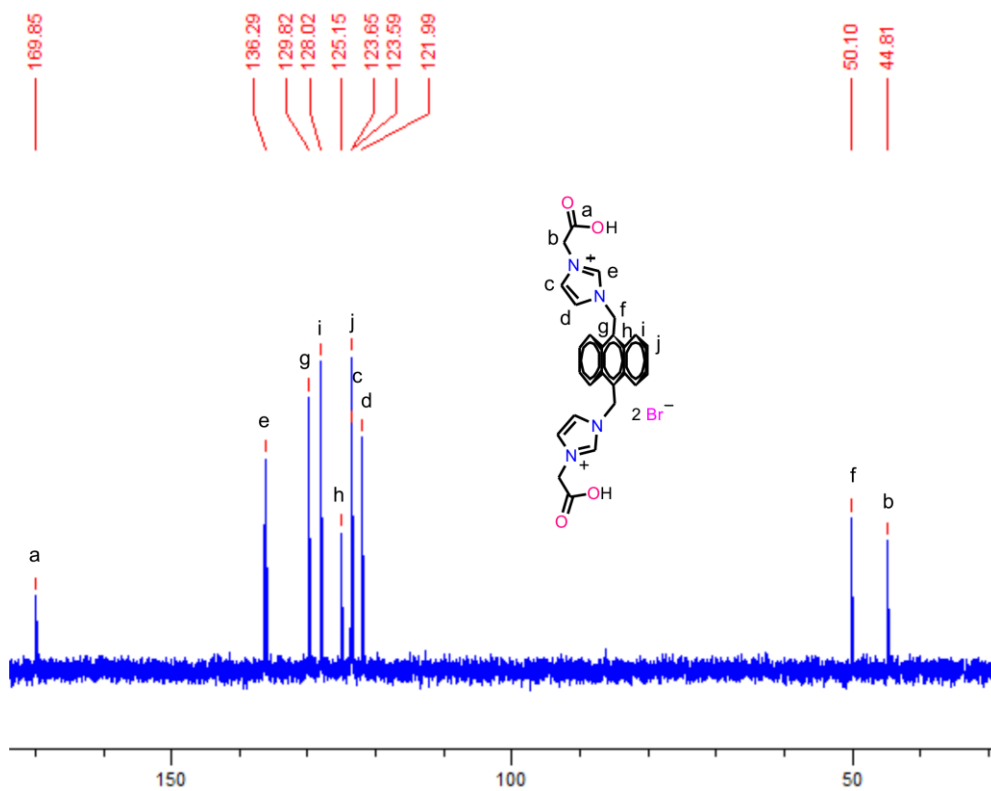


Figure 3.3: ^{13}C NMR spectrum of 3 in D_2O at RT.

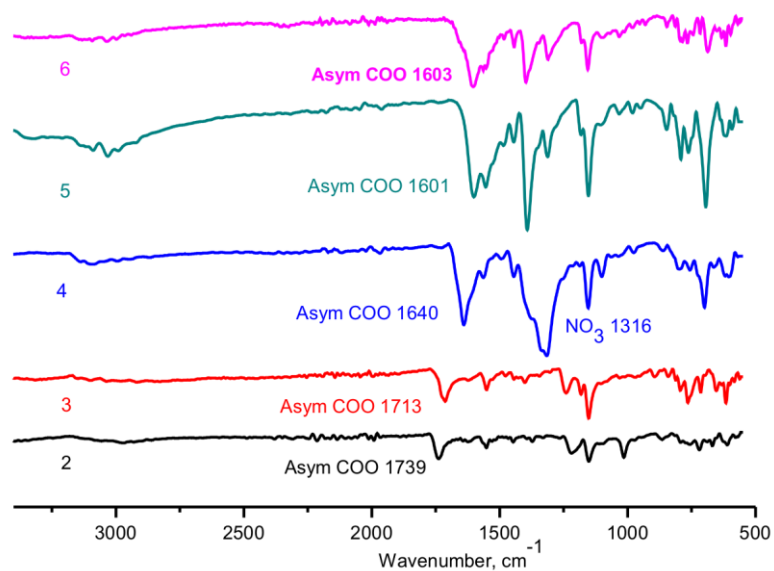
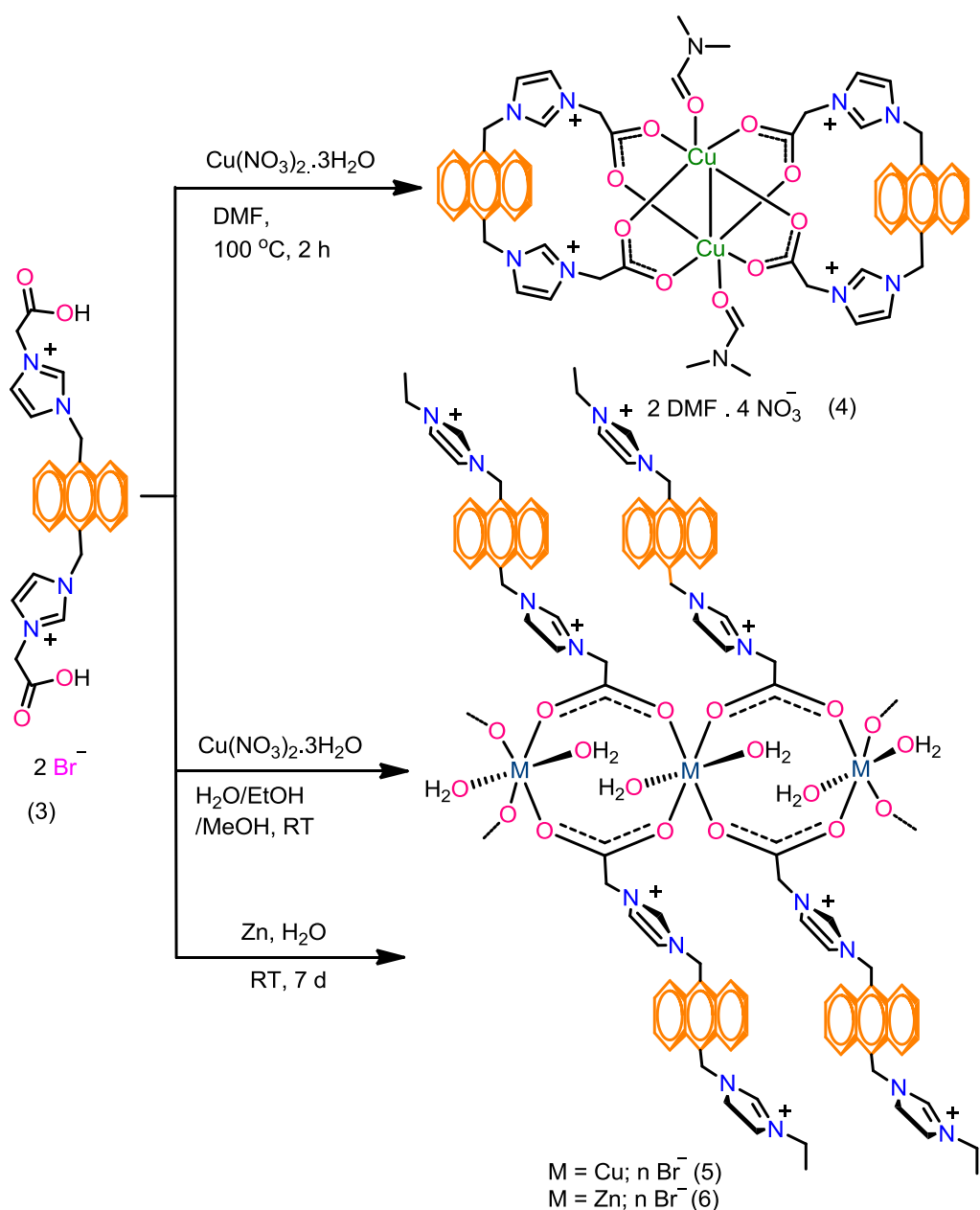


Figure 3.4: FT-IR (neat) spectrum of 2–6.



Scheme 3.2: Synthesis of $\{[(\text{L})\text{Cu}(\text{DMF})_2(\text{NO}_3)_4(\text{H}_2\text{O})(\text{DMF})_2]\}$ (**4**), $\{[(\text{L})_2\text{Cu}(\text{H}_2\text{O})_2]_2(\text{Br})_2\}_\infty$ (**5**) and $\{[(\text{L})_2\text{Zn}(\text{H}_2\text{O})_2]_2(\text{Br})_2\}_\infty$ (**6**)

The presence of bridging carboxylate moieties in **4–6** were confirmed by a decrease in the stretching frequency of the carbonyl group (Fig 3.4). The C=O stretching frequency of **4–6** were about 73 to 110 cm^{-1} lower than **3**. The presence of free NO_3^- ions and solvent molecules in **4–6** were also witnessed by FT-IR. For example the FT-IR vibrations of NO_3^- ions in **4** appeared at 1316 cm^{-1} . In ^1H NMR, the N–CH–N proton of **2** is downfield shifted (δ 9.05 ppm) compare to that of **3** (δ 8.32 ppm). The ^{13}C NMR

chemical shift value of C=O and N-CH-N carbons are virtually comparable (δ 166.5, 136.73 for **2** and 169.85, 136.29 ppm for **3**) in **2** and **3** (Fig. 3.2 and Fig. 3.3). The ^1H NMR spectra of **4-6** have diagnostic peaks corresponding to the N-CH-N proton in the range of δ 8.29–8.51 ppm, which are also comparable with **3** (δ 8.32 ppm).

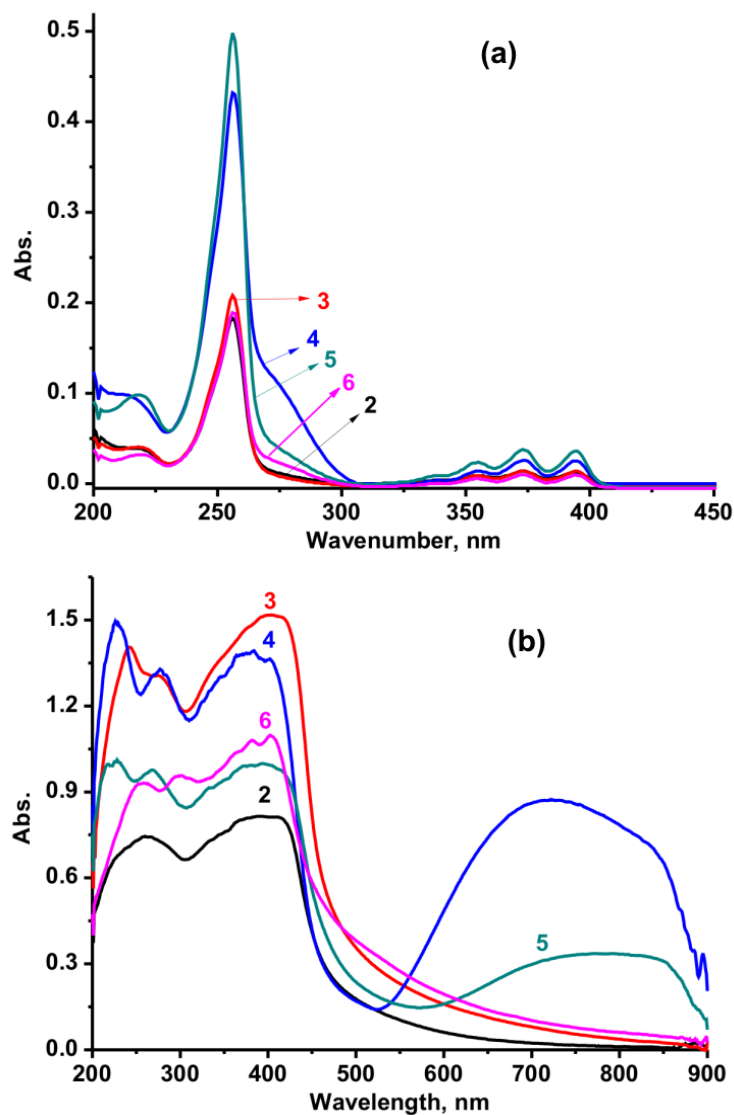


Figure 3.5: (a) The UV-vis absorption spectra of **2-6** in water at RT (1.6×10^{-6} M). (b) The solid-state UV-vis absorption spectra of **2-6**.

UV-visible absorption spectra of **2-6** were measured in water at room temperature and displayed a nearly comparable absorption pattern at 256, 355, 373 and 394 nm (Fig. 3.5). Upon complexation of Cu(II) to **3** as shown in Fig. 3.5a, the increase in the absorption peak at 256 nm was observed, while it was not increased much for zinc (**6**),

with its iso-bestic point at 306 nm. The enhancement of absorption maximum at 256 nm is attributable to stronger coordinative interactions between **3** and Cu(II). The solid-state UV-visible absorption spectra of **2–6** were significantly different from that of solution (Fig. 3.5b). A broad absorption peak from 200 to 450 nm in the solid-state UV-visible absorption spectra of **2–6** were attributed to the π to π^* transition of ligand. In the solid-state UV-visible absorption spectra, the π to π^* transition intensity is decreased in the order of **3**, **4**, **5**, **6** and **2**. In addition, a broad absorption peak from 525 to 900 nm is observed for **4** and **5** in the solid-state UV-visible absorption study.

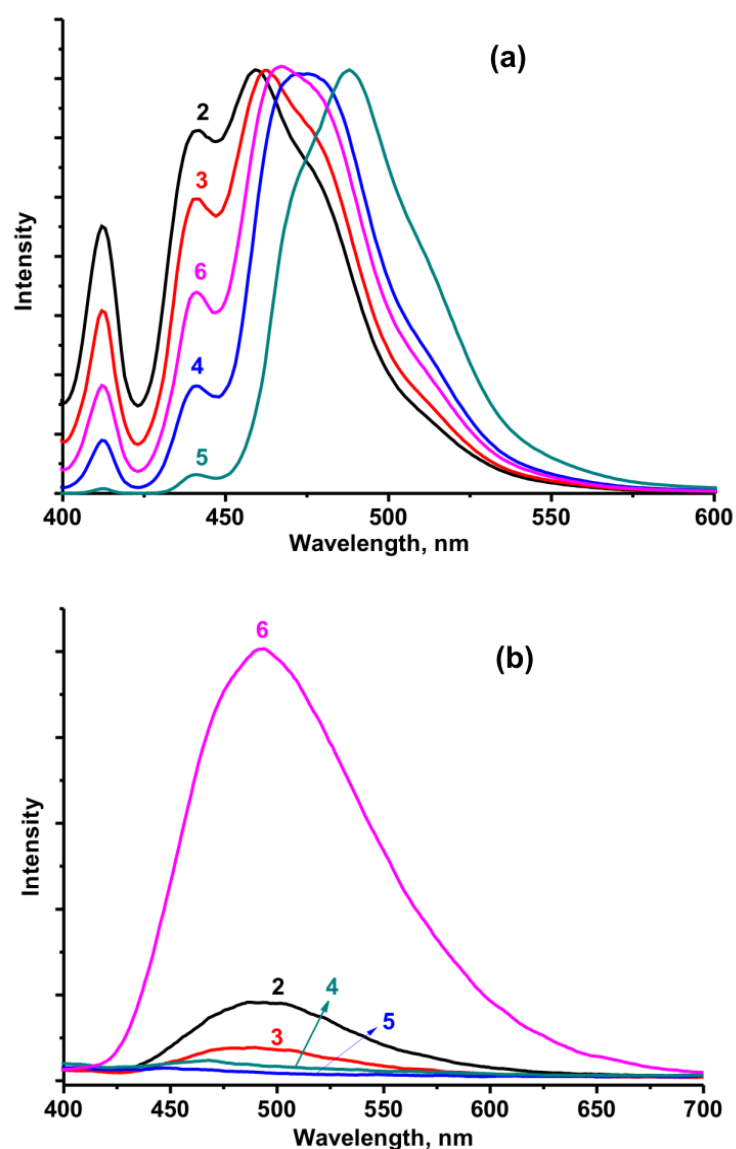


Figure 3.6: (a) The fluorescent spectra of **2–6** in water at RT with excitation wavelength of 370 nm (1.6×10^{-6} M). (d) The solid-state fluorescent spectra of **2–6**.

The fluorescent emission spectra of **2–6** were measured in water at an excitation wave length of 370 nm, in which every band has typically three sets of emission wavelengths in the 412, 441 and 459–488 nm regions (Fig. 3.6a). The emission is indicative of ligand-based intramolecular charge transfer (ICT) character. In 412 and 441 nm regions, a gradual decrease in the emission intensity is observed in the following order of **2, 3, 6, 4,** and **5**. Notably the third set of fluorescent emission maxima of **2–6** are in the range of 459–488 nm wavelengths, in which the emission maxima of **2** is 459 nm, while the emission maximum shifts towards a longer wavelength from **3** (462), **6** (467), **4** (472) to **5** (488 nm). In the 459–488 nm wavelength region, compound **2–6** exhibits almost the same peak intensity. The solid-state fluorescent emission spectra of **2–6** were measured at excitation wave length of 370 nm, in which the intensity of **6** is much stronger than **2–5** (Fig. 3.6b). Moreover, the fluorescent emission spectral intensity of **2–6** in the solid-state and solution state is distinctly different.

3.3.2 Crystal structural description of **2** and **4–6**

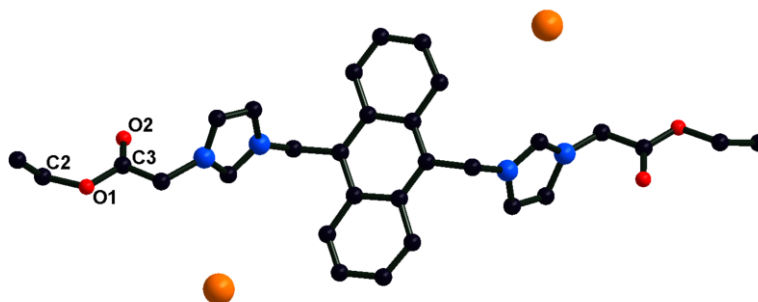


Figure 3.7: Structure of molecule 2. Hydrogen atoms have been omitted for clarity. Selected bond lengths [Å] and angles [°]: C(2)–O(1) 1.478(6), C(3)–O(2) 1.189(6), C(3)–O(1) 1.300(5), O(2)–C(3)–O(1) 125.3(4).

Single crystal X-ray structure of $L(C_2H_5)_2Br_2$ (2**):** The solid state structure of **2** was further confirmed by single crystal X-ray diffraction (Fig. 3.7). Compound **2** crystallized in the triclinic space group $P\bar{1}$. Selected bond lengths and bond angles are listed in the caption of Fig. 3.7. Compound **2** is crystalized with two bromide ions. The solid state structure of **2** reveals that the charge of imidazolium ion is balanced by bromide ion; the width and length of **2** are measured as nearly 7 Å and 15 Å, respectively. Packing diagram of molecule **2** shown in Fig. 3.8. The molecules were packed one by another as a slipped manner along the *a*-diagonal plane (Fig. 3.8). The

similar pattern of packing was observed in metal complexes **5** and **6**, which are discussed in detail at their following crystallographic description.

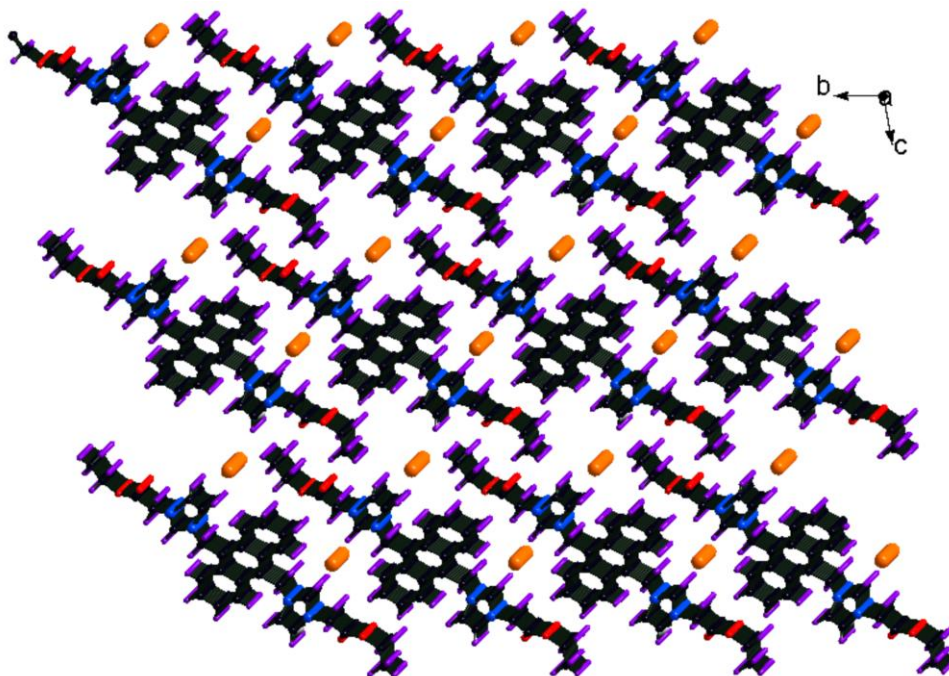


Figure 3.8: Packing diagram of molecule 2.

Table 3.1: Summary of crystallographic data and structure refinement results for **2** and **4**

Parameters	2	4
Empirical formula	C ₃₀ H ₃₂ Br ₂ N ₄ O ₄	C ₃₂ H ₃₆ CuN ₇ O ₉
Formula weight	672.42	726.22
Temperature (K)	150	150(2)
Crystal system	Triclinic	Triclinic
Space group	<i>P</i> $\bar{1}$	<i>P</i> $\bar{1}$
<i>a</i> /Å	4.6681(2)	11.5604(7)
<i>b</i> /Å	11.6004(7)	12.3073(8)

$c/\text{\AA}$	13.7298(8)	13.3623(8)
α°	99.221(5)	78.556(5)
β°	93.928(4)	80.590(5)
γ°	96.670(4)	67.806(6)
Volume (\AA^3)	726.04(7)	1717.1(2)
Z	1	2
$\rho_{\text{calc}}/\text{mg mm}^{-3}$	1.538	1.405
Absorption coefficient (mm^{-1})	3.888	1.435
$F(000)$	342	756
Data collected,	4648	7888
Unique data	2735	6472
R_{int}	0.0519	0.0258
GOF on F^2	1.090	1.046
$R_1 (I > 2\sigma(I))$	0.0546	0.0553
$wR_2 (I > 2\sigma(I))$	0.1554	0.1601
R_1 values (all data)	0.0569,	0.0628
wR_2 values (all data)	0.1576	0.1658

Table 3.2: Summary of crystallographic data and structure refinement results for **5** and **6**

Parameters	5	6
Empirical formula	$\text{C}_{26}\text{H}_{26}\text{Br}_{0.5}\text{CuN}_4\text{O}_6$	$\text{C}_{13}\text{H}_{13}\text{Br}_{0.5}\text{N}_2\text{O}_3\text{Zn}_{0.5}$
Formula weight	594.00	317.89

Temperature (K)	150	150(2)
Crystal system	Triclinic	Triclinic
Space group	<i>P</i> $\bar{1}$	<i>P</i> $\bar{1}$
<i>a</i> /Å	4.5328(5)	4.5284(4)
<i>b</i> /Å	11.3109(12)	11.4135(9)
<i>c</i> /Å	13.2988(14)	13.2801(11)
α °	77.560(9)	78.119(7)
β °	82.903(9)	83.978(7)
γ °	84.026(9)	84.959(7)
Volume (Å ³)	658.61(12)	666.42(10)
<i>Z</i>	1	2
$\rho_{\text{calc}}/\text{mg mm}^{-3}$	1.498	1.584
Absorption coefficient (mm ⁻¹)	2.466	3.445
<i>F</i> (000)	305	323
Data collected	4147	4525
Unique data	2429	2505
<i>R</i> _{int}	0.0293	0.0355
GOF on <i>F</i> ²	1.057	1.033
<i>R</i> ₁ (<i>I</i> > 2σ(<i>I</i>))	0.0693	0.0671
w <i>R</i> ₂ (<i>I</i> > 2σ(<i>I</i>))	0.2095	0.1991
<i>R</i> ₁ values (all data)	0.0794	0.0761
w <i>R</i> ₂ values (all data)	0.2201	0.2115

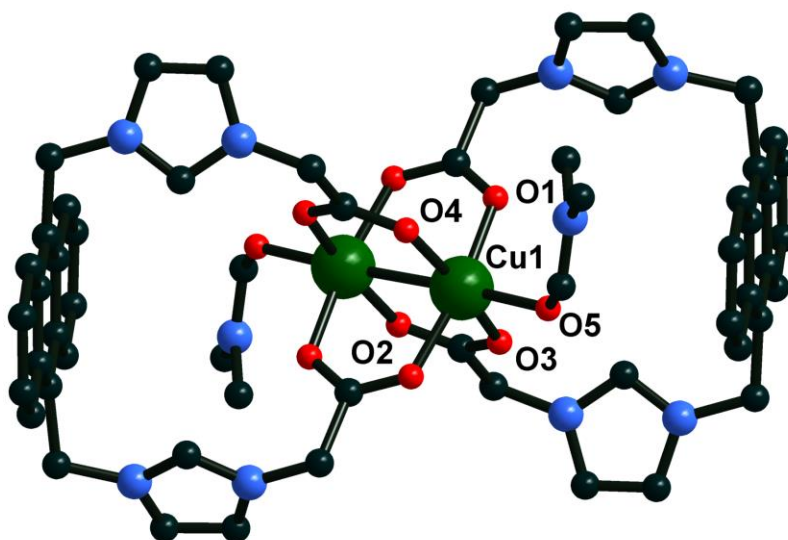


Figure 3.9: Structure of the Cu dimer **4**. Hydrogen atoms, NO_3^- and DMF have been omitted for clarity.

Single crystal X-ray structure of $\{[(\text{L})\text{Cu}(\text{DMF})]_2(\text{NO}_3)_4(\text{H}_2\text{O})(\text{DMF})_2\}$ (4**):**

Compound **4** crystallizes in the triclinic space group, $P\bar{1}$. Data collection parameters are listed in Table 3.1. Molecule **4** is a tetra cationic copper dimer with a ‘‘paddle-wheel’’ structure, which represent the first example of a tetracationic copper dimer (Fig. 3.9). The asymmetric unit of this molecule contains one copper atom, one carboxylate anions **3**, one coordinated molecule of DMF, one uncoordinated molecule of DMF and one uncoordinated NO_3^- anion. In addition one of the heavily disordered uncoordinated NO_3^- anions is excluded for the refinement. The coordination environment around each copper is fulfilled by four carboxylate moieties of two **3** and oxygen atoms of DMF. In each copper centre, the four carboxylate oxygen atoms are arranged nearly in the basal plane while the oxygen atoms of DMF and a Cu(II) centre are in the apical position. The core structure of **4** is comparable with that of $[\text{Cu}(\text{O}_2\text{CPh})_2(\text{DMF})]_2$ [17] and $[\text{Cu}(\text{O}_2\text{CPh-N}_{3-p})_2(\text{DMF})]_2$ [18].

The Cu(1)–Cu(2) bond length is 2.6614(8) Å, which is slightly longer than that of $[\text{Cu}(\text{O}_2\text{CPh})_2(\text{DMF})]_2$ (2.63 Å), $[\text{Cu}(\text{O}_2\text{CPh-N}_{3-p})_2(\text{DMF})]_2$ (2.6366 (5) Å) and copper(II) acetate (2.64 Å) [19]. The different copper–carboxylate oxygen bond distances around Cu(1) and Cu(2) are observed. The Cu(1)– O_{COO} bond lengths are in the range from 1.961(2) to 1.981(2) Å. The carboxylate C–O bond lengths are in the range between 1.253(4)–1.261(4) Å. Notably, the Cu(1)– $\text{O}(5)_{\text{DMF}}$ bond length (2.144(2) Å) is longer than that of Cu(1)– O_{COO} . The $\text{OOC-O-Cu(1)-O}_{\text{COO}}$ angle falls in the range of

118.8(3)° to 127.5(3)°. Therefore, the overall structural features of **4** are slightly different from the known similar class of neutral copper carboxylate dimers, [Cu(O₂CPh)₂(DMF)]₂ and [Cu(O₂CPh-N_{3-p})₂(DMF)]₂.

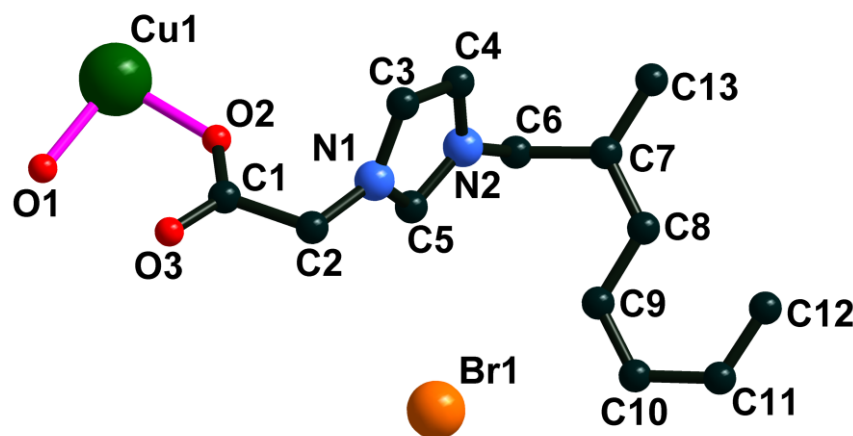


Figure 3.10: Structure of the asymmetric unit of **5**. Hydrogen atoms have been omitted for clarity.

Single crystal X-ray structure of $\{[(L)_2Cu(H_2O)_2]_2(Br)_2\}_\infty$ (5**):** Compound **5** crystallizes in the triclinic space group with *P*₁. Data collection parameters and selected bond lengths and angles are given in Table 3.2 and 3.3, respectively. The asymmetric unit of **5** contains one copper atom, a half anthracene imidazolium carboxylate anion **3** and a bromide ion (Fig. 3.10). The structure comprises a two-dimensional (2D) slipped packing along the *a*-diagonal plane as shown Fig. 3.11, in which the [Cu(H₂O)₂] units are connected by the anthracene imidazolium carboxylate ligand, **3**. The bromide ions are packed in alternative sequences between the layers. The major interaction in the crystal packing is C–H⋯Br in nature (Fig. 3.11). These interactions occur pairwise, and link the porous sheets into the framework. The C–H⋯Br interactions in **5** originate from both N(N)CH (2.598 Å) and alkyl chain hydrogens (2.698 Å). The distance between Br⋯Br centres within the layer is 4.533 Å. Each copper atom adopts a distorted octahedral coordination environment, which is formed by four oxygen atoms (O(2), O(3), O(2') and O(3')) from two carboxylate anions of **3** and two oxygen atoms (O(1) and O(1')) from the water. The carboxylate anions display bidentate bridging coordination modes that results in the formation of a nonplanar eight membered ring which consists of [Cu–O–C–O]₂, which are linked through anthracene imidazolium spacers. The bond distances between copper and oxygen atoms of carboxylate group are

not equal. The axial contact, Cu(1)–O(3) (2.448(4) Å), is longer than those in the basal plane Cu(1)–O(1) (1.970(4)) and Cu(1)–O(2) (1.961(4) Å). Similarly the C(1)–O(2) bond distance (1.271(6) Å) is longer than C(1)–O(3) (1.246(6) Å). The distance between two copper atoms within the layer is 4.533 (5) Å, while the Cu⋯Cu separation between the layer is 11.311(12) Å. The shortest O–Cu–O angle is observed for O(2′)–Cu–O(1) (85.72(16)°). The structural pattern of **5** can be comparable with the recently reported $\{[\text{La}_2(\text{dbtz})_3(\text{H}_2\text{O})_2](\text{H}_2\text{O})_6\}_n$ (dbtz = 3,3′-(1,2,4,5-tetrazine-3,6-diy)ldibenzoate) [20].

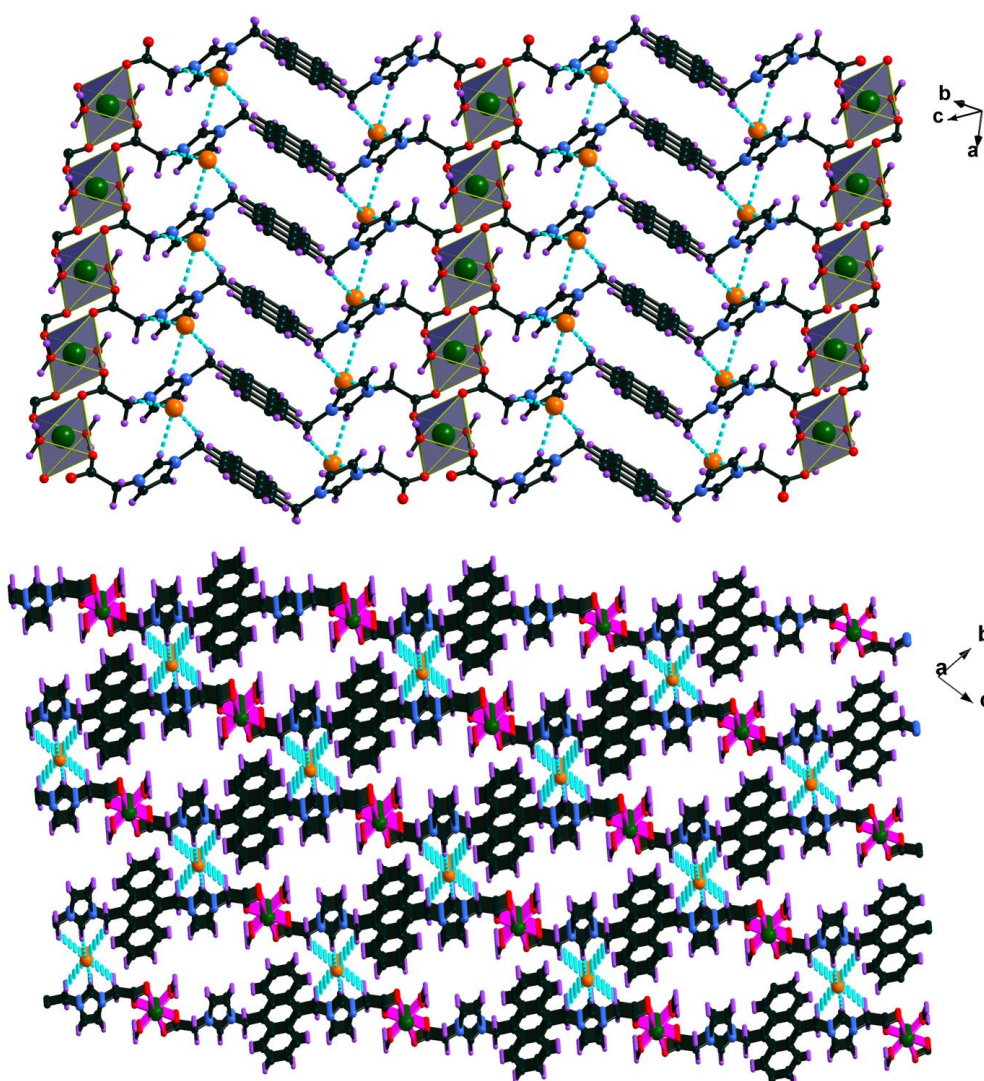


Figure 3.11: Top: A view of the 2D layer of **5**, where polyhedra represent CuO₆; Bottom: A close view of the hydrogen bonding between the neighboring 2D layer in **5** viewed along the *a* axis showing the 3D framework by hydrogen bonding between Br and C–H groups.

Table 3.3: Selected bond lengths and angles of **5** and **6**

Bond lengths [Å]			
	5		6
Cu1–O1	1.970(4)	Zn1–O1	2.055(4)
Cu1–O2	1.961(4)	Zn1–O2	2.169(4)
Cu1–O3	1.246(6)	Zn1–O3	2.092(5)
O2–C1	1.271(6)	O2–C1	1.249(8)
O3–C1	1.246(6)	O2–C1 ¹	1.263(7)

Bond angles [°]			
O2 ¹ –Cu1–O1 ¹	94.28(16)	O2 ¹ –Zn1–O1 ¹	89.01(17)
O2 ¹ –Cu1–O1	85.72(16)	O2 ¹ –Zn1–O1	90.99(17)
O3 ² –Cu1–O1	87.37(15)	O3 ¹ –Zn1–O1	86.53(19)
O3 ² –Cu1–O1 ¹	92.62(15)	O3 ¹ –Zn1–O1 ¹	93.47(19)
O3 ² –Cu1–O2 ¹	88.46(14)	O3 ¹ –Zn1–O2 ¹	92.45(18)
O3 ² –Cu1–O2	91.53(14)	O3 ¹ –Zn1–O2	87.55(18)
O3–C1–O2	127.5(5)	O2–C1–O1 ³	127.0(6)

Single crystal X-ray structure of $\{[(L)_2Zn(H_2O)_2]_2(Br)_2\}_\infty$ (6**):** Compound **6** crystallizes in the triclinic space group *P*₁. Data collection parameters and selected bond lengths and angles are presented in Tables 3.2 and 3.3, respectively. The single crystal X-ray structure of **6** is isostructural with **5** (Fig. 3.12). Thus, **6** has not been discussed in detail. However, the structural parameters of **5** and **6** are significantly different. In **6**, the C(1)–O(1) (1.249(8) Å) and C(1²)–O(2) (1.263(7) Å) bond distance are nearly comparable. The coordination geometry of Zn is octahedral. As with **5**, hydrogen bonds are observed between the N(N)CH groups of the imidazolium cations and alkyl CH groups, with bromide ions acting as hydrogen bond acceptors. These hydrogen bonds link the two-dimensional coordination polymers into a three-dimensional network (Fig. 3.13). However, C–H \cdots Br bond nature of **6** is significantly different to **5**. The C–H \cdots Br bond distances in **6** falls in the narrow range of 2.675 to 2.779 Å. The distance between Br \cdots Br centres within the layer is 4.528 Å. The Zn(1)–O(1) bond distance (2.055(4) Å) in **6** is considerably shorter than the Zn(1)–O(2) (2.169(4) Å). The Zn \cdots Zn separation in **6** is 4.528 Å (within the layer) and 11.413 Å (between adjacent layers).

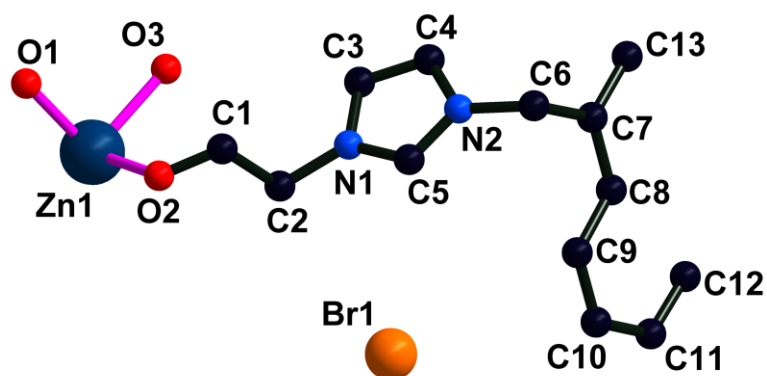


Figure 3.12: Structure of the asymmetric unit of **6**. Hydrogen atoms have been omitted for clarity.

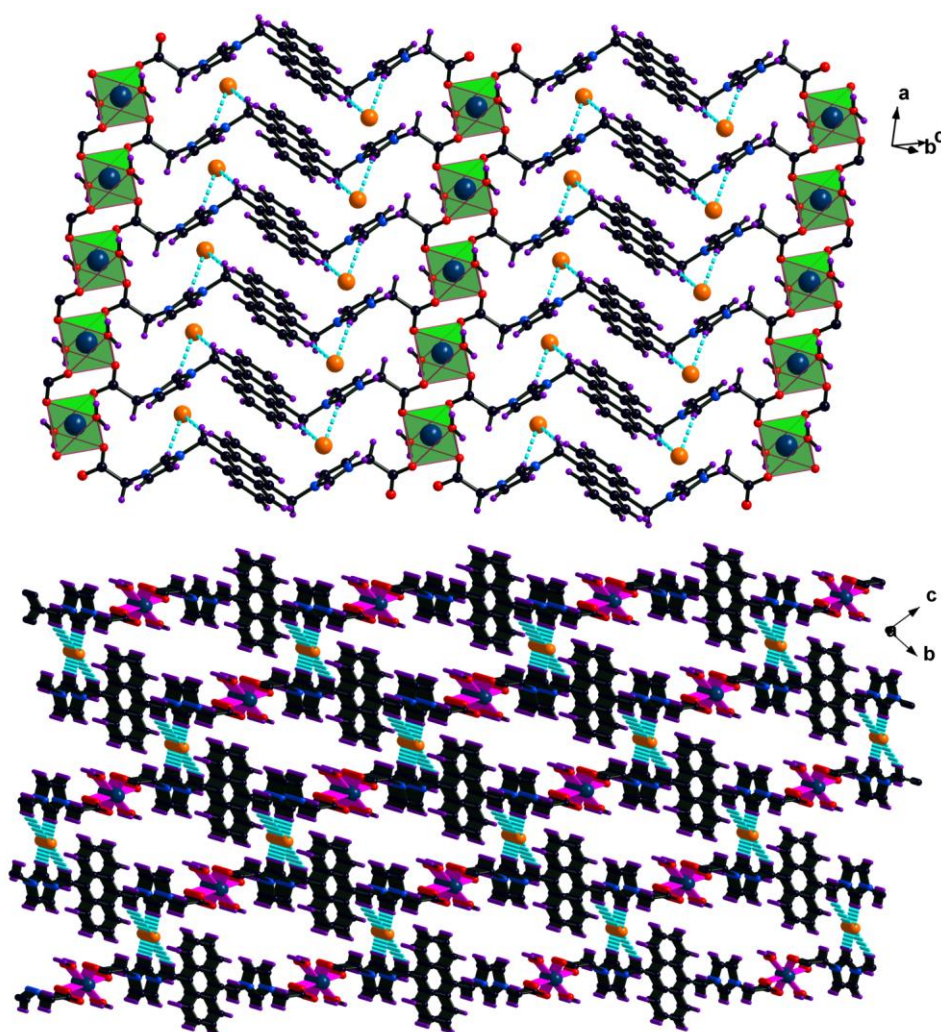


Figure 3.13: Top: A view of the 2D layer of **6** where polyhedral represent ZnO_6 ; Bottom: A close view of the hydrogen bonding between the neighboring 2D layer in **6** viewed along the a -axis showing the 3D framework by hydrogen bonding between Br and C–H groups.

3.3.3 TGA analysis

In order to understand the thermal decomposition pathway of **2–6**, thermogravimetric analysis (TGA) (10 °C/min, 30–1000 °C, under N₂ atmosphere) was carried out on **2–6** (Fig. 3.14). A small weight loss about 2–8% was observed for **2–6** in the initial stage (<80 °C), attributable to the loss of moisture. TGA profile of **2** and **3** are nearly comparable, however the thermal stability of **3** (stable up to 238 °C with 8% weight loss) is relatively higher than **2** (stable up to 196 °C with 6% weight loss). The complete decomposition (0% residue) of **2** and **3** occurred through two steps within 673 °C and 782 °C, respectively.

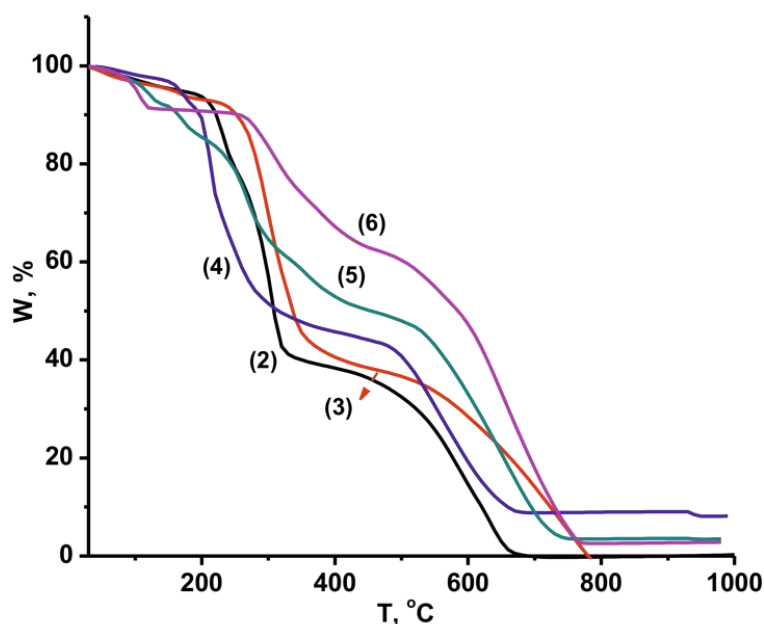


Figure 3.14: TGA curves for compounds 2-6.

In spite of having DMF, water and nitro groups, the thermal history of **4** shows enough stability up to 154 °C (with 4% weight loss) then the major weight loss occurred with two well defined intervals of weight loss, one starting at 154 °C and ending at 476 °C (with 53% weight loss) and then 480 °C to 685 °C (with 34% weight loss), attributable to decomposition of ligand, solvent molecules and nitro groups. The TGA profile of **5** reveals the gradual weight loss from beginning to 516 °C (53%) then the second weight loss up to 774 °C (43%) due to the combustion of organic spacers and Br⁻. Unlike **5**, the TGA profile of **6** shows a much earlier weight loss from 84–129 °C (8%) then a major

weight loss was detected from 248 to 489 °C followed by continues weight loss upto 784 °C (89%, for evacuation of the Br⁻ and organic part).

3.4 Conclusions

In conclusion, a novel flexible biscarboxy imidazolium anthracene spacer **3** was successfully synthesized, and it efficiently underwent complexation with metal ions to result in the hydrogen bonded three dimensional coordination networks of copper (**5**) and zinc (**6**) including the discrete copper dimer (**4**). Molecules **4–6** represent the first example of the luminescent imidazolium carboxylate supported metal rich assemblies. The NMR, UV-vis, and fluorescent data clearly display the smooth formation of **4–6**. The thermal stability of **2–6** was studied by TGA. Molecule **4** is one of the rare examples of a tetracationic copper dimer, where the copper centres are bridged by the carboxylate groups and the cationic charges on the copper-carboxylate aggregate is balanced by the presence of four nitrate anions. Furthermore, two isostructural 3D copper and zinc MOFs **5** and **6** were built from the corresponding Cu(NO₃)₂·3H₂O or zinc powder. The solid state structure of **5** and **6** consists of an infinite weakly bonded three dimensional network having luminescent carboxylate linkers connected to metal atoms, which are interconnected by C–H···Br interactions to form a 3D framework structure.

3.5 References

- [1] (a) K. Sanderson. *Nature* 448, (2007) 746; (b) L. Brunsveld, B. J. B. Folmer, E. W. Meijer, and R. P. Sijbesma. *Chem. Rev.* 101, (2001) 4071; (c) S. Kitagawa, R. Kitaura, and S.-I. Noro. *Angew. Chem., Int. Ed.* 43, (2004) 2334; (d) R. D. Archer. *Coord. Chem. Rev.* 128, (1993) 49; (e) J. M. Lehn. *Angew. Chem., Int. Ed. Engl.* 27, (1988) 89; (f) J. R. Long, and O. M. Yaghi. *Chem. Soc. Rev.* 38, (2009) 1213; (g) N. Stock, and S. Biswas. *Chem. Rev.* 112, (2012) 933.
- [2] (a) Z. Fei, T. J. Geldbach, R. Scopelliti, and P. J. Dyson. *Inorg. Chem.* 45, (2006) 6331; (b) X.-W. Wang, L. Han, T.-J. Cai, Y.-Q. Zheng, J.-Z. Chen, and Q. Deng. *Cryst. Growth Des.* 7, (2007) 1027; (c) G.-Q. Kong, and C.-D. Wu. *CrystEngComm* 14, (2012) 847; (d) J. Chun, G. Jung, H. J. Kim, M. Park, M. S. Lah, and S. U. Son. *Inorg. Chem.* 48, (2009) 6353; (e) J. Y. Lee, J. M. Roberts, O. K. Farha, A. A.

- Sarjeant, K. A. Scheidt, and J. T. Hupp. *Inorg. Chem.* 48, (2009) 9971; (f) L. Han, S. Zhang, Y. Wang, X. Yan, and X. Lu. *Inorg. Chem.* 48, (2009) 786; (g) S. Sen, N. N. Nair, T. Yamada, H. Kitagawa, and P. K. Bharadwaj. *J. Am. Chem. Soc.* 134, (2012) 19432; (h) X.-C. Chai, Y.-Q. Sun, R. Lei, Y.-P. Chen, S. Zhang, Y.-N. Cao, and H.-H. Zhang. *Cryst. Growth Des.* 10, (2010) 658; (i) J. Chun, H. S. Lee, G. Jung, S. W. Lee, H. J. Kim, and S. U. Son. *Organometallics* 29, (2010) 1518; (j) Z. Fei, T. J. Geldbach, D. Zhao, R. Scopelliti, and P. J. Dyson. *Inorg. Chem.* 44, (2005) 5200; (k) B. Wang, J. Li, G. Li, L. Zhu, and G. Bao. *Synth. React. Inorg., Met.–Org., Nano–Met. Chem.* 38, (2008) 750; (l) Z. Fei, W. H. Ang, T. J. Geldbach, R. Scopelliti, and P. J. Dyson. *Chem.–Eur. J.* 12, (2006) 4014; (m) Z. Fei, D. Zhao, T. J. Geldbach, R. Scopelliti, P. J. Dyson, S. Antonijevic, and G. Bodenhausen. *Angew. Chem., Int. Ed.* 44, (2005) 5720; (n) R. S. Crees, M. L. Cole, L. R. Hanton, and C. J. Sumbly. *Inorg. Chem.* 49, (2010) 1712.
- [3] K. Oisaki, Q. Li, H. Furukawa, A. U. Czaja, and O. M. Yaghi. *J. Am. Chem. Soc.* 132, (2010) 9262.
- [4] G.-Q. Kong, X. Xu, C. Zou, and C.-D. Wu. *Chem. Commun.* 47, (2011) 11005.
- [5] G.-Q. Kong, S. Ou, C. Zou, and C.-D. Wu. *J. Am. Chem. Soc.* 134, (2012) 19851.
- [6] J. M. Roberts, O. K. Farha, A. A. Sarjeant, J. T. Hupp, and K. A. Scheidt. *Cryst. Growth Des.* 11, (2011) 4747.
- [7] Y. Cui, Y. Yue, G. Qian, and B. Chen. *Chem. Rev.* 112, (2012) 1126.
- [8] D. D. Perrin, and W. L. F. Armarego. *Purification of laboratory chemicals*. 3rd edition. Pergamon Press, London, 1988.
- [9] P. P. Neelakandan, and D. Ramaiah. *Angew. Chem., Int. Ed.* 47, (2008) 8407.
- [10] SHELXS-97, Program for structure solution: G. M. Sheldrick, Phase annealing in SHELX-90: direct methods for larger structures. *Acta Crystallogr., Sect. A: Found. Crystallogr.* 46, (1990) 467.
- [11] G. M. Sheldrick, SHELXL-97, Program for Crystal Structure Refinement, Universität Göttingen, Göttingen, 1997.
- [12] P. van der Sluis, and A. L. Spek, BYPASS: an effective method for the refinement of crystal structures containing disordered solvent regions. *Acta Crystallogr., Sect. A: Found. Crystallogr.* 46, (1990) 194.
- [13] O. V. Dolomanov, L. J. Bourhis, R. J. Gildea, J. A. K. Howard, and H. Puschmann, OLEX2: a complete structure solution, refinement and analysis program. *J. Appl. Crystallogr.* 42, (2009) 339.
- [14] SUPERFLIP. *J. Appl. Crystallogr.* 40, (2007) 786.

- [15] olex2.refine (L. J. Bourhis, O. V. Dolomanov, R. J. Gildea, J. A. K. Howard, and H. Puschmann, 2011).
- [16] A. L. Spek. *Acta Crystallogr., Sect. A: Fundam. Crystallogr.* 46, (1990) C34.
- [17] R. E. D. Sesto, A. M. Arif, and J. S. Miller. *Inorg. Chem.* 39, (2000) 4894.
- [18] A. Wang. *Acta Crystallogr., Sect. E: Struct. Rep. Online.* 68, (2012) m43.
- [19] (a) J. van Niekerk, and F. Schoening. *Acta Crystallogr.* 6, (1953) 227; (b) W. Bateman, and D. Conrad. *J. Am. Chem. Soc.* 37, (1915) 2553; (c) J. Lewis, Y. Lin, L. Royston, and R. Thompson. *J. Chem. Soc.* (1965) 6464.
- [20] A. J. Calahorro, A. Peñas-Sanjuan, M. Melguizo, D. Fairen-Jimenez, G. Zaragoza, B. Fernández, A. Salinas-Castillo, and A. Rodríguez-Diéguez. *Inorg. Chem.* 52, (2013) 546.

Chapter 4

Imidazolium Carboxylate Based Ionic Calcium Coordination Polymers and Discrete Molecules with Diversified Calcium Coordination geometry

4.1 Introduction

The key strategy to design the functional porous coordination polymers (PCPs) or metal-organic frameworks (MOFs) for a specific application has been well documented, which allows better understanding of their structural-physicochemical relationships [1,2]. Most of the PCPs/MOFs are constructed using multidentate rigid aromatic bridging ligands, such as aromatic multicarboxylate ligands [3-6]. Of late, the azolium carboxylate linkers with a flexible backbone have been widely used in construction of coordination frameworks [7,8], owing to their versatility in both structural and $[\text{C-H}]^{\delta+}$ functional aspects. The first azolium carboxylate coordination polymer was reported by Dyson *et al.* in 2005 using an ionic imidazolium carboxylate linker [8]. The bio-inspired supramolecular network of one-dimensional water chains (comparable to the water chains present in aquaporin channels) was trapped by the helical channels of a zinc zwitterionic tubular coordination polymer $[(\text{ZnBr}(\text{H}_2\text{O})_4(\mathbf{BCI}))(\text{H}_2\text{O})]_{\infty}$, \mathbf{BCI} = 1,3-bis(carboxymethyl)-imidazolium, derived from reaction between N,N'-diacetic acid, imidazolium bromide and zinc. Later, the high proton conductivity of the zinc- \mathbf{BCPI} MOF, \mathbf{BCPI} = 1,3-bis(4-carboxyphenyl)imidazolium Chloride was demonstrated, where the methylene protons of imidazolium group played an important role to conduct protons [9]. Recently, we have reported the first photoluminescent ionic zinc and copper

imidazolium carboxylate coordination polymers using a luminescent imidazolium carboxylate ligand [10a].

Collective efforts by a number of groups have expanded the metal-azolium carboxylate chemistry to provide a variety of routes toward desired PCPs/MOFs. Nevertheless, the imidazolium carboxylate supported coordination assemblies constructed from lighter alkaline-earth metals have been understudied [11-13] in comparison to the plethora of examples of d-block-based imidazolium carboxylate assemblies [7-10a,14-16], perhaps due to their unpredictable geometries, coordination numbers and limited reactivity.

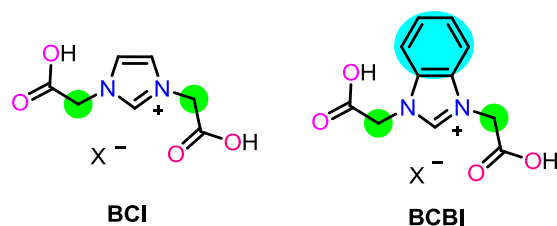


Figure 4.1: The structure of 1,3-bis(carboxymethyl)imidazolium (**BCI**) and 1,3-bis(carboxymethyl)benzimidazolium (**BCBI**) salts.

The first *s*-block coordination chemistry of imidazolium carboxylate was explored by Dyson *et al.* in 2005 [11]. The two-dimensional strontium-imidazolium carboxylate polymer, $\{[\text{Sr}(\mathbf{BCI}')_2(\text{H}_2\text{O})_4]\}_\infty$, $\mathbf{BCI}' =$ zwitterionic 1,3-bis(carboxymethyl)imidazolium, derived from \mathbf{BCI}' salt and SrCO_3 , where the polymeric sheet is separated by water sheets in which the water molecules form near-planar hexagons. Later, coordination polymers containing calcium, strontium, barium and cesium metal ions connected *via* the **BCI** ligand were reported with different structural motifs of water molecules in the structural framework [12]. Recently, the structural properties of $\text{Mg}(\mathbf{BCBI})_2(\text{H}_2\text{O})_4 \cdot 2\text{H}_2\text{O}$, $[\text{Ca}(\mathbf{BCBI})_2(\text{H}_2\text{O})_4] \cdot 2\text{H}_2\text{O}$ and $[\text{Ba}(\mathbf{BCBI})_2(\text{H}_2\text{O})_2 \cdot 2\text{H}_2\text{O}]_n$, $\mathbf{BCBI} =$ 1,3-bis(carboxymethyl)benzimidazolium, were studied [13]. Notably, only two structurally characterized calcium coordination complexes, a three-dimensional calcium-**BCI** supported coordination network and monomeric calcium-**BCBI** has been reported using **BCI** or **BCBI** salts. As shown in Fig. 4.1, the structural motifs of known calcium-imidazolium carboxylates were tuned up by two flexible “methyl” arms and steric hindrance bestowed by **BCI** and **BCBI** ligands. In particular, the ionic calcium complexes derived from imidazolium or benzimidazolium carboxylate ligands bearing more than two flexible nodes are not known.

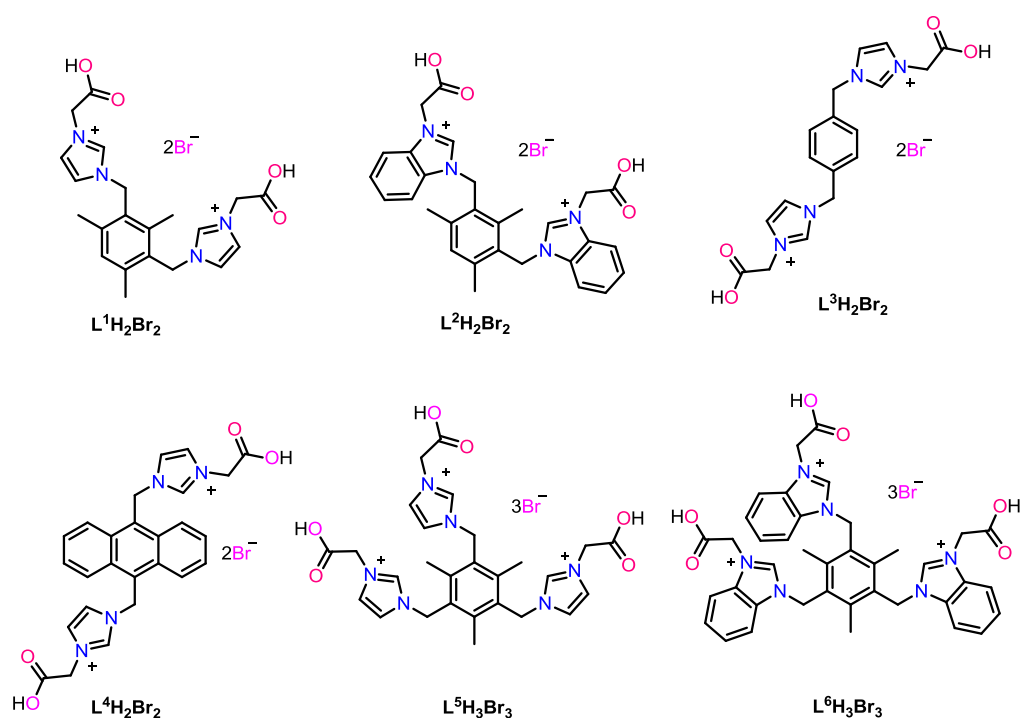


Figure 4.2: Molecular structure of the bis-imidazolium carboxylic acids ($L^1H_2Br_2$, $L^2H_2Br_2$, $L^3H_2Br_2$ and $L^4H_2Br_2$) and tris-imidazolium carboxylic acids ($L^5H_2Br_2$ and $L^6H_2Br_2$).

Continuing our efforts on photoluminescent ionic metal-azolium carboxylates [10a], herein we report the synthesis and isolation of ionic calcium dimers and extended networks supported by bis- (with four flexible nodes) and tris- (with six flexible nodes)azolium carboxylic acid ligands (Fig. 4.2). The first structurally authenticated calciumazolium carboxylate complexes with diversified calcium coordination geometry and photoluminescent property are described.

4.2 Experimental

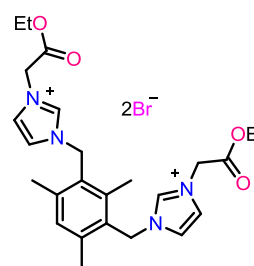
4.2.1 Materials and methods

The solvents were purchased from commercial sources and purified according to standard procedures [17]. Unless otherwise stated, the chemicals were purchased from commercial sources. Imidazolium carboxylates were prepared as reported [10]. FT-IR measurement (neat) was carried out on a Bruker Alpha-P Fourier Transform spectrometer. NMR spectra were recorded on Bruker Ultrashield-400 spectrometers at

25 °C unless otherwise stated. Chemical shifts are given relative to TMS and were referenced to the solvent resonances as internal standards. Elemental analyses were performed by the Euro Vector EA-300 elemental analyzer. The UV–vis spectra were measured on a T90+ UV-visible spectrophotometer using ultrapure water with a resistivity 18.2 M cm, obtained through the Millipore Direct-Q 3 UV system. The fluorescent emission spectra were measured on a Horiba Scientific fluorescence spectrophotometer using ultrapure water with a resistivity 18.2 M cm, obtained through the Millipore Direct-Q 3 UV system. The excitation and emission slit width in fluorescence study is 5 nm for all the compounds, and the spectra were recorded at room temperature. The thermogravimetric analysis (TGA) was performed using a TA-SDT Q600, Tzeropress.

4.2.2 Synthesis of bis- and tris-imidazolium carboxylates and 1-6

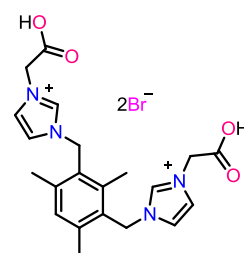
L¹(C₂H₅)₂Br₂: Mixture of compounds 1,3-bis(N-imidazolymethyl)-2,4,6-trimethylbenzene (2 g, 7.13 mmol) and ethyl 2-bromoacetate (2.382 g, 14.26 mmol) in acetone (20 mL) was refluxed for 16 h. The solvent was filtered using cannula and then solid was washed with acetone (10 mL) and diethyl ether (10 mL). The resultant was subsequently dissolved in 10 mL water and filtered. The solvent was removed under reduced pressure and dried under vacuum. Yield: 85% (based on 1,3-bis(N-imidazolymethyl)-2,4,6-trimethylbenzene). Anal. Calcd. (%) for C₂₅H₃₄N₄O₄Br₂ (614.3688): C, 48.87; H, 5.58; N, 9.12; found: C, 48.9; H, 5.5; N, 9.1. ¹H NMR (400 MHz, D₂O): δ = 8.70 (s, 2H, ImH), 7.57 and 7.49 (s, 2 x 2H, 2 x ImH), 7.28 (s, 1H, ArH), 5.57 (s, 4H, CH₂), 5.14 (s, 4H, CH₂), 4.29-4.24 (q, 4H, CH₂), 2.37 (s, 6H, CH₃), 2.24 (s, 3H, CH₃), 1.26 (t, 6H, CH₃) ppm. ¹³C NMR (100 MHz, D₂O): δ = 168.03 (C=O), 140.94 (ArC), 139.11 (ArC), 136.50 (ImC), 131.61 (ArC), 127.72 (ArC), 124.08 (ImC), 122.08 (ImC), 63.63 (OCH₂), 50.20 (CH₂), 48.09 (CH₂), 19.08 (CH₃), 14.89 (CH₃), 13.25 (CH₃) ppm. FT-IR (neat): $\bar{\nu}$ = 3394 (br), 3065 (m), 2982 (m), 2907 (m), 1746 (s), 1559 (m), 1373(m), 1337 (w), 1316 (w), 1232 (s), 1200 (m), 1149 (s), 1112 (w), 1043 (w), 1018 (s), 974 (w) cm⁻¹.



L¹(H)₂Br₂: To the ester compound **L¹(C₂H₅)₂Br₂** (3 g, 4.88 mmol) was added 12% HCl aqueous solution (60 mL) and refluxed for 12 h. The solution was removed under

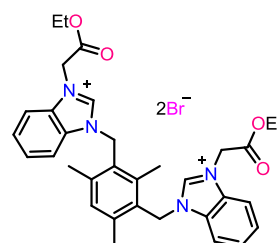
reduced pressure and the remaining solid was washed with acetone (20 mL) and diethyl ether (10 mL). The solvent was removed under reduced pressure and dried under high vacuum.

Yield: 86% (based on $L^1(C_2H_5)_2Br_2$). Anal. Calcd. (%) for $C_{21}H_{26}N_4O_4Br_2$ (558.2635): C, 45.18; H, 4.69; N, 10.04; found: C, 45.1; H, 4.6; N, 10.0. 1H NMR (400 MHz, D_2O): δ = 8.59 (s,



2H, *ImH*), 7.52 and 7.43 (s, 2 x 2H, 2 x *ImH*), 7.25 (s, 1H, *ArH*), 5.53 (s, 4H, CH_2), 5.04 (s, 4H, CH_2), 2.34 (s, 6H, CH_3), 2.18 (s, 3H, CH_3) ppm. ^{13}C NMR (100 MHz, D_2O): δ = 169.94 (C=O), 140.92 (*ArC*), 139.12 (*ArC*), 136.35 (*ImC*), 131.51 (*ArC*), 127.72 (*ArC*), 124.00 (*ImC*), 121.97 (*ImC*), 50.18 (CH_2), 47.98 (CH_2), 19.00 (CH_3), 14.75 (CH_3) ppm. FT-IR (neat): $\bar{\nu}$ = 3390 (br), 3086 (w), 2954 (w), 1738 (s), 1562 (m), 1445 (w), 1430 (w), 1401 (w), 1336 (w), 1229 (s), 1151 (s), 1101 (w), 1033 (w), 1018(w) cm^{-1} .

$L^2(C_2H_5)_2Br_2$: $L^2(C_2H_5)_2Br_2$ was prepared as reported for $L^1(C_2H_5)_2Br_2$, using 1,3-bis(N-benzimidazolylmethyl)-2,4,6-trimethylbenzene (1 g, 2.63 mmol) and ethyl 2-bromoacetate (0.878 g, 5.26 mmol). Yield: 86% (based on 1,3-bis(N-benzimidazolylmethyl)-2,4,6-trimethylbenzene). Anal.

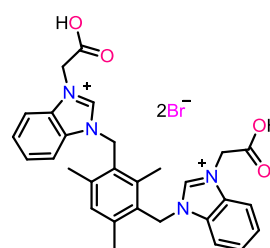


Calcd. (%) for $C_{33}H_{38}Br_2N_4O_4$ (714.48): C, 55.47; H, 5.36;

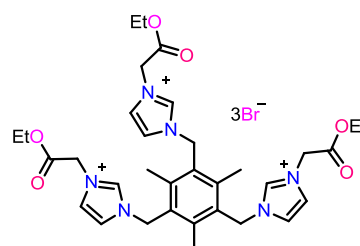
N, 7.84; found: C, 55.2; H, 5.2; N, 7.8. 1H NMR (400 MHz, D_2O): δ = 9.02 (s, 2H, *NCHN*), 7.90-7.66 (m, 8H, *ArH*), 7.33 (s, 1H, *Ar H*), 5.76 (s, 4H, CH_2), 5.38 (s, 4H, CH_2), 4.23-4.18 (q, 4H, CH_2), 2.36 (s, 6H, CH_3), 2.12 (s, 3H, CH_3), 1.19 (t, 6H, CH_3) ppm. ^{13}C NMR (100 MHz, D_2O): δ = 167.67 (C=O), 141.24 (*ArC*), 141.12 (*NCHN*), 139.22 (*ArC*), 131.83 (*ArC*), 131.07 (*ArC*), 127.75 (*ArC*), 127.41 (*ArC*), 127.14 (*ArC*), 113.48 (*ArC*), 113.03 (*ArC*), 63.65 (OCH_2), 47.60 (CH_2), 46.14 (CH_2), 19.11 (CH_3), 15.03 (CH_3), 13.15 (CH_3) ppm. FT-IR (neat): $\bar{\nu}$ = 3396 (br), 2983 (w), 1739 (s), 1563 (s), 1432 (w), 1371 (w), 1343 (m), 1223 (s), 1191 (s), 1031 (m), 983 (w), 758 (s) cm^{-1} .

$L^2(H)_2Br_2$: $L^2(H)_2Br_2$ was prepared as reported for $L^1(H)_2Br_2$, using $L^2(C_2H_5)_2Br_2$ (1.5 g, 2.10 mmol) and 30 mL of 12% HCl. Yield: 85% (based on $L^2(C_2H_5)_2Br_2$). Anal. Calcd. (%) for $C_{29}H_{30}Br_2N_4O_4$ (658.38): C, 52.90; H, 4.59; N, 8.51; found: C, 52.8; H, 4.7; N, 8.5. 1H NMR (400 MHz, DMSO- d_6): δ = 9.16 (s, 2H, *NCHN*), 8.26 (d, 2H, *ArH*), 8.07 (d, 2H, *ArH*), 7.78-7.70 (m, 4H, *ArH*), 7.31 (s, 1H, *ArH*), 5.81 (s, 4H, CH_2), 5.34 (s, 4H, CH_2), 2.35 (s, 6H, CH_3), 2.20 (s, 3H, CH_3) ppm. ^{13}C NMR (100 MHz,

DMSO-d₆): δ = 168.31 (C=O), 142.13 (ArC), 140.38 (NCHN), 139.54 (ArC), 131.91 (ArC), 130.99 (ArC), 127.68 (ArC), 126.94 (ArC), 126.55 (ArC), 113.99 (ArC), 113.82 (ArC), 48.22 (CH₂), 45.36 (CH₂), 19.53 (CH₃), 15.28 (CH₃) ppm. FT-IR (neat): $\bar{\nu}$ = 3333 (br), 2914 (br), 2496 (w), 1730 (s), 1611 (w), 1565 (s), 1485 (w), 1433 (m), 1393 (m), 1345 (m), 1267 (w), 1183 (s), 1020 (m), 982 (w) cm⁻¹.

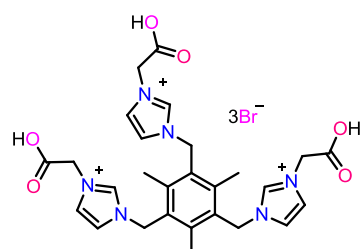


L⁵(C₂H₅)₃Br₃: A mixture of compound 1,3,5-tris(N-imidazolylmethyl)-2,4,6-trimethylbenzene (1 g, 2.77 mmol) and ethyl 2-bromoacetate (1.389 g, 8.32 mmol) in acetone (10 mL) was refluxed for 24 h. The solvent was filtered using cannula and solid was washed with acetone (10 mL) and diethyl ether (10 mL). The resultant was subsequently dissolved in 10 mL water and filtered. The solvent



was removed under reduced pressure and dried under high vacuum. Yield: 95% (based on 1,3,5-tris(N-imidazolylmethyl)-2,4,6-trimethylbenzene). Anal. Calcd. (%) for C₃₃H₄₅N₆O₆Br₃ (861.4590): C, 46.01; H, 5.27; N, 9.76; found: C, 46.1; H, 5.2; N, 9.7. ¹H NMR (400 MHz, D₂O): δ = 8.84 (s, 3H, ImH), 7.58 (d, 6H, ImH), 5.67 (s, 6H, CH₂), 5.17 (s, 6H, CH₂), 4.29-4.24 (q, 4H, CH₂), 2.36 (s, 9H, CH₃), 1.26 (t, 9H, CH₃) ppm. ¹³C NMR (100 MHz, D₂O): δ = 168.06 (C=O), 141.81 (ArC), 136.46 (ImC), 129.07 (ArC), 124.21 (ImC), 122.19 (ImC), 63.60 (OCH₂), 50.23 (CH₂), 48.51 (CH₂), 15.81 (CH₃), 13.24 (CH₃) ppm. FT-IR (neat): $\bar{\nu}$ = 3389 (br), 2980 (br), 1743 (s), 1634 (w), 1561 (m), 1473 (w), 1447 (w), 1374 (m), 1338 (w), 1317 (w), 1224 (s), 1154 (s), 1110 (w), 1015 (m), 972 (w) cm⁻¹.

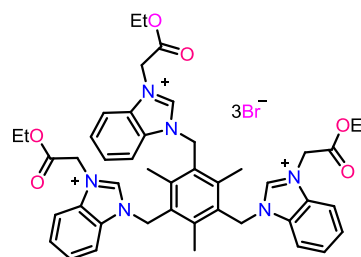
L⁵(H)₃Br₃: To the ester compound **L⁵(C₂H₅)₃Br₃** (1.5 g, 1.19 mmol) was added 12% HCl aqueous solution (45 mL) and refluxed for 12 h. The solution was removed under reduced pressure and the remaining solid was washed with acetone (10 mL) and diethyl ether (10 mL). The solvent was removed



under reduced pressure and dried under high vacuum (Yield: 88%). Anal. Calcd. (%) for C₂₇H₃₃N₆O₆Br₃ (777.29): C, 41.72; H, 4.28; N, 10.81; found: C, 41.7; H, 4.3; N, 10.9.

^1H NMR (400 MHz, D_2O): $\delta = 8.73$ (s, 3H, ImH), 7.55-7.52 (m, 6H, ImH), 5.64 (s, 6H, CH_2), 5.08 (s, 6H, CH_2), 2.34 (s, 9H, CH_3) ppm. ^{13}C NMR (100 MHz, D_2O): $\delta = 169.96$ (C=O), 141.73 (ArC), 136.34 (ImC), 129.12 (ArC), 124.14 (ImC), 122.08 (ImC), 50.29 (CH_2), 48.44 (CH_2), 15.77 (CH_3) ppm. FT-IR (neat): $\bar{\nu} = 3320$ (br), 3041 (w), 2922 (w), 1732 (s), 1561 (m), 1429 (w), 1377 (w), 1337 (w), 1311 (w), 1229 (m), 1202 (m), 1151 (s), 1032 (w), 973 (w) cm^{-1} .

$\text{L}^6(\text{C}_2\text{H}_5)_3\text{Br}_3$: $\text{L}^6(\text{C}_2\text{H}_5)_3\text{Br}_3$ was prepared as reported for $\text{L}^6(\text{C}_2\text{H}_5)_3\text{Br}_3$, using 1,3,5-tris(N-benzimidazolymethyl)-2,4,6-trimethylbenzene (1 g, 1.96 mmol), and ethyl 2-bromoacetate (0.981 g, 5.87 mmol). Yield: 89% (based on 1,3,5-tris(N-benzimidazolymethyl)-2,4,6-trimethylbenzene).

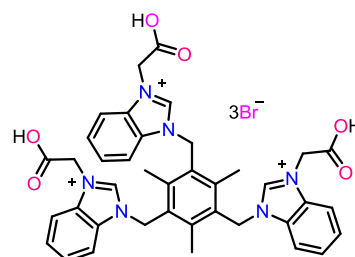


Anal. Calcd. (%) for $\text{C}_{45}\text{H}_{51}\text{Br}_3\text{N}_6\text{O}_6$ (1011.63): C, 53.43; H, 5.08; N, 8.31; found: C, 54.0; H, 5.1; N, 8.3. ^1H NMR (400 MHz, D_2O): $\delta = 9.39$ (s, 3H, NCHN), 8.03-8.01 (m, 3H, ArH), 7.86-7.84 (m, 3H, ArH), 7.78-7.75 (m, 6H, ArH), 5.92 (s, 6H, CH_2), 5.48 (s, 6H, CH_2), 4.28-4.23 (q, 6H, CH_2), 2.38 (s, 9H, CH_3), 1.23 (t, 9H, CH_3) ppm. ^{13}C NMR (100 MHz, D_2O): $\delta = 167.83$ (C=O), 142.32 (ArC), 141.12 (NCHN), 131.95 (ArC), 131.10 (ArC), 128.85 (ArC), 127.94 (ArC), 127.57 (ArC), 113.47 (ArC), 113.09 (ArC), 63.71 (OCH_2), 47.70 (CH_2), 46.49 (CH_2), 15.97 (CH_3), 13.22 (CH_3) ppm. FT-IR (neat): $\bar{\nu} = 3397$ (br), 2982 (w), 1745 (s), 1566 (s), 1430 (w), 1372 (w), 1343 (m), 1222 (s), 1192 (s), 1030 (m), 983 (w), 759 (s) cm^{-1} .

$\text{L}^6(\text{H})_3\text{Br}_3$: $\text{L}^6(\text{H})_3\text{Br}_3$ was prepared for $\text{L}^5(\text{H})_3\text{Br}_3$, using $\text{L}^6(\text{C}_2\text{H}_5)_3\text{Br}_3$ (1.5 g, 1.48 mmol) and 45 mL of 12% HCl. Yield: 86% (based on $\text{L}^6(\text{C}_2\text{H}_5)_3\text{Br}_3$). Anal.

Calcd. (%) for $\text{C}_{39}\text{H}_{39}\text{Br}_3\text{N}_6\text{O}_6$ (927.47): C, 50.50; H, 4.24; N, 9.06; found: C, 50.4; H, 4.3; N, 9.07. ^1H NMR (400 MHz, D_2O): $\delta = 9.24$ (s, 3H, NCHN),

8.01-7.98 (m, 3H, ArH), 7.84-7.82 (m, 3H, ArH), 7.74-7.72 (m, 6H, ArH), 5.89 (s, 6H, CH_2), 5.37 (s, 6H, CH_2), 2.34 (s, 9H, CH_3) ppm. ^{13}C NMR (100 MHz, D_2O): $\delta = 169.77$ (C=O), 142.26 (ArC), 141.06 (NCHN), 131.98 (ArC), 131.12 (ArC), 128.87 (ArC), 127.82 (ArC), 127.45 (ArC), 113.38 (ArC), 113.14 (ArC), 47.83 (CH_2), 46.40 (CH_2), 15.89 (CH_3) ppm. FT-IR (neat): $\bar{\nu} = 3225$ (br), 3030 (br), 1729 (s), 1566 (s), 1435 (w), 1393 (w), 1346 (w), 1188 (s), 741 (s) cm^{-1} .



{[(L¹)₂Ca₂(H₂O)₄](Br)₄·6H₂O}_∞ (1): The solution of L¹H₂Br₂ (0.100 g, 0.179 mmol) in water (10 mL) was added into a suspension of CaCO₃ (0.018 g, 0.180 mmol) in water (5 mL), stirred at ambient temperature for 24 h. The resultant cloudy solution was filtered and washed with water (10 mL). The crystals were formed through slow evaporation of the filtered solution. Yield: 42% (based on CaCO₃). Anal. Calcd. (%) for C₂₁H₃₄N₄O₉Br₂Ca (686.42): C, 36.75; H, 4.99; N, 8.16; found: C, 36.8; H, 5.1; N, 8.3. ¹H NMR (400 MHz, D₂O): δ = 7.43 (d, 2H, ImH), 7.35 (s, 2H, ImH), 7.24 (s, 1H, ArH), 5.50 (s, 4H, CH₂), 4.73 (s, 4H, CH₂), 2.33 (s, 6H, 2 x CH₃), 2.12 (s, 3H, CH₃) ppm. ¹³C NMR (100 MHz, D₂O): δ = 172.2 (C=O), 140.8, 139.2, 131.4, 127.7 (ArC), 123.7, 121.5 (ImC), 52.0 (CH₂), 47.7 (CH₂), 18.9 (2 x CH₃), 14.7 (CH₃) ppm. FT-IR (neat): $\bar{\nu}$ = 3355 (br), 3138 (w), 3045 (w), 2967 (w), 1590 (s), 1444 (m), 1404 (s), 1322 (s), 1212 (w), 1150 (s), 1104 (w), 1036 (w), 981 (w) cm⁻¹.

{[(L²)₂Ca₂(H₂O)₉](Br)₄·4H₂O} (2): **2** was prepared as described for **1**, using L²H₂Br₂ (0.100 g, 0.152 mmol) and CaCO₃ (0.016 g, 0.160 mmol). Yield: 41% (based on CaCO₃). Anal. Calcd. (%) for C₅₈H₈₂N₈O₂₁Br₄Ca₂ (1627.08): C, 42.81; H, 5.08; N, 6.89; found: C, 44.1; H, 5.0; N, 7.3. FT-IR (neat): $\bar{\nu}$ = 3333 (br), 2972 (m), 2839 (w), 2775 (m), 1604 (s), 1565 (w), 1433 (w), 1397 (s), 1343 (w), 1309 (m), 1265 (w), 1190 (m), 1136 (w), 1020 (m), 986 (w) cm⁻¹. ¹H and ¹³C NMR spectra of **2** were not clear due to the dissociative nature of **2** in D₂O.

{[(L³)₂Ca₂(H₂O)₂]₂(Br)₂}_∞ (3): **3** was prepared as described for **1**, using L³H₂Br₂ (0.100 g, 0.194 mmol) and CaCO₃ (0.019 g, 0.194 mmol). Yield: 39% (based on CaCO₃). Anal. Calcd. (%) for C₁₈H₂₂N₄O₆CaBr (510.38): C, 42.36; H, 4.34; N, 10.98; found: C, 42.4; H, 4.33; N, 10.9. ¹H NMR (400 MHz, D₂O): δ = 7.46-7.48 (m, 8H, ArH and ImH), 5.44 (s, 4H, CH₂), 4.80 (s, 4H, CH₂) ppm. ¹³C NMR (100 MHz, D₂O): δ = 172.2 (C=O), 134.4, 129.4 (ArC), 123.8, 122.0 (ImC), 52.4 (CH₂), 52.0 (CH₂) ppm. FT-IR (neat): $\bar{\nu}$ = 3370 (br), 3034 (w), 2980 (w), 2941 (w), 1600 (s), 1555 (w), 1487 (w), 1441 (m), 1398 (s), 1306 (m), 1189 (w), 1156 (s), 1104 (w), 1024 (w), 979 (w) cm⁻¹.

{[(L⁴)₂Ca(H₂O)₂]₂(Br)₂}_∞ (4): **4** was prepared as described for **1**, using L⁴H₂Br₂ (0.100 g, 0.162 mmol) and CaCO₃ (0.016 g, 0.162 mmol). Yellow crystals were formed through slow evaporation of the yellow filtrate solution. Yield: 36% (based on CaCO₃).

Anal. Calcd. (%) for $C_{26}H_{26}N_4O_6BrCa$ (610.50): C, 51.15; H, 4.29; N, 9.18; found: C, 51.2; H, 4.2; N, 9.2. 1H NMR (400 MHz, D_2O): δ = 8.25 (s, 2H, ImH), 8.11-8.08 (dd, 4H, ArH), 7.73-7.70 (dd, 4H, ArH), 7.31-7.30 (m, 2H, ImH), 7.25-7.24 (m, 2H, ImH), 5.83 (s, 4H, CH_2), 4.55 (s, 4H, CH_2) ppm. ^{13}C NMR (100 MHz, D_2O): δ = 171.9 (C=O), 135.9 (ImC), 129.9, 128.0, 125.3, 123.7 (ArC), 123.6, 121.7 (ImC), 51.9 (CH_2), 44.7 (CH_2) ppm. FT-IR (neat): $\bar{\nu}$ = 3342 (br), 3152 (w), 3091 (w), 3039 (w), 2992 (w), 1605 (s), 1481 (w), 1442 (m), 1397 (s), 1311 (m), 1180 (w), 1154 (s) 1103 (w) cm^{-1} .

$\{[(L^5)_2Ca_3(Na)(H_2O)_9(Cl)](Br)_6 \cdot 2H_2O\}_\infty$ (**5**): **5** was prepared as described for **1**, using $L^5H_3Br_3$ (0.100, 0.128 mmol) and $CaCO_3$ (0.013 g, 0.128 mmol). Yield: 33% (based on $CaCO_3$). Anal. Calcd. (%) for $C_{54}H_{82}Br_6Ca_3ClN_{12}NaO_{23}$ (1925.40): C, 33.69; H, 4.29; N, 8.73; found: C, 36.4; H, 4.2; N, 9.8. 1H NMR (400 MHz, D_2O): δ = 8.58 (s, 3H, ImH), 7.49 (s, 3H, ImH), 7.41 (s, 3H, ImH), 5.63 (s, 6H, CH_2), 4.74 (s, 6H, CH_2), 2.37 (s, 9H, CH_3) ppm. ^{13}C NMR (100 MHz, D_2O): δ = 172.2 (C=O), 141.7 (ArC), 136.0 (ImC), 129.1 (ArC), 124.0 (ArC), 123.9 (ArC), 121.6 (ImC), 121.6 (ImC), 52.1 (CH_2), 48.2 (CH_2), 15.7 (CH_3) ppm. FT-IR (neat): $\bar{\nu}$ = 3365 (br), 3090 (w), 1601 (s), 1445 (w), 1399 (s), 1308 (m), 1154 (s), 1104 (w), 1018 (w), 978 (w), 931 (w) cm^{-1} .

$\{[(L^6)_2Ca_2(H_2O)_9](Br)_6\}$ (**6**): **6** was prepared as described for **1**, using $L^6H_3Br_3$ (0.100 g, 0.108 mmol) and $CaCO_3$ (0.011 g, 0.108 mmol). Yield: 41% (based on $CaCO_3$). Anal. Calcd. (%) for $C_{78}H_{90}Br_6Ca_3N_{12}O_{21}$ (2131.27): C, 43.96; H, 4.26; N, 7.89; found: C, 42.2; H, 4.4; N, 7.7. 1H NMR (400 MHz, D_2O): δ = 8.93 (s, 3H, ImH H/D exchange), 7.96-7.94 (m, 3H, ArH), 7.77-7.68 (m, 9H, ArH), 5.86 (s, 6H, CH_2), 5.01 (s, 6H, CH_2), 2.36 (s, 9H, CH_3) ppm. ^{13}C NMR (100 MHz, D_2O): δ = 171.8 (C=O), 142.2, 132.1, 131.2, 128.8, 127.5, 127.2, 113.2 (ArC), 49.6 (CH_2), 46.2 (CH_2), 15.9 (CH_3) ppm. FT-IR (neat): $\bar{\nu}$ = 3310 (br), 3020 (w), 1605 (s), 1565 (m), 1481 (w), 1429 (w), 1397 (s), 1345 (w), 1307 (m), 1271 (w), 1194 (m), 1133 (w), 1020 (m), 985 (w), 930 (w) cm^{-1} .

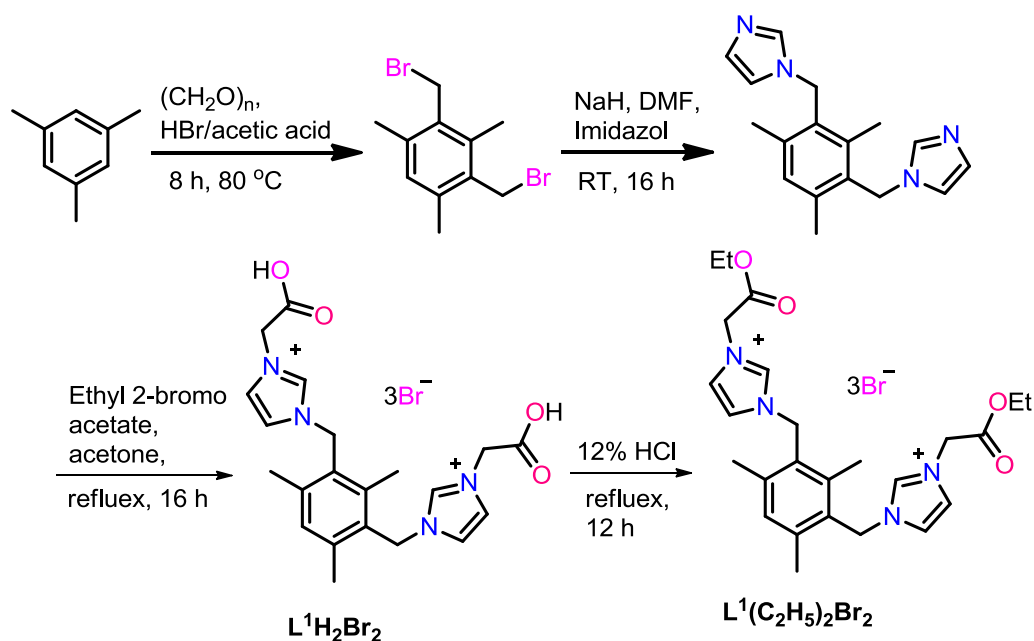
4.2.3 Crystallography

The crystal structures of **1-6** were measured on an Oxford Xcalibur 2 diffractometer. A suitable crystal was selected and mounted on a SuperNova, Dual, Cu at zero, Eos diffractometer. Data were collected at 150 K or 298 K. Using Olex2 [18], the structures **1-6** were solved with the olex2.solve structure solution program using Charge Flipping

and refined with the olex2.refine refinement package using Gauss-Newton minimization. The six crystals reported were crystallized using water as a solvent. In molecule **6**, approximately 31% (1710 Å³) of the unit cell volume comprises heavily disordered solvent molecules, which could not be modelled as discrete atomic sites, and were “squeezed” out with the program PLATON. The estimated total count of 114 electrons per unit cell was removed as disordered solvents.

4.3 Results and discussion

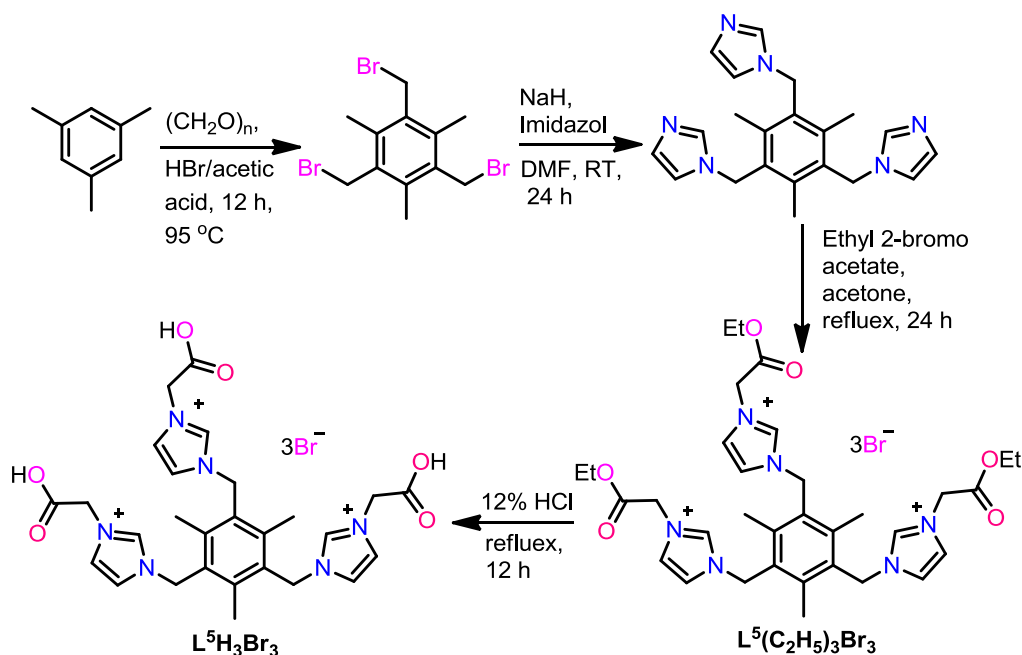
4.3.1 Synthesis and characterization of bis- and tris-imidazolium carboxylates and 1-6



Scheme 4.1: Synthesis of $L^1H_2Br_2$.

The bis-azolium carboxylate ($L^1H_2Br_2$ (Scheme 4.1), $L^2H_2Br_2$, $L^3H_2Br_2$ and $L^4H_2Br_2$) and tris-azolium carboxylate ($L^5H_2Br_2$ and $L^6H_2Br_2$ (Scheme 4.2)) ligands were synthesized as reported in good yield [10]. Compounds **1-6** were synthesized from the reaction of corresponding azolium carboxylic acid with calcium carbonate in aqueous solution. Compounds **1-6** are soluble only in water and were characterized by FT-IR, multinuclear (¹H and ¹³C) NMR, TGA, UV-vis and fluorescent spectroscopy techniques. The FT-IR spectra of **1-6** showed a characteristic peak for the asymmetric stretching frequency at 1590-1605 cm⁻¹ and the symmetric stretching frequency at 1397-1404

cm^{-1} . The ^{13}C NMR spectra of **1-6** showed the diagnostic peak for C=O carbon at 170-173 ppm, which were shifted to downfield compare to corresponding azolium carboxylic acids (Table 4.1). The solid-state UV-visible absorption spectra of **1-6** were significantly different from those in solution. The solid UV-visible absorption spectra of **1-6** are nearly comparable with those of corresponding azolium carboxylic acids (Fig. 4.4).



Scheme 4.2. Synthesis of $\text{L}^5\text{H}_3\text{Br}_3$.

The solid state fluorescent emission spectra of **1-6** were measured at an excitation wavelength of 370 nm (Fig. 4.5). The emission wavelength (440 nm) of **1**, **3**, **5** and **6** are comparable. The emission wavelength intensity for **1**, **3** and **6** are enhanced compared to their corresponding ligands, $\text{L}^1\text{H}_2\text{Br}_2$ (444 nm), $\text{L}^3\text{H}_2\text{Br}_2$ (440 nm), $\text{L}^6\text{H}_3\text{Br}_3$ (440 nm), respectively. The emission wavelength of **2** (445 nm) and **4** (447 nm) are slightly shifted towards higher wavelengths compared to **1**, **3**, **5** and **6**. Moreover, the emission intensity of **2** is comparable with $\text{L}^2\text{H}_2\text{Br}_2$ (447 nm), while the emission intensity of **4** is enhanced compared to $\text{L}^4\text{H}_2\text{Br}_2$ (447 nm).

Table 4.1: Selected FT-IR spectra and NMR peak values for bis- and tris-imidazolium carboxylate spacers and corresponding calcium molecules (**1-6**)

Compound	¹ H NMR NCHN (ppm)	¹³ C NMR C=O (ppm)	FT-IR of asym COO str	FT-IR of sym COO str
L¹H₂Br₂	8.59	169.9	1738	1562
L²H₂Br₂	9.16	168.3	1730	1565
L³H₂Br₂	8.80	170.4	1733	1567
L⁴H₂Br₂	8.32	169.8	1713	1552
L⁵H₃Br₃	8.73	170.0	1732	1561
L⁶H₃Br₃	9.24	169.8	1729	1566
1	H/D exchange	172.2	1590	1404
2	H/D exchange	171.7	1604	1397
3	H/D exchange	172.2	1600	1398
4	8.25	171.9	1605	1397
5	H/D exchange	172.2	1601	1399
6	H/D exchange	171.8	1605	1397

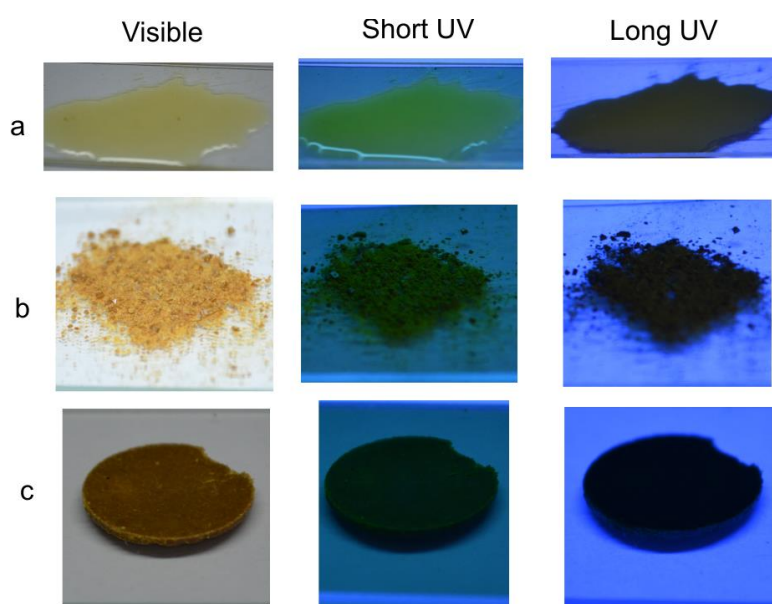


Figure 4.3: Molecule 4 shows color variation in different lights (Visible, short UV and long UV); a = sample in water, b = powder form, c = pellet form.

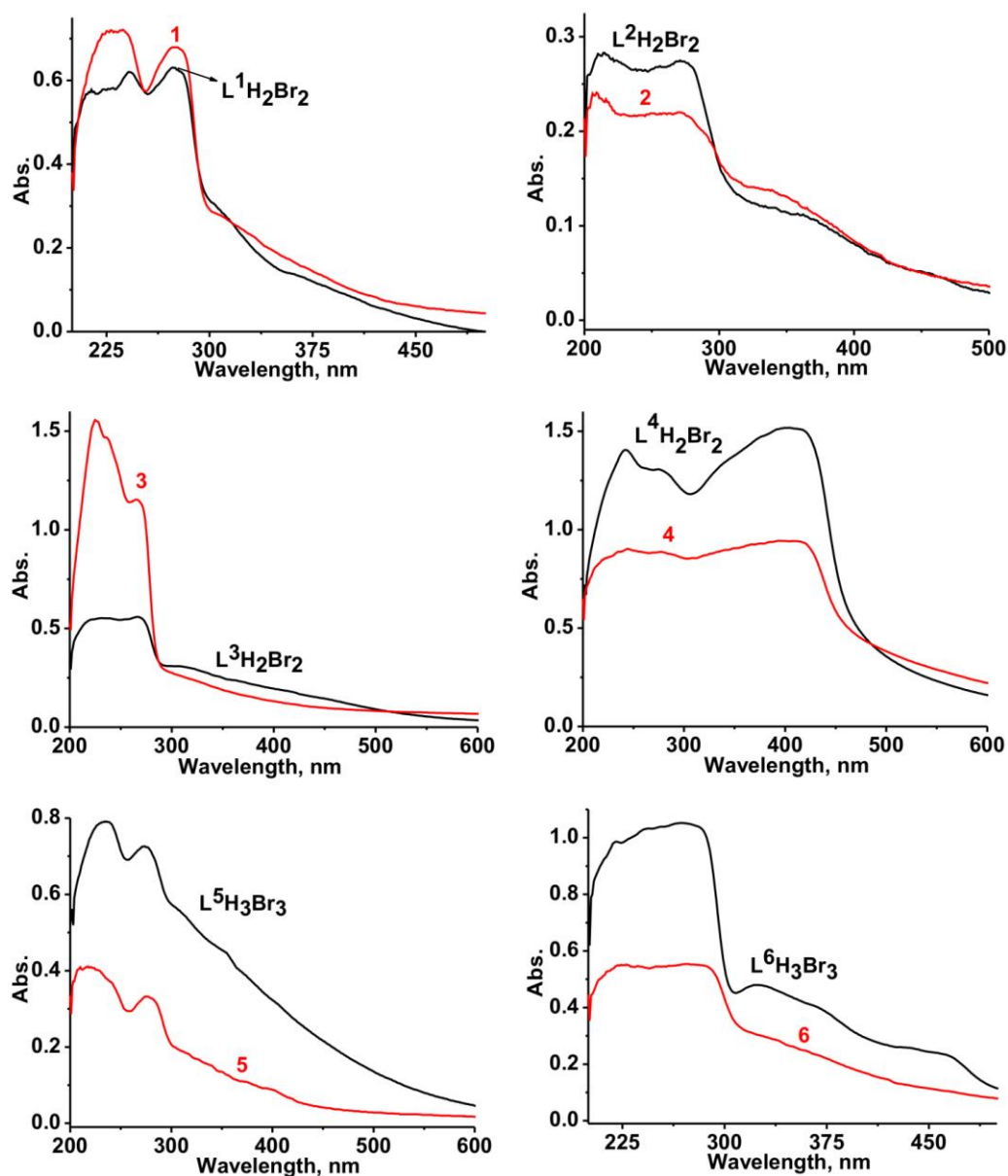


Figure 4.4: The solid-state UV-vis absorption spectra of 1-6 and corresponding organic spacers.

Molecule **4** was exhibited color variation under different lights. Under visible light, it was displayed as yellow color and under short UV light, it was exhibited light green color, while long UV light, it was given blackish blue color (Fig. 4.3). Furthermore, the solid state structures of **1-6** were unambiguously determined by the single crystal X-ray diffraction technique. The data collection parameters are listed in Table 4.2 and Table 4.3.

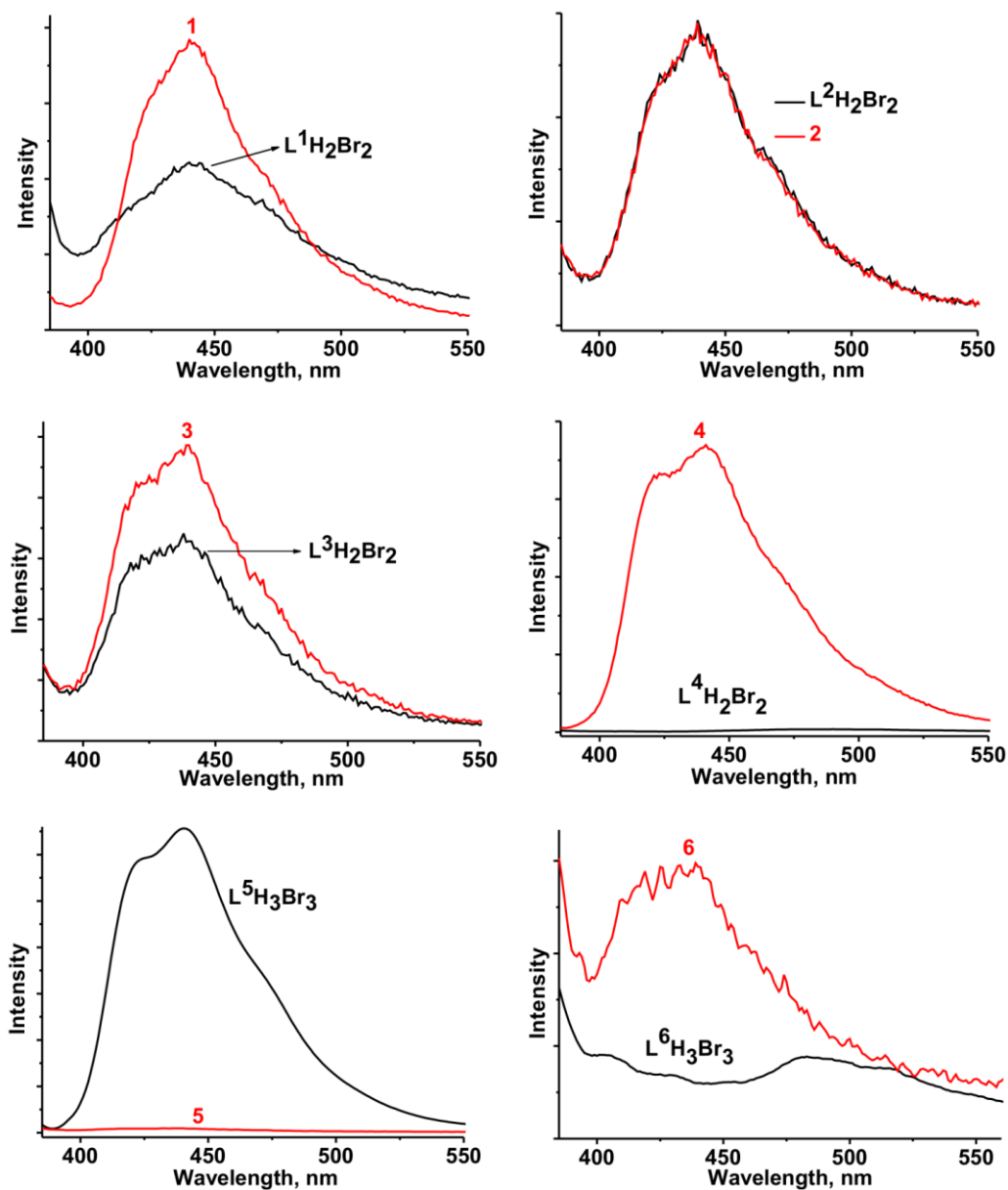


Figure 4.5: The solid-state fluorescent spectra of 1-6 and corresponding organic spacers.

4.3.2 Description of crystal structures

Single crystal X-ray structure of $\{[(L^1)_2Ca_2(H_2O)_4](Br)_4 \cdot 6H_2O\}_\infty$ (1): Complex **1** is a 3D supramolecular network connected through hydrogen bonding in the triclinic space group, $P\bar{1}$ (Fig. 4.6). The molecular structure of **1** is depicted in Fig. 4.6a.

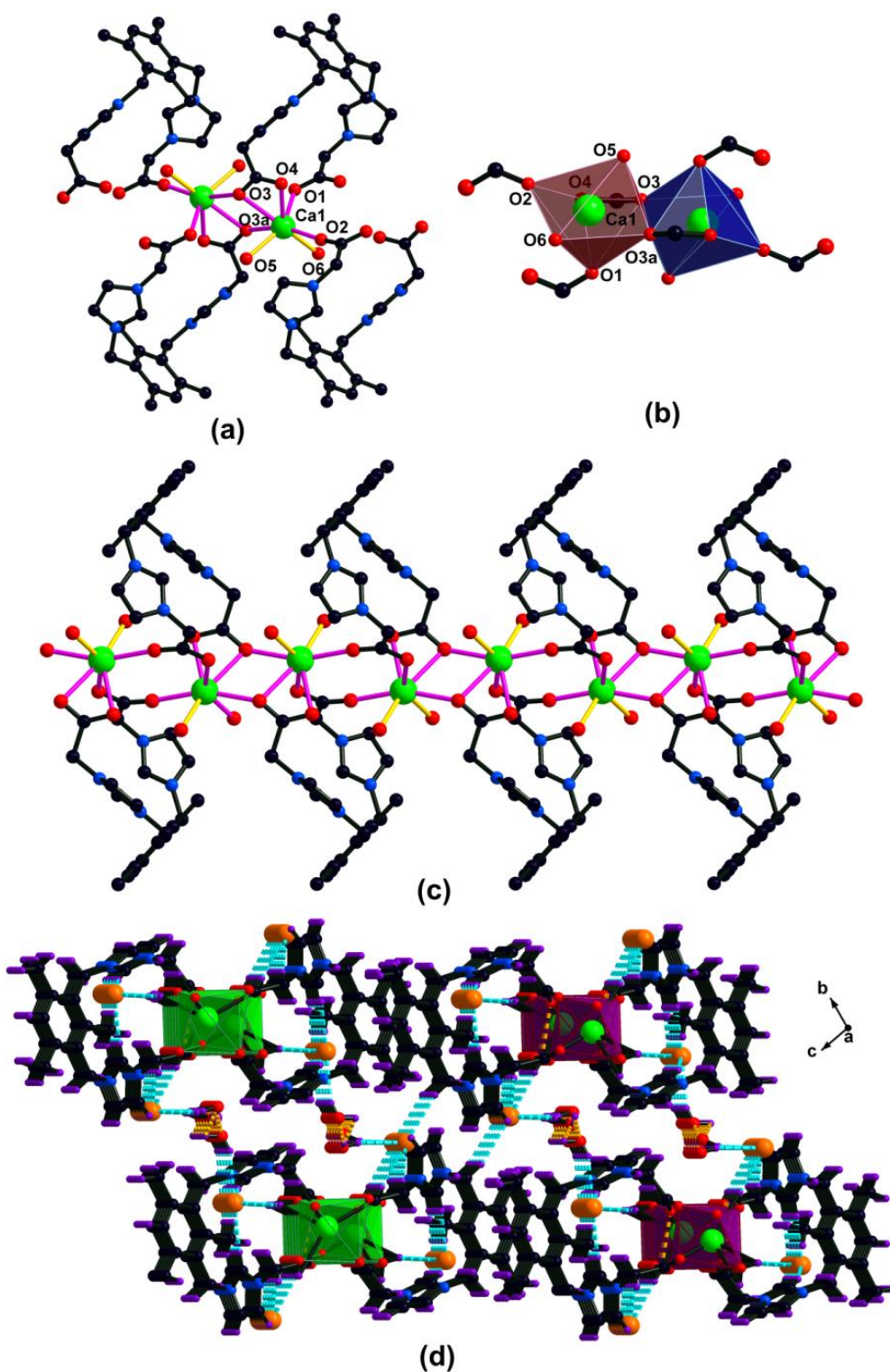


Figure 4.6: (a) Coordination environment of the Ca(II) centers in 1. The hydrogen atoms have been omitted for clarity. (b) View of the edge shared polyhedrons in 1. (c) View of the 1D coordination polymer. (d) 3D supramolecular network through hydrogen bond O-H \cdots Br and C-H \cdots Br.

The calcium(II) coordination number is seven and the geometry is distorted square-face monocapped trigonal-prismatic. The coordination environment of calcium is fulfilled by five oxygen atoms of carboxylates and two oxygen atoms of water molecules (Fig. 4.6b). Each organic spacer is connecting three calcium centers through bridging coordination modes. One of the bridging carboxylate groups are in the $\mu_2\text{-}\eta^1:\eta^1$ COO bridging mode, while the second carboxylate group is in the $\mu_2\text{-}\eta^1:\eta^2$ COO bridging mode. Two seven-coordinated calcium polyhedrons are fused through edge sharing (Fig. 4.6b). The similar dimers are bridged by carboxylate group to form a 1D coordination polymer. The cationic charge of the 1D calcium coordination polymer is balanced by bromine anions, where the calcium centers are alternatively connected by the $\mu_2\text{-}\eta^1:\eta^2$ and $\mu_2\text{-}\eta^1:\eta^1$ bridging mode of carboxylate groups (Fig. 4.6c).

As shown in Fig. 4.6d, the 1D polymer chains are further connected through C–H \cdots Br and O–H \cdots Br hydrogen bonding to form a 3D supramolecular network. In the supramolecular network, two sets of bromine interactions are observed, namely (i) (NCHN)C–H \cdots Br, (coordinated H₂O)O–H \cdots Br and (lattice H₂O)O–H \cdots Br; (ii) (CH₂)C–H \cdots Br, (coordinated H₂O)O–H \cdots Br and (lattice H₂O)O–H \cdots Br. The different Ca–O_{COO} bond distances are observed in the range from 2.324(3) to 2.552(3) Å. Similarly, the Ca–O_{water} bond lengths are different (2.396(3) and 2.409(3) Å). The O_{COO}–Ca–O_{COO} angles vary from 52.18(9)° to 160.58(11)°.

Single crystal X-ray structure of $\{[(L^2)_2Ca_2(H_2O)_9](Br)_4\cdot 4H_2O\}$ (2): The molecule **2** is a discrete tetra-cationic calcium dimer (Fig. 4.7). As shown in Fig. 4.7b, each organic spacer is coordinated to two calcium centers, where one carboxylate group is coordinated to calcium in the $\mu_1\text{-}\eta^0:\eta^1$ mode, while the other carboxylate group is coordinated to two calcium centers in the $\mu_2\text{-}\eta^1:\eta^2$ COO bridging mode. The geometries of the calcium (II) centers are different; One is distorted square-face bicapped trigonal-prismatic and square-face tricapped trigonal-prismatic (Fig. 4.7b). The coordination environment of Ca1 is satisfied by four oxygen atoms of carboxylates and four water molecules, while the Ca2 center is satisfied by four oxygen atoms of carboxylates and five water molecules. The tetra-cationic charge is fulfilled by four bromine anions. The Ca and Ca separation distance is 4.068(13) Å. The Ca(1)–O_{COO} bond lengths (2.413(4) Å to 2.579(4) Å) around Ca(1) are different from the Ca(2)–O_{COO} bond lengths (2.412(3) Å to 2.462(4) Å) around Ca(2). Similarly, the Ca(1)–O_{water} bond lengths

(2.365(4) to 2.633(12) Å) are different from those of Ca(2)–O_{water} (2.386(4) to 2.454(4) Å).

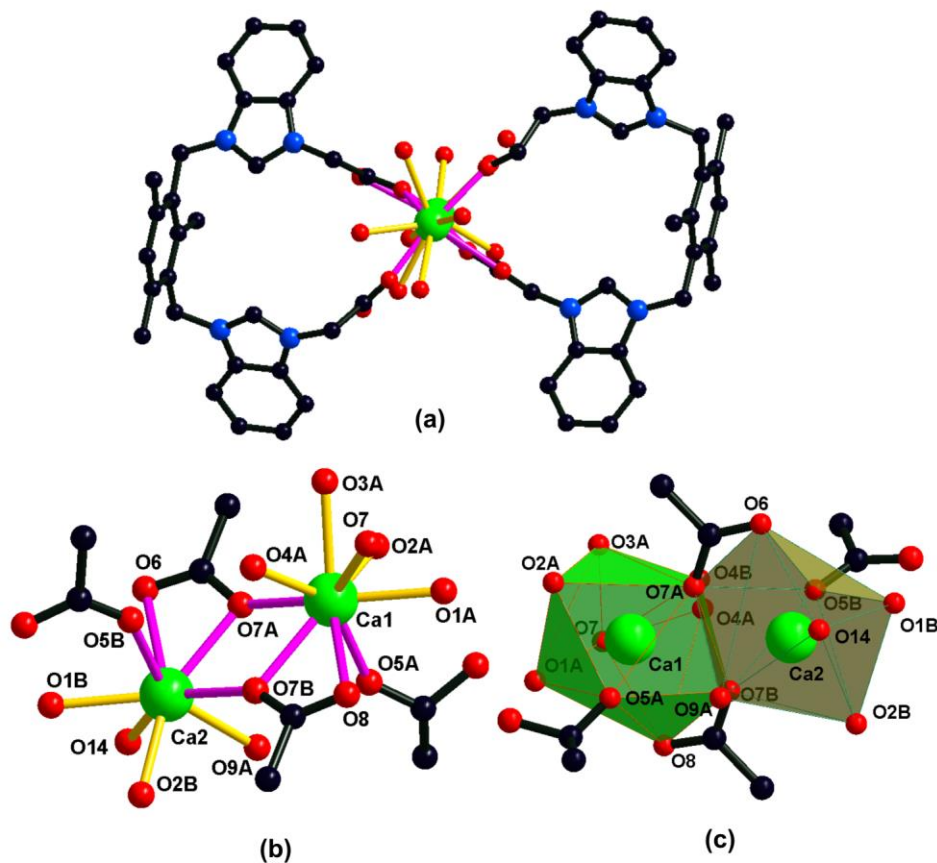


Figure 4.7: (a) Coordination environment of the Ca(II) centers in **2**. The hydrogen atoms have been omitted for clarity. (b) Core unit of molecule **2**. (c) Polyhedron view of Ca(II) centers.

Single crystal X-ray structure of $\{[(L^3)_2Ca_2(H_2O)_2]_2(Br)_2\}_\infty$ (3**):** The molecule **3** is a three dimensional metal organic framework (Fig. 4.8). As shown in Fig. 4.8c, CaO₈ polyhedrons are edge shared by two carboxylate oxygen atoms and create inorganic motifs in the form of zigzag 1D chains running along the *c* axis. These chains are linked together by L³ organic spacer in the rhomboidal channels. The channel size is about 4.8 x 2.9 nm (Fig. 4.8d and 4.8e). The Ca(II) ion is eight-coordinated by six oxygen atoms of carboxylate groups associated to four organic spacers and two oxygen atoms of coordinated water molecules (Fig. 4.8b). The calcium(II) coordination geometry is a distorted square-face biccapped trigonal-prismatic geometry. The different Ca–O_{COO} bond distances are observed in the range from 2.327(5) to 2.540(5) Å. The Ca–O_{water}

bond lengths are 2.405(8) and 2.56(2) Å. The Ca and Ca separation distance is 3.95(7) Å. The $O_{\text{COO}}\text{-Ca-O}_{\text{COO}}$ angles fall in the range from $51.23(15)^\circ$ to $159.3(4)^\circ$.

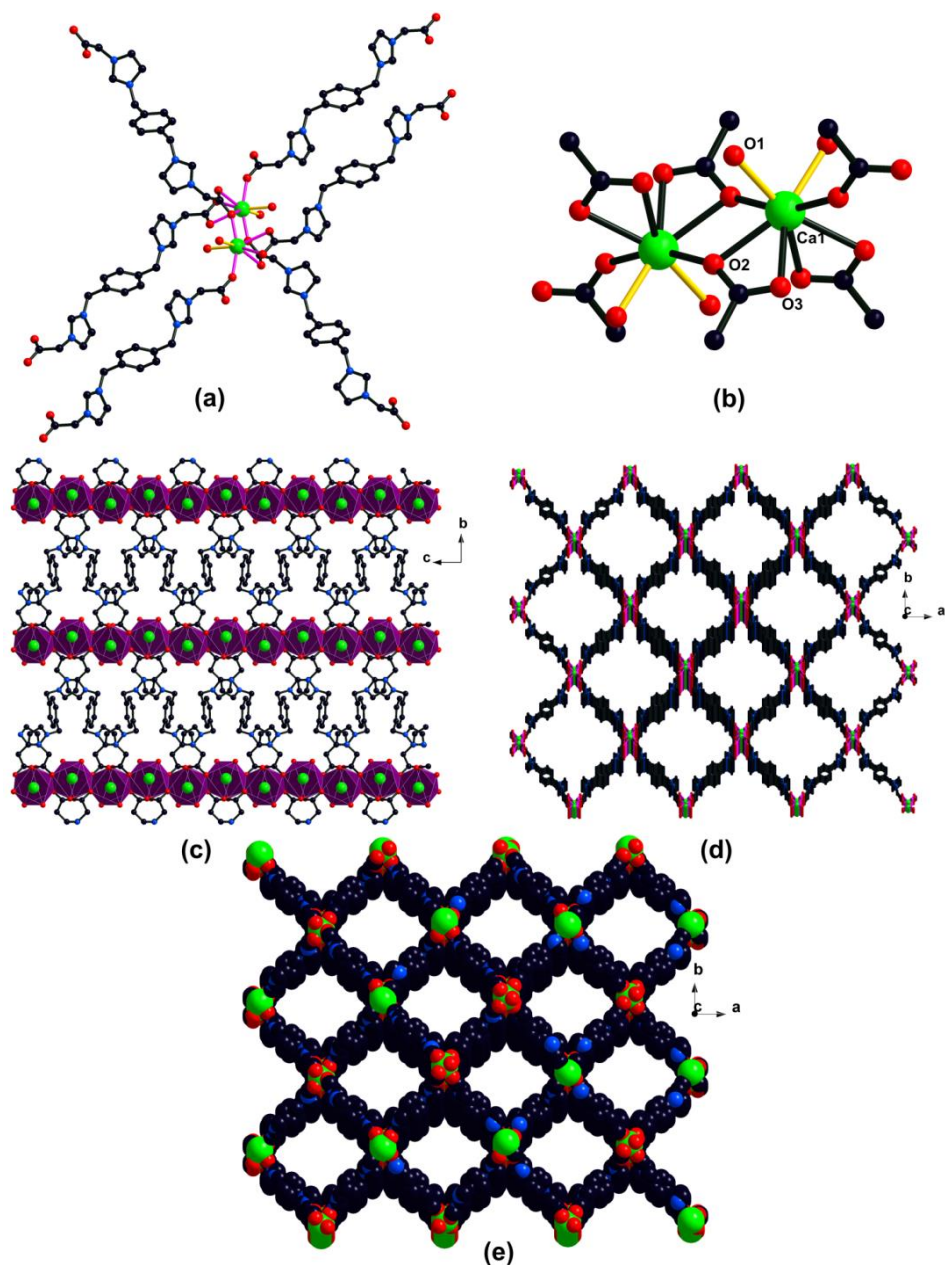


Figure 4.8: (a) Coordination environment of the Ca(II) centers in 3. The hydrogen atoms have been omitted for clarity. (b) Core unit of molecule 3. (c) View of zig-zag arrangement of the Ca(II) centers. (d) View of molecule 3 in the direction of the *c* axis. (e) Space filling model of 3 (views along *c* axis).

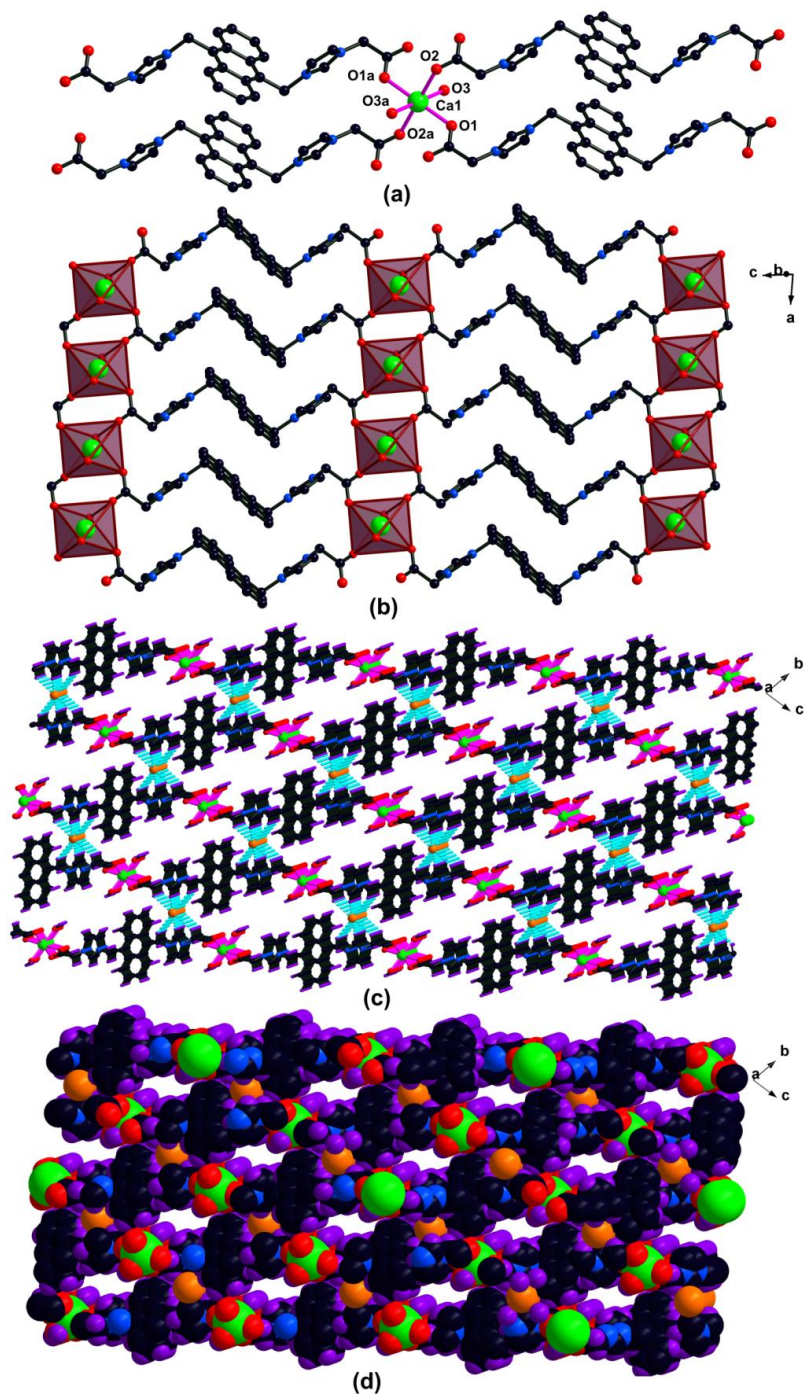


Figure 4.9: (a) Coordination environment of the Ca(II) center in 4. The hydrogen atoms and bromine ions have been omitted for clarity. (b) The polyhedron arrangement in two-dimensional layers of 4. (c) Three-dimensional network through Br \cdots H hydrogen bonding. (d) Space filling model of 3D network of 4.

Single crystal X-ray structure of $\{[(L^4)_2Ca(H_2O)_2]_2(Br)_2\}_\infty$ (4**):** The solid state structure of **4** was further confirmed by the single crystal X-ray diffraction study (Fig. 4.9). Molecule **4** crystallized in the triclinic space group, $P\bar{1}$. The asymmetric unit of **4** is composed of one calcium atom, a half anthracene imidazolium carboxylate anion of L^4 and a bromide ion. The coordination environment of Ca is a distorted octahedron and the coordination sites are satisfied by four carboxylate oxygen atoms of four L^4 and the oxygen atoms of two water molecules (Fig. 4.9a). The anthracene imidazolium carboxylate ligand in **4** acts as a μ_4 -bridge with a bis-monodentate bridging mode to link four calcium atoms, in which each deprotonated carboxylic group bridges between two calcium atoms. The $O_{COO}-Ca-O_{COO}$ angles fall in the range from $85.26(15)^\circ$ to $180.00(0)^\circ$. The calcium and carboxylate oxygen bond distances are nearly comparable, and the $Ca(1)-O(2)$ ($2.335(4)$ Å) bond distance is slightly longer than that of $Ca(1)-O(1)$ ($2.311(4)$ Å), which implies a nearly symmetric coordination mode of the carboxylate group. The bond distance of the calcium and the oxygen atom of water ($Ca(1)-O(3)$) is $2.294(6)$ Å, which is considerably shorter than that of found in the calcium N,N' -diacetic acid imidazolium bromide network ($2.390(5)$ Å). As shown in Fig. 4.9c, the extended network of calcium anthracene imidazolium carboxylate forms a two dimensional layer structure, in which the neighboring layers slipped with respect to each other. The bromide anion occupies the inner layer site through which the layers are connected ($NCHN$ and two H_2CN groups) by $C-H\cdots Br$ hydrogen bonding ($HC-H\cdots Br$, 2.850 and 2.859 Å; $NNCH\cdots Br$, 2.701 Å).

Single crystal X-ray structure of $\{[(L^5)_2Ca_3(Na)(H_2O)_9(Cl)](Br)_6\cdot 2H_2O\}_\infty$ (5**):** Molecule **5** is a rare 1D coordination polymer constructed by a trinuclear $Ca(II)$ and $Na(I)$ carboxylate cluster (Fig. 4.10). The coordination environment of $Ca(1)$ is fulfilled by six oxygen atoms of carboxylates, a chlorine anion (with occupancy of 85%) and a bromine anion (with occupancy of 15%), while $Ca(3)$ center is surrounded by seven oxygen atoms of carboxylates and the $Ca(4)$ center is satisfied by three oxygen atoms of carboxylates and four oxygen atoms of water molecules. The $Na(2)$ center is fulfilled by two oxygen atoms of carboxylates and five oxygen atoms of water molecules. The $Ca-Ca$ separation distances are not comparable ($Ca(1)\cdots Ca(3)$ $4.265(2)$ Å, $Ca(1)\cdots Ca(4)$ $3.907(4)$ Å and $Ca(1)\cdots Ca(1')$ $4.108(2)$ Å). The $Ca(1)-O_{COO}$ ($2.297(5)$ Å- $2.575(5)$ Å), $Ca(3)-O_{COO}$ ($2.333(10)$ Å- $2.682(7)$ Å) and $Ca(4)-O_{COO}$ ($2.570(7)$ Å- $2.652(6)$ Å) bond lengths are different. The $Ca(1)-Cl$ distance is $2.719(7)$ Å and the

Ca(1)–Br distance is 2.953(2) Å. As shown in Fig. 4.10c, the inorganic zig-zag chain contains an alternating orientation of trinuclear Ca(II) and Na(I) polyhedron units.

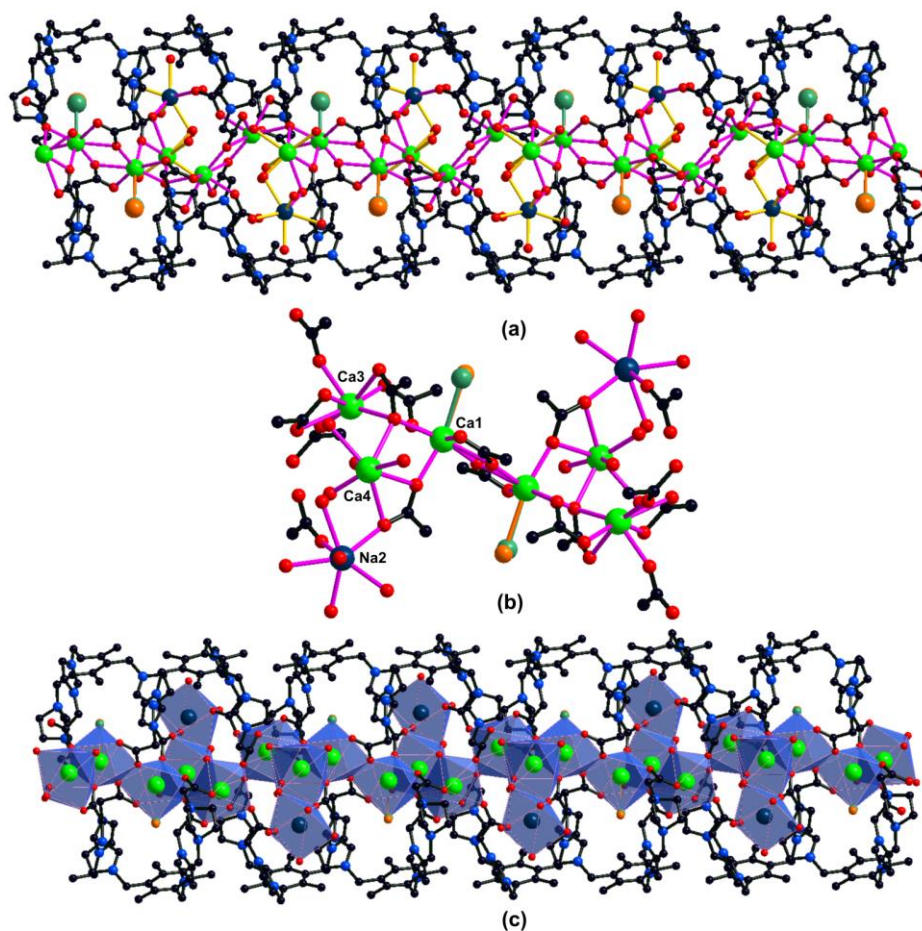


Figure 4.10: (a) One-dimensional coordination polymer of **5**. The hydrogen atoms and counter ions have been omitted for clarity. (b) Repeating unit of molecule **5**. (c) Polyhedron view of the Ca(II) centers in molecule **5**.

Single crystal X-ray structure of $\{[(L^6)_2Ca_2(H_2O)_9](Br)_6\}$ (6**):** Compound **6** crystallized in the triclinic space group, *P* $\bar{1}$. The molecular structure of **6** is depicted in Fig. 4.11. Molecule **6** is a rare calcium trimer (Fig. 4.11a). **6** consisting of three different Ca centers with different geometries, where one calcium(II) center is in a distorted square-face monocapped trigonal-prismatic geometry, the second calcium(II) center is in a distorted square-face bicapped trigonal-prismatic geometry, and the third calcium center is in an inverted tetrahedral geometry (Fig. 4.11b). The coordination environment around the Ca(0A) center is fulfilled by five oxygen atoms of carboxylates and two water molecules. The geometry of Ca(2) center is satisfied by three oxygen atoms of

carboxylates and five water molecules. The Ca(1B) center coordinated by two oxygen atoms of carboxylate group and two water molecules (Fig. 4.11b). The Ca–Ca separation distances are 4.008(16) and 4.655(27) Å. One organic spacer is coordinated to two calcium centers, where one carboxylate group is coordinated to calcium in a $\mu_1-\eta^0:\eta^1$ mode and other carboxylate group is coordinated to two calcium centers in the $\mu_2-\eta^1:\eta^2$ bridging mode. The second organic spacer is coordinated to three calcium centers, where one carboxylate group is coordinated to two calcium centers in the $\mu_1-\eta^1:\eta^2$ mode and other carboxylate group is also coordinated to two calcium centers in the $\mu_2-\eta^1:\eta^2$ bridging mode.

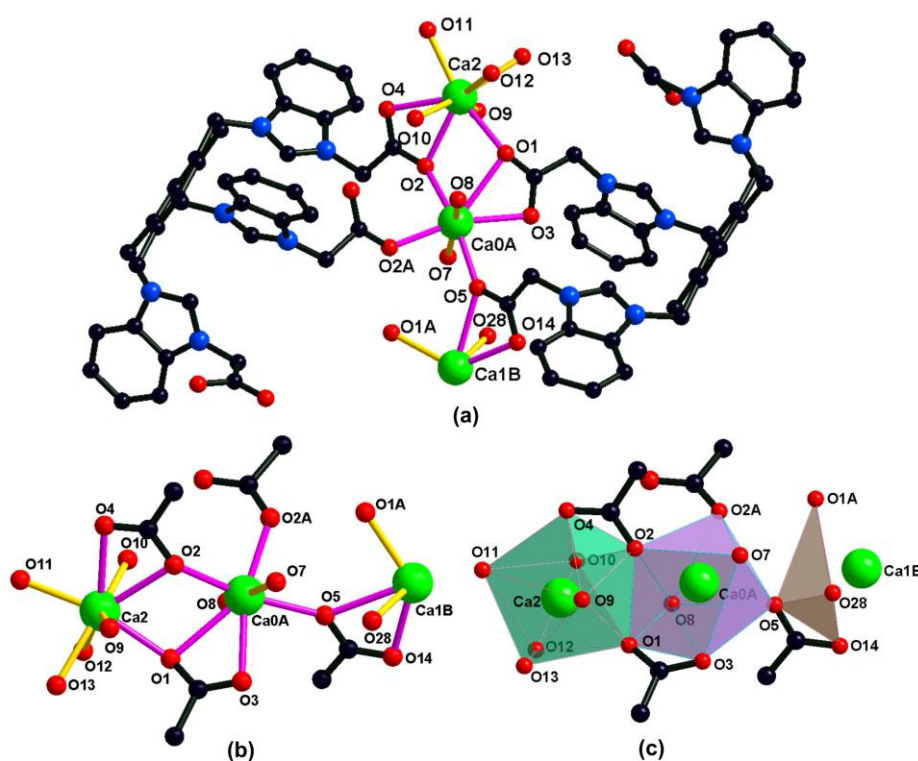


Figure 4.11: (a) Coordination environment of the Ca(II) centers in 6. The hydrogen atoms and bromine ions have been omitted for clarity. (b) Core unit of molecule 6. (c) Polyhedron view of the Ca(II) centers.

The Ca(0A)–O_{COO} (Ca(0A)–O(2) 2.305(4) Å, Ca(0A)–O(1) 2.698(5) Å, Ca(0A)–O(2A) 2.318(5) Å, Ca(0A)–O(3) 2.453(4) Å and Ca(0A)–O(5) 2.353(4) Å), Ca(2)–O_{COO} (Ca(2)–O(2) 2.538(5) Å, Ca(2)–O(1) 2.371(5) Å and Ca(2)–O(4) 2.530(4) Å) and Ca(1B)–O_{COO} (Ca(1B)–O(5) 2.672(5) Å and Ca(1B)–O(14) 2.356(5) Å) bond lengths are different. Similarly, the Ca(0A)–O_{water} (2.368(5) and 2.436(5) Å), Ca(2)–O_{water} (2.354(6) Å to 2.470(6) Å) and Ca(1B)–O_{water} (2.379(9) and 2.469(11) Å) bond lengths

are different. The charge of Ca(II) centers are balanced by carboxylate anions, while the benziimidazol cation charges are balanced by bromine anions.

Table 4.2: Summary of crystallographic data and structure refinement results for **1-3**

Parameters	1	2	3
Empirical formula	C ₂₁ H ₃₄ N ₄ O ₉ CaBr ₂	C ₅₈ H _{80.4} N ₈ O _{23.97} Ca ₂ Br ₄	C ₁₈ H ₂₂ N ₄ O ₆ CaBr
Formula weight	686.42	1673.02	510.38
Temperature (K)	150	150	150
Crystal system	Triclinic	Triclinic	Monoclinic
Space group	<i>P</i> $\bar{1}$	<i>P</i> $\bar{1}$	<i>P2/c</i>
<i>a</i> /Å	8.2450(6)	14.1675(7)	11.8051(15)
<i>b</i> /Å	11.6571(9)	16.5118(9)	14.1508(16)
<i>c</i> /Å	15.3212(13)	17.3328(8)	7.6915(5)
α /°	100.778(7)	94.247(4)	90.00
β /°	99.668(7)	109.921(4)	91.038(9)
γ /°	91.324(6)	110.838(5)	90.00
Volume (Å ³)	1423.8(2)	3473.6(3)	1284.7(2)
<i>Z</i>	2	2	2
ρ_{calc} /mg mm ⁻³	1.601	1.600	1.319
Absorption coefficient (mm ⁻¹)	5.652	4.821	4.242
<i>F</i> (000)	700.0	1712.0	522.0
Data collected	10212	26432	2326
Unique data	5338	13074	2326

R_{int}	0.0412	0.0359	0.0424
GOF on F^2	1.041	1.023	0.952
R_1 ($I > 2\sigma(I)$)	0.0490	0.0652	0.0697
wR_2 ($I > 2\sigma(I)$)	0.1229	0.1920	0.1975
R_1 values (all data)	0.0647	0.0816	0.0963
wR_2 values (all data)	0.1345	0.2107	0.2293

Table 4.3: Summary of crystallographic data and structure refinement results for **4-6**

Parameters	4	5	6
Empirical formula	$\text{C}_{13}\text{H}_{13}\text{N}_2\text{O}_3\text{Ca}_{0.5}\text{Br}_{0.5}$	$\text{C}_{54}\text{H}_{72.5}\text{N}_{12}\text{O}_{21.75}\text{Ca}_{2.5}\text{Cl}_{0.85}$	$\text{C}_{78}\text{H}_{88}\text{N}_{12}\text{O}_{20}\text{Br}_6\text{Ca}_{2.5}$
Formula weight	305.25	1842.55	2093.26
Temperature (K)	150	150	150
Crystal system	Triclinic	Triclinic	Triclinic
Space group	$P\bar{1}$	$P\bar{1}$	$P\bar{1}$
$a/\text{\AA}$	4.6746(12)	14.4574(8)	14.3416(7)
$b/\text{\AA}$	11.632(3)	15.3803(6)	20.7798(8)
$c/\text{\AA}$	13.537(3)	19.4570(11)	21.1629(8)
α°	76.891(18)	103.011(4)	89.717(3)
β°	84.108(19)	107.177(5)	74.471(4)
γ°	85.173(19)	99.571(4)	75.245(4)

Volume (Å ³)	711.7(3)	3899.4(4)	5862.7(5)
Z	2	1	2
$\rho_{\text{calc}}/\text{mg mm}^{-3}$	1.424	1.569	1.186
Absorption coefficient (mm ⁻¹)	3.930	5.896	3.898
F(000)	313.0	1855.0	2120.0
Data collected	2562	27821	21809
Unique data	2562	13719	21809
R_{int}	0.0000	0.0161	0.0560
GOF on F^2	1.027	1.023	1.036
R_1 ($I > 2\sigma(I)$)	0.0787	0.0837	0.0975
wR_2 ($I > 2\sigma(I)$)	0.1897	0.2304	0.2682
R_1 values (all data)	0.0954	0.0983	0.1176
wR_2 values (all data)	0.2054	0.2523	0.2916

4.3.3 Comparison of solid state structures of 1-6

The coordination geometry of the calcium centres in **1-6** are compared with known calcium imidazolium carboxylates, $\{[\text{Ca}_2(\mathbf{BCI})_3(\text{Br})](\text{H}_2\text{O})_5\}_\infty$ [12] and $[\text{Ca}(\mathbf{BCBI})_2(\text{H}_2\text{O})_4]\cdot 2\text{H}_2\text{O}$ [13] in Fig. 4.12. Highly diversified and flexible coordination numbers and geometries are observed for the calcium centres in **1-6**. The geometry of calcium(II) in known calcium imidazolium carboxylates, $\{[\text{Ca}_2(\mathbf{BCI})_3(\text{Br})](\text{H}_2\text{O})_5\}_\infty$ and $[\text{Ca}(\mathbf{BCBI})_2(\text{H}_2\text{O})_4]\cdot 2\text{H}_2\text{O}$ is a distorted octahedron. The molecules **1** and **4** are isolated

as 3D supramolecular networks through Br \cdots H hydrogen bonding. However the geometry of calcium centres in **1** is distorted square-face monocapped trigonal-prismatic (CN = 7) and geometry of **4** is a distorted octahedron. The Ca–O_{COO} bond lengths of **4** are comparable with those of the reported molecules.

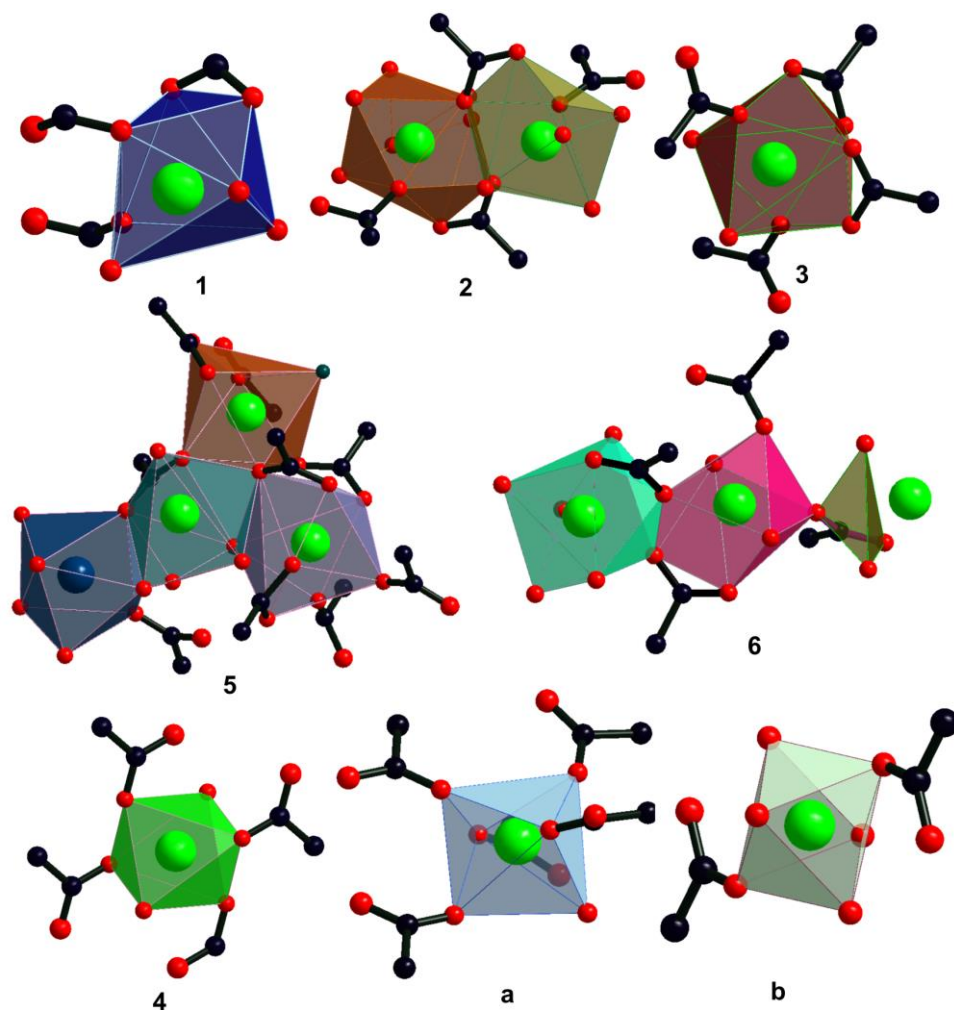


Figure 4.12: Polyhedra of Ca coordination compounds **1-6** and the reported Ca molecules based on imidazolium carboxylates; **a** = $\{[\text{Ca}_2(\text{BCI})_3(\text{Br})](\text{H}_2\text{O})_5\}_\infty$ and **b** = $[\text{Ca}(\text{BCBI})_2(\text{H}_2\text{O})_4]\cdot 2\text{H}_2\text{O}$.

The molecules **2** and **6** are discrete binuclear and trinuclear calcium molecules, respectively. The geometries of calcium centers in **2** are distorted square-face bicapped trigonal-prismatic (CN = 8) and distorted square-face tricapped trigonal-prismatic (CN = 9), while **6** exhibits three different geometries (distorted square-face monocapped trigonal-prismatic (CN = 7), distorted square-face bicapped trigonal-prismatic (CN = 8) and inverted tetrahedral geometry (CN = 4)). The molecule **5** is a complicated 1D

coordination polymer, where the molecule exists in three different calcium coordination environments with hepta-coordinated sodium ions. The molecule **3** is constructed as a three-dimensional metal-organic framework with a distorted square-face bicapped trigonal-prismatic (CN = 8) geometry. Among all the complexes reported in this work, the geometry of calcium center in **4** is most comparable with known Ca imidazolium carboxylate complexes. In **1-3**, **5** and **6** the calcium centers are in distorted square-face monocapped trigonal-prismatic and/or distorted square-face bicapped trigonal-prismatic geometries (besides the third calcium center in **6**, which shows inverted tetrahedral geometry (CN = 4), and in compound **2**, the calcium centers exist in distorted square-face bicapped trigonal-prismatic and square-face tricapped trigonal-prismatic geometries, where the Ca–O_{COO} bond lengths are slightly larger than Ca–O_{COO} bond lengths found in **4**.

4.3.4 Thermal analyses

In order to understand the thermal decomposition pathway of **1-6**, thermogravimetric analysis (TGA) (10 °C/min, 30-1000 °C under a N₂ atmosphere) was carried out on **1-6** (Fig. 4.13). The initial weight loss (11.6%) observed up to 170 °C in **1** can be attributed to the loss of lattice water and coordinated water molecules. Framework **1** showed stability until 320 °C. Subsequently two major weight loss stages were observed (due to loss of the organic part and Br anions). In the first stage (320-490 °C), a weight loss of about 33% was observed, and in the second stage (550-770 °C) a weight loss of about 25% was observed. Compound **2** exhibited an initial weight loss of 10% up to 224 °C, which may be due to the loss of coordinated and lattice water molecules. Then the molecule **2** slowly degraded in two stages, from 224-460 °C with a weight loss of 52% and from 461-840 °C with a weight loss of 19%. Subsequently, the weight loss was constant till 940 °C. Compound **3** displayed an initial weight loss of 7% up to 140 °C, which can be assigned to the loss of coordinated and lattice water molecules. Then the framework was stable upto 280 °C. Later the framework was slowly disturbed. Then sudden weight loss was observed from 280-460 °C with a weight loss of 36%, and then slow weight loss was observed from 460-970 °C with a weight loss of 35%. A small weight loss about 10% was observed for **4** in the initial stage (< 150 °C), attributable to the loss of moisture. From 150 to 320 °C, the compound was almost stable with 7% weight loss. Later, three stages of weight losses were occurred: 320-420 °C with 21%

weight loss, 490-830 °C with 37% weight loss, and 840-920 °C with 11% weight loss (due to evacuation of the Br⁻ and organic part).

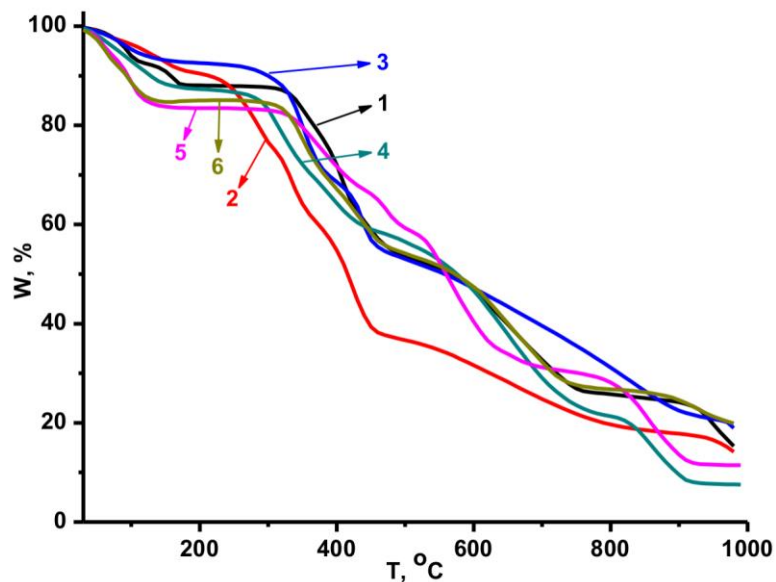


Figure 4.13: The TGA profiles of 1-6 (10 °C min⁻¹, 30-1000 °C under a N₂ atmosphere).

1D coordination polymer **5** displayed an initial weight loss of 15% up to 127 °C, which can be assigned to the loss of coordinated and lattice water molecules. Then the framework was stable up to 326 °C. Later the framework was slowly disturbed. Subsequently, the sudden weight loss was observed from 326-680 °C, with a weight loss of 50%, and then further weight loss was observed from 780-923 °C, with a weight loss of 17.4%. **6** was stable up to 145 °C with a loss of 5%, which may be due to the loss of water molecules. Later the framework was stable up to 306 °C. Then the framework was degraded in different stages: 310-470 °C with 28% weight loss, 500-750 °C with 26% weight loss, and 760-970 °C with 8% weight loss.

4.4 Conclusions

Azolium carboxylate ligands featuring flexible bis- and tris-carboxylic acid groups have been used to assemble the first cationic calcium binuclear (**2**), trinuclear (**6**), one dimensional coordination polymer (**5**) and three dimensional calcium coordination networks (**1**, **3** and **4**) *via* carbonic acid elimination reactions. The flexible carboxylic acid groups in these ligands facilitated the isolation of calcium complexes existing in

unusual coordination environments. The solid state structures of **2** and **6** reveal tetra-cationic binuclear and hexa-cationic trinuclear calcium molecules, respectively, which are rare examples of cationic calcium complexes supported by imidazolium carboxylate ligands. Complex **5** is a one-dimensional coordination polymer consisting of three different calcium coordination environments. Elusive changes in the position of the imidazolium carboxylate group at the aryl spacer (substitution at the 1,3- or 1,4-positions of aryl spacer) yield three dimensional calcium coordination networks (**1**, **3** and **4**), which do not feature any structural resemblances. Changing the aryl spacer between the azolium carboxylates in these solids not only changes the topology of the network but also affects the thermal and luminescence properties exhibited by the network. These calcium azolium carboxylate assemblies (except for **5**) exhibit interesting solid-state photoluminescence behaviors, driven by the imidazolium carboxylate ligand. Variation of the bridging chromophore produced significant effects on the fluorescent behaviors. Moreover **1-4** and **6** represent the first luminescent calcium complexes derived using azolium carboxylate ligands. These results show that azolium carboxylate ligands can be used as potential functional spacers for the isolation of discrete molecules, one dimensional and three dimensional calcium complexes.

4.5 References

- [1] J. R. Long, and O. M. Yaghi. *Chem. Soc. Rev.* 38, (2009) 1213.
- [2] J.-P. Zhang, Y.-B. Zhang, J.-B. Lin, and X.-M. Chen. *Chem. Rev.* 112, (2012) 1001.
- [3] A. Y. Robin, and K. M. Fromm. *Coord. Chem. Rev.* 250, (2006) 2127.
- [4] S. Kitagawa, R. Kitaura, and S. I. Noro. *Angew. Chem., Int. Ed.* 44, (2005) 5720.
- [5] N. Stock, and S. Biswas. *Chem. Rev.* 112, (2012) 933.
- [6] H. Furukawa, K. E. Cordova, M. O'keeffe, and O. M. Yaghi. *Science* 341, (2013) 6149.
- [7] (a) G.-Q. Kong, X. Xu, C. Zou, and C.-D. Wu. *Chem. Commun.* 47, (2011) 11005; (b) G.-Q. Kong, S. Ou, C. Zou, and C.-D. Wu. *J. Am. Chem. Soc.* 134, (2012) 19851; (c) J. M. Roberts, O. K. Farha, A. A. Sarjeant, J. T. Hupp, and K. A. Scheidt. *Cryst. Growth Des.* 11, (2011) 4747; (d) G.-Q. Kong, and C.-D. Wu. *CrystEngComm* 14, (2012) 847; (e) S. Wang, Q. Yang, J. Zhang, X. Zhang, C. Zhao, L. Jiang, and C.-Y. Su. *Inorg. Chem.* 52, (2013) 4198; (f) X. Wang, X.-B. Li, R.-H. Yan, Y.-Q. Wang, and E.-Q. Gao. *Dalton Trans.* 42, (2013) 10000; (g) C. N.

- Babu, A. Sathyanarayana, S. M. Mobin, and G. prabusankar. *Inorg. Chem. Commun.* 37, (2013) 222; (h) P. Suresh, C. N. Babu, and G. Prabusankar. *Polyhedron* 89, (2015) 322.
- [8] Z. Fei, D. Zhao, T. J. Geldbach, R. Scopelliti, P. J. Dyson, S. Antonijevic, and G. Bodenhausen. *Angew. Chem., Int. Ed.* 44, (2005) 5720.
- [9] S. Sen, N. N. Nair, T. Yamada, H. Kitagawa, and P. K. Bharadwaj. *J. Am. Chem. Soc.* 134, (2012) 19432.
- [10] (a) P. Suresh, S. Radhakrishnan, C. N. Babu, A. Sathyanarayana, N. Sampath, and G. Prabusankar. *Dalton Trans.* 42, (2013) 10838 and references there in. (b) A. W. van der Made, and R. H. van der Made. *J. Org. Chem.* 58, (1993) 1262. (c) Y. Yuan, Z.-L. Jiang, J.-M. Yan, G. Gao, A. S. C. Chan, and R.-G. Xie. *Synth. Commun.* 30, (2000), 4555; (d) S. Kohmoto, S. Okuyama, N. Yokota, M. Takahashi, K. Kishikawa, H. Masu, and I. Azumaya. *Cryst. Growth Des.* 11, (2011) 3698.
- [11] Z. Fei, T. J. Geldbach, D. Zhao, R. Scopelliti, and P. J. Dyson. *Inorg. Chem.* 44, (2005) 5200.
- [12] Z. Fei, T. J. Geldbach, R. Scopelliti, and P. J. Dyson. *Inorg. Chem.* 45, (2006) 6331.
- [13] L. Huang, A.-G. Zhong, D.-B. Chen, D. Qiu, and H.-D. Liang. *J. Mol. Struct.* 984, (2010) 39.
- [14] G. Nickerl, A. Notzon, M. Heitbaum, I. Senkovska, F. Glorius, and S. Kaskel. *Cryst. Growth Des.* 13, (2013) 198.
- [15] S. Sen, T. Yamada, H. Kitagawa, and P. K. Bharadwaj. *Cryst. Growth Des.* 14, (2014) 1240.
- [16] S. Sen, S. Neogi, A. Aijaz, Q. Xu, and P. K. Bharadwaj. *Inorg. Chem.* 53, (2014) 7591.
- [17] D. D. Perrin, and W. L. F. Armarego. *Purification of laboratory chemicals*, third ed., Pergamon Press, London, 1988.
- [18] O. V. Dolomanov, L. J. Bourhis, R. J. Gildea, J. A. K. Howard, and H. Puschmann. *J. Appl. Cryst.* 42, (2009) 339.

Chapter 5

Rare-earth Discrete Molecules and Coordination Polymers from Zwitterionic Imidazolium Carboxylates

5.1 Introduction

The design and synthesis of lanthanide coordination compounds has engrossed wide attention during the last few decades because of their fascinating architectures and physical properties with widespread applications in catalysis [1], sensors [2], single molecule magnets (SMMs) [3], light-emitting diodes [4], laser systems [5] and display devices [6]. In contrast with transition metal ions, the lanthanides own higher coordination numbers and more flexible coordination geometries. Thus lead to the formation of coordination polymers with versatile motifs [7]. Moreover, lanthanide contraction may also impact the coordination numbers and generate diverse structures [8]. Exclusively, synthesizes of Dy(III) and Gd(III) coordination compounds are much more attractive in the field of molecular magnetism [9-11]. The first imidazolium carboxylic organic spacer based coordination polymer was reported by Dyson *et al.* in 2005 [12]. The chemistry of imidazolium carboxylate based d-block coordination polymers were well studied compared to lanthanide based coordination polymers. The first imidazolium carboxylate supported lanthanide coordination compound was first reported by Lu *et al.* in 2009 [13]. Later, Zhang *et al.* was reported the different La and Nd coordination polymers in 2012 [14].

In this chapter, we report the first time design and synthesis of zwitterionic bis-imidazolium carboxylates (L^1), tris-imidazolium carboxylate (L^2) for the isolation of coordination compounds (Fig. 5.1). The deca-coordinated dimers $\{[(L^1)_2(RE)_2(NO_3)_2(H_2O)_4(DMF)_2](NO_3)_4\}$ (RE = La (**1**) and Ce (**2**)), nona-coordinated

dimer $\{[(L^1)_2(RE)_2(NO_3)_2(H_2O)_2(DMF)_2](NO_3)_4\}$ (RE = Sm (**3**)), octa-coordinated dimers $\{[(L^1)_2(RE)_2(NO_3)_2(H_2O)_2(DMF)_2](NO_3)_4\}$ (RE = Gd (**4**), Dy (**5**) and Y (**6**)) were derived using L^1 and corresponding metal salts. The 1D coordination polymers $\{[(L^2)(RE)(NO_3)(H_2O)](H_2O)_3(NO_3)_2\}_\infty$ (RE = Sm (**7**), Gd (**8**), Dy (**9**) and Y (**10**)) and monomers $\{[(L^2)_2(RE)](NO_3)_3\}$ (RE = Sm (**11**), Gd (**12**), Dy (**13**) and Y (**14**)) were isolated from the reaction between L^2 and corresponding metal salts.

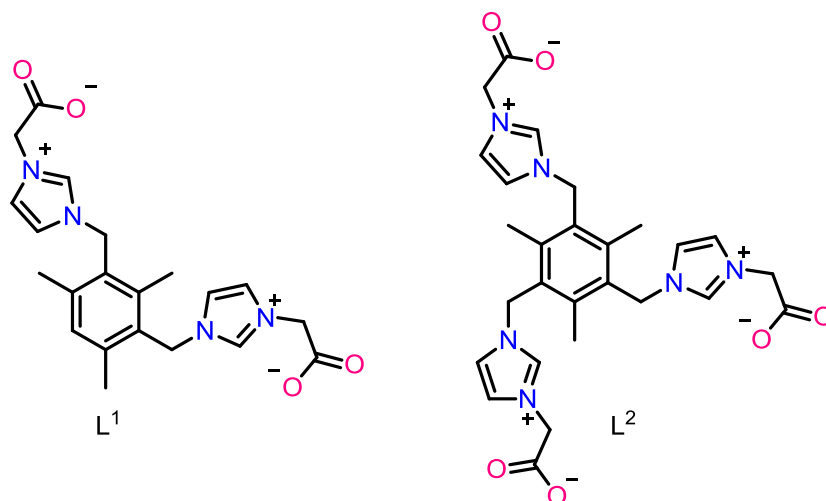


Figure 5.1: Zwitterionic bis- and tris-imidazolium carboxylates.

5.2 Experimental section

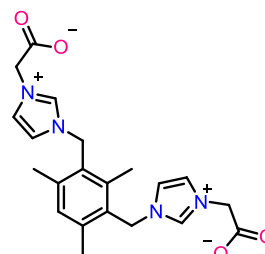
5.2.1 Materials and methods

The solvents were purchased from commercial sources and purified according to standard procedures [15]. Unless otherwise stated, the chemicals were purchased from commercial sources. L^1 and L^2 were prepared as reported [16,17]. FT-IR measurement (neat) was carried out on a Bruker Alpha-P Fourier transform spectrometer. NMR spectra were recorded on Bruker Ultrashield-400 spectrometers at 25 °C unless otherwise stated. Chemical shifts are given relative to TMS and were referenced to the solvent resonances as internal standards. The UV-vis spectra were measured on a T90+ UV-visible spectrophotometer. Elemental analyses were performed by the Euro Vector EA-300 elemental analyzer. The crystal structures of **1-14** were measured on an Oxford Xcalibur 2 diffractometer. Data were collected at 298 K or 150 K. Using Olex2 [18], the structure were solved with the Olex2 structure solution program using Direct Methods

and refined with the olex2.refine refinement package using Gauss-Newton minimisation.

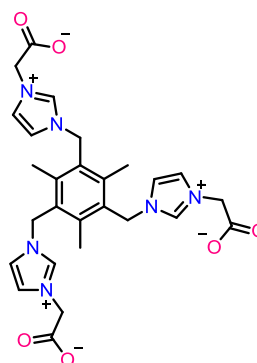
5.2.2 Synthesis of L^1 , L^2 and 1-14

L^1 : A reaction mixture of $L^1H_2Br_2$ (1 g, 1.791 mmol) and dry triethylamine (1.5 mL) in dry DCM (50 mL) was stirred for 24 h at room temperature. The resultant solid was filtered and washed with DCM (20 mL) and dried under vacuum. Yield: 92% (based on $L^1H_2Br_2$). Anal. Calcd. (%) for $C_{21}H_{24}N_4O_4$ (396.44): C, 63.62; H, 6.10; N,



14.13; found: C, 63.6; H, 6.1; N, 14.2. 1H NMR (400 MHz, D_2O): δ = 8.50 (s, 2H, ImH), 7.45 and 7.36 (s, 2 x 2H, 2 x ImH), 7.24 (s, 1H, ArH), 5.51 (s, 4H, CH_2), 4.75 (s, 4H, CH_2), 2.34 (s, 6H, CH_3), 2.23 (s, 3H, CH_3) ppm. ^{13}C NMR (100 MHz, D_2O): δ = 172.0 (C=O), 140.8 (ArC), 139.2 (ArC), 135.9 (ImC), 131.4 (ArC), 127.7 (ArC), 123.8 (ImC), 121.55 (ImC), 52.02 (CH_2), 47.67 (CH_2), 18.94 (CH_3), 14.71 (CH_3) ppm. FT-IR (neat): $\bar{\nu}$ = 3467 (w), 3072 (w), 3002 (w), 1618 (s), 1559 (m), 1460 (w), 1371 (s), 1333 (w), 1305 (m), 1221 (w), 1156 (s), 1023 (w) cm^{-1} .

L^2 : The compound L^2 was synthesized similar method as L^1 using $L^2H_3Br_3$ (1 g, 1.286 mmol) and dry triethylamine (2 mL) in dry DCM (50 mL). Yield: 87% (based on $L^2H_3Br_3$). Anal. Calcd. (%) for $C_{27}H_{30}N_6O_6$ (534.56): C, 60.66; H, 5.66; N, 15.72; found: C, 60.2; H, 5.7; N, 15.7. 1H NMR (400 MHz, D_2O): δ = 8.56 (s, 3H, ImH), 7.48 (s, 3H, ImH), 7.40 (s, 3H, ImH), 5.63 (s, 4H, CH_2), 4.79 (s, 4H, CH_2), 2.36 (s, 9H, CH_3) ppm. ^{13}C NMR (100 MHz,



D_2O): δ = 172.0 (C=O), 141.7 (ArC), 136.00 (ImC), 129.1 (ArC), 123.9 (ImC), 121.6 (ImC), 52.1 (CH_2), 48.1 (CH_2), 15.7 (CH_3) ppm. IR (neat): $\bar{\nu}$ = 3361 (w), 3089 (w), 1626 (s), 1569 (m), 1495 (w), 1372 (s), 1333 (w), 1303 (m), 1247 (w), 1158 (s), 1113 (w) cm^{-1} .

$\{(L^1)_2(La)_2(NO_3)_2(H_2O)_4(DMF)_2\}(NO_3)_4$ (**1**): L^1 (0.200 g, 0.500 mmol) and $La(NO_3)_3 \cdot 6H_2O$ (0.219 g, 0.506 mmol) were taken into schlenk tube and added 1:1

DMF and MeOH (2 mL). The reaction mixture was heated at 70 °C for 12 h. Then the reaction mixture was slowly brought RT to isolate the colorless crystals. Crystals were washed with MeOH and dried under vacuum. Yield: 62% (based on $\text{La}(\text{NO}_3)_3 \cdot 6\text{H}_2\text{O}$). Anal. Calcd. (%) for $\text{C}_{48}\text{H}_{70}\text{N}_{16}\text{O}_{32}\text{La}_2$ (1660.99): C, 34.71; H, 4.25; N, 13.49; found: C, 34.7; H, 4.3; N, 13.4. FT-IR (neat): $\bar{\nu} = 3096$ (w), 1667 (w), 1622 (s), 1571 (w), 1442 (m), 1397 (w), 1378 (w), 1335 (w), 1307 (s), 1155 (s), 1104 (m), 1037 (w), 1019 (w), 980 (w) cm^{-1} .

$\{[(\text{L}^1)_2(\text{Ce})_2(\text{NO}_3)_2(\text{H}_2\text{O})_4(\text{DMF})_2](\text{NO}_3)_4\}$ (**2**): **2** was synthesized as reported for **1**, using $\text{Ce}(\text{NO}_3)_3 \cdot 6\text{H}_2\text{O}$ (0.219 g, 0.504 mmol). Yield: 59% (based on $\text{Ce}(\text{NO}_3)_3 \cdot 6\text{H}_2\text{O}$). Anal. Calcd. (%) for $\text{C}_{48}\text{H}_{70}\text{N}_{16}\text{O}_{32}\text{Ce}_2$ (1663.41): C, 34.66; H, 4.24; N, 13.47; found: C, 34.7; H, 4.2; N, 13.4. FT-IR (neat): $\bar{\nu} = 3097$ (w), 1668 (w), 1624 (s), 1571 (w), 1443 (m), 1397 (w), 1379 (w), 1336 (w), 1309 (s), 1155 (s), 1104 (m), 1038 (w), 1019 (w), 980 (w) cm^{-1} .

$\{[(\text{L}^1)_2(\text{Sm})_2(\text{NO}_3)_2(\text{H}_2\text{O})_2(\text{DMF})_2](\text{NO}_3)_4\}$ (**3**): **3** was synthesized as reported for **1**, using $\text{Sm}(\text{NO}_3)_3 \cdot 6\text{H}_2\text{O}$ (0.225 g, 0.506 mmol). Yield: 58% (based on $\text{Sm}(\text{NO}_3)_3 \cdot 6\text{H}_2\text{O}$). Anal. Calcd. (%) for $\text{C}_{48}\text{H}_{66}\text{N}_{16}\text{O}_{30}\text{Sm}_2$ (1647.85): C, 34.99; H, 4.04; N, 13.60; found: C, 34.9; H, 4.1; N, 13.6. FT-IR (neat): $\bar{\nu} = 3148$ (w), 3092 (w), 1674 (w), 1636 (s), 1569 (w), 1449 (m), 1402 (w), 1364 (w), 1336 (w), 1307 (s), 1156 (s), 1102 (m), 1036 (w), 1019 (w), 980 (w) cm^{-1} .

$\{[(\text{L}^1)_2(\text{Gd})_2(\text{NO}_3)_2(\text{H}_2\text{O})_2(\text{DMF})_2](\text{NO}_3)_4\}$ (**4**): **4** was synthesized as reported for **1**, using $\text{Gd}(\text{NO}_3)_3 \cdot 6\text{H}_2\text{O}$ (0.228 g, 0.505 mmol). Yield: 56% (based on $\text{Gd}(\text{NO}_3)_3 \cdot 6\text{H}_2\text{O}$). Anal. Calcd. (%) for $\text{C}_{48}\text{H}_{66}\text{N}_{16}\text{O}_{30}\text{Gd}_2$ (1661.67): C, 34.70; H, 4.00; N, 13.49; found: C, 34.8; H, 4.0; N, 13.5. FT-IR (neat): $\bar{\nu} = 3094$ (w), 2030 (w), 1678 (w), 1641 (s), 1568 (w), 1452 (m), 1405 (w), 1381 (w), 1308 (s), 1156 (s), 1105 (m), 1024 (m), 980 (w) cm^{-1} .

$\{[(\text{L}^1)_2(\text{Dy})_2(\text{NO}_3)_2(\text{H}_2\text{O})_2(\text{DMF})_2](\text{NO}_3)_4\}$ (**5**): **5** was synthesized as reported for **1**, using $\text{Dy}(\text{NO}_3)_3 \cdot x\text{H}_2\text{O}$ (0.194 g, 0.506 mmol). Yield: 52% (based on $\text{Dy}(\text{NO}_3)_3 \cdot x\text{H}_2\text{O}$). Anal. Calcd. (%) for $\text{C}_{48}\text{H}_{66}\text{N}_{16}\text{O}_{30}\text{Dy}_2$ (1672.17): C, 34.48; H, 3.98; N, 13.40; found: C, 34.5; H, 4.0; N, 13.3. FT-IR (neat): $\bar{\nu} = 3107$ (w), 1692 (m), 1642 (s), 1568 (w), 1451 (m), 1410 (w), 1381 (w), 1303 (w), 1303 (s), 1156 (m), 1110 (w), 1034 (w), 980 (w) cm^{-1} .

$\{[(L^1)_2(Y)(NO_3)_2(H_2O)_2(DMF)_2](NO_3)_4\}$ (**6**): **6** was synthesized as reported for **1**, using $Y(NO_3)_3 \cdot 6H_2O$ (0.231 g, 0.506 mmol). Yield: 54% (based on $Y(NO_3)_3 \cdot 6H_2O$). Anal. Calcd. (%) for $C_{48}H_{66}N_{16}O_{30}Y_2$ (1524.94): C, 37.81; H, 4.36; N, 14.70; found: C, 37.7; H, 4.4; N, 14.7. FT-IR (neat): $\bar{\nu} = 3107$ (w), 3060 (w), 1695 (m), 1643 (s), 1567 (m), 1469 (w), 1451 (m), 1411 (m), 1380 (m), 1306 (s), 1254 (w), 1203 (w), 1155 (m), 1111 (m), 1033 (m), 981 (w) cm^{-1} .

$\{[(L^2)(Sm)(NO_3)(H_2O)](H_2O)_3(NO_3)_2\}_\infty$ (**7**): L^2 (0.200 g, 0.374 mmol) and $Sm(NO_3)_3 \cdot 6H_2O$ (0.167 g, 0.376 mmol) were taken into schlenk tube and added 1:1 DMF, EtOH and H_2O (2 mL). The reaction mixture was heated at 100 °C for 12 h, and then the reaction mixture was slowly brought to RT to obtain the colorless crystals. The crystals were washed with MeOH and dried under vacuum. Yield: 53% (based on $Sm(NO_3)_3 \cdot 6H_2O$). Anal. Calcd. (%) for $C_{27}H_{38}N_9O_{19}Sm$ (943.02): C, 34.39; H, 4.06; N, 13.37; found: C, 34.4; H, 4.2; N, 13.3. FT-IR (neat): $\bar{\nu} = 3388$ (w), 3143 (w), 3112 (w), 3066 (w), 1635 (w), 1607 (m), 1566 (w), 1449 (m), 1368 (m), 1338 (m), 1311 (s), 1154 (s), 1107 (w), 1035 (m) cm^{-1} .

$\{[(L^2)(Gd)(NO_3)(H_2O)](H_2O)_3(NO_3)_2\}_\infty$ (**8**): **8** was synthesized as reported for **7**, using $Gd(NO_3)_3 \cdot 6H_2O$ (0.169 g, 0.374 mmol). Yield: 56% (based on $Gd(NO_3)_3 \cdot 6H_2O$). Anal. Calcd. (%) for $C_{27}H_{38}N_9O_{19}Gd$ (949.90): C, 34.14; H, 4.03; N, 13.27; found: C, 34.2; H, 4.1; N, 13.3. FT-IR (neat): $\bar{\nu} = 3142$ (w), 3087 (w), 1636 (w), 1606 (s), 1566 (w), 1452 (m), 1368 (m), 1339 (w), 1317 (s), 1153 (s), 1036 (m), 981 (w) cm^{-1} .

$\{[(L^2)(Dy)(NO_3)(H_2O)](H_2O)_3(NO_3)_2\}_\infty$ (**9**): **9** was synthesized as reported for **7**, using $Dy(NO_3)_3 \cdot xH_2O$ (0.171 g, 0.374 mmol). Yield: 55% (based on $Dy(NO_3)_3 \cdot xH_2O$). Anal. Calcd. (%) for $C_{27}H_{38}N_9O_{19}Dy$ (955.15): C, 33.95; H, 4.01; N, 13.20; found: C, 34.4; H, 4.2; N, 13.3. FT-IR (neat): $\bar{\nu} = 3396$ (br), 3143 (w), 3112 (w), 1640 (w), 1608 (s), 1566 (w), 1454 (s), 1389 (w), 1297 (s), 1154 (s), 1105 (w), 1037 (m), 981 (w) cm^{-1} .

$\{[(L^2)(Y)(NO_3)(H_2O)](H_2O)_3(NO_3)_2\}_\infty$ (**10**): **10** was synthesized as reported for **7**, using $Y(NO_3)_3 \cdot 6H_2O$ (0.144 g, 0.376 mmol). Yield: 48% (based on $Y(NO_3)_3 \cdot 6H_2O$). Anal. Calcd. (%) for $C_{27}H_{38}N_9O_{19}Y$ (882.56): C, 36.75; H, 4.34; N, 14.28; found: C, 36.8; H, 4.3; N, 14.3. FT-IR (neat): $\bar{\nu} = 3393$ (br), 3142 (w), 3114 (w), 1639 (w), 1609 (s), 1565 (m), 1457 (s), 1389 (w), 1368 (w), 1321 (s), 1155 (s), 1109 (w), 1038 (m) cm^{-1} .

{[(L²)₂(Sm)](NO₃)₃} (11): L² (0.2 g, 0.374 mmol) and Sm(NO₃)₃·6H₂O (0.084 g, 0.189 mmol) were taken into schlenk tube and added 1:1:1:3 DMF, MeOH and H₂O, 4,4'-bipyridene (0.1 g, 0.641 mmol) and pyridene (2 mL). The reaction mixture was heated at 80 °C for 12 h, and then the reaction mixture was slowly brought to RT to obtain the colorless crystals. The crystals washed with MeOH and dried under vacuum. Yield: 58% (based on Sm(NO₃)₃·6H₂O). Anal. Calcd. (%) for C₅₄H₆₀N₁₅O₂₁Sm (1405.53): C, 46.15; H, 4.30; N, 14.95; found: C, 46.2; H, 4.3; N, 14.9. FT-IR (neat): $\bar{\nu}$ = 3103 (w), 1623 (s), 1446 (m), 1397 (w), 1304 (s), 1155 (s), 1107 (w), 1033 (m) cm⁻¹.

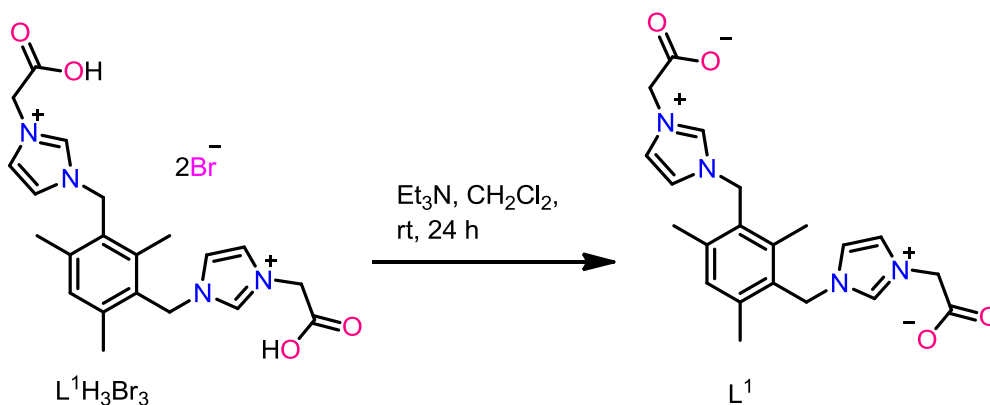
{[(L²)₂(Gd)](NO₃)₃} (12): 12 was synthesized as reported for 11, using Gd(NO₃)₃·6H₂O (0.085 g, 0.188 mmol). Yield: 64% (based on Gd(NO₃)₃·6H₂O). Anal. Calcd. (%) for C₅₄H₆₀N₁₅O₂₁Gd (1412.42): C, 45.92; H, 4.28; N, 14.88; found: C, 45.7; H, 4.3; N, 14.8. FT-IR (neat): $\bar{\nu}$ = 3142 (w), 3094 (w), 2998 (w), 1627 (s), 1563 (w), 1366 (s), 1329 (s), 1282 (s), 1199 (w), 1151 (s), 1109 (w), 1037 (w), 981 (w) cm⁻¹.

{[(L²)₂(Dy)](NO₃)₃} (13): 13 was synthesized as reported for 11, using Dy(NO₃)₃·xH₂O (0.086 g, 0.188 mmol). Yield: 74% (based on Dy(NO₃)₃·xH₂O). Anal. Calcd. (%) for C₅₄H₆₀N₁₅O₂₁Dy (1417.66): C, 45.75; H, 4.27; N, 14.82; found: C, 45.9; H, 4.2; N, 14.8. FT-IR (neat): $\bar{\nu}$ = 3136 (w), 3089 (w), 2994 (w), 1626 (s), 1563 (w), 1435 (w), 1355 (m), 1329 (s), 1301 (m), 1280 (m), 1201 (w), 1152 (s), 1111 (w), 1037 (w), 984 (w) cm⁻¹.

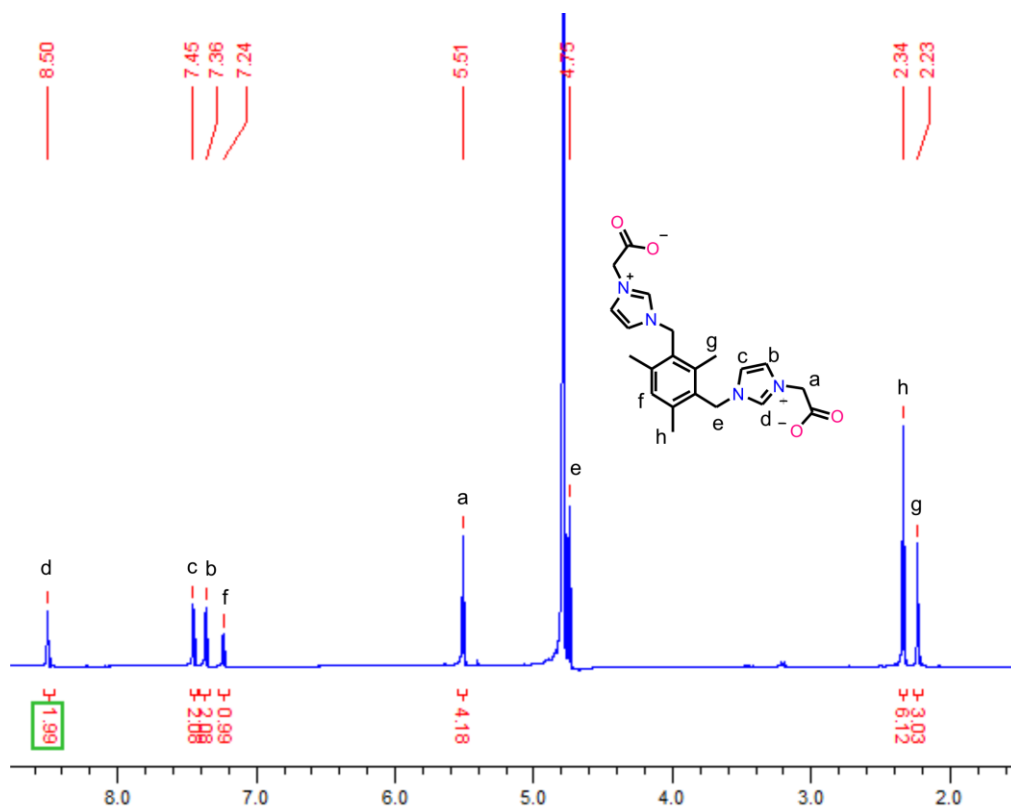
{[(L²)₂(Y)](NO₃)₃} (14): 14 was synthesized as reported for 11, using Y(NO₃)₃·6H₂O (0.072 g, 0.188 mmol). Yield: 73% (based on Y(NO₃)₃·6H₂O). Anal. Calcd. (%) for C₅₄H₆₀N₁₅O₂₁Y (1345.07): C, 48.26; H, 4.50; N, 15.62; found: C, 48.1; H, 4.4; N, 15.7. FT-IR (neat): $\bar{\nu}$ = 3140 (w), 3092 (w), 2999 (w), 1627 (s), 1566 (w), 1478 (w), 1453 (w), 1373 (m), 1324 (s), 1203 (w), 1154 (s), 1112 (w), 1034 (w) cm⁻¹.

5.3 Results and discussion

5.3.1 Synthesis and characterization of L¹ and 1-6



Scheme 5.1: Synthesis of L^1 .



Compound L^1 was synthesized from deprotonation of corresponding imidazolium salt $\text{L}^1\text{H}_3\text{Br}_3$ with Et_3N in DCM at RT (Scheme 5.1). The FT-IR spectrum of L^1 exhibited a characteristic peak for asymmetric stretching frequency at 1618 cm^{-1} and symmetric stretching frequency at 1370 cm^{-1} . The ^1H NMR spectrum of L^1 showed the diagnostic peak for NCHN at 8.50 ppm (Fig. 5.2), while ^{13}C NMR spectrum of L^1 displayed the diagnostic peaks for NCHN at 139 ppm and C=O at 172 ppm (Fig. 5.3). The compounds

1-6 were synthesized from the reaction of **L**¹ and RE(NO₃)₃·6H₂O (RE = La, Ce, Sm, Gd, Dy, and Y) in DMF and methanol at 70 °C. These are insoluble in almost all common organic solvents and soluble in water.

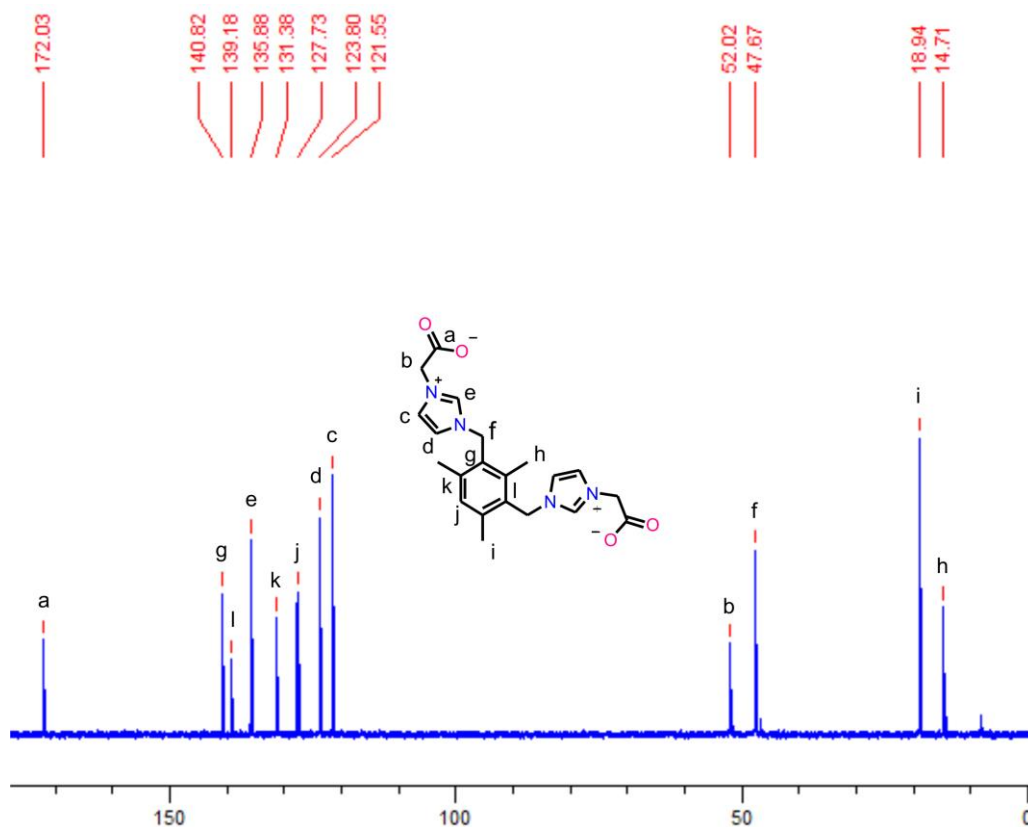


Figure 5.3: ¹³C NMR spectrum of **L**¹ in D₂O at RT.

In FT-IR spectroscopy (Fig. 5.4), **1-6** shows characteristic peaks for DMF C=O group at 1667-1695 cm⁻¹ (**1** 1667 cm⁻¹, **2** 1668 cm⁻¹, **3** 1674 cm⁻¹, **4** 1678 cm⁻¹, **5** 1692 cm⁻¹ and **6** 1695 cm⁻¹), asymmetric stretching frequency at 1622-1643 cm⁻¹ (**1** 1622 cm⁻¹, **2** 1624 cm⁻¹, **3** 1636 cm⁻¹, **4** 1640 cm⁻¹, **5** 1642 cm⁻¹ and **6** 1643 cm⁻¹), symmetric stretching frequency at 1441-1451 cm⁻¹ (**1** 1441 cm⁻¹, **2** 1442 cm⁻¹, **3** 1449 cm⁻¹, **4** 1451 cm⁻¹, **5** 1451 cm⁻¹ and **6** 1451 cm⁻¹) and nitrate group stretching frequency at 1303-1310 cm⁻¹.

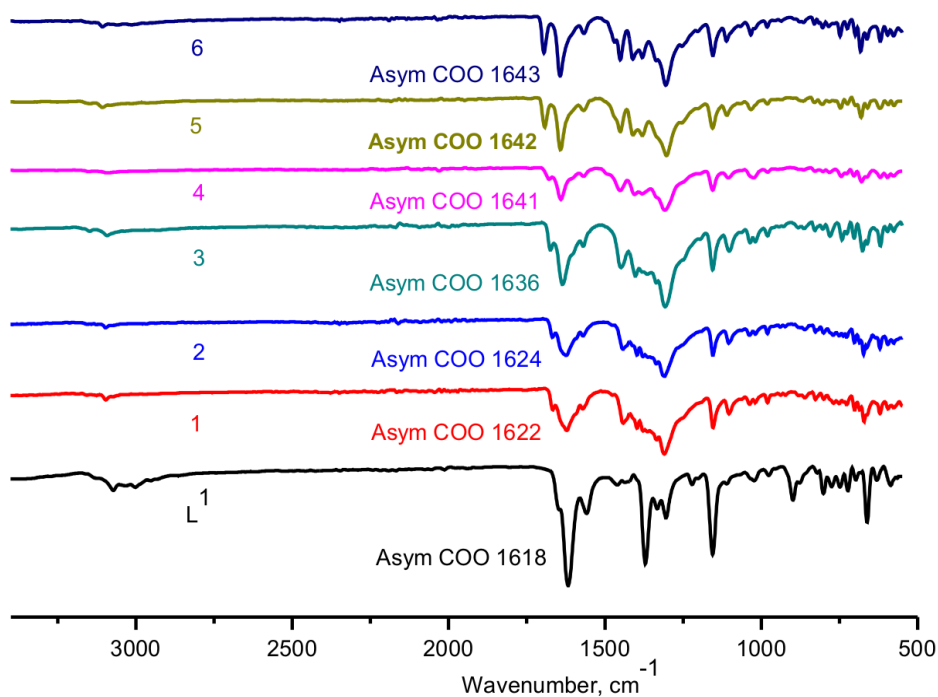


Figure 5.4: FT-IR (neat) spectrum of L^1 and 1–6.

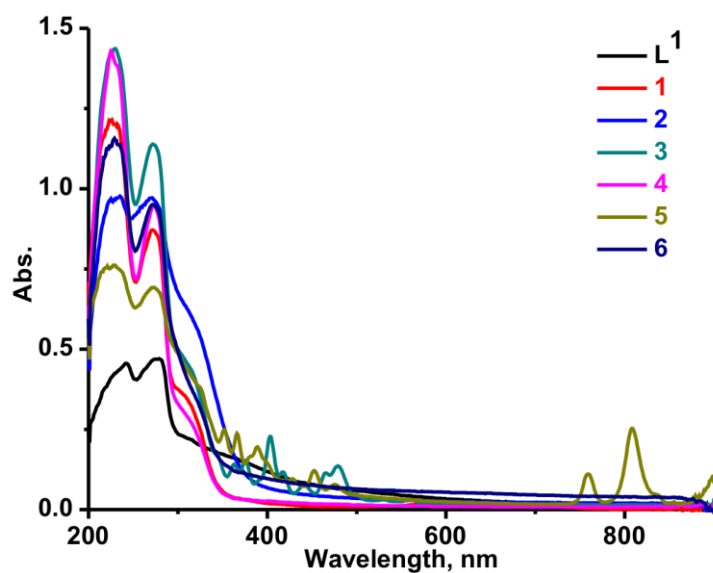


Figure 5.5: The solid-state UV-vis absorption spectra of L^1 and 1-6.

The solid UV-visible absorption spectra of L^1 and 1-6 were measured at room temperature (Fig. 5.5). L^1 shows two absorption bands at 243 and 279 nm which are attributed due to π to π^* transitions. Compounds 1-6 were slightly shifted to higher

wavelength and shows strong bands compare to L^1 absorption bands at 243 and 279 nm (**1** (226 and 271 nm), **2** (235 and 271 nm), **3** (230 and 272 nm), **4** (225 and 273 nm), **5** (221 and 273 nm) and **6** (229 and 272 nm)). As shown in Fig. 5.5, in the case of compounds **3** and **5** shows f-f transitions. The compound **3** shows additional (f-f transitions) absorption bands at 363, 376, 403 and 479 nm, while **5** shows additional (f-f transitions) absorption bands at 352, 366, 389, 428, 452, 475, 759, 808 and 899 nm.

5.3.2 Description of crystal structures 1-6

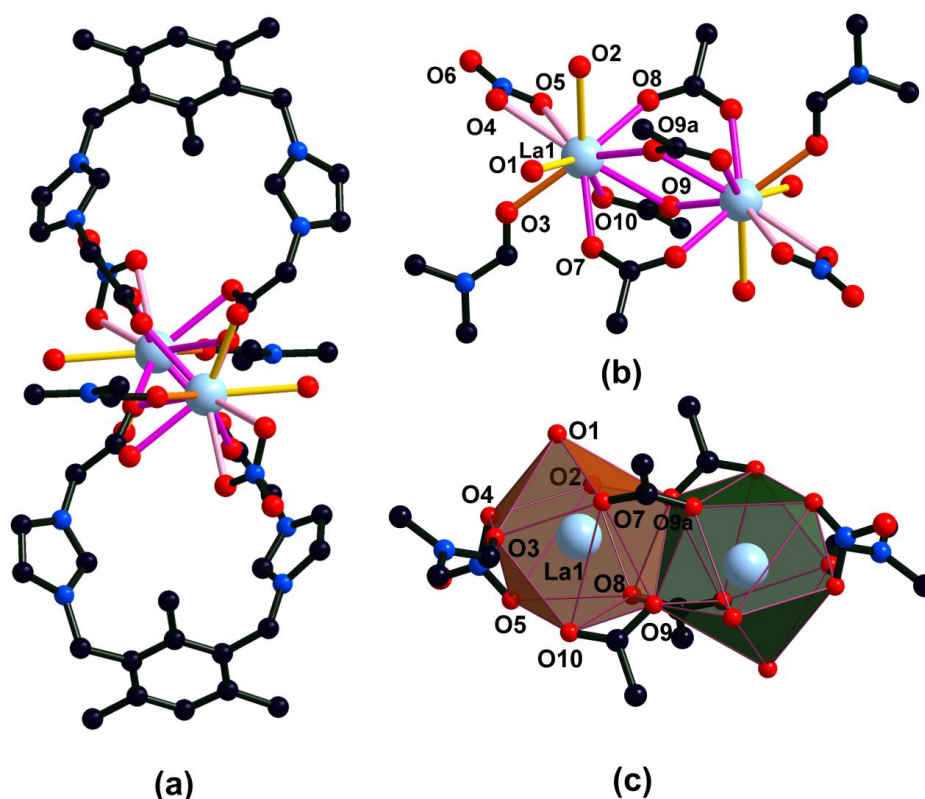


Figure 5.6: (a) The solid state structure of **1**. The hydrogen atoms have been omitted for clarity. (b) Core unit of **1**. (c) Polyhedron view of La(III) centers in **1**.

Crystal X-ray structure of $\{[(L^1)_2(RE)_2(NO_3)_2(H_2O)_4(DMF)_2](NO_3)_4\}$ (RE = La (1**) and Ce (**2**)):** The solid state structure of **1** revealed the formation of ionic dinuclear compound and crystallized in the triclinic space group, $P\bar{1}$. The dimer **1** consisting of two La(III), two ligands (L^2), two coordinated DMF molecules, four coordinated water molecules, two coordinated NO_3^- anions and four counter anions (NO_3^-) (Fig. 5.6). The La(III) cation charge is balanced by coordinated carboxylates and coordinated NO_3^- anion. The each imidazolium cation charge is balanced by one counter anion (NO_3^-).

The NO₃⁻ anion is coordinated to La(III) in $\mu_1\text{-}\eta^1:\eta^1$ mode, and carboxylate groups of organic spacer coordinated to metal in two different modes ($\mu_2\text{-}\eta^1:\eta^2$ and $\mu_2\text{-}\eta^1:\eta^1$). Both La(III) ions exist in the symmetrical coordination environment and adopt distorted bicapped square antiprism geometry. The La and La separation distance is 4.327(5) Å. The La(III) polyhedron are edge shared by carboxylate oxygen's (O9 and O9a) (Fig. 5.6c). The solid state structure of **2** is isostructural with **1**. Thus, **2** has not been discussed in detail. However, the structural parameters of **1** and **2** are significantly different. Selected bond lengths and bond angles are listed in Table 5.1.

Single crystal X-ray structure of $\{[(L^1)_2(RE)_2(NO_3)_2(H_2O)_2(DMF)_2](NO_3)_4\}$ (RE = Sm (3)):

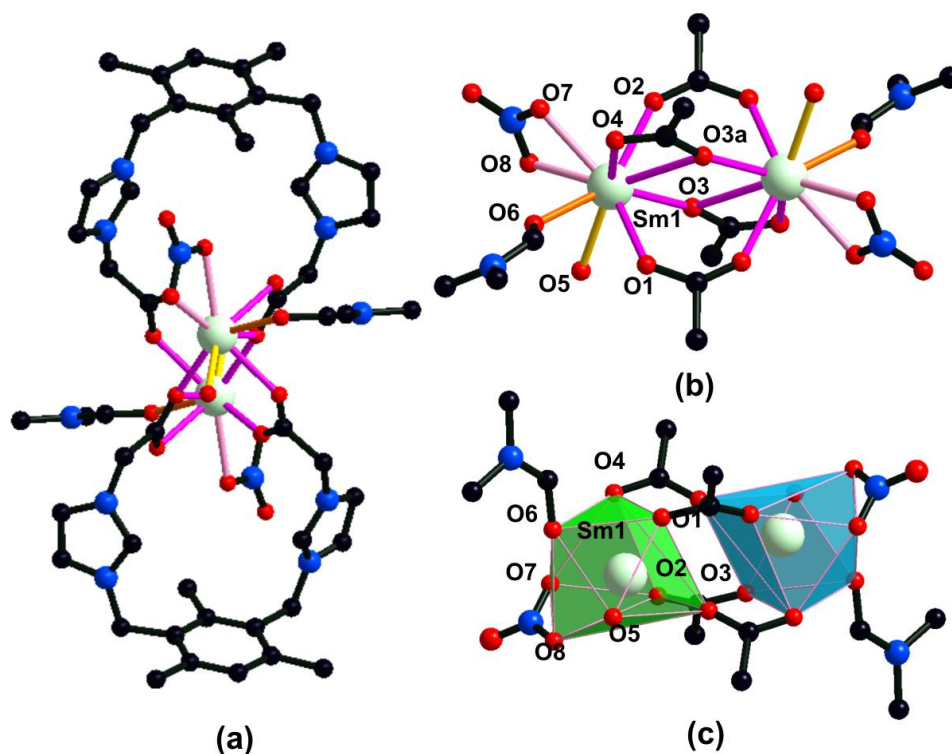


Figure 5.7: (a) The solid state structure of **3**. The hydrogen atoms have been omitted for clarity. (b) Core unit of **3**. (c) Polyhedron view of Sm(III) centers in **3**.

The molecule **3** is a dimer, consisting of two Sm(III), two ligands (L²), two coordinated DMF molecules, two coordinated water molecules, two coordinated NO₃⁻ anions and four counter anions (NO₃⁻) (Fig. 5.7). The Sm(III) cationic charge is balanced by coordinated carboxylate groups and coordinated NO₃⁻ anion. The each imidazolium

cation charge is balanced by one counter anion (NO_3^-). The NO_3^- anion is coordinated to Sm(III) in $\mu_1\text{-}\eta^1:\eta^1$ mode, carboxylate groups are coordinated to metal in two different modes ($\mu_2\text{-}\eta^1:\eta^2$ and $\mu_2\text{-}\eta^1:\eta^1$). The Sm and Sm separation distance is 4.242(2) Å. Selected bond lengths and bond angles are listed in Table 5.1. The Sm–O_{COO} bond lengths are in the range from 2.354(16) to 2.458(14) Å. The Sm–O_{nitrate} (2.505(15) and 2.531(12) Å) bond lengths are longer than Sm–O_{water} (2.453(13) Å), Sm–O_{DMF} (2.445(2)) and Sm–O_{COO}. The O_{COO}–Sm–O_{COO} angles fall in the range from 46.9 (5)^o to 128.9(5)^o.

Table 5.1: Selected bond lengths and bond angles of **1-3**

	1 (La)	2 (Ce)	3 (Sm)
RE···RE (Å)	4.327(5)	4.291(4)	4.291(4)
RE–O _{COO} (Å)	2.453(4) to 2.815(4)	2.443(3) to 2.779(3)	2.354(16) to 2.458(14)
RE–O _{NO3} (Å)	2.651(4) and 2.699(4)	2.614(3) and 2.665(3)	2.505(15) and 2.531(12)
RE–O _{DMF} (Å)	2.548(4)	2.525(3)	2.445(2)
RE–O _{water} (Å)	2.606(4) and 2.729(4)	2.569(3) and 2.703(3)	2.453(13)
O _{COO} –RE–O _{COO} (°)	47.55(9) to 128.79(11)	48.31(8) to 129.30(9)	46.9 (5) to 128.9(5)

Table 5.2: Selected bond lengths and bond angles of **4-6**

	4 (Gd)	5 (Dy)	6 (Y)
RE···RE (Å)	4.3101(10)	4.314(9)	4.325(3)
RE–O _{COO} (Å)	2.294(12) to 2.425(12)	2.268(9) to 2.374(9)	2.268(17) to 2.330(18)
RE–O _{NO3} (Å)	2.457(14) to 2.515(10)	2.451(10) to 2.501(8)	2.407(17) to 2.456(18)
RE–O _{DMF} (Å)	2.376(10) and 2.382(11)	2.312(9) and 2.364(9)	2.301(15) and 2.356(18)
RE–O _{water} (Å)	2.423(13) and 2.469(13)	2.409(10) and 2.432(10)	2.410(16) and 2.449(16)
O _{COO} –RE–O _{COO} (°)	72.6(4) to 128.1(4)	73.0(3) to 126.7(3)	72.4(6) to 125.3(6)

Single crystal X-ray structure of $\{[(L^1)_2(RE)_2(NO_3)_2(H_2O)_2(DMF)_2](NO_3)_4\}$ (RE = Gd (4), Dy (5) and Y (6)):

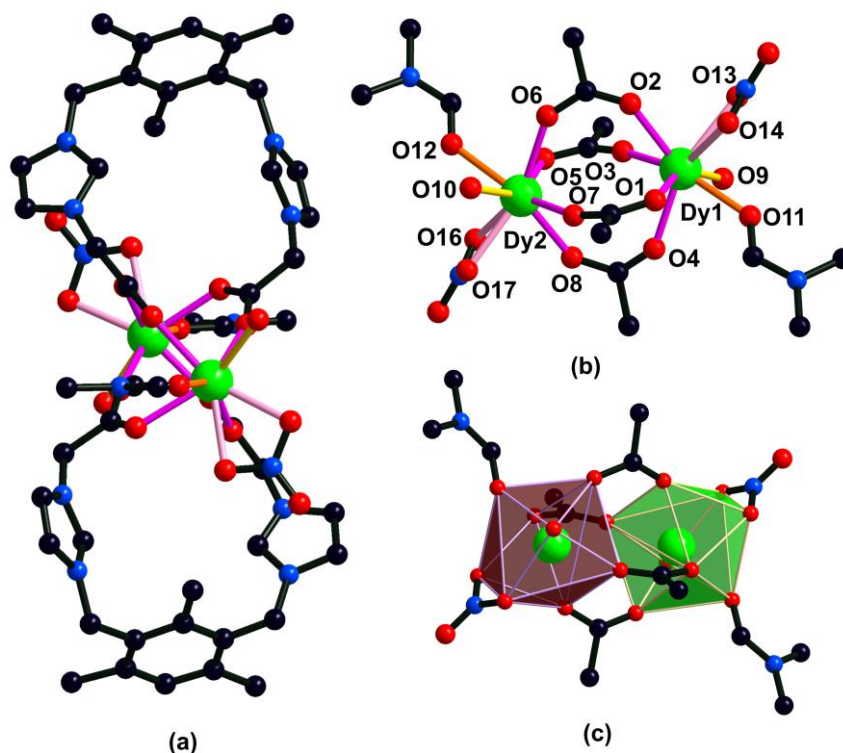
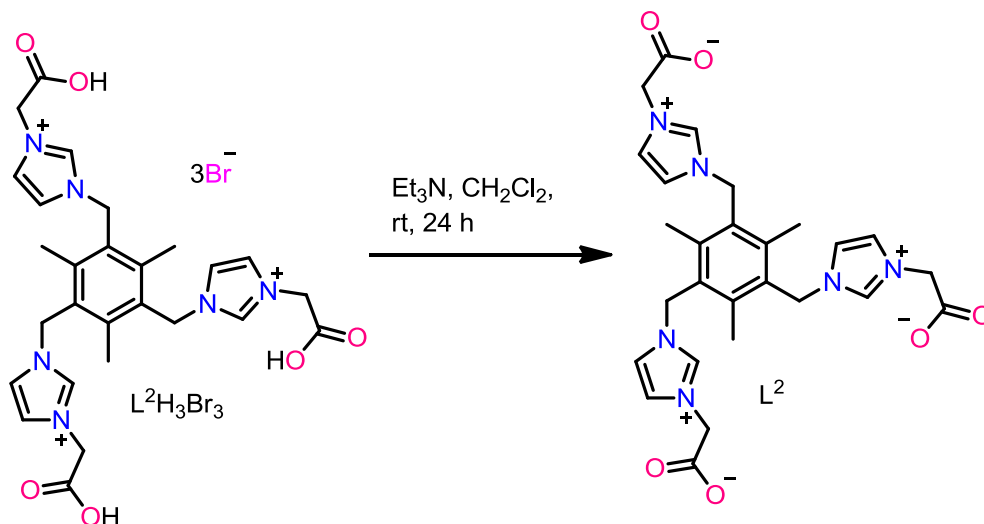


Figure 5.8: (a) The solid state structure of **5**. The hydrogen atoms have been omitted for clarity. (b) Core unit of **5**. (c) Polyhedron view of Dy(III) center in **5**.

The molecules **4-6** are isostructural discrete dimers. Thus the structural feature of **5** is described as a typical. The selected bond lengths and angles are given in Table 5.2. The crystal structure data of **5** reveal that it is dinuclear. Each dinuclear unit consists of two Dy(III), two organic spacers, two coordinated DMF molecules, two coordinated NO_3^- , two coordinated water and three counter anions (NO_3^-) (Fig. 5.8). The NO_3^- anion is coordinated to Dy(III) in $\mu_1-\eta^1:\eta^1$ mode, while the carboxylate are coordinated to Dy(III) in $\mu_2-\eta^1:\eta^1$ modes. The Dysprosium (III) coordination number is eight with geometry trigonal prismatic square-face bicapped in compound **5** (Fig. 5.8c). The Dy and Dy separation distance is 4.314(9) Å. The Dy–O_{COO} bond lengths are in the range from 2.268(9) Å to 2.374(9) Å. The Dy–O_{nitrate} (2.451(10) Å to 2.501(8) Å) bond lengths are longer than Dy–O_{water} (2.409(10) Å and 2.432(10) Å), Dy–O_{DMF} (2.312(9) and 2.364(9)) and Dy–O_{COO}. The O_{COO}–Dy–O_{COO} angle falls in the range from 73.0(3)^o to 126.7(3)^o. The Dy(III) cation charge is balanced by coordinated carboxylate and

coordinate NO_3^- anion. The each imidazolium cation charge balanced with one counter anion (NO_3^-).

5.3.3 Synthesis and characterization of L^2 and 7-10



Scheme 5.2: Synthesis of L^2 .

L^2 was synthesized from deprotonation of corresponding imidazolium salt $\text{L}^1\text{H}_2\text{Br}_3$ with Et_3N in DCM at RT (Scheme 2). The FT-IR spectrum of L^2 has shown a characteristic peak for asymmetric stretching frequency at 1624 cm^{-1} and symmetric stretching frequency at 1376 cm^{-1} . The asymmetric and symmetric stretching frequencies of L^2 are longer than L^1 . The ^1H NMR spectrum of L^2 exhibited the diagnostic peak for NCHN at 8.50 ppm (Fig. 5.9), while ^{13}C NMR spectrum of L^2 displayed the diagnostic peaks for NCHN at 139 ppm and C=O at 172 ppm (Fig. 5.10). The compounds **7-10** were synthesized from the reaction of L^2 and $\text{RE}(\text{NO}_3)_3 \cdot 6\text{H}_2\text{O}$ (RE = Sm, Gd, Dy, and Y) in DMF, ethanol and water at $100\text{ }^\circ\text{C}$.

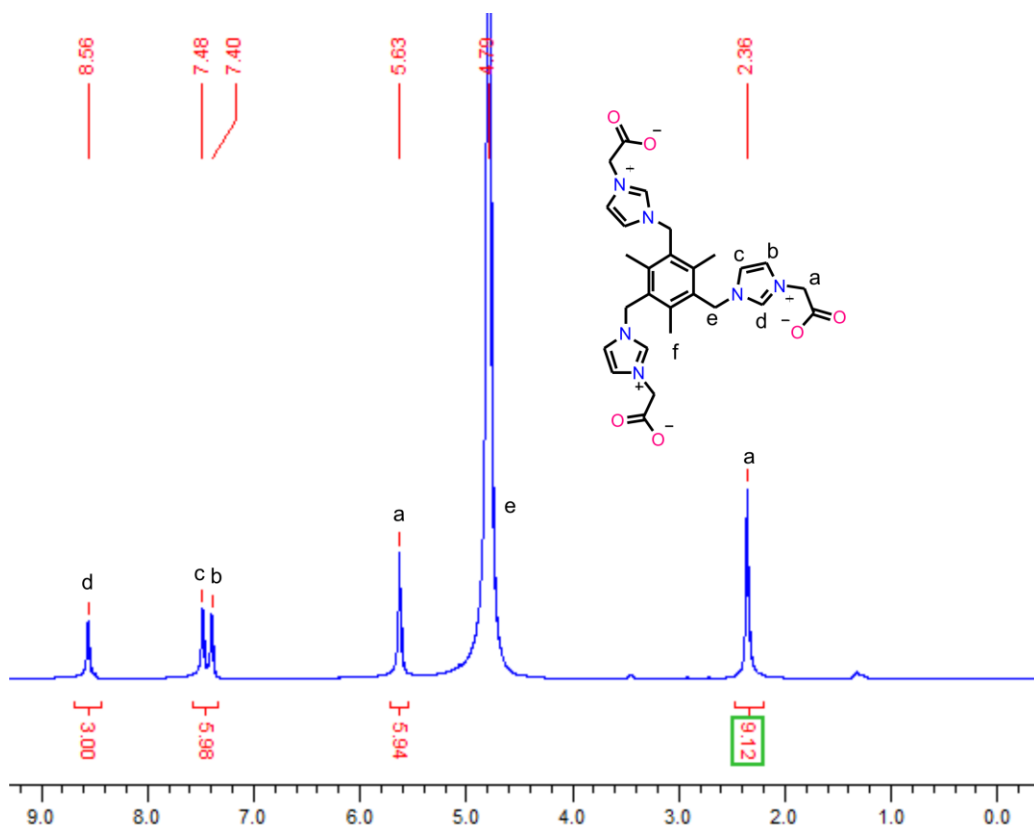


Figure 5.9: ^1H NMR spectrum of L^2 in D_2O at RT.

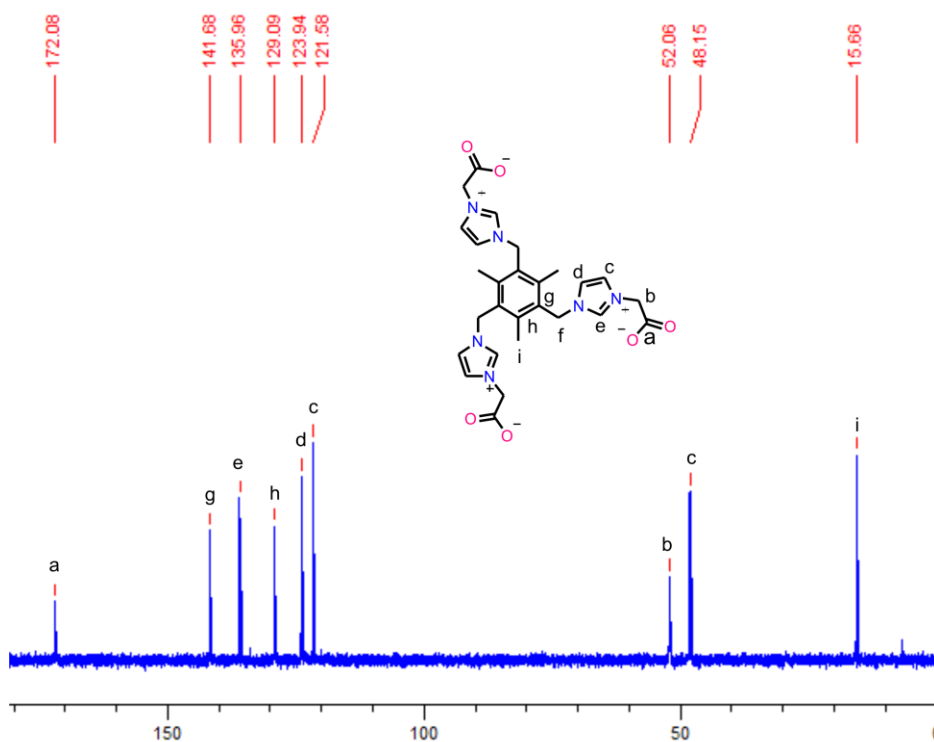


Figure 5.10: ^{13}C NMR spectrum of L^2 in D_2O at RT.

In FT-IR spectroscopy, **7-10** shows characteristic peaks for DMF C=O group at 1635-1640 cm^{-1} (**7** 1635 cm^{-1} , **8** 1636 cm^{-1} , **9** 1640 cm^{-1} and **10** 1639 cm^{-1}), asymmetric stretching frequency at 1606-1609 cm^{-1} (**7** 1606 cm^{-1} , **8** 1606 cm^{-1} , **9** 1608 cm^{-1} and **10** 1609 cm^{-1}), symmetric stretching frequency at 1448-1457 cm^{-1} (**7** 1448 cm^{-1} , **8** 1452 cm^{-1} , **9** 1454 cm^{-1} and **10** 1457 cm^{-1}) and nitrate group at 1297-1321 cm^{-1} (Fig. 5.11).

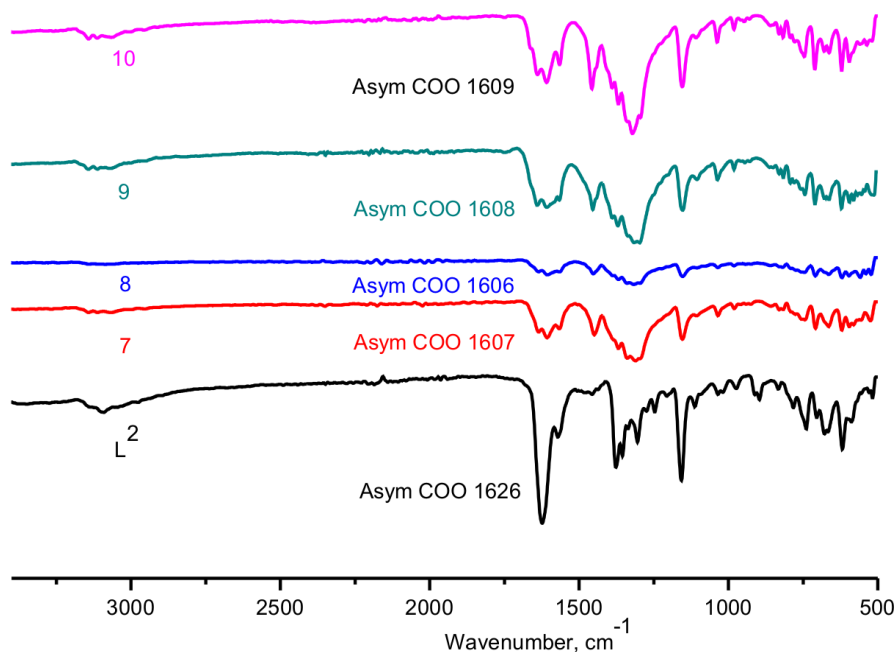


Figure 5.11: FT-IR (neat) spectrum of L^2 and 7-10.

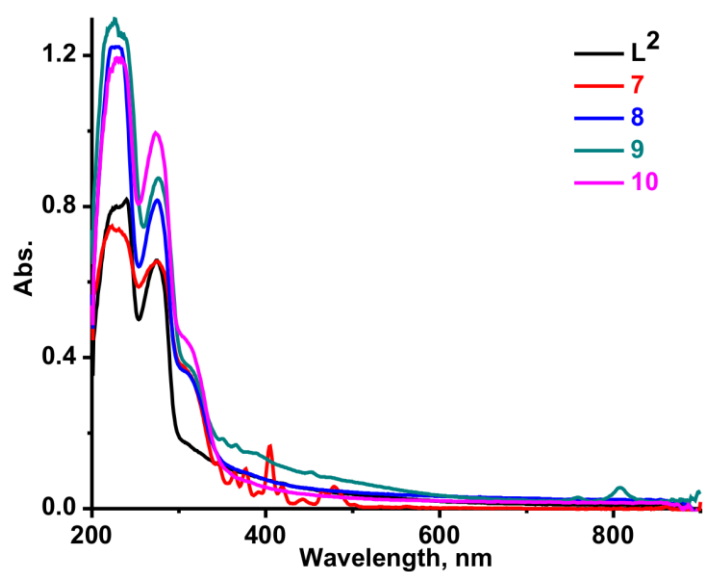


Figure 5.12: The solid-state UV-vis absorption spectra of L^2 and 7-10.

The solid UV-visible absorption spectra of L^2 and **7-10** were measured at room temperature (Fig. 5.12). The tris-zwitterionic organic spacer L^2 displays two absorption bands at 240 and 274 nm which are accredited due to intraligand transitions. Compounds **7-10** were displays absorption peaks (**7** (223 and 275 nm), **8** (230 and 275 nm), **9** (234 and 275 nm) and **10** (231 nm)) blue shifted compare to organic spacer (L^2) absorption peaks at 240 nm. The compound **7** shows f-f transitions at 364, 377, 405, 419 and 479 nm, while **9** displays weak f-f transitions at 352, 365, 389, 452, 475, 759, 809 and 899 nm.

5.3.4 Description of crystal structures 7-10

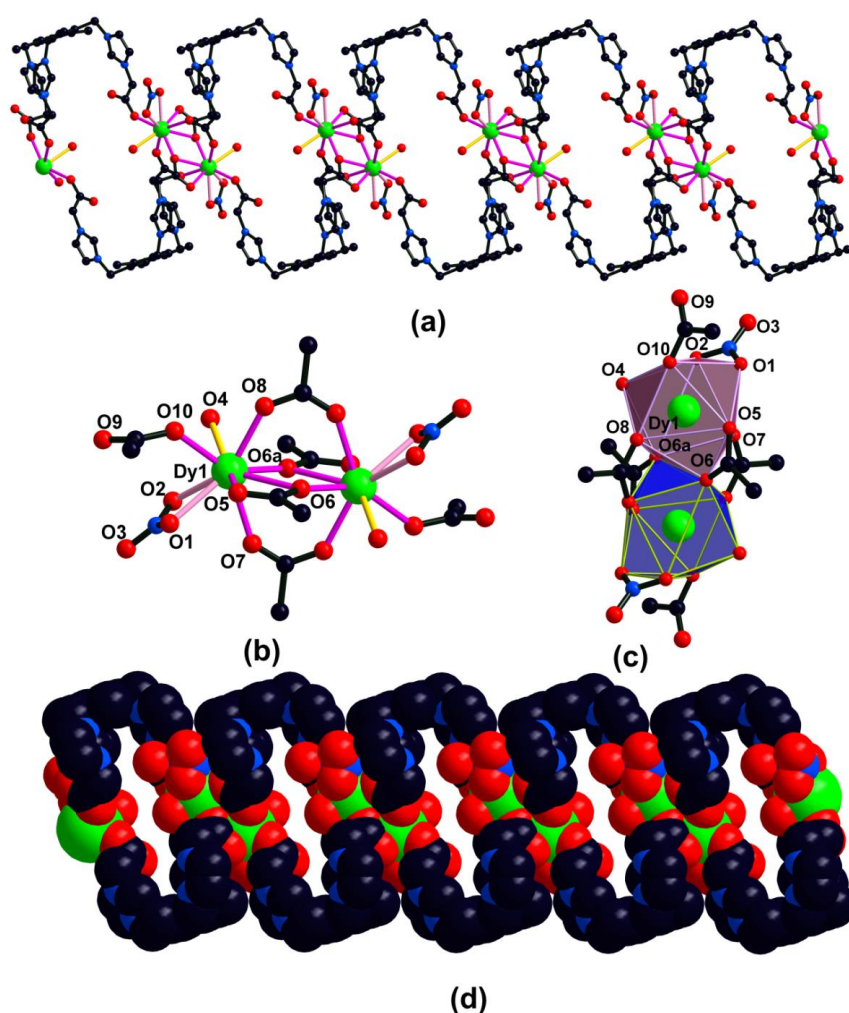


Figure 5.13: (a) The 1D nano tubular coordination polymer of **9**. The hydrogen atoms have been omitted for clarity. (b) Core unit of molecule **9**. (c) Polyhedron view of Dy(III) center in **9**. (d) Space filling model of **9**.

Single crystal X-ray structure of $\{[(L^2)(RE)(NO_3)(H_2O)](H_2O)_3(NO_3)_2\}_\infty$ (RE = Sm (7), Gd (8), Dy (9) and Y (10)): The molecules **7-10** are isostructural 1D coordination polymers. Thus the structural feature of **9** is described as a model. The selected bond lengths and angles are given in Table 5.3. The molecular structure of **9** is depicted in Fig. 5.13. The geometry of Dy(II) is distorted tricapped trigonal prismatic. The coordination environment of Dy(III) is fulfilled by six carboxylate oxygen atoms of ligands, one oxygen of water molecule and two oxygen of nitro group. The NO_3^- anion is coordinated to Dy(III) in $\mu_1-\eta^1:\eta^1$ mode and the carboxylate groups are coordinated to metal in three different modes ($\mu_2-\eta^1:\eta^1$, $\mu_2-\eta^1:\eta^2$ and $\mu_1-\eta^0:\eta^1$). The molecule is constructed as one-dimensional nanotubular porous coordination polymer (Fig. 5.13a and Fig. 5.13d). The separation of Dy(III) ions in the dimer is 4.002(7) Å. The imidazolium cationic charge is balanced by nitrates (as counter anions). Each polyhedron is edge shared by two oxygen atoms of different carboxylates (O6 and O6a) (Fig. 5.13c). The Dy–O_{COO} bond lengths are in the range from 2.289(4) Å to 2.597(5) Å. The Dy–O_{nitrate} bond lengths are 2.435(5) and 2.536(5) Å. The Dy–O_{water} bond length is 2.425 Å. The O_{COO}–Dy–O_{COO} angle falls in the range from 51.73(14)° to 143.56(17)°.

Table 5.3: Selected bond lengths and bond angles of **7-10**

	7 (Sm)	8 (Gd)	9 (Dy)	10 (Y)
RE···RE (Å)	4.026(8)	4.010(6)	4.002(7)	3.960(4)
RE–O _{COO} (Å)	2.340(6)	to 2.326(3)	to 2.289(4)	to 2.88(2) to
	2.614(6)	2.599(4)	2.597(5)	2.582(2)
RE–O _{NO3} (Å)	2.476(6)	and 2.457(4)	and 2.435(5)	and 2.406(2) and
	2.540(6)	2.523(4)	2.536(5)	2.500(2)
RE–O _{water} (Å)	2.462(5)	2.455(4)	2.425	2.409(2)
O _{COO} –RE–O _{COO}	51.13(17) to	51.36(11) to	51.73(14) to	51.92(7) to
(°)	141.27(19)	144.95(14)	143.56(17)	145.21(8)

5.3.5 Synthesis and characterization of **11-14**

The compounds **11-14** were synthesized from the reaction of L^2 and $RE(NO_3)_3 \cdot 6H_2O$ (RE = Sm, Gd, Dy, and Y) in DMF, methanol, water and Py at 80 °C. These are insoluble in almost all common organic solvents and soluble in water. The compounds

11-14 shows characteristic peaks for asymmetric stretching frequency at 1623-1627 cm^{-1} (**11** 1623 cm^{-1} , **12** 1627 cm^{-1} , **13** 1626 cm^{-1} and **14** 1627 cm^{-1}), symmetric stretching frequency at 1435-1453 cm^{-1} and nitrate group at 1288-1366 cm^{-1} (Fig. 5.14 and Fig. 5.16). The solid UV-visible absorption spectra of **11-14** were measured at room temperature (Fig. 5.8). Compounds **11-14** were displays absorption peaks (**11** (228 and 271 nm), **12** (232 nm), **13** (233 and 276 nm) and **14** (231 and 275 nm)) blue shifted compare to organic spacer (L^2) absorption peaks at 240 nm. The compound **11** shows f-f transitions at 376, 404 and 479 nm, while **13** displays weak f-f transitions at 365, 389, 452, 475, 759, 808 and 899 nm (Fig. 5.15).

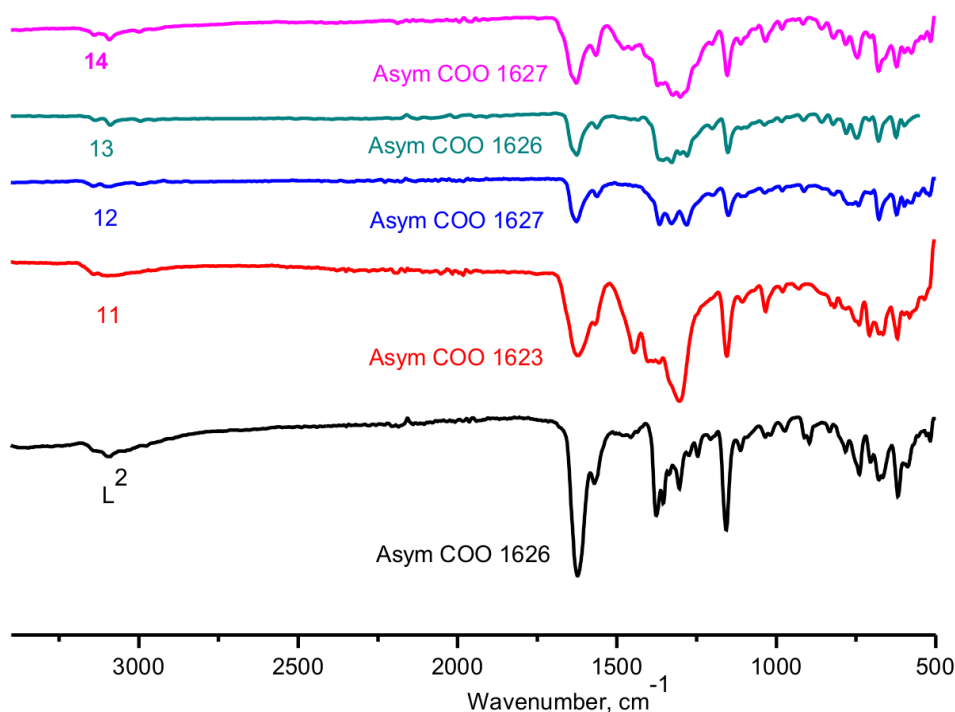


Figure 5.14: FT-IR (neat) spectrum of L^2 and **11-14**.

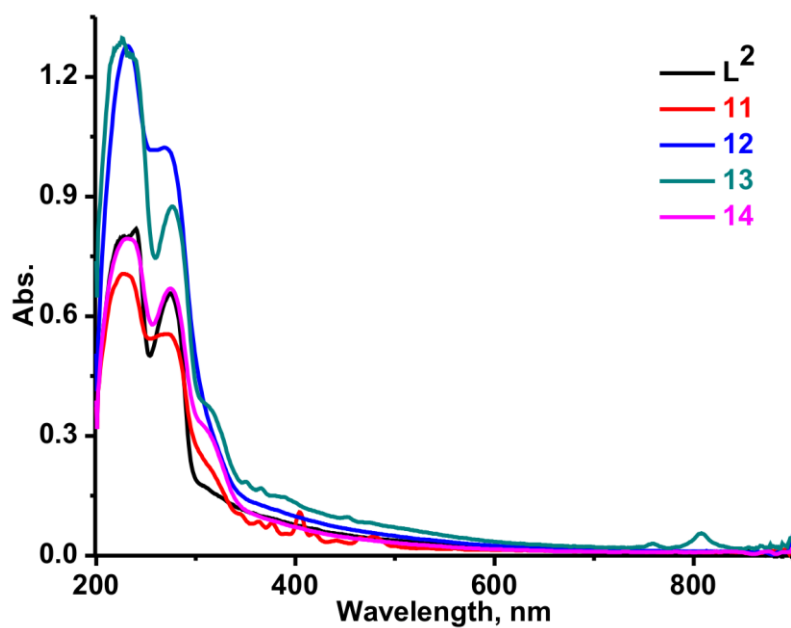


Figure 5.15: The solid-state UV-vis absorption spectra of L^2 and 11-14.

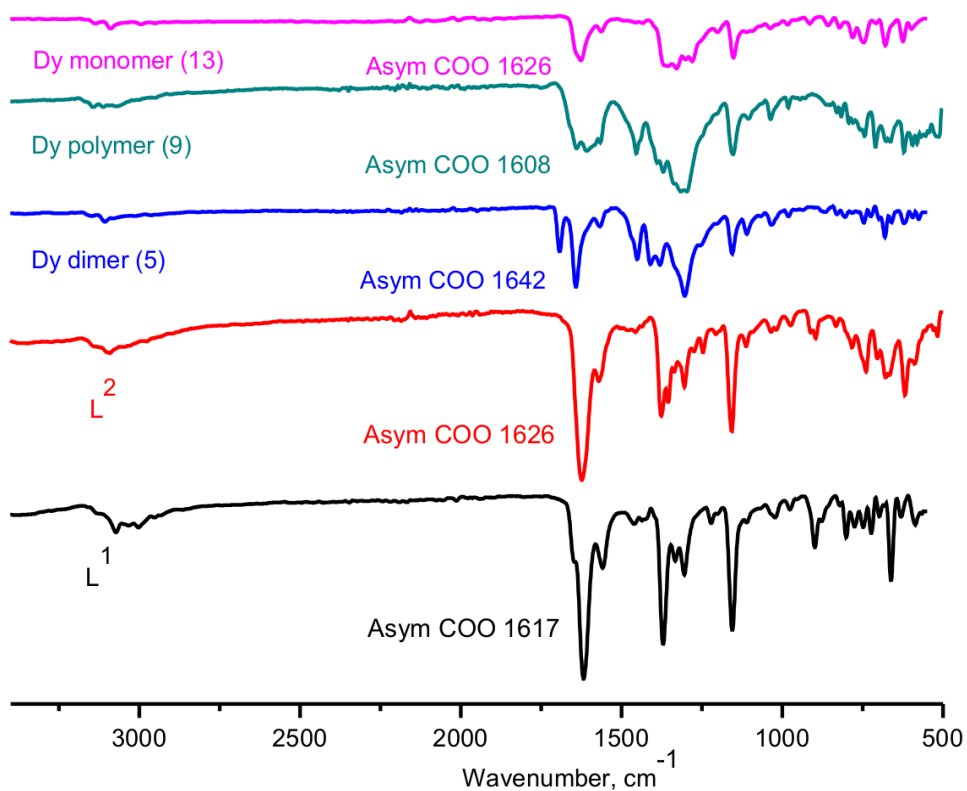


Figure 5.16: FT-IR spectra of L^1 , L^2 and Dy molecules (5, 9 and 13).

5.3.6 Description of crystal structures 11-14

Single crystal X-ray structure of $\{[(L^2)_2(RE)](NO_3)_3\}$ (RE = Sm (11), Gd (12), Dy (13) and Y (14)):

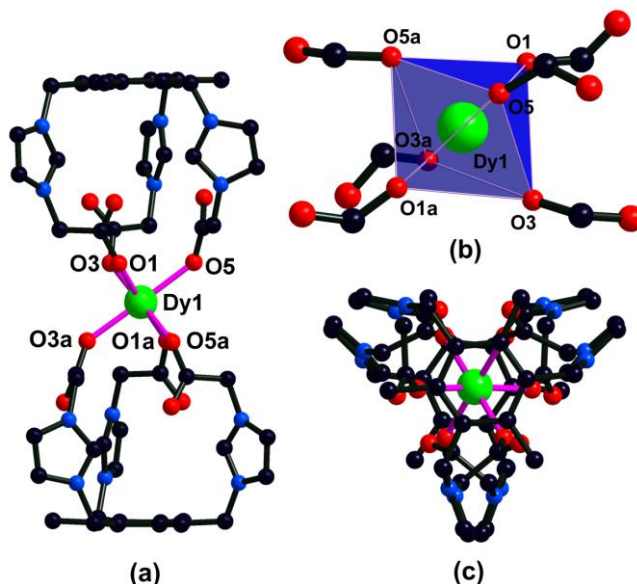


Figure 5.17: (a) Coordination environment of the Dy(III) center in **13**. The hydrogen atoms have been omitted for clarity. (b) Polyhedron view of Dy(III) center in **13**. (c) View along through phenyl ring of molecule **13**.

The molecules **11-14** are isostructural discrete monomers. Thus the solid state structure of Dy monomer (**13**) is discussed in detail as a model. The selected bond lengths and angles are given in Table 5.4. The molecule **13** crystallized in the monoclinic space group Cc . The molecular structure of **13** is depicted in Fig. 5.17a. The geometry of Dy(III) is distorted octahedron. The coordination environment of Dy(III) is fulfilled by six carboxylate oxygen atoms of ligands. The carboxylate groups of each organic spacer is coordinated to Dy(III) in $\mu_1-\eta^0:\eta^1$ mode. An interesting structural feature of **13** is the ionic monomeric lanthanide molecule, which has never been isolated. The Dy(III) charge is balanced by three carboxylate anions. The six imidazolium cations charge is balanced by three carboxylate anions and three counter anions of NO_3^- anions. The organic spacer behaves as tripodal ligand. Two tripodal organic spacers are coordinated with one Dy(III) center in capping mode. The Dy(III) metal and four coordinated carboxylate oxygen atoms (O3, O5, O3a and O5a) are arranged in the basal plane, and other coordinated carboxylate oxygen atoms (O1 and O1a) are arranged in axial plane

(Fig. 5.17b). The different Dy–O_{COO} bond distances are observed (2.242(4) Å, 2.246(4) and 2.288(9) Å). The bond distance of axial Dy–O_{COO} (2.288(9) Å) are longer than basal Dy–O_{COO} (2.242(4) and 2.246(4) Å). The O_{COO}–Dy–O_{COO} angles fall in the range of 87.1(4)° to 179.0(4)°. As shown in Fig 5.18, molecules are packed in head to tail triangle shape and each corner is occupied by two imidazole groups, while Dy(III) is occupied by at the center.

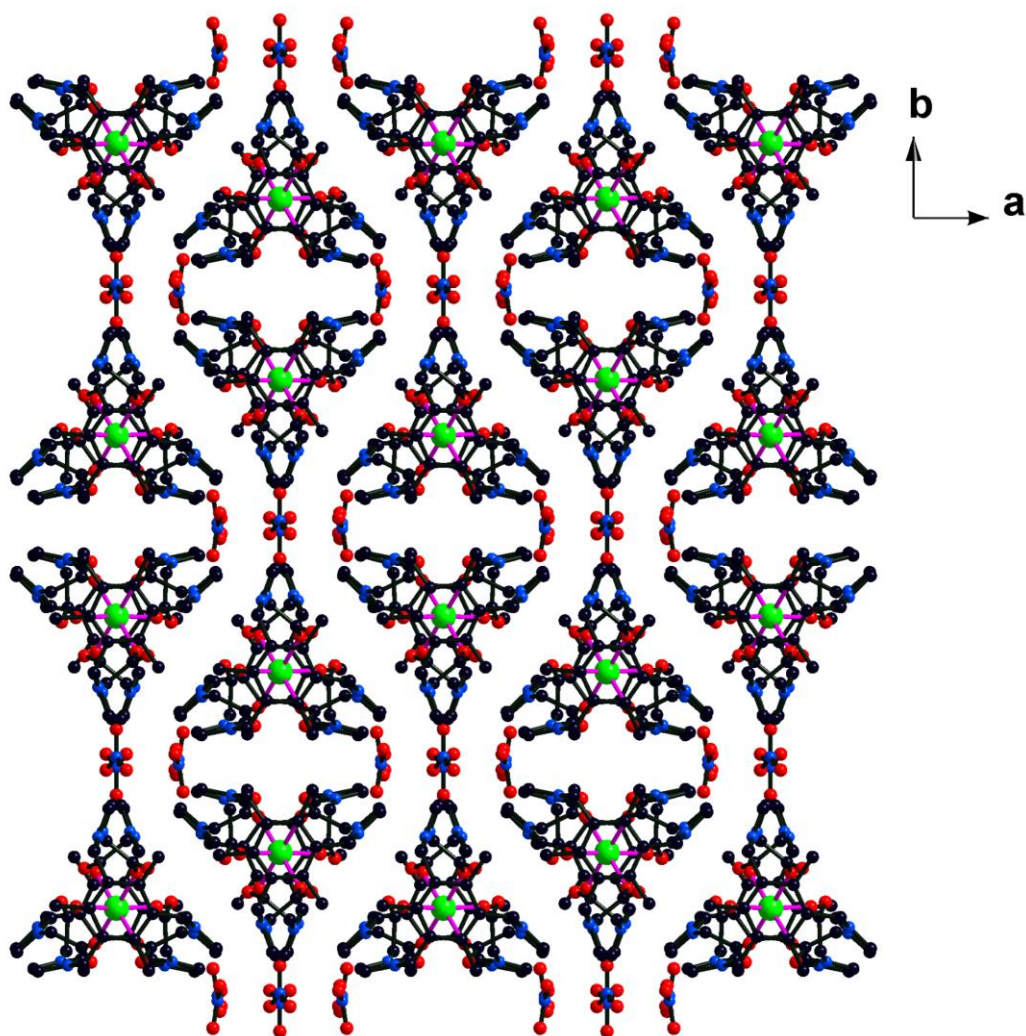


Figure 5.18: Molecular packing of 13.

Table 5.4: Selected bond lengths and bond angles of **11-14**

	11(Sm)	12 (Gd)	13 (Dy)	14 (Y)
RE–O _{COO} (Å)	2.288(3), 2.296(3) 2.310(3)	and 2.261(3), 2.267(3) 2.284(3)	and 2.242(4), 2.246(4) 2.268(5)	and 2.223(5), 2.224(5) and 2.268(5)
O _{COO} –RE–O _{COO} (°)	85.92(10) 178.05(10)	to 86.32(10) 178.36(9)	to 86.77(16) 178.57(14)	to 87.44(19) to 178.8(2)

Table 5.5: Summary of crystallographic data and structure refinement results for **1-3**

Parameters	1	2	3
Empirical formula	C ₄₈ H ₇₀ N ₁₆ O ₃₂ La ₂	C ₄₈ H ₇₀ N ₁₆ O ₃₂ Ce ₂	C ₄₈ H ₆₆ N ₁₆ O ₃₀ Sm ₂
Formula weight	1660.99	1663.41	1643.85
Temperature (K)	298	150	150
Crystal system	Triclinic	Triclinic	Triclinic
Space group	<i>P</i> $\bar{1}$	<i>P</i> $\bar{1}$	<i>P</i> $\bar{1}$
<i>a</i> /Å	9.6504(4)	9.5606(5)	9.4649(6)
<i>b</i> /Å	13.3336(8)	13.1819(6)	13.3075(12)
<i>c</i> /Å	13.7284(7)	13.6536(6)	13.3577(9)
α /°	81.220(5)	90.112(4)	80.526(7)
β /°	70.211(5)	109.922(4)	73.830(6)
γ /°	78.488(4)	101.845(4)	80.971(6)
Volume (Å ³)	1621.81(15)	1578.45(14)	1582.9(2)
<i>Z</i>	1	1	1
ρ_{calc} /mg mm ⁻³	1.7005	1.7498	1.7244
Absorption coefficient	10.941	11.925	14.674

(mm ⁻¹)			
<i>F</i> (000)	840.6	841.6	818.2
Data collected	11404	11395	12305
Unique data	6081	5947	5973
<i>R</i> _{int}	0.0497	0.0408	0.0444
GOF on <i>F</i> ²	1.031	1.051	1.056
<i>R</i> ₁ (<i>I</i> > 2σ(<i>I</i>))	0.0442	0.0357	0.1351
w <i>R</i> ₂ (<i>I</i> > 2σ(<i>I</i>))	0.1183	0.0937	0.3113
<i>R</i> ₁ values (all data)	0.0517	0.0399	0.1558
w <i>R</i> ₂ values (all data)	0.1183	0.0937	0.3264

Table 5.6: Summary of crystallographic data and structure refinement results for **4-6**

Parameters	4	5	6
Empirical formula	C ₄₈ H ₆₆ N ₁₆ O ₃₀ Gd ₂	C ₄₈ H ₆₆ N ₁₆ O ₃₀ Dy ₂	C ₄₈ H ₆₆ N ₁₆ O ₃₀ Y ₂
Formula weight	1661.67	1672.17	1364.48
Temperature (K)	150	150	150
Crystal system	Monoclinic	Monoclinic	Monoclinic
Space group	Cc	Cc	Cc
<i>a</i> /Å	20.1417(3)	20.1497(3)	20.1022(4)
<i>b</i> /Å	17.5019(3)	17.5103(2)	17.4609(3)
<i>c</i> /Å	18.4165(4)	18.3580(3)	18.3272(4)
α°	90.00	90.00	90.00

$\beta/^\circ$	101.6824(17)	101.7626(16)	102.2423(19)
$\gamma/^\circ$	90.00	90.00	90.00
Volume (\AA^3)	6357.62(19)	6341.19(17)	6286.6(2)
<i>Z</i>	4	4	4
$\rho_{\text{calc}}/\text{mg mm}^{-3}$	1.736	1.752	1.4394
Absorption coefficient (mm^{-1})	14.235	13.351	3.238
<i>F</i> (000)	3336.0	3352.0	2687.7
Data collected	12625	13459	13644
Unique data	8033	8014	7703
R_{int}	0.0419	0.0395	0.0337
GOF on F^2	1.046	1.051	3.015
R_1 ($I > 2\sigma(I)$)	0.0771	0.0607	0.1456
wR_2 ($I > 2\sigma(I)$)	0.1971	0.1506	0.3834
R_1 values (all data)	0.0778	0.0615	0.1578
wR_2 values (all data)	0.1979	0.1513	0.4027

Table 5.7: Summary of crystallographic data and structure refinement results for **7-9**

Parameters	7	8	9
Empirical formula	$\text{C}_{27}\text{H}_{38}\text{N}_9\text{O}_{19}\text{Sm}$	$\text{C}_{27}\text{H}_{38}\text{N}_9\text{O}_{19}\text{Gd}$	$\text{C}_{27}\text{H}_{38}\text{N}_9\text{O}_{19}\text{Dy}$
Formula weight	943.02	949.90	955.15
Temperature (K)	150	150	150
Crystal system	Triclinic	Triclinic	Triclinic

Space group	$P\bar{1}$	$P\bar{1}$	$P\bar{1}$
$a/\text{\AA}$	11.5886(9)	11.6273(9)	11.6061(7)
$b/\text{\AA}$	12.6167(9)	12.6535(10)	12.7106(7)
$c/\text{\AA}$	13.7024(9)	13.6034(12)	13.3958(8)
α°	79.699(6)	79.677(7)	79.790(5)
β°	77.863(6)	77.909(7)	77.975(5)
γ°	68.018(7)	67.723(7)	68.054(5)
Volume (\AA^3)	1805.2(2)	1801.0(3)	1781.94(19)
Z	2	2	2
$\rho_{\text{calc}}/\text{mg mm}^{-3}$	1.7348	1.7515	1.7800
Absorption coefficient (mm^{-1})	13.051	12.746	12.064
$F(000)$	946.7	942.1	946.0
Data collected	13115	12921	12929
Unique data	6799	6784	6681
R_{int}	0.0662	0.0486	0.0499
GOF on F^2	1.048	1.053	1.047
$R_1 (I > 2\sigma(I))$	0.0661	0.0522	0.0574
$wR_2 (I > 2\sigma(I))$	0.1960	0.1433	0.1574
R_1 values (all data)	0.0753	0.0572	0.0703
wR_2 values (all data)	0.1960	0.1433	0.1574

Table 5.8: Summary of crystallographic data and structure refinement results for **10-12**

Parameters	10	11	12
Empirical formula	C ₂₇ H ₃₈ N ₉ O ₁₉ Y	C ₅₄ H ₆₀ N ₁₅ O ₂₁ Sm	C ₅₄ H ₆₀ N ₁₅ O ₂₁ Gd
Formula weight	882.56	1405.53	1412.42
Temperature (K)	150	298	298
Crystal system	Triclinic	Monoclinic	Monoclinic
Space group	<i>P</i> $\bar{1}$	C2/c	C2/c
<i>a</i> /Å	11.5681(6)	15.8163(8)	15.8184(5)
<i>b</i> /Å	12.5947(6)	20.9878(9)	20.9781(6)
<i>c</i> /Å	13.6791(6)	18.7201(9)	18.6400(7)
α /°	80.178(4)	90.00	90.00
β /°	78.380(4)	113.110(6)	113.059(4)
γ /°	67.301(5)	90.00	90.00
Volume (Å ³)	1791.41(16)	5715.4(5)	5691.3(4)
<i>Z</i>	2	4	4
$\rho_{\text{calc}}/\text{mg mm}^{-3}$	1.6342	1.6333	1.6483
Absorption coefficient (mm ⁻¹)	3.159	8.530	8.354
<i>F</i> (000)	910.9	2864.2	2855.0
Data collected	12686	11941	11800
Unique data	6734	5412	5379
<i>R</i> _{int}	0.0271	0.0369	0.0417
GOF on <i>F</i> ²	1.046	1.053	1.034

$R_1 (I > 2\sigma(I))$	0.0448	0.0396	0.0409
$wR_2 (I > 2\sigma(I))$	0.1242	0.1030	0.1029
R_1 values (all data)	0.0485	0.0448	0.0498
wR_2 values (all data)	0.1242	0.1030	0.1029

Table 5.9: Summary of crystallographic data and structure refinement results for **13** and **14**

Parameters	13	14
Empirical formula	C ₅₄ H ₆₀ N ₁₅ O ₂₁ Dy	C ₅₄ H ₆₀ N ₁₅ O ₂₁ Y
Formula weight	1417.66	1345.07
Temperature (K)	298	298
Crystal system	Monoclinic	Monoclinic
Space group	C2/c	C2/c
$a/\text{\AA}$	15.8008(9)	15.8317(14)
$b/\text{\AA}$	21.0142(9)	21.0166(11)
$c/\text{\AA}$	18.5831(8)	18.5403(13)
α°	90.00	90.00
β°	112.889(8)	112.747(10)
γ°	90.00	90.00
Volume (\AA^3)	5684.5(5)	5689.1(8)
Z	4	4
$\rho_{\text{calc}}/\text{mg mm}^{-3}$	1.6564	1.5691
Absorption coefficient (mm^{-1})	7.851	2.277
$F(000)$	2862.8	2792.8

Data collected	11674	11776
Unique data	5360	5345
R_{int}	0.0598	0.0701
GOF on F^2	1.026	1.075
R_1 ($I > 2\sigma(I)$)	0.0642	0.0726
wR_2 ($I > 2\sigma(I)$)	0.1879	0.1997
R_1 values (all data)	0.0757	0.01108
wR_2 values (all data)	0.1879	0.1997

5.4 Conclusions

A novel discrete dimers $\{[(L^1)_2(RE)_2(NO_3)_2(H_2O)_4(DMF)_2](NO_3)_4\}$ (RE = La (**1**) and Ce (**2**)), $\{[(L^1)_2(RE)_2(NO_3)_2(H_2O)_2(DMF)_2](NO_3)_4\}$ (RE = Sm (**3**)), $\{[(L^1)_2(RE)_2(NO_3)_2(H_2O)_2(DMF)_2](NO_3)_4\}$ (RE = Gd (**4**), Dy (**5**) and Y (**6**)), coordination polymers $\{[(L^2)(RE)(NO_3)(H_2O)](H_2O)_3(NO_3)_2\}_\infty$ (RE = Sm (**7**), Gd (**8**), Dy (**9**) and Y (**10**)) and monomers $\{[(L^2)_2(RE)](NO_3)_3\}$ (RE = Sm (**11**), Gd (**12**), Dy (**13**) and Y (**14**)) were synthesized from zwitterionic bis-imidazolium carboxylate (**L**¹) or zwitterionic tris-imidazolium carboxylate (**L**²) and corresponding metal nitrates. The solid state structures of compounds **1-14** were confirmed by single-crystal X-ray diffraction technique. Molecules **1-14** were constructed in ionic nature. The crystal structure analysis revealed that **1-2** were isostructural discrete dimers with deca-coordinated metal centers. **3** was discrete dimer with nona-coordinated metal centers, while compound **4-6** were formed as isostructural discrete dimers with octa-coordinated metal centers. The molecules **7-10** were formed as a 1D nanotubular coordination polymer. Interestingly, molecules **11-14** were formed as novel and rare ionic lanthanide discrete monomers.

5.5 References

- [1] N. Wei, M. Y. Zhang, X.-N. Zhang, G.-M. Li, X.-D. Zhang, and Z.-B. Han. *Cryst. Growth Des.* 14, (2014) 3002.
- [2] (a) D. Parker. *Coord. Chem. Rev.* 205, (2000) 109; (b) K. Kuriki, and Y. Koike. *Chem. Rev.* 102, (2002) 2347; (c) J. Kido, and Y. Okamoto. *Chem. Rev.* 102, (2002) 2357.
- [3] N. Ishikawa, M. Sugita, T. Ishikawa, S.-Y. Koshihara, and Y. Kaizu. *J. Am. Chem. Soc.* 125, (2003) 8694.
- [4] (a) K. Kuriki, Y. Koike, and Y. Okamoto. *Chem. Rev.* 102, (2002) 2347; (b) J. Kido, and Y. Okamoto. *Chem. Rev.* 102, (2002) 2357.
- [5] (a) H. Yokoyama. *Science* 256, (1992) 66; (b) J. I. Adam. *Chem. Rev.* 102, (2002) 2461; (c) S. Kuck. *Appl. Phys. B: Laser Opt.* 72, (2001) 515.
- [6] (a) E.-G. Moore, J. Xu, C.-J. Jocher, E. J. Werner, and K.-N. Raymond. *J. Am. Chem. Soc.* 128, (2006) 10648; (b) X.-P. Yang, and R.-A. Jones. *J. Am. Chem. Soc.* 127, (2005) 7686.
- [7] (a) B. Q. Ma, D. S. Zhang, S. Gao, T. Z. Jin, C. H. Yan, and G. X. Xu. *Angew. Chem., Int. Ed.* 39, (2000) 3644; (b) G. Mancino, A. J. Ferguson, A. Beeby, N. J. Long, and T. S. Jones. *J. Am. Chem. Soc.* 127, (2005) 524.
- [8] (a) J.-W. Cheng, S.-T. Zheng, and G.-Y. Yang. *Dalton Trans* (2007) 4059; (b) Z.-P. Deng, W. Kang, L.-H. Huo, H. Zhao, and S. Gao. *Dalton Trans* 39, (2010) 6276 and reference therein; (c) W.-G. Lu, L. Jiang, and T.-B. Lu. *Cryst. Growth Des.* 10, (2010) 4310; (d) G.-L. Zhuang, X.-J. Kong, L.-S. Long, R.-B. Huang, and L.-S. Zheng. *CrystEngComm* 12, (2010) 2691.
- [9] (a) S.-D. Jiang, B.-W. Wang, G. Su, Z.-M. Wang, and S. Gao. *Angew. Chem., Int. Ed.* 49, (2010) 7448; (b) D.-P. Li, X.-P. Zhang, T.-W. Wang, B.-B. Ma, C.-H. Li, Y.-Z. Li, and X.-Z. You. *Chem. Commun.* 47, (2011) 6867; (c) G.-J. Chen, C.-Y. Gao, J.-L. Tian, J. Tang, W. Gu, X. Liu, S.-P. Yan, D.-Z. Liao, and P. Cheng. *Dalton Trans.* 40, (2011) 5579.
- [10] (a) Y.-M. Song, F. Luo, M.-B. Luo, Z.-W. Liao, G.-M. Sun, X.-Z. Tian, Y. Zhu, Z.-J. Yuan, S.-J. Liu, W.-Y. Xu, and X.F. Feng. *Chem. Commun.* 48, (2012) 1006; (b) L. Liang, G. Peng, G. Li, Y. Lan, A. K. Powell, and H. Deng. *Dalton Trans.* 41,

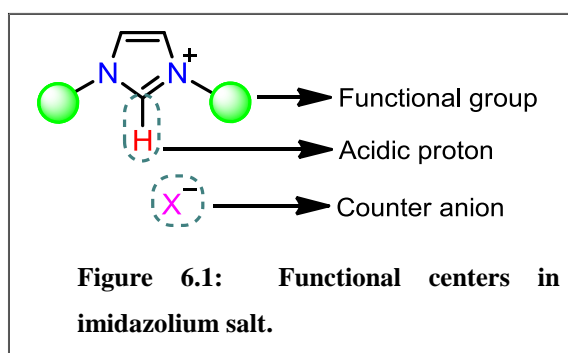
- (2012) 5816; (c) P.-H. Lin, W.-B. Sun, M.-F. Yu, G.-M. Li, P.-F. Yan, and M. Murugesu. *Chem. Commun.* 48, (2012) 1006.
- [11] (a) S. Biswas, H. S. Jena, S. Goswami, S. Suresh, and S. Konar. *Cryst. Growth Des.* 14, (2014) 1287; (b) S. Biswas, H. S. Jena, A. Adhikary, and S. Konar. *Inorg. Chem.* 53, (2014) 3926.
- [12] Z. Fei, D. Zhao, T. J. Geldbach, R. Scopelliti, P. J. Dyson, S. Antonijevic, and G. Bodenhausen. *Angew. Chem., Int. Ed.* 44, (2005) 5720.
- [13] L. Han, S. Zhang, Y. Wang, X. Yan, and X. Lu. *Inorg. Chem.* 48, (2009) 786.
- [14] X.-C. Chai, Y.-Q. Sun, R. Lei, Y.-P. Chen, S. Zhang, Y.-N. Cao, and H.-H. Zhang. *Cryst. Growth Des.* 10, (2010) 658.
- [15] D. D. Perrin, and W. L. F. Armarego. *Purification of laboratory chemicals*, 3rd Ed., Pergamon Press, London, 1988.
- [16] P. Suresh, S. Radhakrishnan, C. Naga Babu, A. Sathyanarayana, N. Sampath, and G. Prabusankar. *Dalton Trans.* 42, (2013) 10838.
- [17] Fei, D. Zhao, T. J. Geldbach, R. Scopelliti, and P. J. Dyson. *Chem. Eur. J.* 10, (2004) 4886.
- [18] O. V. Dolomanov, L. J. Bourhis, R. J. Gildea, J. A. K. Howard, and H. Puschmann. *OLEX2: a complete structure solution, refinement and analysis program*, *J. Appl. Cryst.* 42, (2009) 339.

Chapter 6

Summary and Conclusion

Construction of functionalized coordination polymers (FCPs) have been the subject of interest over the last few decades due to their fascinating architectures and versatile applications in catalysis, gas storage, separation, luminescence, electrical conductivity, magnetism and nonlinear optics. Suitable organic spacers, metal precursors and synthetic methodologies are essential criteria to design FCPs with different physical properties. In addition, non-covalent interactions such as hydrogen bond, $\pi \cdots \pi$, $M \cdots \pi$, $C-H \cdots \pi$ and anion $\cdots \pi$ interactions play a key role in FCPs to increase their dimensionality, supramolecular topology and porosity. Therefore, the choice of organic spacer is extremely important to fine-tune the structural and desired functional properties of FCPs through the coordination mode or non-covalent interaction mode.

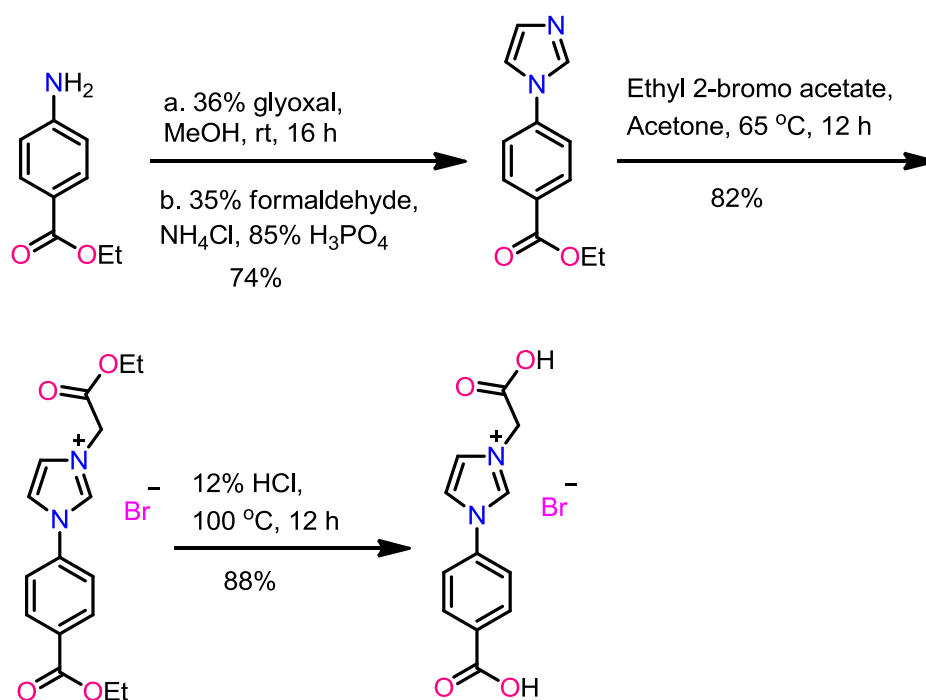
Amongst these organic spacers, imidazolium carboxylic acids are of special interest as they have $[C-H]^{\delta+}$ functional group (potential functional group for anion reorganization and post modification to generate N-heterocyclic carbene tethered catalytically active metal centers)



along with excellent functional group tolerance at the N-positions (Fig. 6.1). Thus, the thesis dealt (i) the design, synthesis and characterization of new imidazolium carboxylic acid organic spacers, (ii) synthesis and characterization of novel imidazolium carboxylate based coordination polymers, (iii) structural diversity and close interracial relationships between main group, transition metal and rare earth imidazolium carboxylate based coordination assemblies.

A thorough literature survey on imidazolium carboxylate coordination polymers (till August 2014) and seven new imidazolium carboxylate organic spacers along with their thirty synthetically intriguing metal aggregates have been reported in the thesis. These new molecules have been fully characterized. Chapter 1 (Introduction) reviews the

recent literature on imidazolium carboxylate based coordination assemblies. Chapter two to five deals with the synthesis and structural features of newly prepared imidazolium carboxylate supported coordination assemblies. The final section of each chapter lists the references from the literature, which are indicated in the text (Chapters 1-6) by appropriate numbers appearing as square brackets. Lists of abbreviations, table, scheme, and figure captions appearing in this report are collected together in the beginning of the thesis chapters.



Scheme 6.1: Synthesis of L^1H_2Br .

In second chapter dealt the design and synthesis of semi rigid mono-imidazolium carboxylate (Scheme 6.1) and its zwitterion coordination polymers. Zwitterion coordination networks, $[(L^1)_2Mn(H_2O)_2]_\infty$, where $L^1 = \{[1-(CH_2CO_2)-3-(C_6H_4-4-CO_2)][(HCN)_2CH]\}$, $[(L^1)_2Co(H_2O)_2]_\infty$, $[(L^1)_2Ni(H_2O)_4]_\infty$, $[(L^1)_2Cu]_\infty$, $[(L^1)_2Zn(H_2O)_2]_\infty$ and $[(L^1)_3Cd_2(Br)_2]_\infty$ have been synthesized from the reaction between semi rigid mono-imidazolium carboxylate spacer L^1H_2Br and corresponding metal nitrates. The molecules $[(L^1)_2Mn(H_2O)_2]_\infty$, $[(L^1)_2Co(H_2O)_2]_\infty$ and $[(L^1)_2Zn(H_2O)_2]_\infty$ are isostructural one-dimensional coordination polymers, where metal geometry is distorted octahedron and imidazolium cation charge is balanced by coordinated carboxylate anions. $[(L^1)_2Ni(H_2O)_4]_\infty$ has been isolated as monomer and the monomers are associated in a

three dimensional fashion through O–H···O hydrogen bond, in which imidazolium cation charge is balanced by free carboxylate anion. $[(L^1)_2Cu]_\infty$ has been isolated as a 1D coordination polymer where carboxylic coordination modes are different and imidazolium cation charge is balanced by coordinated carboxylate anions (Fig. 6.2). Compound $[(L^1)_3Cd_2(Br)_2]_\infty$ is isolated as the two-dimensional coordination framework with a rare $[Cd_2(\mu_2-Br)_2]$ core (Fig. 6.3), where cadmium(II) geometry is distorted octahedron.

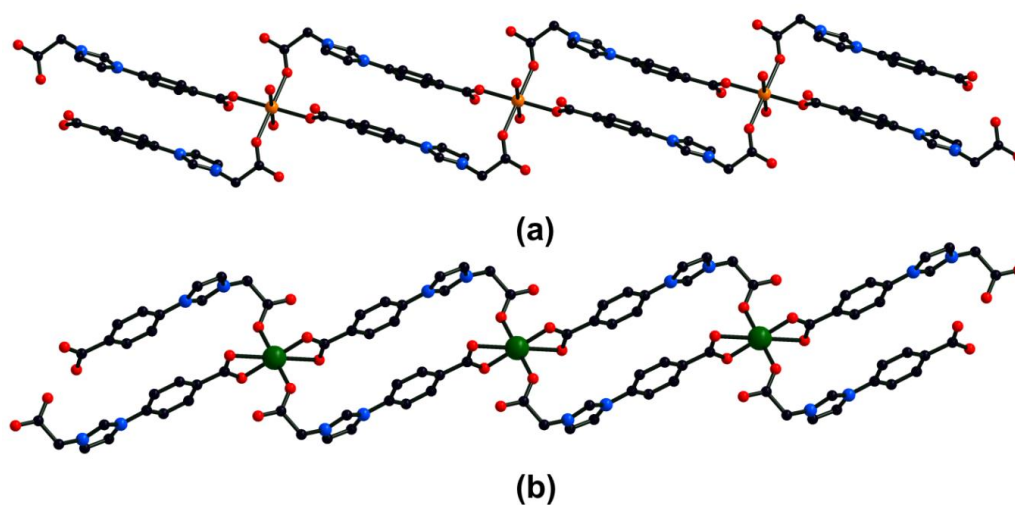


Figure 6.2: (a) Molecular structure of $[(L^1)_2Mn(H_2O)_2]_\infty$. (b) Molecular structure of $[(L^1)_2Cu]_\infty$.

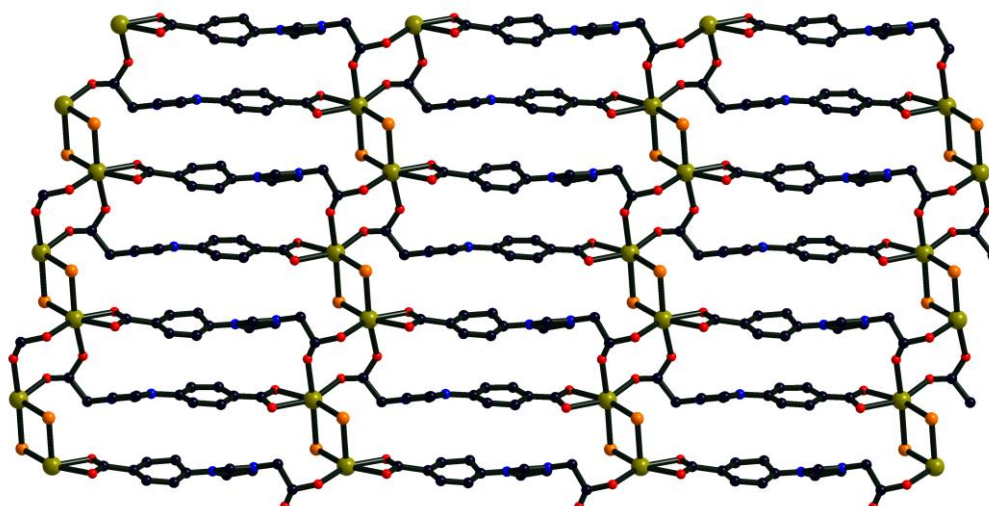
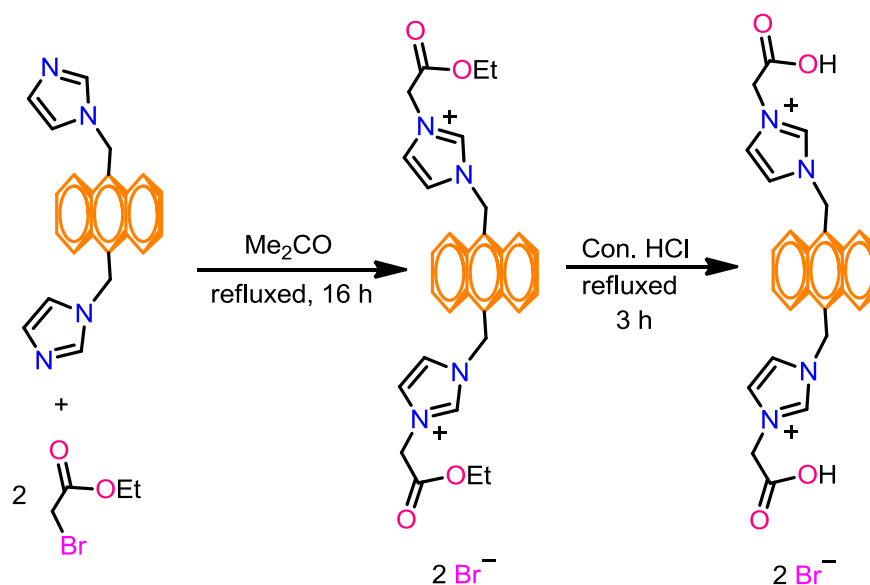


Figure 6.3: Representation of two-dimensional framework in $[(L^1)_3Cd_2(Br)_2]_\infty$.

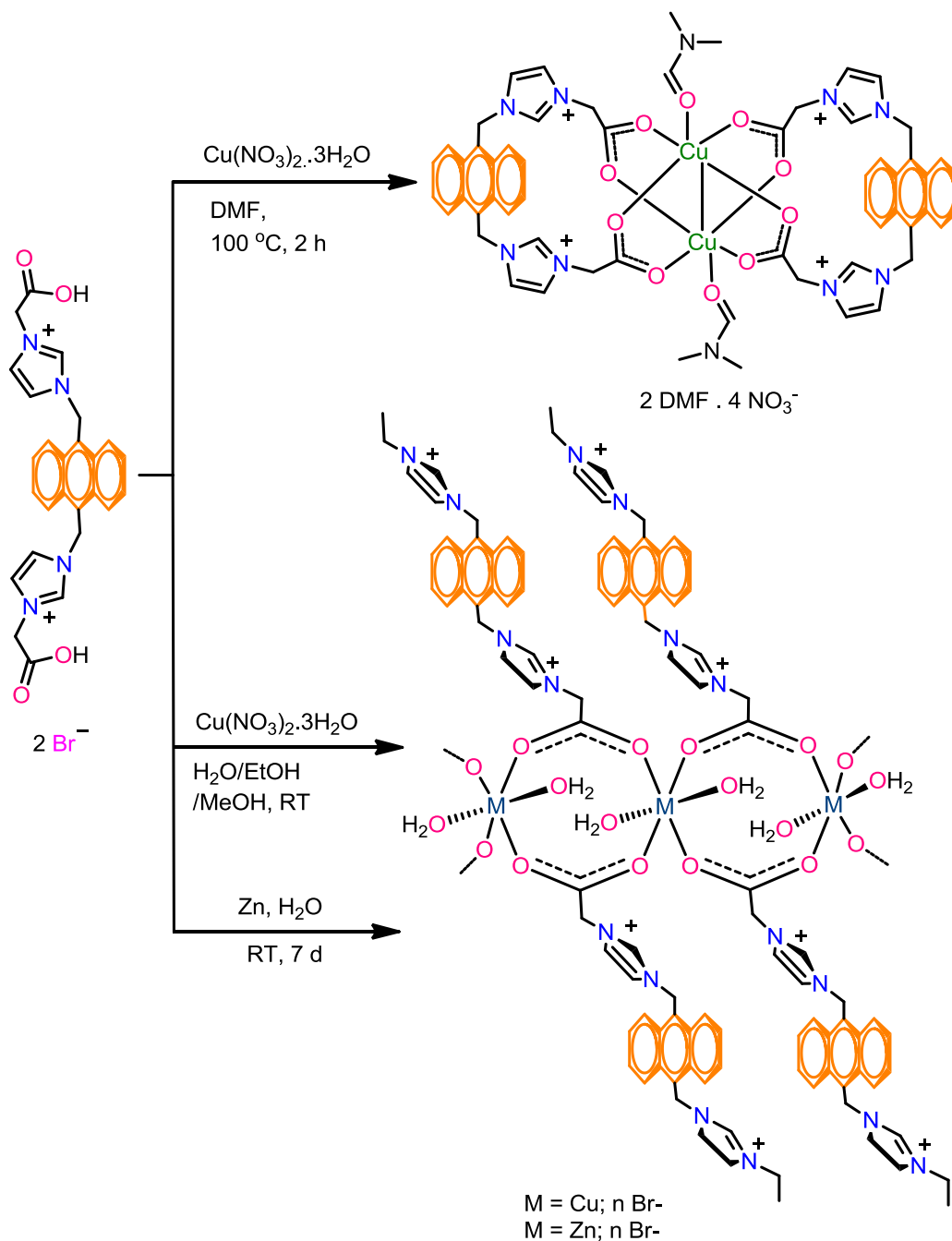


Scheme 6.2: Synthesis of $L^2H_2Br_2$.

Third chapter dispensed for design and synthesis of luminescent bis-imidazolium carboxylate (Scheme 6.2) and its aggregative and infinite coordination networks of copper and zinc. New copper dimer $\{[(L^2)Cu(DMF)]_2(NO_3)_4(H_2O)(DMF)_2\}$, where $L^2 = \{[1,1'-(CH_2)_2-C_{14}H_8]-3,3'-(CH_2CO_2)_2[(HCN)_2CH]_2\}$ and coordination polymers $\{[(L^2)_2Cu(H_2O)_2]_2(Br)_2\}_\infty$ and $\{[(L^2)_2Zn(H_2O)_2]_2(Br)_2\}_\infty$ have been isolated from reactions of luminescent bis-imidazolium carboxylate ligand, $L^2H_2Br_2$ and the corresponding metal precursors (Scheme 6.3).

The reaction between $Cu(NO_3)_2 \cdot 3H_2O$ and $L^2H_2Br_2$ in DMF at $100^\circ C$ yielded bluish green crystals of tetracationic discrete copper dimer $\{[(L^2)Cu(DMF)]_2(NO_3)_4(H_2O)(DMF)_2\}$, the structure of which contains rare tetracationic $[(DMF)Cu(II)]_2$ dimer unit is that bridged by four carboxylates of two L^2 in “paddle-wheel” structure. The same reaction in the presence of water/ethanol/methanol mixture resulted in the formation of light green crystals of $\{[(L^2)_2Cu(H_2O)_2]_2(Br)_2\}_\infty$. Molecule $\{[(L^2)_2Cu(H_2O)_2]_2(Br)_2\}_\infty$ is a two-dimensional (2D) porous coordination polymeric sheet consisting of unique symmetrical dinuclear $[(C(O)O)Cu(OH_2)_2(O(O)C)_2]_2$ building blocks, which are connected by imidazolium anthracene spacers. The infinite 2D porous coordination polymeric sheets are further linked by significant intermolecular hydrogen-bonding interactions by the bromide anions to form a three-dimensional supramolecular framework (Fig. 6.4). Interestingly, the reaction between zinc dust and $L^2H_2Br_2$ in H_2O at room temperature gave similar

structural features to those in $\{[(L^2)_2Cu(H_2O)_2]_2(Br)_2\}_\infty$, though they differ in terms of C–O bond distances and M–O–C angles.



Scheme 6.3: Synthesis of $\{[(L^2)Cu(DMF)]_2(NO_3)_4(H_2O)(DMF)_2\}$, $\{[(L^2)_2Cu(H_2O)_2]_2(Br)_2\}_\infty$ and $\{[(L^2)_2Zn(H_2O)_2]_2(Br)_2\}_\infty$.

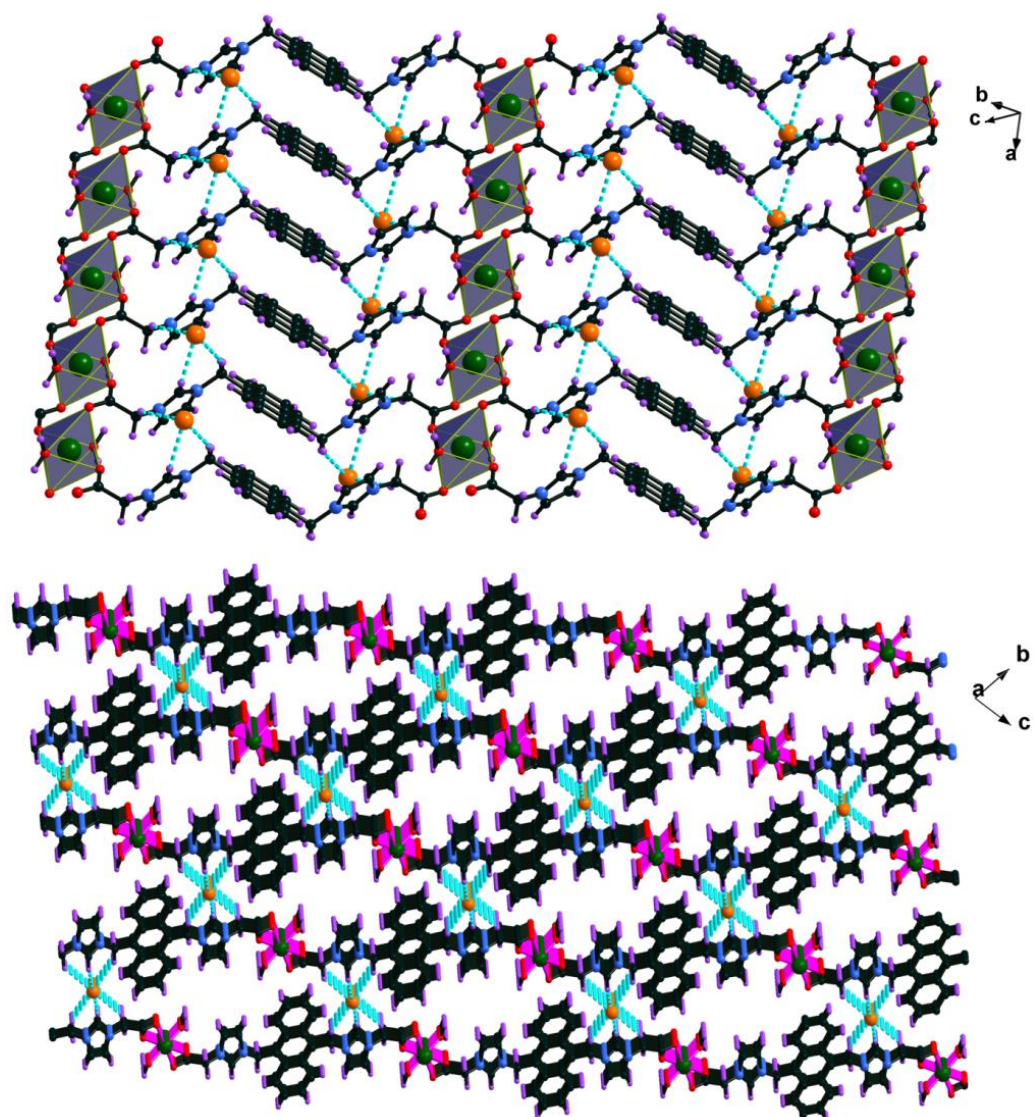


Figure 6.4: Top: A view of the 2D layer of $[(L^2)_2Cu(H_2O)_2]_2(Br)_2$, where polyhedra represent CuO_6 ; Bottom: A close view of the hydrogen bonding between the neighboring 2D layer in $[(L^2)_2Cu(H_2O)_2]_2(Br)_2$ viewed along the a axis showing the 3D framework by hydrogen bonding between Br and C-H groups.

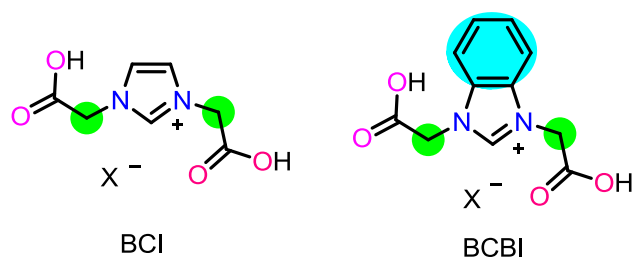


Figure 6.5: The structure of 1,3-bis(carboxymethyl)imidazolium (BCI) and 1,3-bis(carboxymethyl)benzimidazolium (BCBI) salts.

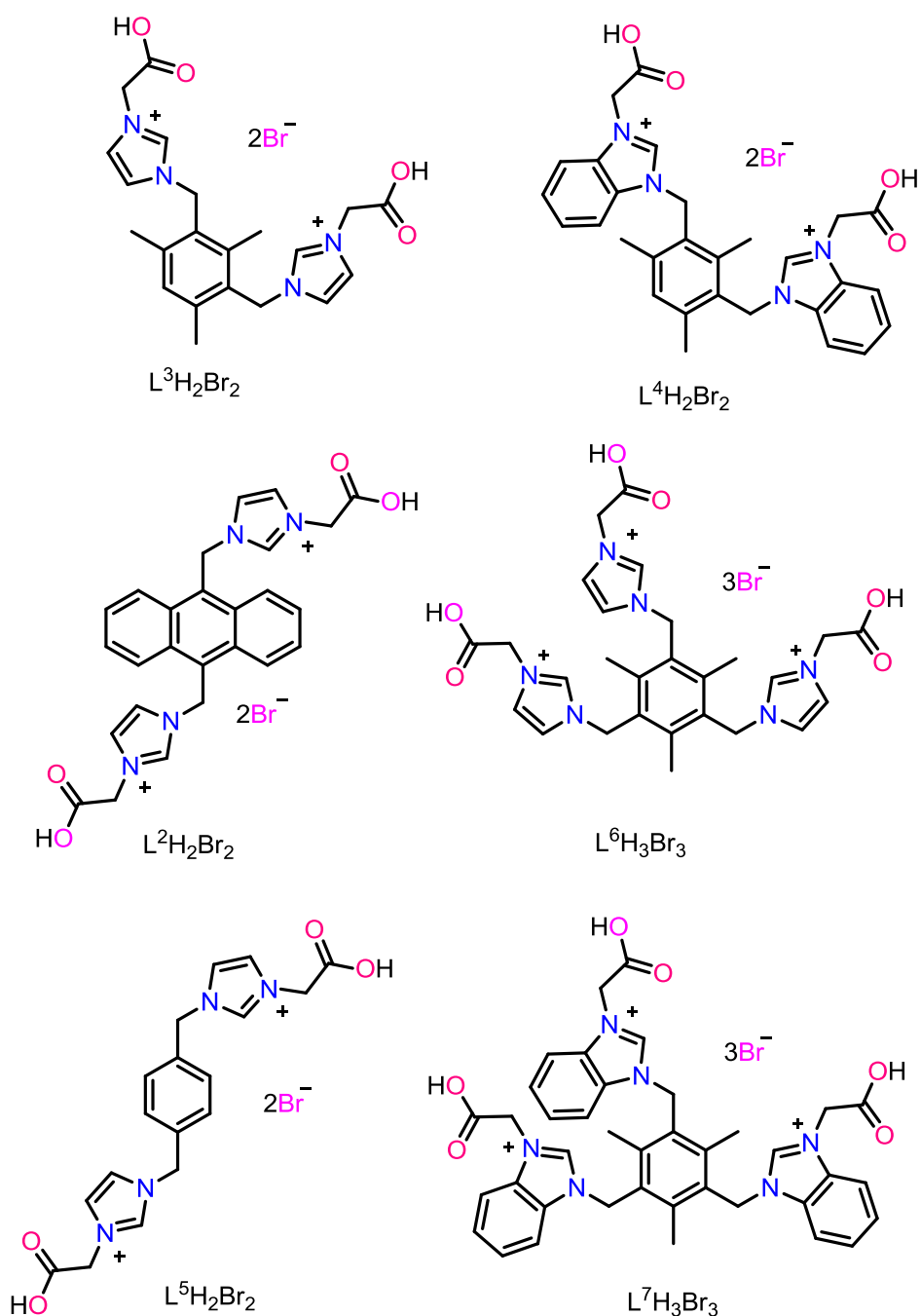
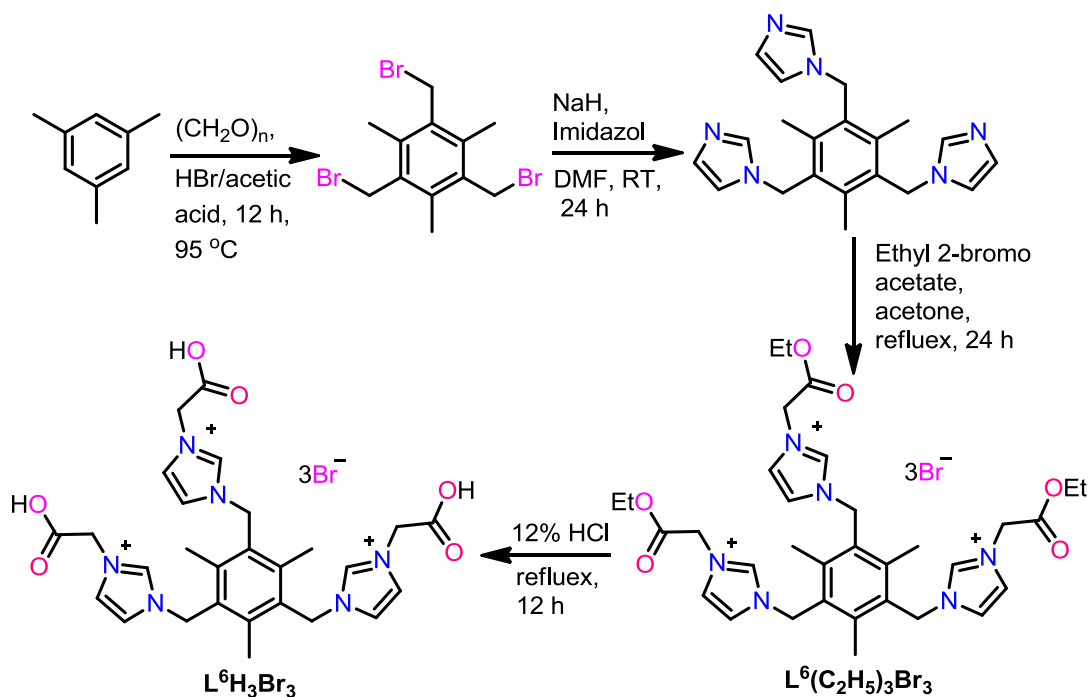


Figure 6.6: Molecular structure of bis-imidazolium carboxylic acids ($L^3H_2Br_2$, $L^4H_2Br_2$, $L^5H_2Br_2$ and $L^2H_2Br_2$) and tris-imidazolium carboxylic acids ($L^6H_3Br_3$ and $L^7H_3Br_3$).

Subsequently, we have designed the new bis- and tris-imidazolium carboxylate organic spacer for isolation of calcium coordination polymers in fourth chapter (Fig. 6.6). The first *s*-block coordination chemistry of imidazolium carboxylate was explored by Dyson *et al.* in 2005. The transition metal or rare earth metal chemistry of imidazolium carboxylate has been explored very well since 2005, while less effort has been devoted

for the *s*-block coordination chemistry of imidazolium carboxylates. The two-dimensional strontium-imidazolium carboxylate polymer, $\{[\text{Sr}(\text{BCI}')_2(\text{H}_2\text{O})_4]\}_\infty$, $\text{BCI}' =$ zwitterionic 1,3-bis(carboxymethyl)imidazolium, derived from BCI' salt and SrCO_3 , where the polymeric sheet is separated by water sheets in which the water molecules form near-planar hexagons. Later, coordination polymers containing calcium, strontium, barium and cesium metal ions, connected *via* the BCI ligand were reported with different structural motifs of water molecules in the structural framework. Recently, the structural properties of $\text{Mg}(\text{BCBI})_2(\text{H}_2\text{O})_4 \cdot 2\text{H}_2\text{O}$, $[\text{Ca}(\text{BCBI})_2(\text{H}_2\text{O})_4] \cdot 2\text{H}_2\text{O}$ and $[\text{Ba}(\text{BCBI})_2(\text{H}_2\text{O})_2 \cdot 2\text{H}_2\text{O}]_n$, $\text{BCBI} =$ 1,3-bis(carboxymethyl)benzimidazolium, were studied.

Notably, only two structurally characterized calcium coordination complexes, namely three-dimensional calcium BCI supported coordination network and monomeric calcium BCBI were reported using BCI or BCBI salts. As shown in Fig. 6.5, the structural motifs of known calcium-imidazolium carboxylates were tuned up by two flexible “methyl” arms and steric hindrance bestowed by BCI and BCBI ligands. In particular, the ionic calcium complexes of imidazolium or benzimidazolium carboxylate ligands with more than two flexible nodes are not known.



Scheme 6.4.: Synthesis of $\text{L}^6\text{H}_3\text{Br}_3$.

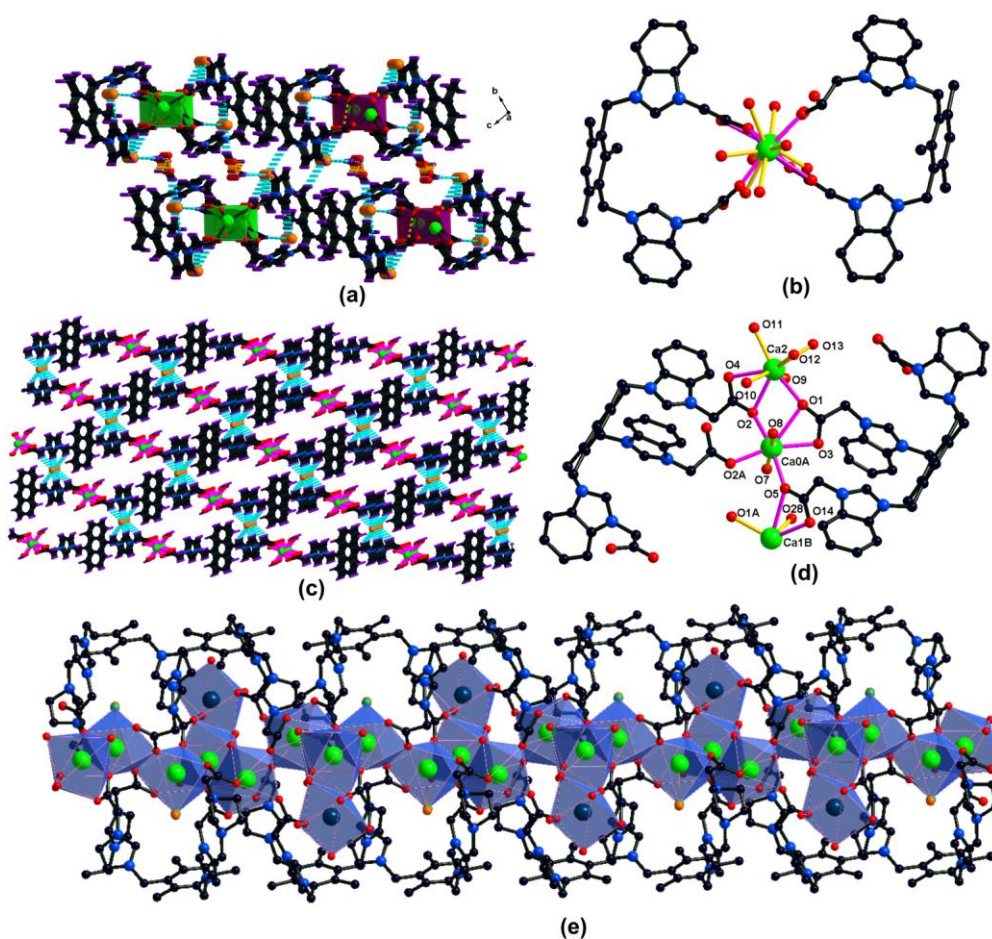


Figure 6.7: (a) 3D supramolecular network through hydrogen bond of $\{[L^3]_2Ca_2(H_2O)_4(Br)_4 \cdot 6H_2O\}_\infty$. (b) Molecular structure of $\{[L^4]_2Ca_2(H_2O)_9(Br)_4 \cdot 4H_2O\}$. (c) Three-dimensional network through $Br \cdots H$ hydrogen bonding of $\{[L^2]_2Ca(H_2O)_2]_2(Br)_2\}_\infty$. (d) Molecular structure of $\{[L^7]_2Ca_2(H_2O)_9(Br)_6\}$. (e) One-dimensional coordination polymer of $\{[L^6]_2Ca_3(Na)(H_2O)_9(Cl)](Br)_6 \cdot 2H_2O\}_\infty$.

In this chapter, the discrete and polymeric calcium coordination compounds $\{[L^4]_2Ca_2(H_2O)_9(Br)_4 \cdot 4H_2O\}$, where $L^4 = \{[1,1'-(CH_2)_2-C_9H_{10}-3,3'-(CH_2CO_2)_2][(C_6H_4N)_2CH]_2\}$, $\{[L^3]_2Ca_2(H_2O)_4(Br)_4 \cdot 6H_2O\}_\infty$, where $L^3 = \{[1,1'-(CH_2)_2-C_9H_{10}-3,3'-(CH_2CO_2)_2][(CHN)_2CH]_2\}$, $\{[L^5]_2Ca_2(H_2O)_2]_2(Br)_2\}_\infty$, where $L^5 = \{[1,1'-(CH_2)_2-C_6H_4-3,3'-(CH_2CO_2)_2][(HCN)_2CH]_2\}$, $\{[L^2]_2Ca(H_2O)_2]_2(Br)_2\}_\infty$, $\{[L^6]_2Ca_3(Na)(H_2O)_9(Cl)](Br)_6 \cdot 2H_2O\}_\infty$, $L^6 = \{[1,1',1''-(CH_2)_3-C_9H_9-3,3',3''-(CH_2CO_2)_3][(HCN)_2CH]_3\}$ and $\{[L^7]_2Ca_2(H_2O)_9(Br)_6\}$ (Scheme 6.4), $L^7 = \{[1,1',1''-(CH_2)_3-C_9H_9-3,3',3''-(CH_2CO_2)_3][(C_6H_4N)_2-CH]_3\}$ have been isolated from the reaction between corresponding imidazolium carboxylates and calcium carbonate in aqueous solution. The molecules $\{[L^3]_2Ca_2(H_2O)_4(Br)_4 \cdot 6H_2O\}_\infty$ and $\{[L^2]_2Ca(H_2O)_2]_2(Br)_2\}_\infty$ are isolated as 3D supramolecular network through $Br \cdots H$ hydrogen bonding, while

$\{[(L^4)_2Ca_2(H_2O)_9](Br)_4 \cdot 4H_2O\}$ and $\{[(L^7)_2Ca_2(H_2O)_9](Br)_6\}$ are the tetra-cationic binuclear and hexa-cationic trinuclear calcium molecules, respectively (Fig. 6.7). The coordination polymer $\{[(L^5)_2Ca_2(H_2O)_2]_2(Br)_2\}_\infty$ has been isolated as 3D metal-organic framework (Fig. 6.8). The coordination polymer $\{[(L^6)_2Ca_3(Na)(H_2O)_9(Cl)](Br)_6 \cdot 2H_2O\}_\infty$ has been isolated as ionic 1D coordination polymer.

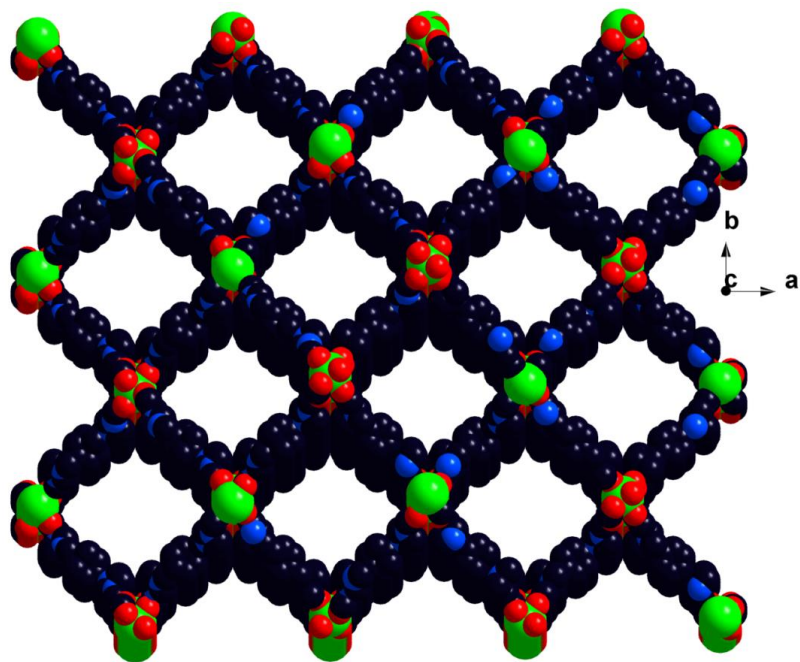
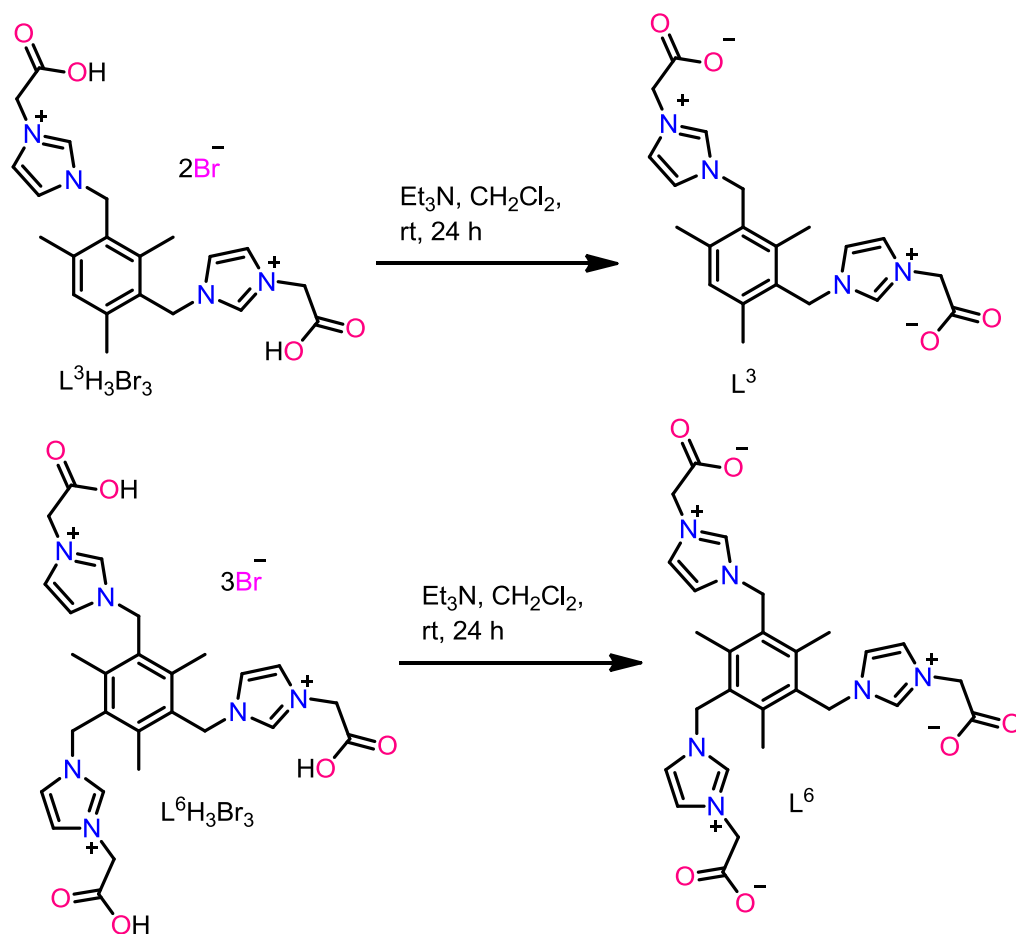


Figure 6.8: Space filling model of 3D MOF $\{[(L^5)_2Ca_2(H_2O)_2]_2(Br)_2\}_\infty$.

Besides, we have extended our study towards rare-earth metals in chapter 5. We have designed and synthesized the new zwitterionic bis- and tris-imidazolium carboxylate organic spacers (Scheme. 6.5). The novel discrete dimers $\{[(L^3)_2(RE)_2(NO_3)_2(H_2O)_4(DMF)_2](NO_3)_4\}$ (RE = La and Ce), $\{[(L^3)_2(RE)_2(NO_3)_2(H_2O)_2(DMF)_2](NO_3)_4\}$ (RE = Sm), $\{[(L^3)_2(RE)_2(NO_3)_2(H_2O)_2(DMF)_2](NO_3)_4\}$ (RE = Gd, Dy and Y), coordination polymers $\{[(L^6)(RE)(NO_3)(H_2O)](H_2O)_3(NO_3)_2\}_\infty$ (RE = Sm, Gd, Dy and Y) and discrete monomers $\{[(L^6)_2(RE)](NO_3)_3\}$ (RE = Sm, Gd, Dy and Y) have been derived from poly-zwitterionic imidazolium carboxylates and corresponding metal nitrates in the presence of DMF/MeOH or DMF/EtOH/H₂O or DMF/MeOH/H₂O/Py/4,4'-bpy.



Scheme 6.5: Synthesis of L^3 and L^6 .

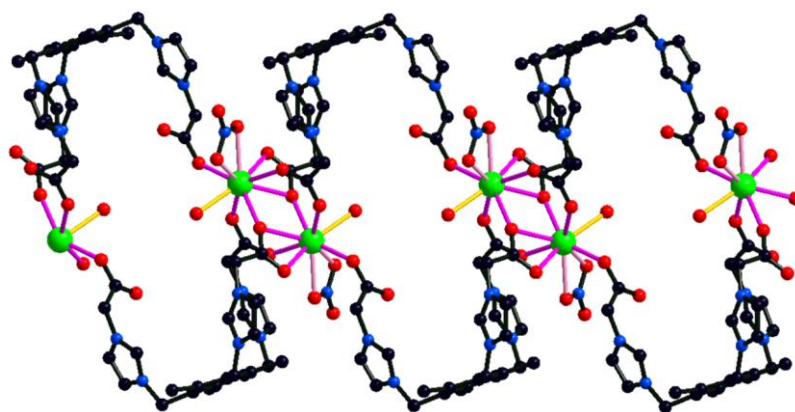


Figure 6.9: 1D nano tubular coordination polymer of $\{[L^6(Dy)(NO_3)(H_2O)](H_2O)_3(NO_3)_2\}_\infty$.

The first discrete dimers $\{[L^3]_2(RE)_2(NO_3)_2(H_2O)_4(DMF)_2\}(NO_3)_4$ ($RE = La$ and Ce) have been isolated with decacoordinated metal centers. Similarly, the first discrete dimer $\{[L^3]_2(RE)_2(NO_3)_2(H_2O)_2(DMF)_2\}(NO_3)_4$ ($RE = Sm$) has been isolated with

nano-coordinated metal centers. The first isostructural discrete dimers $\{[(L^3)_2(RE)_2(NO_3)_2(H_2O)_2(DMF)_2](NO_3)_4\}$ (RE = Gd, Dy and Y) have been obtained with octacoordinated metal centers. The coordination polymer $\{[(L^6)(RE)(NO_3)(H_2O)](H_2O)_3(NO_3)_2\}_\infty$ (RE = Sm, Gd, Dy and Y) have been formed as a 1D nanotubular structure, where metal geometry is distorted tricapped trigonal prismatic (Fig. 6.9). Interestingly, the hitherto unknown ionic rare-earth discrete monomers $\{[(L^6)_2(RE)](NO_3)_3\}$ (RE = Sm, Gd, Dy and Y) have been isolated using L^6 , where metal geometry is distorted octahedron (Fig. 6.10).

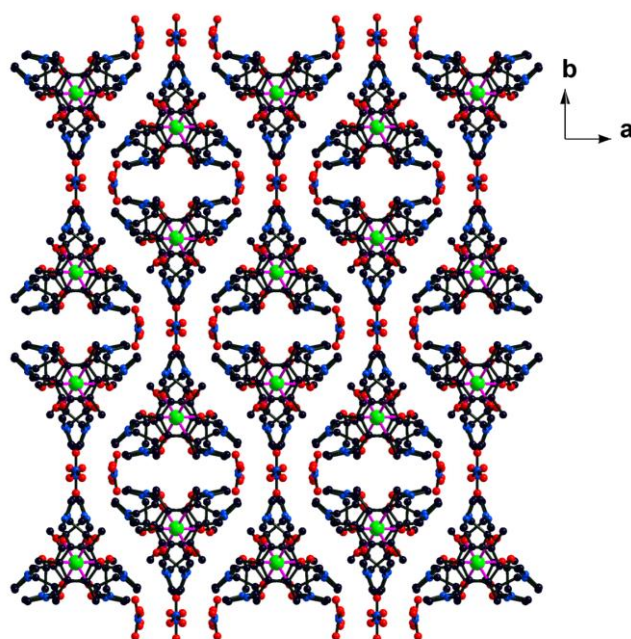


Figure 5.10: Molecular packing of $\{[(L^6)_2(Dy)](NO_3)_3\}$.

The results presented in this thesis contribute to a better understanding of the imidazolium carboxylic acid spacers based coordination assemblies. Efforts have been made to expand the Mn, Co, Ni, Cu, Zn and Cd metal-azolium carboxylate chemistry to provide a variety of routes toward desired PCPs/MOFs. The late transition metal (Mn, Co, Ni, Cu, Zn and Cd) based dinuclear or 1D coordination polymers or 2D coordination grids or 3D metal organic frameworks have been derived using imidazolium carboxylic acid spacers (with one flexible node) or anthracene derivative of imidazolium carboxylic acid spacer (with four flexible nodes) (Chapter 2 and 3). Interestingly, only the nickel imidazolium carboxylate has been isolated as a rare monomer. The first luminescent 3D Cu and Zn imidazolium carboxylates have been reported. Despite the popularity and versatility of transition-metal-azolium carboxylate

coordination polymers, there are very few examples of group 2 complexes supported by azolium carboxylate ligands in the literature. There are none featuring the luminescent calcium azolium carboxylates and the first luminescent calcium azolium carboxylates with different thermal properties have been reported with the help of bis- (with four flexible nodes) azolium carboxylic acid ligands in chapter 4. Interestingly, the variation of the bridging chromophore produced significant effects on the fluorescent as well as thermal properties in calcium azolium carboxylates. Like dinuclear copper and calcium azolium complexes depicted in chapters 3-4, the bis-(with four flexible nodes) azolium carboxylic acid ligand resulted the formation of first discrete rare-earth dinuclear azolium molecules of La, Ce, Sm, Gd, Dy and Y (as reported in chapter 5). Whereas the tris-(with six flexible nodes) azolium carboxylic acid led the formation of one-dimensional Sm, Gd, Dy and Y nanotubular rare-earth coordination polymers and first discrete Sm, Gd, Dy and Y monomers (as reported in chapter 5). As can be observed in the thirty synthetically intriguing metal-azolium carboxylate aggregates presented in this thesis, a combination of carboxylate groups with flexible or rigid arms and steric hindrance affect not only the structural topology, also the physical properties of the resultant solids. The potential applications of metal-imidazolium carboxylates in carbon-carbon bond formation reactions along with magnetic properties of some of the molecules depicted in this thesis along with several new molecules will be submitted as a separate thesis by my colleague Mr. Chatla Naga Babu in due course.

List of Publications

- [1] **P. Suresh**, A. Samanta, A. Sathyanarayana and G. Prabusankar*, Synthesis and characterization of vinyl imidazolium salts: solution state study to realize the influence of different anions, *Journal of Molecular Structure*, **2012**, 1024, 170-175.
- [2] A. Sathyanarayana, **P. Suresh** and G. Prabusankar*, A mild approach to the synthesis of 1,2-diferrocenylethanedione from ferrocenealdehyde, *Journal of Organometallic Chemistry*, **2012**, 720, 46-51.
- [3] **P. Suresh**, A. Sathyanarayana, G. Prabusankar*, O. Hernandez and S. Golhen, The first monomeric β -Diketiminato stabilized four coordinated bismuth(III) bistrifluoromethanesulfonate, *Journal of Inorganic and General Chemistry*, **2012**, 638, 617–620.
- [4] **P. Suresh**, S. Radhakrishnan, C. N. Babu, A. Sathyanarayana, N. Sampath and G. Prabusankar*, Luminescent imidazolium carboxylate supported aggregate and infinite coordination networks of copper and zinc, *Dalton Transactions*, **2013**, 42, 10836-10846.
- [5] **P. Suresh** and G. Prabusankar*, Cationic zinc (II) dimers and one dimensional coordination polymer from ionic carboxylic acid, *Journal of Chemical Sciences*, **2014**, 126, 1409-1415 (Invited paper in special issue on “Chemical Crystallography”).
- [6] G. Prabusankar*, A. Sathyanarayana, **P. Suresh**, C. N. Babu, K. Srinivas and M. B. P. Rao, N-heterocyclic carbene supported heavier group 14 elements: recent progress and challenges, *Coordination Chemistry Review*, **2014**, 269, 96-133.
- [7] C. N. Babu, **P. Suresh**, P. Das, A. Sathyanarayana, R. Ranjith, N. Sampath and G. Prabusankar*, Synthesis, crystal structure and spectral properties of copper(II) monomer decorated copper(II) coordination polymer, *Journal of Molecular Structure*, **2014**, 1062, 141-146.
- [8] C. N. Babu, **P. Suresh**, N. Sampath and G. Prabusankar*, Cadmium coordination polymers based on flexible bis(imidazole) ligands: A rare example for doublet of doublet cadmium polyhedron arrangements, *Journal of Molecular Structure*, **2014**, 1075, 147-153.
- [9] K. Srinivas, **P. Suresh**, C. N. Babu, A. Sathyanarayana and G. Prabusankar*, Heavier chalcogenone complexes of bismuth(III) trihalides: potential catalysts for acylative cleavage of cyclic ethers, *RSC Advance*, **2015**, 5, 15579-15590.

- [10] **P. Suresh**, C. N. Babu and G. Prabusankar*, Semi rigid imidazolium carboxylate controlled structural topologies in zwitterionic coordination networks, *Polyhedron*, **2015**, 89, 322-329.
- [11] **P. Suresh**, C. N. Babu, N. Sampath and G. Prabusankar*, Photoluminescent calcium azolium carboxylates with diversified calcium coordination geometry and thermal stability, *Dalton Transactions*, **2015**, 44, 7338-7346.
- [12] **P. Suresh**, V. Munisamy and G. Prabusankar*, Synthesis, characterization and applications of vinyl functionalized N-heterocyclic carbene supported ruthenium(II) derivatives, *Indian Journal of Chemistry*, **2015**, 54A, 588-595.
- [13] **P. Suresh**, C. N. Babu and G. Prabusankar*, A rare binuclear metallocyclic planar 20, 26 and 34 membered zinc-organic rings, *Polyhedron*, **2015**, 93, 84-90.
- [14] **P. Suresh** and G. Prabusankar*, Rare-earth discrete molecules and coordination polymers from zwitterionic imidazolium carboxylates, *Dalton Transactions*, to be Submitted.

List of Conferences and Workshops

- [1] **P. Suresh** and G. Prabusankar*, Semi rigid imidazolium carboxylate controlled structural topologies in zwitterionic coordination networks, *National symposium in chemistry (CRSI-NSC-17)*, CSIR-NCL Pune, India, Feb, 6-8, **2015** (poster presentation).
- [2] **P. Suresh**, C. N. Babu and G. Prabusankar*, Unprecedented cyclic zinc dimer and polynuclear cadmium coordination polymers based on imidazole ligands, symposium on *International Conference on Coordination Chemistry (ICCC-41)*, Suntec Singapore convention & exhibition centre, Singapore, July 21-25, **2014** (flash presentation).
- [3] **P. Suresh** and G. Prabusankar*, Luminescent flexible imidazolium carboxylate supported aggregate and infinite coordination polymers, symposium on *Modern Trends in Inorganic Chemistry (MTIC-XV)*, Indian Institute of Technology Roorkee, India, Dec 13-16, **2013** (poster).
- [4] **P. Suresh**, Introduction of Gaussian: theory and practice, *Gaussian, Inc.* Central Leather Research Institute and Indian Institute of Technology Madras, India, Jan 2-6, **2012** (workshop).
- [5] **P. Suresh** and G. Prabusankar*, Π -Functionalized N-heterocyclic carbenes (NHCs) and its applications, symposium on *Modern Trends in Inorganic Chemistry (MTIC-XIV)*, University of Hyderabad, India, Dec 10-13, **2011** (poster).

